Final Report

Design Synthesis Exercise (Project 07)

June 27, 2016

Delft University of Technology

Tom Gulikers	4270282	Dave Kroezen	4097890
Daan van Hoogstraten	4229517	Lukas Müller	4275659
Radu Iordache	4181018	Marleen Otting	4276027
Imke Kleinbekman	4289757	Marc Pieters	4282248
Mike Koch	4232313	Pieter-Jan Proesmans	4275063

TUDelft

Preface

We are a group of prospective aerospace engineers, currently in the final year of the Bachelor of Aerospace Engineering at Delft University of Technology. As a part of our concluding bachelor assignment, the Design Synthesis Exercise (DSE), our supervisors have given us the task to design an aircraft which will have a performance similar to current narrow-body airliners, such as the Airbus A320 or the Boeing 737NG, but with a 30 % reduction in direct operating cost and a significant increase in sustainability. The objectives of the DSE are to allow us to enhance our skills in engineering, to work as a team and to apply previously apprehended knowledge to a realistic problem. This report is aimed at readers with technical knowledge and some parts of the report can be challenging due to the nature of the content.

We would like to thank our tutor Wim Verhagen and our coaches Marianella Hernandez Santana and Navi Rajan for their guidance and support. Furthermore, we would like to express our gratitude to the DSE supporting staff for providing the facilities for this project and to all experts helping us in any way.

<div align="right">

Group 07
Delft, June 2016

</div>

Summary

As more and more people choose the airplane as a means of transportation, the aviation industry faces new challenges in order to fulfill the increasing demand, while decreasing the costs and emissions. In this report, the authors present a design of a narrow-body aircraft that is meant to provide a 30 % direct operating costs reduction, as well as a 20 % reduction in NO_x and CO_2 emissions while being ready for market introduction by 2030. Furthermore, the aircraft should provide a noise reduction of 10 % which translates to a reduction of 29 $[EPNdB]$ and it should house 177 passengers.

As this is the last report in a series of four, this report elaborates on a more detailed design. Previously, the requirements of the aircraft and the market analysis were investigated. The latter showed that the narrow-body aircraft will capture a large part of the market by 2034 and thus the project continued with the concepts generation. These concepts were sized during the preliminary design phase, and based on the found performances a trade-off was made. The blended wing body was the most promising one and was thus investigated further in this report.

The authors then continue by breaking down the chosen design into components. A detailed analysis on the aerodynamic, structural, propulsion, stability and aircraft system components is made, while performing iterations between the departments in order to completely integrate the design. The result is a canard aircraft with a rear placed wing and two ultra high bypass turbofans placed between two vertical stabilizers. Its flight deck design introduces the possibility of a single pilot operations system, which accounts for a possible change of regulations. That, in turn, would allow the airlines to further reduce the crew costs by 7.2 %. A noise assessment is also performed by positioning the powerplant system on top of the fuselage in order to meet the noise reduction requirements. With the noise shielding due to the top mounted engines, vertical twin tails and other smaller adaptions, a total noise reduction of 29.6 $[EPNdB]$ is achieved.

The design analysis concludes with a final overview of the aircraft and its integrated systems and components. The authors wrap up by giving recommendations for the future stages of development such as reviewing the life cycle estimation, considering the implementation of a geared turbofan and analyzing a possible blending between the fuselage and the wing. A project risk mitigation is also performed, in which the authors state that the overall approach was as conservative as possible with respect to the technology available by 2025, when the production phase should commence.

A market analysis is performed, to see the necessity of such an aircraft in respect to the forecasted market expectations by the year 2030. With the enlarged range of 6500 km and the reduction of 30.4 % in DOC, the aircraft is assumed to easily capture 5% of the market. Furthermore, only a 2% market capture, is needed to have a Return of investment of 5 % in 5 years. Thus, a 172 aircraft will need to be produced. With this, the aircraft needs to be sold for 90 M$ each, which is found in line with the competitors. A requirements analysis is used to describe the expected standards the new aircraft would need to reach in order to breach such a market successfully. The authors claim that the design of each component is made while keeping in mind objectives such as safety, maintenance or sustainable development. The aircraft is thus able to reach all requirements except for the dispatch reliability. This assessment concludes that a noticeable improvement in this regard is not possible by 2030 and the reliability will remain comparable to the dispatch reliability of the competitors, namely 99.0 %

Contents

List of Abbreviations & Symbols

Abbreviations

AC	Alternating Current
ACARS	Aircraft Communication Addressing and Reporting System
AMPR	Aeronautical Manufacturing Planning Report
APU	Auxiliary Power Unit
ATC	Air Traffic Control
BLI	Boundary Layer Ingestion
BWB	Blended Wing Body
CFD	Computational Fluid Dynamics
CFRP	Carbon Fibre Reinforced Plastics
DC	Direct Current
DD	Direct Drive
DOC	Direct Operating Cost
DOT	Design Option Tree
DSE	Design Synthesis Exercise
EGPWS	Enhanced Ground Proximity Warning System
EMI	Electromagnetic Interference
FAA	Federal Aviation Administration
FBD	Functional Breakdown Diagram
FEM	Finite Element Method
FFD	Functional Flow Diagram
FLTA	Forward Looking Terrain Avoidance
FND	Fan Nozzle Diameter
FW	Fuel Weight
GSP	Gas turbine Simulation Program
GTF	Geared Turbo Fan
HLD	High Lift devices
HPC	High Pressure Compressor
HPS	High Pressure Shaft
HPT	High Pressure Turbine
HUD	Head Up Display
HWB	Hybrid Wing Body
ICAO	International Civil Aviation Organization
ISA	International Standard Atmosphere
LCC	Life Cycle Cost
LPC	Low Pressure Compressor
LPS	Low Pressure Shaft
LPT	Low Pressure Turbine
LTO	Landing Take Off cycle
MAC	Mean Aerodynamic Chord
MEA	More Electric Aircraft
MFN	Mid-Fuselage Nacelle
MRB	Maintenance Review Board
MSG	Maintenance Steering Group
MTOW	Maximum Take-Off Weight
MWG	Maintenance Working Group
OEW	Operating Empty Weight
OPR	Overall Pressure Ratio
OWN	Over-Wing Nacelle
PF	Pilot Flying
PHM	Prognostic Health Monitoring
PM	Pilot Monitoring
PMG	Permanent Magnet Generators
QoS	Quality of Service
RDTE	Research Development Test and Evaluation
RELOAD	Reliable Low-cost Aircraft Design
ROI	Return On Investment
RPK	Revenue Passenger Kilometer
SFC	Specific Fuel Consumption
SMART	Specific, Measurable, Attainable, Realistic, Time-Bound
SPO	Single Pilot Operations
SST	Shear Stress Transport
TCAS	Traffic Collision Avoidance System
TIT	Turbine Inlet Temperature
VFSG	Variable Frequency Starter Generator

Symbols

α	Design angle of attack	$[rad]$
$\alpha_{0L,h}$	Angle of attack of the horizontal tail plane at zero lift	$[rad]$
α_{stall}	Stall angle of attack	$[rad]$
β	Ground Turn radius	$[m]$
δ	Thickness of the runway construction	$[m]$
η_s	Shock absorption efficiency	$[-]$
η_t	Tyre efficiency	$[-]$
Γ	Dihedral angle of the main wing	$[rad]$
Λ	Sweep of the main wing measured at the MAC	$[rad]$
λ	Taper ratio of the main wing	$[rad]$
Λ_c	Sweep of the canard measured at the MAC	$[rad]$
Λ_v	Sweep of the vertical tail measured at the MAC	$[rad]$
Λ_{LE}	Sweep of the main wing measured at the leading edge	$[rad]$
Λ_{QC}	Sweep of the main wing measured at the quarter chord	$[rad]$
μ	friction coefficient	$[-]$
μ_b	Dimensionless asymmetrical mass parameter	$[-]$
μ_c	Dimensionless symmetrical mass parameter	$[-]$
ν	Kinematic viscosity	$[m^2/s]$
ν_m	Material's Poisson's ratio	$[-]$
ψ	Lateral tip over angle	$[°]$
ρ	Density	$[\frac{kg}{m^3}]$
$\rho_{biofuel}$	Density of biofuel	$[\frac{kg}{m^3}]$
$\rho_{kerosine}$	Density of kerosine	$[\frac{kg}{m^3}]$
σ_{ult}	Material's ultimate stress	$[MPa]$
σ_{yield}	Material's yield stress	$[MPa]$
τ_{max}	Material's maximum shear stress	$[MPa]$

θ	Tail cone angle	[°]
φ	Castor angle	[°]
A	Aspect ratio of the main wing	[-]
A_c	Aspect ratio of the canard plane	[-]
A_s	Area surface	$[m^2]$
A_v	Aspect ratio of the vertical tail	[-]
b	Wingspan	$[m]$
B_r	Boom area	$[m]$
$b_{i,j}$	Boom location	$[m]$
BPR	Engine bypass ratio	[-]
c'/c	Ratio between the chord of the airfoil with extended flap and the chord in clean configuration	[-]
c_j	Specific fuel consumption	$[\frac{kg}{Ns}]$
C_{D0}	Design zero lift drag coefficient	[-]
C_{D_f}	Drag coefficient of the fuselage	[-]
$C_{D0,c}$	Design zero lift drag coefficient of the canard	[-]
$C_{D0,fuselage}$	Design zero lift drag coefficient of the fuselage	[-]
$C_{D0,v}$	Design zero lift drag coefficient of the vertical tail	[-]
$C_{D0,w}$	Design zero lift drag coefficient of the main wing	[-]
$C_{D_{L,c}}$	Lift dependent drag coefficient of the canard	[-]
$C_{D_{L,fuselage}}$	Lift dependent drag coefficient of the fuselage	[-]
$C_{D_{L,v}}$	Lift dependent drag coefficient of the vertical tail	[-]
$C_{D_{L,w}}$	Lift dependent drag coefficient of the main wing	[-]
C_{Di}	Induced drag coefficient	[-]
C_{Dw}	Wave drag coefficient	[-]
C_{L0}	Lift coefficient of the airfoil at zero angle of attack	[-]
$C_{L_{\alpha_c}}$	Lift curve slope of the canard	$[\frac{1}{rad}]$
$C_{L_{\alpha_v}}$	Lift curve slope of the vertical tail	$[\frac{1}{rad}]$
$C_{L_{\alpha_{wf}}}$	Lift curve slope of the main wing and fuselage	$[\frac{1}{rad}]$
C_{L_α}	Lift curve slope of the main wing	$[\frac{1}{rad}]$
$C_{l_{\beta/\dot{\beta}/p/r/\delta_a/\delta_r}}$	Roll moment coefficient	$[\frac{1}{rad}]$
$C_{L_{landing}}$	Landing lift coefficient	[-]
$C_{L_{max}}$	Maximum lift coefficient	[-]
$C_{L_{TO}}$	Take-off lift coefficient	[-]
C_L	Design lift coefficient	[-]
C_l	2D lift coefficient	[-]
C_{m_0}	Pitching moment coefficient of the airfoil	[-]
$C_{m_{engines}}$	Pitching moment coefficient due to the engines	[-]
$C_{m_{u/\alpha/\dot{\alpha}/q/\delta_c}}$	Pitch moment coefficient	$[\frac{1}{rad}]$
$C_{n_{\beta/\dot{\beta}/p/r/\delta_a/\delta_r}}$	Yaw moment coefficient	$[\frac{1}{rad}]$
C_{rivet}	End fixity coefficient	[-]
c_{root}	Chord of the main wing at the root	$[m]$
c_{tip}	Chord of the main wing at the tip	$[m]$
$C_{X_{u/\alpha/\dot{\alpha}/q/\delta_c}}$	Force coefficient in X-direction	$[\frac{1}{rad}]$
$C_{Y_{\beta/\dot{\beta}/p/r/\delta_a/\delta_r}}$	Force coefficient in Y-direction	$[\frac{1}{rad}]$
$C_{Z_{u/\alpha/\dot{\alpha}/q/\delta_c}}$	Force coefficient in Z-direction	$[\frac{1}{rad}]$
d_f	Fuselage structural depth	$[m]$
$D_{engines}$	Diameter of the engine inlet	$[m]$
$D_{lg_{main}}$	Diameter of main landing gear wheel	$[m]$
$D_{lg_{nose}}$	Diameter of nose landing gear wheel	$[m]$
D_{strut}	Diameter if the landing gear struts	$[m]$
D_{wheel}	Diameter of the wheels	$[m]$
E	Young's modulus	$[GPa]$
e	Oswald factor of the main wing	[-]
e_c	Oswald factor of the horizontal tail	[-]
$e_{b/D/M}$	Oswald factor components	[-]
F	Vertical tail force at various positions	$[N]$
G	Shear modulus	$[GPa]$
h	Cruise altitude	$[m]$
h_f	Mean fuselage height	$[m]$
H_t/H_v	T-tail configuration ratio	[-]
h_{lg}	Height of the landing gear	$[m]$
$h_{nacelle}$	Height of the nacelles	$[m]$
I_y	Yawing moment of inertia	$[kg \cdot m^2]$
$I_{xx,yy,zz}$	Moment of inertia around x,y or z axis	$[m^4]$
K	Aerodynamic form factor	[-]
K_c	Compression buckling coefficient	[-]
K_s	Shear buckling coefficient	[-]
K_x	Various estimation constants	[-]
K_Λ	Sweep correction factor	[-]
l_a	Electrical routing distance (generators to avionics to cockpit)	$[m]$
l_c	Distance between aerodynamic centers of the main wing and canard	$[m]$
l_f	Total fuselage length	$[m]$
l_u	Length available at the end of the fuselage to place upsweep	$[m]$
l_{engine}	Length of the engine	$[m]$
$l_{f_{structure}}$	Length of the fuselage structure	$[m]$
$l_{landing}$	Landing field length	$[m]$
$l_{MAC_{root}}$	Distance from the MAC to the root of the main wing	$[m]$
l_m	Distance between the main landing gear and center of gravity	$[m]$
$l_{nosecone}$	Nosecone length	$[m]$
l_n	Distance between the nose landing gear and center of gravity	$[m]$
$l_{tailcone}$	Tailcone length	$[m]$
l_{TO}	Take-off field length	$[m]$
l_{track}	Distance between main and nose landing gear	$[m]$
l_{vortex}	Distance between the horizontal tail and the vortex shed plane	$[m]$
$LEMAC$	Longitudinal position of the leading edge mean aerodynamic chord	$[m]$
m	Mass	$[kg]$
$m_{batteries}$	Total weight of the batteries	$[kg]$
M_{cruise}	Cruise Mach number	[-]
M_{cr}	Critical Mach number	[-]
m_{engine}	Mass of the engine	$[kg]$
m_{FG}	Mass of the fuselage group	$[kg]$
m_F	Fuel mass	$[kg]$
$m_{landing}$	Aircraft mass during landing	$[kg]$
m_{LUG}	Luggage mass including hand luggage	$[kg]$

Symbol	Description	Unit
M_{min}	Minimum Mach number	[-]
m_{OE}	Operating empty mass	[kg]
$m_{pax_{luggage}}$	Mass of the passenger luggage	[kg]
m_{PAX}	Passenger mass including hand luggage	[kg]
m_{UAV}	Mass of the uninstalled avionics	[kg]
m_{WG}	Wing group mass	[kg]
$M_{x,y,z}$	Moment around x,y or z axis	[Nm]
MAC	Mean aerodynamic chord length	[m]
mu_1	Pitching moment factor 1	[-]
mu_2	Pitching moment factor 2	[-]
mu_3	Pitching moment factor 3	[-]
n	Load factor	[-]
N_g	Landing load factor	[-]
n_{aisles}	Number of aisles	[-]
$n_{c_{functions}}$	Number of functions performed by the controls	[-]
n_{crew}	Number of crew members	[-]
$n_{engines}$	Number of engines	[-]
$n_{generators}$	Number of generators	[-]
$n_{m_{functions}}$	Number of mechanical functions	[-]
n_{mss}	Number of main landing gear shock struts	[-]
$n_{mwheels}$	Number of main landing gear wheels	[-]
$n_{nwheels}$	Number of nose landing gear wheels	[-]
$n_{pax/row}$	Number of passengers per row	[-]
n_{pax}	Number of passengers	[-]
n_{tanks}	Number of fuel tanks	[-]
$N_{ult_{landing}}$	Ultimate load factor during landing	[-]
N_z	Ultimate load factor	[-]
$P_{internal}$	Internal pressure of the wheels	[kg/m²]
$P_{mainlg_{landing}}$	Load on main landing gear during landing	[N]
$P_{mainlg_{TO}}$	Load on main landing gear during take-off	[N]
$P_{noselg_{landing}}$	Load on nose landing gear during landing	[N]
$P_{noselg_{TO}}$	Load on nose landing gear during take-off	[N]
q_s	Shear flow	[N/m]
q_{distr}	Distributed load	[N/m]
R_{kva}	System electrical rating	[kvA]
Re	Reynolds number	[-]
S	Surface area of the main wing	[m²]
S_c	Surface area of the canard	[m²]
S_e	Elevator area	[m²]
S_f	Wetted area of the fuselage	[m²]
S_v	Surface area of the vertical tail	[m²]
S_wheels	Width between the wheels	[m]
S_y	Vertical tail force	[N]
S_{csw}	Control surface area	[m²]
S_{cs}	Total area of control surfaces	[m²]
S_{e_c}	Elevator area of the canard	[m²]
$S_{effected}$	Surface area of the main wing affected by flaps or slats	[m²]
S_{HLD}/S	Ratio of area high lift devices by total wing area	[-]
S_{wet}	Wetted surface	[m²]
S_{wf}/S	High lift device surface area over total wing surface area	[-]
T	Temperature	[K]
t/c_{root_c}	Thickness over chord ratio at the root of the canard plane	[-]
t/c_{root_v}	Thickness over chord ratio at the root of the vertical tail plane	[-]
t/c_{root}	Thickness over chord ratio of the main wing at the root	[-]
T/W	Thrust loading	[-]
t_{skin}	Thickness of the fuselage skin	[m]
V_F	Fuel volume	[m³]
V_i	Integral tank volume	[m³]
V_p	Pressurized fuselage volume	[m³]
$V_s s$	Self-sealing 'protected' tanks volume	[m³]
V_t	Touch down speed	[m/s]
V_v	Vertical tail volume	[m³]
$V_{biofuel}/V_F$	Fraction of biofuel in the total fuel volume	[-]
V_{stall}	Stall air speed	[m/s]
$V_{x,y,z}$	Shear forces in x,y or z direction	[N]
w_f	Mean fuselage width	[m]
W_x	Weight of various components	[N]
w_{f_t}	Fuselage width at tail intersection	[m]
$w_{fuselage_c}$	Width of the fuselage at the canard intersection	[m]
$w_{nacelle}$	Width of the nacelle	[m]
x_{ac}/c	Longitudinal position of the aerodynamic center divided by the chord	[-]
$x_{cg_{aft}}$	Most aft center of gravity position possible	[m]
$x_{cg_{engine}}$	Center of gravity of the main engines	[m]
$x_{cg_{FG}}$	Center of gravity of the fuselage group	[m]
$x_{cg_{fwd}}$	Most forward center of gravity position possible	[m]
x_{cg_F}	Fuel center of gravity position	[m]
$x_{cg_{OEW}}$	Operational empty weight center of gravity position	[m]
$x_{cg_{WG}}$	Center of gravity of the wing group	[m]
$y_{cg_{engine}}$	Distance from fuselage centerline to engines in y-direction	[m]
z_{cg_E}	Engine center of gravity position in z-direction	[m]
$z_{cg_{landing}}$	Total aircraft center of gravity location at landing in z-direction	[m]
$z_{cg_{TO}}$	Total aircraft center of gravity location at take-off in z-direction	[m]

1

Introduction

Rather than starting anew, the current trend in the aviation industry is to redesign an existing aircraft to increase its efficiency. However, with the ongoing tightening of environmental sustainability requirements and demands for cost reduction, these designs are reaching their limit of improvement. An innovative aircraft is needed that can fulfill the future demands. This is what the project RELOAD aims to do: to develop a REliable LOw-cost Aircraft Design for narrow-body aircraft. Reference aircraft are the Airbus A320 and Boeing 737. The RELOAD mission statement is as follows: *"Design a narrow-body aircraft with a 30 % reduction in direct operating cost, compared to 2015 competitors such as the Boeing 737NG and the Airbus A320, for market introduction by 2030, with a group of 10 students in 11 weeks time."* By choosing radically new design concepts and technologies, the problem of lowering the direct operating cost and increasing the sustainability will be tackled in a manner allowing for a high amount of innovation to find its place in the final design. The outcome of this project will be a completely new aircraft design with a mission statement as follows: *"Perform at similar levels as current competitors, with at least a 30 % reduction in direct operating costs and a 20 % reduction in emissions, while at the same time maintaining equal development and production costs."*

This report is the fourth and last report that covers this project. It was preceded by the Project Plan, Baseline report and Midterm report. During the project several concepts and technologies were chosen and through a first conceptual sizing of these concepts a final design was selected. This design is further analyzed in this report. This covers wing sizing, strength analysis, fuselage layout and many more aspects that are considered. After coming up with a final design for the aircraft, future activities are being planned as well. Plans for production, ground operations and logistics are investigated in the last part of this report. Since many different names exist for the phases in an aircraft design process, RELOAD now defines the conventions used during the project. Figure 1.1 presents the top level flow of an aircraft lifespan. The lowest level presents the efforts of the RELOAD project.

To present the content as clear as possible, this report is divided into multiple parts. It first shortly recaps the Baseline and the Mid Term report in Part I. After this, Part II presents the engineering of the detailed design. It pursues the following structure: Chapter 5 discusses the aerodynamic design such as the airfoil selection and wing planform design. The structural analysis is investigated in Chapter 6. The engines are sized in Chapter 7. To see whether the aircraft remains stable, the stability and control is investigated in Chapter 8. Furthermore,the landing gear sizing and flight deck design are performed in Chapter 9 and 10. This part is concluded by the aircraft system design and noise assessment in Chapter 11 and 12. Part III states the design objectives such as maintenance, sustainability and cost analysis and elaborates how these are factored in the design. The last part, Part IV, summarizes the performance of the final aircraft. The report is concluded by Chapter 22. Some appendices are present to support the content.
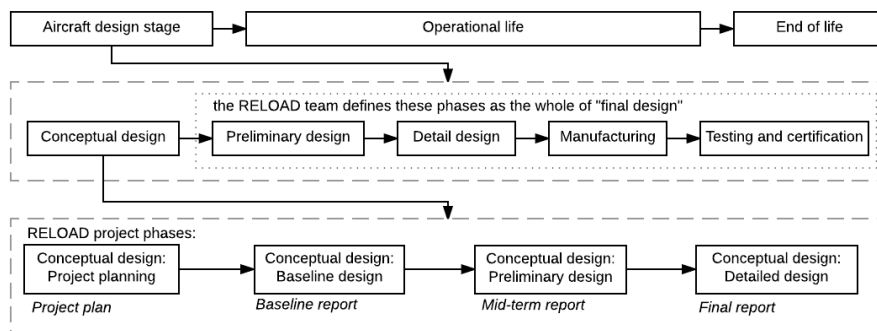
Figure 1.1: Aircraft life and the design stages needed to complete it

I

Baseline & Conceptual Design

To clarify the initial phases of the RELOAD project, a metaphor is proposed. The final product, the aircraft design, is placed inside a rigid box. The box represents the regulations, the needed functions, the nominal mission, and so on. It is rigid in the sense that its dimensions are fixed, comparable to the regulations that need to be met. The box itself forms the boundary to the outside world; the connection to environment. Outside the box, the environment, represents the market and the demand of the aircraft. To create an aircraft which is able to fit inside the box, it is necessary to work from the outside inwards; firstly investigating the environment, the market, the demand and so on. Then, the box itself, the regulations, the nominal mission, the functions etc. are defined. Finally, the product can be established, since the environment and the container are now also defined. Figure 1.2 shows the steps in which the initial project phase was split up; outside the box (the environment), the box itself (the constraints) and inside the box (the product).
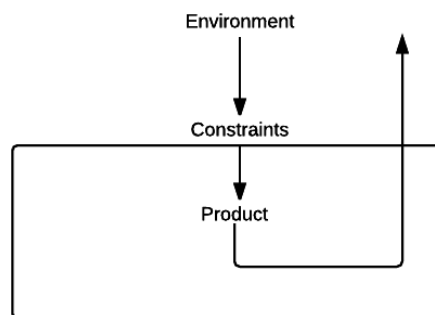
Figure 1.2: The stages in the initial project phase: outside the box, the box itself and inside the box

The first chapters of this part follow the same approach. Firstly, in Chapter 2, the market and cost analysis, the requirements and the mission are presented. Secondly, Chapter 3, presents the initial definition of the aircraft; the four baseline concepts.

After these chapters, one of the formed concepts has to be selected to design into great detail. To make this trade-off as fair as possible more information and hard numbers should be known about the concepts. The conceptual design was therefore done for all four concepts on which the trade-off could be based. To make sure that the same level of detail exists among all concepts a overall tool and Database was built. This makes sure that at all times, the most updated parameters are used in that any changes in a parameter will automatically indicate the influence in the whole design. This tool was later updated during the detailed design and will therefore be explained more elaborate in Part II.

The whole conceptual design phase were split up into several engineering tasks, such as wing, engine and fuselage design. But also sustainable development and the performance of the aircraft were considered in the Midterm report [1]. Afterwards, the results could be obtained and were used for the final design trade-off. All this can be read in Chapter 4.

<p style="text-align: right; font-size: 3em;">2</p>

Market, Mission and Requirements

Before the concept generation can be started, a mission and market analysis have to be conducted to make sure that RELOAD will meet market demands. Firstly, a recap of the market analysis and the required cost reduction is presented in Section 2.1. After that, the functions the aircraft has to perform are discussed in Section 2.2. Finally the requirements are determined in Section 2.3. All these sections are a recap of the Baseline report [2].

2.1 Market and Cost Analysis

A market analysis is a crucial first step in the aircraft design. It will not only define the airliners demands, but it also shows where the market will increase or decrease and where competitors are aiming for. With this information, a competitive design can be made and the needed cost reductions can be identified. For RELOAD, the market in 2030 with respect to now is investigated. This shows an increasing trend in aviation transport all over the world, especially Asia shows a rapid growth. Passengers want to fly further and preferably with a direct flight. Together with the increasing demand for narrow-body aircraft, the RELOAD aircraft is a good response to these demands.

To reach the 30 % direct operation cost reduction, a cost analysis is performed. This indicates the most expensive areas to be the fuel, crew and maintenance. Since the technology is not improving equally fast in all categories, different target values are set for each category. The new target values are shown in Figure 2.1.
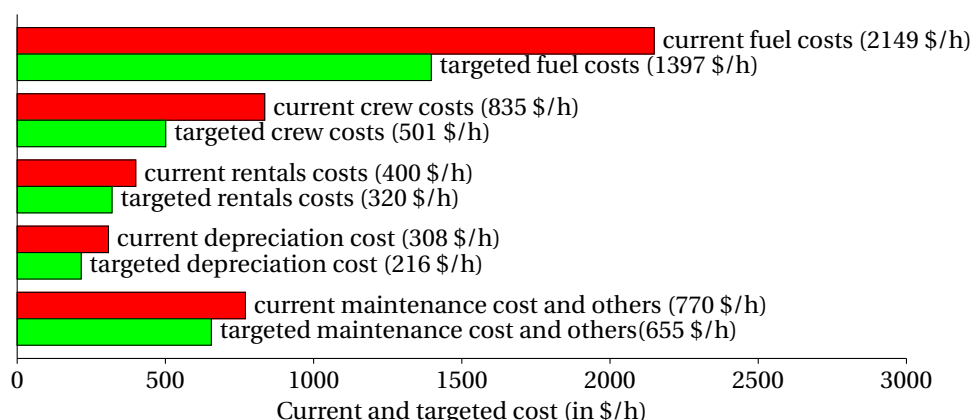
Figure 2.1: Average operating cost in $ per airborne hour for the 737-800, 737-900 and A320 from October 2014 to September 2015 [3] (red), compared to the RELOAD target values [2] (green)

2.2 Aircraft Mission and Functions

The market demands in Section 2.1 must be converted into a nominal mission with actual functions. Therefore, a nominal mission was selected and a functional breakdown was performed on the aircraft's functions.

The range of the RELOAD aircraft is 6500 [km], but next to that it also has to taxi, take-off, climb, descend and land. For safety reasons the aircraft has an extra loiter and second cruise phase so that a different airport can be reached if the aircraft has to divert. This mission profile is indicated in Figure 2.2.

<p style="text-align: center;">3</p>
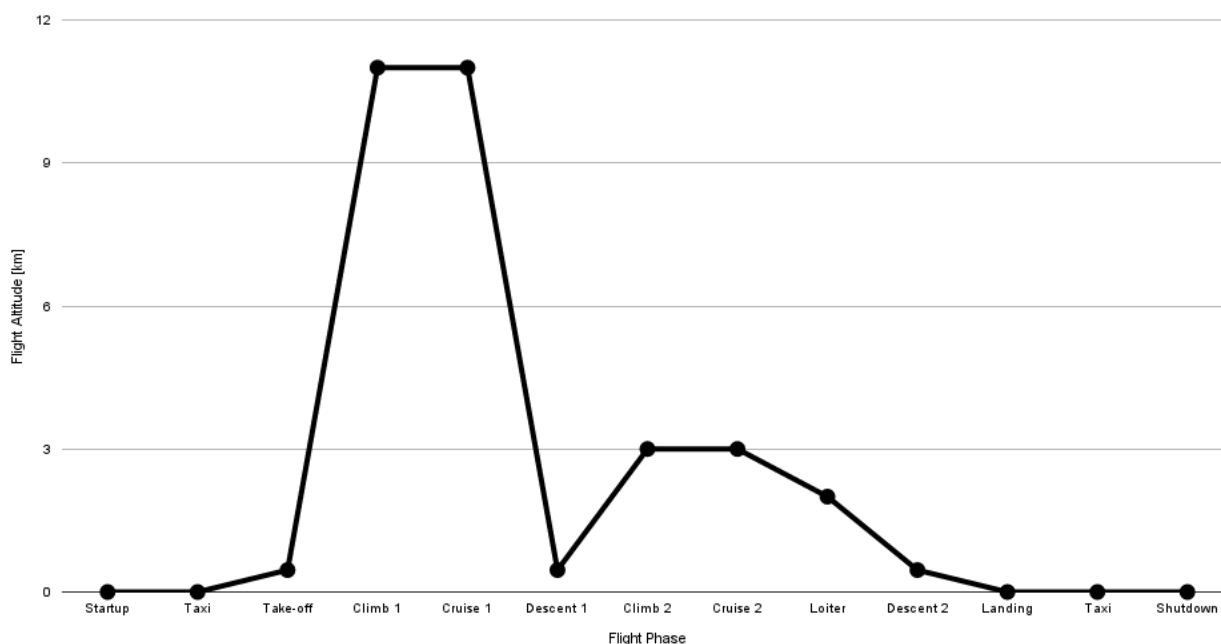
Figure 2.2: Mission profile of the RELOAD aircraft

This mission is split up into four phases; pre-flight, flight, post-flight and abnormal functions. Each of these phases is again subdivided into other subgroups, with the goal of capturing all possible functions. The biggest groups of functions in the pre-flight section are the inspection functions, the loading and the start. The flight group features mainly the flight phases, with their corresponding functions (take-off, climb, cruise, and so on). The post-flight contains parking, shut-down, unloading and maintenance as main groups. As a final example, the abnormal functions group features the following subgroups and functions: enable emergency control, generate emergency power, etc. The definition of all functions is performed by generating a functional flow diagram, which shows in what order all functions are performed. Secondly, the functional breakdown structure provides another view on the functions, grouping them together. Both documents are used in the following design stages; creating the final requirements definition and generating the design options. After the subsystem design, this functional flow diagram is remade into a more detailed level that shows the functions per subsystem.

2.3 Requirements Analysis

This section shortly recaps the requirements identified in [2]. Chapter 20.6 looks back on these requirements and validates the final design by checking whether all the requirements are met.

CS-25 [4] is not the only source of requirements. There are also requirements originating from a development perspective, the product performance and the stakeholder. These requirements are subdivided into four levels; top-level, medium-level, low-level and stakeholder requirements. All the requirements can be seen in Figure 2.3.
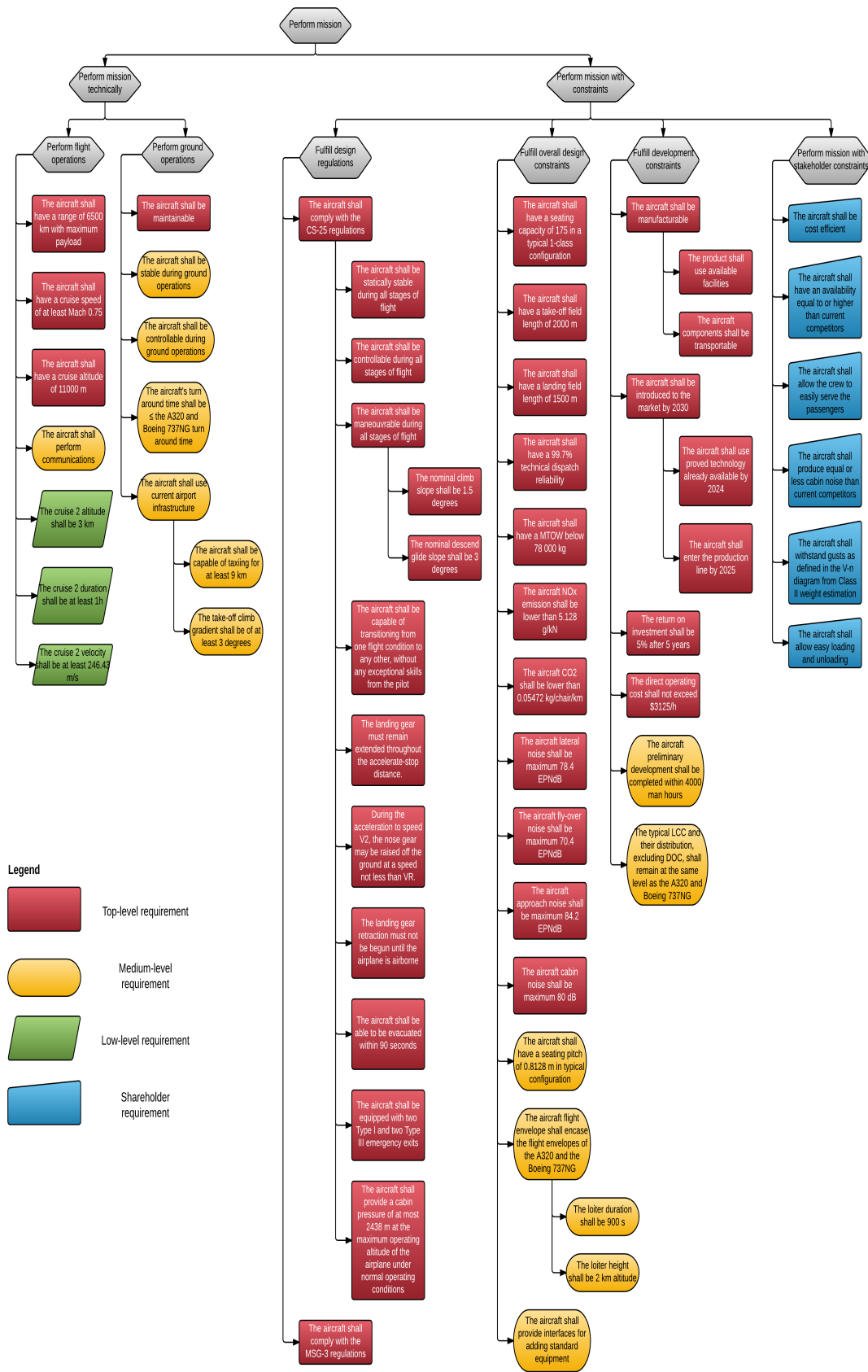
Figure 2.3: The requirements discovery tree [2]

3

Concept Generation

The generating of all possible design options is performed by a large brainstorming session. An initial structure for the design option tree is set up by dividing it in 7 main categories; lift & drag, payload hosting, navigation & communication, structural integrity, safety, stability & control and propulsion. For each category, as much options and new technologies are found as possible. A feasibility study is then executed to eliminate several options. On the remainder options a trade-off is performed, of which the result is listed below. This is further reduced once the final concept is chosen in Chapter 4.2.

- **Wing type:** cantilever, braced, blended wing body
- **Wing tip device options:** vortex turbine, split/dual feather winglet, spiroid
- **Flap options:** plain, morphing, zap
- **Airfoil options:** conventional airfoil series, adaptive airfoils
- **Cross-section options:** single floor/cylindrical, oval
- **Energy source option:** kerosene, hybrid
- **Engine type options:** open rotor, geared turbofan, LEAP engine, CLEEN/NEWAC engine
- **Engine configuration options:** wing podded below, boundary layer ingestion
- **Tail options**: canard, twin, winglets as vertical tail

After completing the trade-off between all design options present in the design option tree, the final concepts are selected.

1. The first concept is a conventional, low-risk design. It is very similar to current narrow-body, single aisle aircraft, with small improvements aiming to meet the requirements. It has a geared turbofan engine, winglets and morphing flaps and slats. This concept is rather straightforward, so the morphing slats and flaps are added to make it technically more interesting.

2. The second concept is a blended wing body (BWB). It features split winglets, a twin tail and zap flaps. To reduce the emissions, biofuel is used and since the engines are mounted on the roof at the rear, a twin tail is designed. This also helps to shield the engine noise.

3. The third concept has three lifting surfaces, a canard, a main cantilever wing and a T-tail. It is equipped with spiroid winglets, morphing flaps & slats and a boundary layer ingestion turbofan engine. A three lifting surface aircraft is chosen since high lift over drag ratios can be reached with this configuration [2]. The spiroids, morphing high lift devices and boundary layer ingestion engine increase the efficiency even more.

4. The fourth concept is the braced wing concept. This extra wing strut allows for high wing aspect ratios, which increases the efficiency. Furthermore the geared turbofan engines use biofuel and make use of boundary layer ingestion. Finally, plain flaps and Krueger slats are installed.

4

Concept Design & Trade-off

After analysis of the project, market and costs related to a narrow-body aircraft design, concepts are generated. This chapter discusses the preliminary design of each concept in Section 4.1. Section 4.2 elaborates on the final concept selection method and choice.

4.1 Concepts Design

From the four concepts chosen in the Baseline report [2] only one can be analyzed into detail and developed. The Midterm report discussed the conceptual design of the four concepts [1]. This design is shortly recapped in this section, starting with the wing and tail planform sizing in Subsection 4.1.1. Afterwards, Subsection 4.1.2 and Subsection 4.1.3 discuss the engine and fuselage design respectively. The landing gear design is explained in Subsection 4.1.4. Finally, Subsection 4.1.5 discusses the performance analysis.

4.1.1 Wing and Tail Planform Sizing

To provide an estimate on the surface area needed to generate enough lift for the aircraft, a thrust and a wing loading diagram is created during the Midterm [1]. These diagrams take into account the requirements related to take-off, landing and cruise and plot several thrust loading lines which constrain the design space. After varying the aspect ratio and lift coefficients a design point is chosen. For concept 1, 3 and 4 the same design point is chosen, having a thrust loading of 0.36 and a wing loading of 5980 [N/m^2]. Concept 2, the BWB, deviated from this comparable layout, such that a thrust loading of 0.26 and a wing loading of 3410 [N/m^2] were chosen. The plots and a more extensive list of values is found in [1]. The wing loading and chosen aspect ratio is used to calculate the trapezoidal wing planform, where a taper ratio of 0.3 is assumed for all concepts.

To ensure stability and controlability, the tail and canard sizing are investigated. This heavily depends on the position of the wing and the center of gravity variation due to loading and unloading the aircraft. Firstly, the needed center of gravity range due to cargo, passenger and fuel loading is estimated by means of a so-called potato diagram. Secondly, the allowed center of gravity range is plotted by means of a scissor plot. Combining these two, a tail surface value and wing location are found at the intersection point. The plots for all four concepts and the first estimates is found in [1].

4.1.2 Engine Design

Three different engines are considered for the concepts; an open rotor, (geared) turbofan engines and electrical engines. To find the the height, length and weight of the first two engines, they are modelled as a cylinder and the rubber sizing method is applied. This same method is applied to the electrical engines, but the nacelles themselves are neglected.

After the size is known, the location of the engines on each concept is considered. The engines of the Conventional aircraft are placed under the wing at the lateral position of the MAC. The Blended Wing Body in the concept stage has open rotors placed on top of the fuselage in order to shield the noise. As the turbofans in the Three Lifting Surface aircraft are using Boundary Layer Ingestion, they are placed at the very end of the fuselage, with their center line aligned with the center line of the fuselage. The electrical engines are placed at the leading edge of the wing, with the

inboard engines at the position of the MAC and the outboard engines 1 [m] next to it. The last concept, the Braced Wing, has two turbofans placed at the same position as the Conventional aircraft.

To see whether the requirements for fuel, noise and emissions is met with these engines, the CFM56-7B24 and LEAP engine is used as reference. As a preliminary check for the performance of each concept, the data from the CFM56 and the LEAP engines are extrapolated to 2025. This way, it is estimated that the requirements for the emissions are met. However, when it comes to noise, only the approach noise and lateral noise requirements are likely to be met. Extra effort is needed for the fly-over noise during the detailed design phase. The fuel cost reduction can only be met with the open rotor according to the preliminary analysis, but wing tips and further design of the geared turbofan might also make it compliant.

4.1.3   Fuselage Design

The layout of the fuselage strives the dimensions of the fuselage. For the conventional fuselage a single aisle is chosen. Since 175 passengers cannot be evenly divided, two extra seats are implemented. The cross-section of this fuselage is chosen to be circular, as this is easier to manufacture and is more structural efficient under pressure loads. The blended wing body cross-section is changed from oval to elliptical in order to make use of the extra room in the wing. For this concept, the capacity is also 177 passengers. Both fuselages are sized such that the cargo compartment can load a unit load device type ULD-3. Also, four type I and type III exits are needed according to the safety regulations. During the detail design phase this is adapted, thus the final layout is seen in Figure A.1. All dimensions of the fuselage, its cross-section and the nose and tail cone is found in the Mid Term Report [1].

4.1.4   Landing Gear and System Design

To design the landing gear, first the type of configuration is selected. The tricycle landing gear is picked because this configuration offers better stability when landing, a leveled cockpit and cabin on the ground and prevents the aircraft from tipping over. Afterwards, the dual wheel configuration is designed for both the main and nose gear [1]. The preliminary and detail design of the fuel and electrical system is found in Chapter 11.

4.1.5   Performance Analysis

Designing for flight performance is a continuous task throughout each design phase. The first parameter that is considered is the MTOW. This is initially calculated using a Class I estimation, but then is refined in the Midterm report [1]. Also, by calculating the moment of each component in respect to the nose, and dividing it by the total OEW, the center of gravity of the aircraft is determined.

Next to that, the climb gradient for each concept is considered. This is highly dependent on the thrust required and is calculated using Raymer [5], which describes the equations for steady sea level climb. All results isar seen in Table 4.1.

The final performance parameter that is considered is range. This is done by means of a payload-range diagram which shows the increase in range with payload and fuel loading. The BWB shows the best performance on this [1].

Table 4.1: Operational Empty Weight and maximum steady climb performance for all concepts

Aircraft type	OEW [kg]	Center of gravity [m]	Rate of Climb [m/s]	Climb Gradient [rad]
Conventional	58651	20.14	47.601	0.299
BWB	55114	19.34	29.553	0.209
Three Lifting Surfaces	53020	21.46	47.155	0.300
Braced Wing	57599	20.16	48.137	0.308

4.1.6   Operations and Maintenance Considerations

Ground operations partially influences the operating costs and the turnaround time of the aircraft. To reduce this time and these costs, a work flow diagram is made to show the main steps during ground operations and each concept is evaluated in operating efficiency. The Conventional aircraft and Braced Wing are considered to be the most favourable for ground operations due to their conventional layout. Some more difficulty will likely arise for the Three Lifting Surfaces due to its amount of engines and lifting surfaces. These will obstruct the gate and passengers bridge. The least efficient is the BWB due to its revolutionary shape and large wing surface.

The ease of maintenance has to be compared between concepts, since maintenance is one of the main sources of the direct operating cost. When looking at engine maintenance specifically, the BWB and the Braced Wing are again the most difficult ones since the engines are placed relatively high. Also, the control surfaces of the Braced Wing are quite difficult to maintain.

4.2 Concept Trade-off and Selection

Finally, a concept can be selected. Weights and criteria are defined, so that by means of a trade-off table a unprejudiced decision can be made. This trade-off method is defined in Subsection 4.2.1 and the final decision is made in Subsection 4.2.2.

4.2.1 Trade-off Method

For the trade-off of the concepts, seven different criteria were defined and given a weight from 1 to 5 based on their importance. These weights were decided on influence and reliability of the values of the factors. The scores are given in a range from 0 to 10. For quantitative factors the best value for a criteria is given a 10 and the other concepts' scores are scaled down to that value to show the relative performance. The resulting final trade-off table can be seen in Table 4.2. Next to that, a decision still has to be made on some subsystems. On most components such as the tail and winglets a trade-off was already performed in the Baseline report [2]. However, a decision on the engines and HLD still has to be made. A range from 1 to 5 is given for these trade-offs based on the importance of their criteria [1].

Furthermore, a sensitivity analysis is performed to show the importance of the trade-off parameters and results when deciding between the concepts. It is found that for some different ranges of the criteria the Braced Wing would perform better, but after careful consideration it is decided not to alter the criteria. This is explained in more detail in the Midterm report [1].

Table 4.2: Concept trade-off

Paramater	Weight	Conventional		BWB		Three Lifting Surfaces		Braced Wing	
		value	score	value	score	value	score	value	score
$\frac{W_5}{W_4}$	5	0.88	9.80	0.90	10.00	0.88	9.83	0.89	9.99
MTOW [kg]	4	58651	9.04	55114	9.62	53020	10.00	57599	9.20
$\frac{L}{D}_{cruise}$	5	17.3	8.48	20.5	10.00	17.7	8.67	20.2	9.87
C_{D_i}	2	0.024	4.47	0.011	10.00	0.023	4.78	0.020	5.49
Ease of maintenance	1	n/a	7.00	n/a	4.00	n/a	5.00	n/a	6.00
Ease of development	1	n/a	5.00	n/a	4.00	n/a	3.00	n/a	6.00
Ease of operations	1	n/a	7.00	n/a	4.00	n/a	5.00	n/a	7.00
Total			155.52		**170.48**		155.06		166.09

4.2.2 Final Concept

According to Table 4.2, the BWB has the best overall performance and will therefore be selected for the further design stages. This design will be worked out together with morphing HLD, a geared turbofan and the application of Boundary Layer Ingestion. Another note should be made on the wing design. Due to the placement of emergency exits it is decided to only blend the last part of the fuselage into the wing, such that the door could still be placed upfront. For stability reasons, also a canard is applied.

An overview of the design point of the final concept is given in Table 4.3.

Table 4.3: Design point final concept

	A [-]	e [-]	Wing Loading [N/m^2]	Thrust Loading [-]	$C_{max_{TO}}$	C_{max_L}
Concept 2	7	0.95	3410	0.26	1.6	1.6

II

Detail Design

In the conceptual design phase the trade-off has been performed and the most viable options have been chosen carefully. The final design was sketched but now it is time to take that sketch and turn it into a technical drawing. Therefore, a detail design will be performed taking into account all the components that have emerged as winners from the conceptual trade-off.

The engineering process can be divided into several steps: firstly, different design departments are established. Secondly, all possible interactions between the departments are collected. Important design parameters that are used by different departments are also specified and normalized. Thirdly, the actual design process starts and the departments develop and execute design methods. As soon as an important design parameter changes this is communicated to other departments as specified during the previous step. In this way possible problems can be detected precociously and every department uses the same dataset. Fourthly the design is iterated partly in order to attain convergent and balanced results. At the same time different design aspects, as specified in Part III, are monitored. Finally, the design is synthesized and validated as described in Part IV. The complete process is also illustrated in Figure 4.1. This part of the report discusses the first three steps.
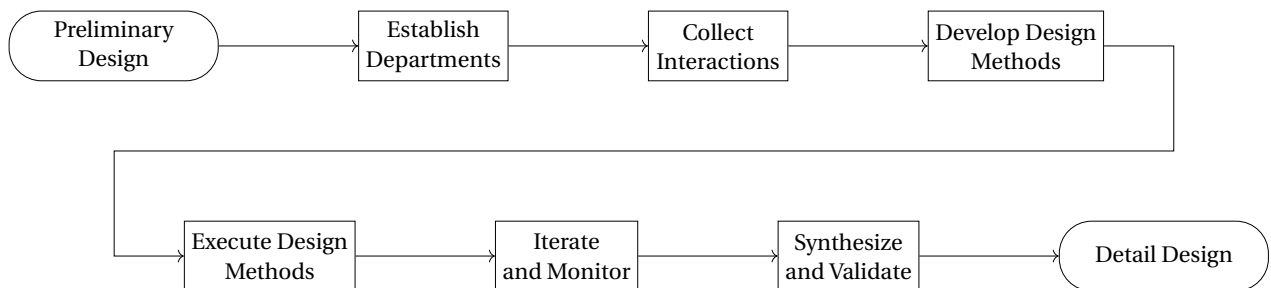
Figure 4.1: Abstraction of the engineering process

Five different departments are created: aerodynamics, structures, propulsion, stability & control and aircraft systems. Each department starts by writing or using software tools that aid them in conceiving an optimal design.

In Chapter 5, the aerodynamics concerning the aircraft are discussed. The airfoil selection process is described and factors such as drag and lift will be further analyzed while keeping in mind the interaction of the wing with other components such as fuselage or the engines. In Chapter 6 the forces, moments, torques and stresses acting on the fuselage and wing at different flight phases are presented and discussed upon. Next, in Chapter 7, the powerplant is designed and the emissions resulting from it are analyzed. Chapter 8 makes sure that the vertical stabilizers and the canard are correctly sized in such a way that the aircraft is stable and controllable at any point during the flight. Taking into account the ground clearance in respect to the tailcone and the wings the landing gear is sized in Chapter 9. Following this, the cockpit design is presented in Chapter 10, while the aircraft systems are elaborated on in Chapter 11. Finally, Chapter 12 tackles the noise reductions provided by the exterior layout of the RELOAD aircraft.

5

Aerodynamic Design

The aerodynamic design of an aircraft influences its configuration and performance substantially. The airfoil sections used along the wing determine the general shape of the overall lift and drag polars. Therefore the very first section of this chapter (Section 5.1) describes the airfoil selection process. Afterwards the detailed wing geometry and additional wing features are determined in Section 5.2. Important aircraft characteristics, such as the maximum lift coefficient, are also presented in this section. Section 5.3 discusses the aerodynamic fuselage design. A detailed drag estimation is illustrated in Section 5.4 based on the results form the preceding sections. This drag estimation serves as main input for the propulsion system design which is considered in one of the following chapters. Verification and validation of the aerodynamic design are explained in Section 5.5. This chapter is then concluded by recommendations for further design activities in Section 5.6. In this chapter cruise conditions and landing/take-off conditions are defined by the properties listed in Table 5.1.

Table 5.1: Aerodynamic properties during different flight phases

Flight Phase	h [m]	M	v_{cruise} [m^2/s]	ρ [kg/m^2]	T [K]
Cruise	11000	0.75	$1.43 \cdot 10^{-5}$	0.364	216.65
Landing/Take-off	0	0.16	$1.51 \cdot 10^{-5}$	1.225	293.15

5.1 Wing Airfoils

This section describes one of the most important design steps during the development of an aircraft, namely the selection of suitable airfoil sections. Firstly, the method is explained in Subsection 5.1.1. Secondly, the results from the detailed analysis of over 1000 airfoils are presented in Subsection 5.1.2. Please note that this section only covers the airfoil selection for the main wing. The airfoils for the canard and horizontal tail are chosen during the design for stability and controllability, see Chapter 8.

5.1.1 Selection Methodology

It is assumed that the majority of fuel is burned during cruise. In order to minimize operating costs the wing should exhibit optimal aerodynamic properties during this flight phase. Therefore the objective of the applied airfoil selection process is straightforward: finding an airfoil that displays a minimal drag coefficient while operating at the desired cruise lift coefficient.

The developed and applied selection process is iterative and consists of several steps. Firstly, the three dimensional cruise lift coefficient, $C_{L_{cruise}}$, is determined based on the preceding preliminary analysis. Secondly, this lift coefficient is reduced to the two dimensional airfoil cruise lift coefficient, $C_{l_{cruise}}$, using standard formulae from literature [6]. Amongst others these formulae include factors to model finite wingspan and dihedral. Furthermore, an optimal wing sweep angle is determined for every airfoil section based on its critical Mach number, thus based on its minimum pressure coefficient following the method outlined in [7]. Thirdly, the atmospheric properties (e.g. M_{cruise}, Re_{cruise}, v_{cruise}) are calculated as "seen" by the airfoil sections, i.e. taking the sweep into account. For the Reynolds number, Re_{cruise}, the mean aerodynamic chord is taken as a reference length. A more detailed analysis also shows that the influence of the Reynolds number reference length on the lift and drag coefficient is quasi-negligible during cruise conditions. Fourthly, a set of airfoils is analyzed with the TSFOIL [8] panel code and the airfoil drag

coefficient ,$C_{d_{cruise}}$, at the given lift coefficient, $C_{l_{cruise}}$, is determined using all previously calculated values as inputs. TSFOIL is capable of modelling compressibility and shock waves rather accurately [8] (in contrast to XFoil [9] or Javafoil [10]). During the final iterations TSFOIL is replaced by SU2_EDU [11] for increased precision. SU2_EDU is set up to calculate the lift curve based on solving Navier-Stokes equations with the shear stress transport (SST) turbulence model using the Roe solver. Subsequently, poorly performing airfoils can be removed from the selection and another iteration (with a higher accuracy setting for TSFOIL or SU2_EDU) can be performed.

5.1.2   Selection Results

Several databases with a large amount of airfoil sections are publicly available[1,2]. Manually unqualified airfoil sets, e.g. sailplane airfoils or model aircraft airfoils, are eliminated. After manual elimination, about 1000 airfoils are initially considered. A tool is developed in order to execute the iterations efficiently. The process usually converges quickly as some airfoil cannot provide the lift coefficient required and others just feature too high drag coefficients.

Subsequently, the best airfoils are examined individually. Several other aspects are considered next to the aerodynamic performance. For example very thin airfoils can not be used over the whole wingspan as this would lead to an unacceptable increase in wing box weight, see Section 6.4. Moreover, in order to straighten the isobares over the wing surface, the airfoil sections at the wing root are required to have a maximum camber location which is closer to the leading edge than the maximum camber location of airfoil sections close to the tip [7].

Eventually two different airfoil sections are selected. The "Whitcomb Integral Supercritical" airfoil is selected for the outboard wing sections until half of the semi-span whereas the "Grumman K-3 Transonic" airfoil is most suitable for the inboard wing sections. As the maximum thickness of the two selected airfoils differs by about 6 % the wing section from the half of the semi-span until the quarter semi-span features a gradual transition. This division is also illustrated in Figure 5.3.

The chosen airfoils shapes can be seen in Figure 5.1. The coefficient curves are shown in Figure 5.2.
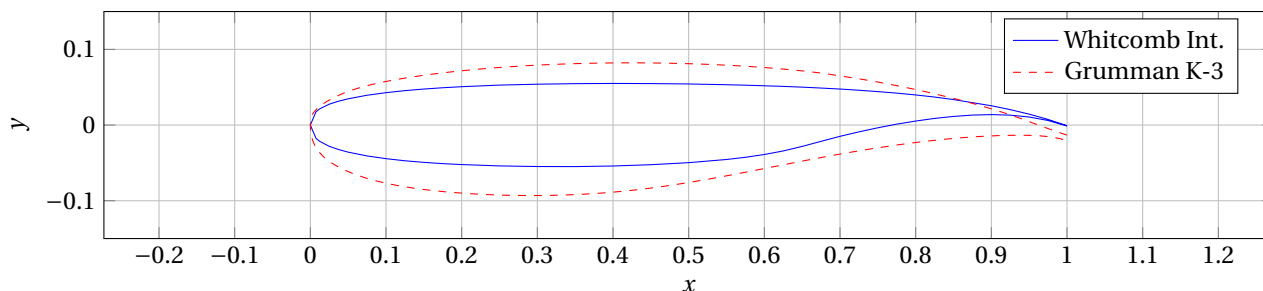
Figure 5.1: Selected airfoils

(a) C_l-α

(b) C_d-C_l
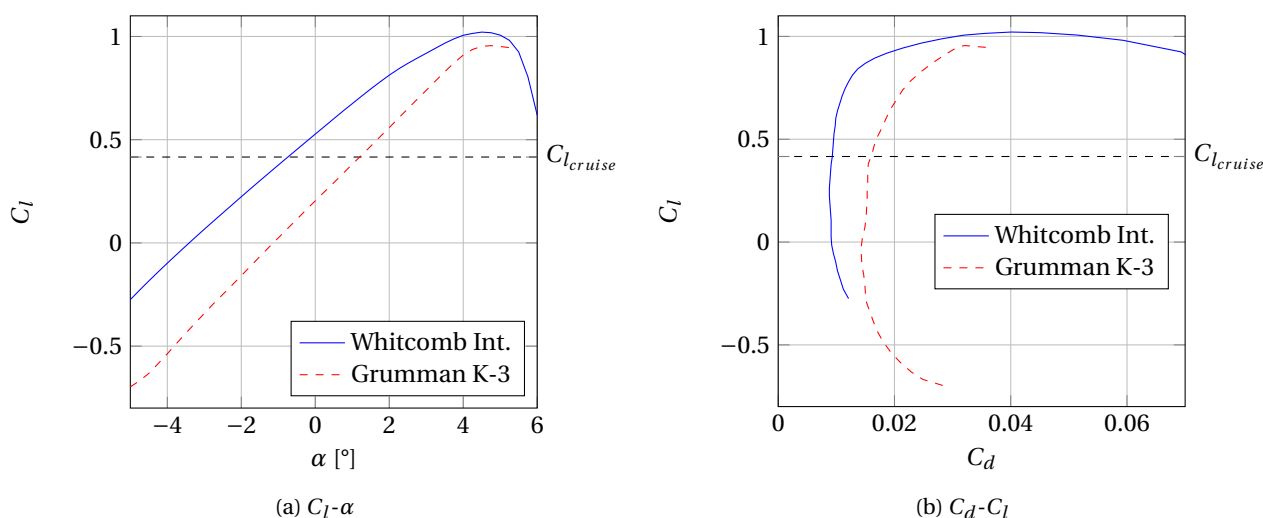
Figure 5.2: Characteristic coefficient plots of the selected airfoils at cruise altitude conditions

---

[1] URL http://m-selig.ae.illinois.edu/ads/coord_database.html [Cited on 14 June 2016]
[2] URL http://airfoiltools.com/index [Cited on 14 June 2016]

5.2 Wing Layout

This section covers the overall wing layout. Firstly, the planform is described in Subsection 5.2.1. Subsequently, more details about incidence, twist and dihedral angles are determined in Subsections 5.2.2 to 5.2.4. Then the sizing of wing tip and high lift devices is explained in Subsections 5.2.5 and 5.2.6 and furthermore the aerodynamic performance estimates are presented.

5.2.1 Planform

A basic trapezoidal reference wing planform was already developed during the previous design phase. An updated sweep angle follows directly from the airfoil selection, see Section 5.1. As two different airfoil sections are selected also two different sweep angles are to be considered. In order to minimize weight sweep angles should never be oversized and wing planforms should not feature too large kinks, compared with Section 6.4. Since the sweep angles for the two selected airfoils differ significantly it is decided to apply the largest sweep angle to the complete wing planform. The updated trapezoidal wing planform parameters are summarized in Table 5.2.

Table 5.2: Trapezoidal wing planform parameters

A	b [m]	c_{root} [m]	c_{tip} [m]	MAC [m]	S [m^2]	λ	Λ_{LE} [°]
7	33.34	7.32	2.20	5.22	158.63	0.3	25.50

Several three dimensional flow effects are influencing the wing performance. Mainly the root and the tip sections need to be reconsidered carefully. Due to the wing-fuselage interaction and wingtip effects, the isobars near the root and tip are bending. Although it is more efficient to have straight isobars [7]. The isobars at the root can be straightened by increasing the local sweep angle. This increase of sweep at the root necessitates a small positive kink in the wing planform. It is assumed that the critical Mach number near the root scales with the factor $\frac{1}{\sqrt{cos(\Lambda)}}$ instead of $\frac{1}{cos(\Lambda)}$ [7]. This implies that the wing sweep angle for the first 30 % of the half wing span can be recalculated. The recalculated local sweep angle equals 35.40 [°]. Additionally the root chord c_r changes to 8.5 [m]. At the tips the flow shows a similar effect. However the RELOAD wing is not featuring an updated local tip sweep angle but winglets. The sizing of the winglets is extensively described in Section 5.2.5.

A sketch of the final wing planform can be seen in Figure 5.3.
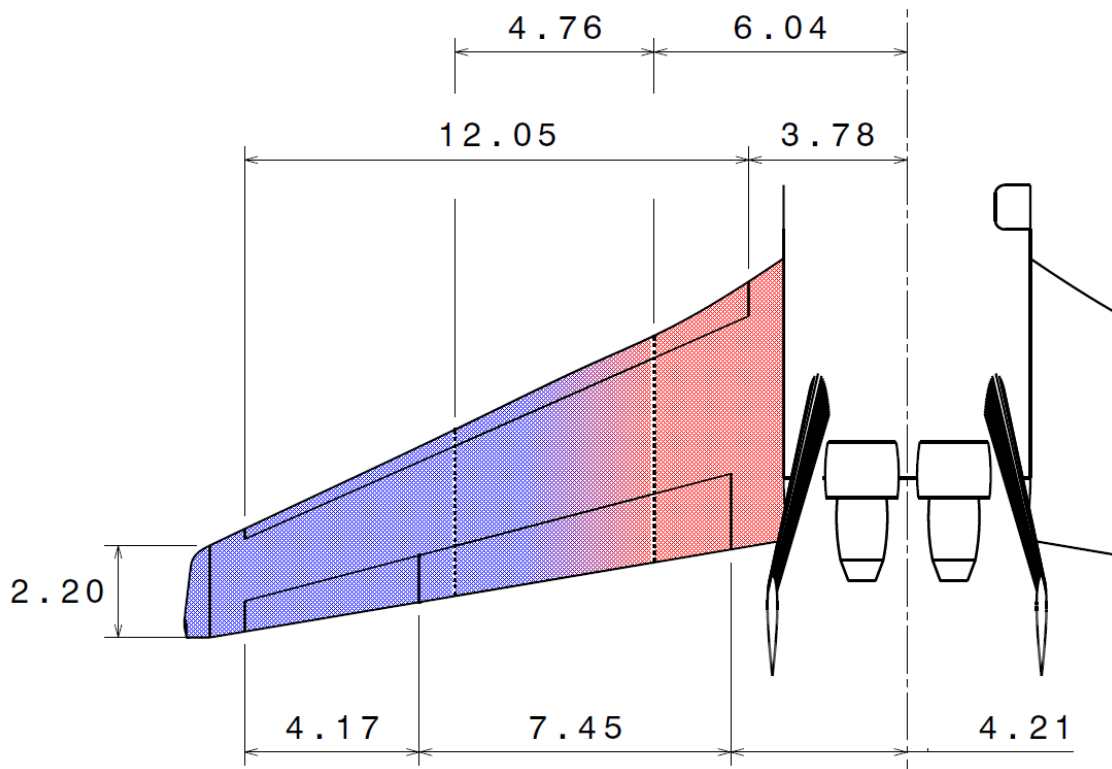
Figure 5.3: Wing planform sketch (dimensions are in [m], blue sections feature the Whitcomb Int. airfoil and red sections the Grumman K3 airfoil)

5.2.2   Incidence Angle

This subsection discusses the wing incidence angle, i.e. the angle of the wing with respect to the fuselage. For the RELOAD aircraft this angle is mainly affected by cruise drag considerations and by the floor attitude during cruising flight. A too large or a too small incidence angle generally implies additional drag because the aircraft needs to fly nose down or nose up respectively. Moreover, the incidence angle influences the floor attitude. If the cruise attitude differs too much from the horizontal, people struggle to walk onboard. Furthermore pushing beverage service carts through the cabin might be a problem [12].

Hence it is preferred that the RELOAD aircraft flies with level fuselage/floor in order to minimize drag and in order to allow passengers and cabin crew walking easily through the cabin. As discussed in Section 5.1 two airfoils have been chosen to ensure that minimum drag is achieved at the design lift coefficient. The angle of attack at the design lift coefficient for the inboard airfoil section is chosen as incidence angle for the wing. In this way the floor attitude is parallel to the horizontal during cruise and the drag of the inboard airfoil sections is minimized. The incidence angle equals 0.56 [°].

5.2.3   Twist Angle

The wing twist angle primarily affects wing tip stall, induced drag and weight. Positive twist decreases the incidence angle of the outboard direction. This delays the tip stall and is undesirable because it occurs in an asymmetrical manner causing roll control problems, see also Chapter 8. It also increases the induced drag. Furthermore, the aerodynamic loading at the tip is decreased which shifts the center of pressure inboard. This might lower the wing weight [12].

The angle of attack at $C_{L_{cruise}}$ for the outboard airfoil equals -1 [°]. To achieve minimum drag the angle of attack for this airfoil during cruise should be -1 [°]. This means a twist of -1.56 [°] is applied at the airfoil transition section.

It is more challenging to optimize the twist angle for the outboard wing section. According to literature [7, 13], the twist angle usually is in the range of 0 to -5 [°]. Furthermore the methods from Culver[3] and Panknin[4] are investigated. The twist for the RELOAD wing is determined using both methods, however both methods yield unrealistic results. The Culver method returns a positive twist angle while a negative one is preferred. Applying the Panknin method results in a too large twist of -7.7 [°]. In this case the wingtip generates negative lift which is not beneficial for the efficiency of the aircraft. The unrealistic outputs probably result from the differences between the two selected airfoils. Ultimately, a twist angle of -3 [°] is chosen for the outboard wing section, which is an average value advised from literature [7, 13] in order to prevent wingtip stall.

Hence the RELOAD wing exhibits two twist angles, the first one at the transition of the two airfoil sections (-1.56 [°]) and the second one at the outboard wing section (-3 [°]). This is illustrated in Figure 5.4.
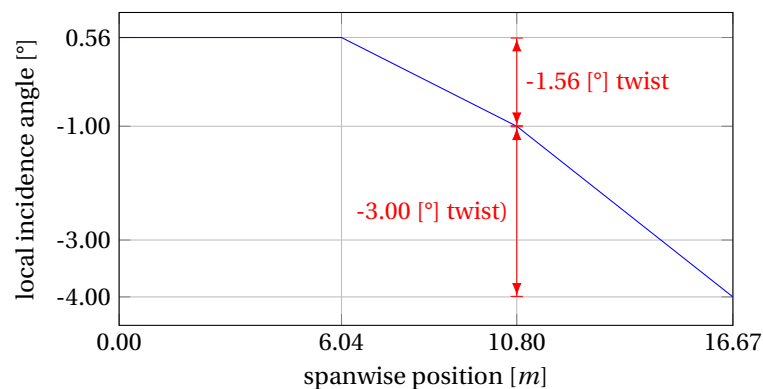
Figure 5.4: Local incidence angle distribution

5.2.4   Dihedral Angle

The choice of the wing dihedral angle influences the spiral stability, dutch roll stability and the ground clearance as described in Chapter 8. A positive wing dihedral causes the rolling moment due to sideslip derivative C_{L_β} to be negative. This derivative influences both the spiral and dutch roll stability. A more negative C_{L_β} results in a more stable spiral stability while it makes the dutch roll stability less stable. According to literature low-wing aircraft with

---

[3]URL http://www.b2streamlines.com/Culver.html [Cited on 8 June 2016]
[4]URL http://www.b2streamlines.com/Panknin.html [Cited on 8 June 2016]

straight wings generally have a dihedral of 5 to 7 [°] [14]. When looking at reference aircraft, see Table 5.3, one can conclude that for these aircraft the dihedral is indeed between 5 and 6 [°].

Table 5.3: Dihedral angles of reference aircraft in [°] [5]

A319	A320	A321	737-700	737-800
6.00	5.11	5.11	6.00	6.00

As can be seen in Figure 5.5, the ground clearance for the wing should be at least 5.00 [°] [15]. To obtain this ground clearance a dihedral angle of minimal -1.56 [°] is needed. Following from the stability derivatives, an optimum value for the dihedral angle of -1.00 [°] is found. In Chapter 8 a more elaborate explanation of the dihedral angle with respect to the stability derivatives is present.

Hence the final dihedral angle for the RELOAD aircraft is set to -1.00 [°]. Actually this implies that the RELOAD wing features anheadral. The significant difference from the reference aircraft in Table 5.3 originates from the unusual configuration of the RELOAD aircraft. The lateral ground clearance criterion is not constraining as the engines are not attached to the wing and thus an optimal dihedral angle for stability can be selected.
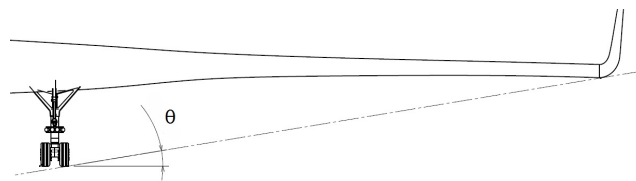
Figure 5.5: Lateral ground clearance criteria adapted from [15]

5.2.5   Tip Devices

Wing tips can improve the performance of the wing significantly. Normally the air under the wing escapes and rotates around the wing tips, resulting in vortex drag. Wing tip devices are intended to counter the before mentioned effects. If the wing tip device is properly designed it even increases the lift coefficient by a small amount. Several wing tip devices have already been investigated during the previous design phase. A trade-off has shown that split winglets suit the needs of RELOAD best [2].

Yet split winglets are not used too often. Boeing currently offers a split winglet option for the 737-700 and 737-800. The company claims[6] that 2.3 % fuel savings can be obtained at a range of 6500 [km], using split winglets instead of blended winglets. Blended winglets provide 3.5-4.0 % fuel savings compared to conventional wings[7]. Together this implies that the use of split winglets on the RELOAD aircraft can lead to an almost 6 % fuel reduction.

However the sizing of winglets appears to be complicated. Neither Boeing nor Airbus publish detailed winglet data. Especially scientific data about split winglets on large aircraft is not publicly accessible. Therefore the RELOAD winglet is developed using estimated reference values along with the numerical wing sizing tool XFLR5 [16]. Since split winglets can not be modelled accurately with XFLR5 a blended winglet is developed and splitting it becomes a recommendation.

For some aircraft the winglet height and the wing span can be found. From Table 5.4 it is concluded that the average blended winglet height is approximately equivalent to 6.5 to 7.5 % of the wingspan length. Using Whitcomb's winglet sizing method, a first estimation of the other winglet parameters is made [17].

Aircraft	Winglet type	Wing span [m]	Winglet height [m]	Relative winglet height (% of wing span)
737-700	Split	34.3	3.5	10
A320-200	Blended	35.8	2.43	6.8
757-200	Blended	38.1	2.5	6.5
767-300ER	Blended	47.6	3.4	7.1
737-300	Blended	28.9	2.1	7.3

Table 5.4: Reference aircraft winglet height[8,9]

---

[5]URL https://www.haw-hamburg.de/ti-ff [Cited on 6 June 2016]

[6]URL http://www.aviationpartnersboeing.com/products_737_700SSW.php [Cited on 7 June 2016]

[7]URL http://blogs.wsj.com/corporate-intelligence/2014/02/18/uniteds-new-plan-for-saving-fuel-more-wings/ [Cited on 7 June 2016]

Based on the initial estimation a winglet model is created in XFLR5 and analyzed with the vortex lattice method. The analysis is done assuming take-off/landing conditions, as it is not possible to model transsonic cruise conditions with XFLR5, see also Section 5.6. Afterwards the winglet is altered using a trial and error method. For example the sweep and taper are varied and subsequently the effects on lift and drag coefficient curves are evaluated. During a sensitivity analysis it can be noticed that increasing the winglet height and the curvature radius eminently improved the efficiency. After careful investigation of lift and drag coefficients an optimized winglet can be selected.

A sketch of the selected RELOAD winglet is depicted in Figure 5.6. Figure 5.7 shows characteristic coefficient curves of the wing and of the wing including the enhanced winglet. From the Figure, the conclusion is drawn that the lift over drag ratio improved on average by 10.8 %. Furthermore it is concluded that the winglets provide better stability since the C_M value becomes more negative, as shown in Chapter 8.

(a) Winglet sketch

(b) XFLR5 winglet model with streamlines
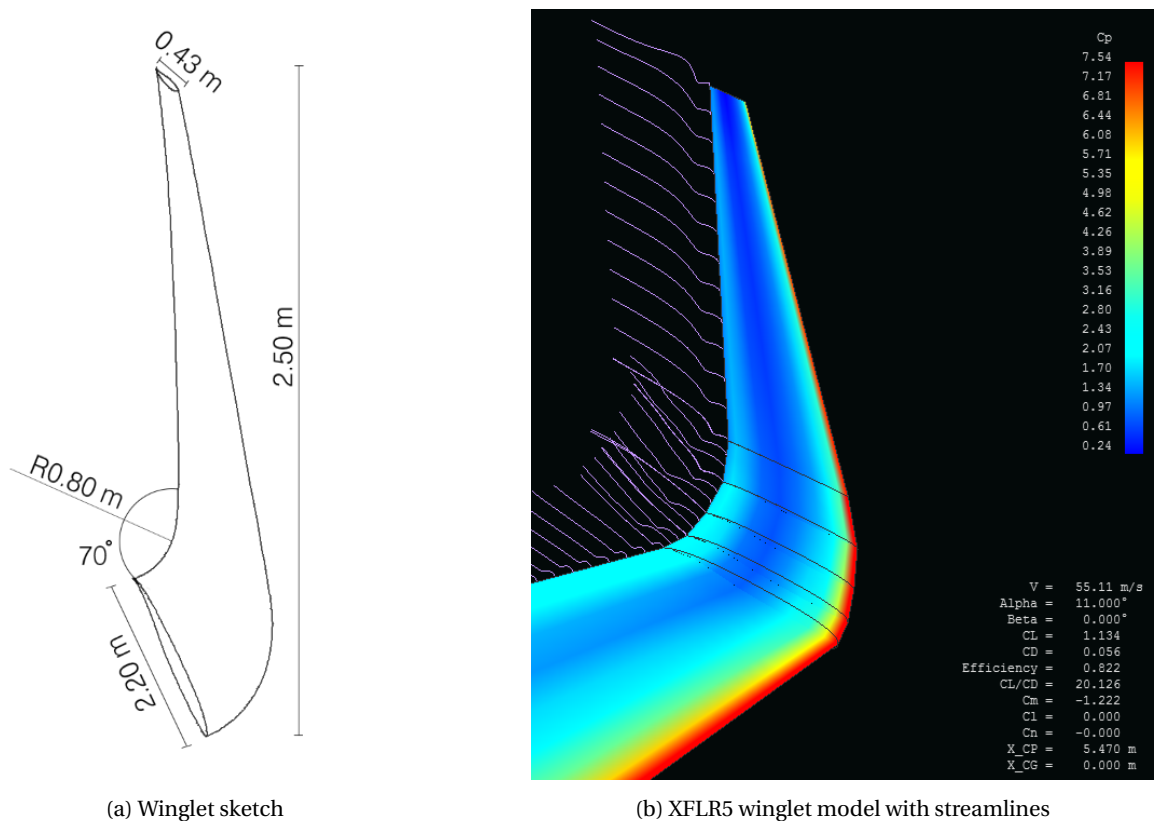
Figure 5.6: Winglet sketch and model

(a) C_D-α

(b) C_L/C_D-α

(c) C_M-α curve
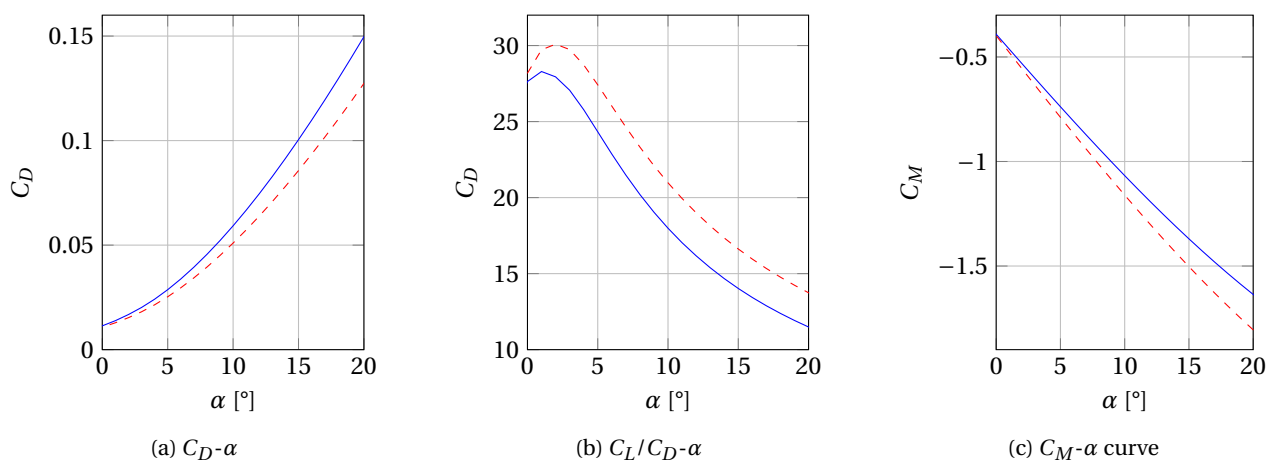
Figure 5.7: Characteristic coefficient plots of the wing alone (continuous line) and including the enhanced winglet (dashed line)

---

[8]URL http://www.aviationpartnersboeing.com/products_737_700SSW.php [Cited on 7 June 2016]
[9]URL http://www.airbus.com/support/maintenance-engineering/technical-data/aircraft-characteristics/ [Cited on 7 June 2016]

5.2.6 High Lift Devices

In the previous design phase, the maximum lift coefficient, $C_{L_{max}}$, of the aircraft was set to 1.6 in order to ensure safe take-offs and landings. Figure 5.7 shows that the wing is able to achieve this $C_{L_{max}}$ at an angle of attack of approximately 16 [°]. Nonetheless high lift devices (HLDs) are necessary because of several reasons. Firstly, the wing lift coefficient is not equal to the aircraft lift coefficient as the wing sections located in the fuselage are not generating lift. Secondly, the rotation angle during landing and take-off is typically 7 [°] to 11 [°] [18] and should not exceed this range due to ground clearance and visibility constraints, compare with Subsection 5.3.3 and Chapter 10. Thus the angle of attack is also limited.

Morphing HLDs were recommended during the previous design phase. These are promising in terms of noise and drag reduction due to their seamless structure. Thus they are currently investigated extensively and the technology is making fast progress. Especially trailing edge morphing HLDs are already in an advanced development stage. In 2014 the trailing edge HLD from FlexSys was flight tested on a business jet[10]. This HLD can increase the camber from -9 to 40 [°] and can reach response rates of 30 [°/s]. During the flight test noise reductions up to 40 % were measured. On top, it is able to reach fuel reductions of 5 % and L/D improvements of 3.3 to 10 %[10]. Projects such as SADE [19], SARISTU [20] and LeaTop [21] are investigating the design options for morphing leading edge HLDs. This appears to be a more challenging topic due to additional stresses in tapered wings and size restrictions. Furthermore maintenance is a problem since the inner structure and actuators are covered with morphing material. Certification issues with regard to de-icing systems and bird strike problems are not yet resolved and also solutions might not be ready before 2025[11].

All the just mentioned arguments make applying morphing leading edge HLDs only a recommendation for the further design phases. For now conventional sealed slats are considered as these also performed well during the trade-off in the previous design phase [1]. On the other hand trailing edge morphing HLDs are applied to the RELOAD aircraft design because de-icing or bird strike problems do not emerge, furthermore successful tests have already been conducted.

The sizing of the HLDs is conducted according to a conventional method from literature [22]. The lift coefficient increase $\Delta C_{L_{slats/flaps}}$ is calculated using Equation 5.1. The total lift coefficient can afterwards be determined using Equation 5.2.

$$\Delta C_{L_{slats/flaps}} = \Delta C_{l_{base_{flaps/slats}}} \frac{S_{effected_{flaps/slats}}}{S} K_\Lambda \tag{5.1}$$

$$C_L = C_{L_{aircraft}} + \Delta C_{L_{flaps}} + \Delta C_{L_{slats}} \tag{5.2}$$

Equation 5.1 incorporates the base change in airfoil lift coefficient due to HLDs ($\Delta C_{l_{base}}$) and a sweepback correction (K_Λ). $\Delta C_{l_{base}}$ is usually determined using a set of different figures. These figures are not applicable to morphing high lift devices and thus $\Delta C_{l_{base}}$ is estimated by designing and analyzing the modified airfoil shape with HLDs in XFLR5 in order to model the morphing effects accurately. K_Λ can be calculated with Equation 5.3.

$$K_\Lambda = (1 - 0.08 cos^2(\Lambda_{QC})) \cdot cos^{0.75}(\Lambda_{QC}) \tag{5.3}$$

Using above mentioned formulae the HLD sizing can be performed recursively. Several constraints arise from the wingbox, aileron and landing gear design (see Chapters 6, 8 and 9 respectively). For example flaps and slats cannot intersect the back spar and front spar of the wingbox respectively.

The sizing of HLDs is especially sensitive too a change in the area effected by the devices, S_{HLD}, and to the percentage of the chord that is used for HLDs. Varying the maximum deflection has a comparatively small effect.

The final sizing and positioning of the HLDs is illustrated in Figure 5.3. The final modified airfoil shape can be seen in Figure 5.8. The maximum deflection of the trailing edge flap is 35 [°] and the pivot point is located at 70 % of the airfoil section chord. The maximum deflection of the leading edge is 15 [°] and the pivot point is located at 10 % of the airfoil section chord. The aircraft is assumed to be at 11 [°] angle of attack during take-off and landing and without HLDs it shows a lift coefficient $C_{L_{aircraft}}$ of 0.952, the slats add a $\Delta C_{L_{slats}}$ of 0.339 and the flaps a $\Delta C_{L_{flaps}}$ of 0.334. Together this results in a $C_{L_{max}}$ of 1.625. The approximations for the HLD sizing are all conservative, i.e. minimum speed airspeed is assumed instead of approach speed and the fuselage-wing intersection is not assumed to generate any lift, to ensure absolute safety.

---

[10]URL http://www.flxsys.com/flexfoil [Cited on 7 June 2016]
[11]Dr. J. Sodja, Aerospace Structures & Computational Mechanics, TU Delft, 30 May 2016, Personal interview
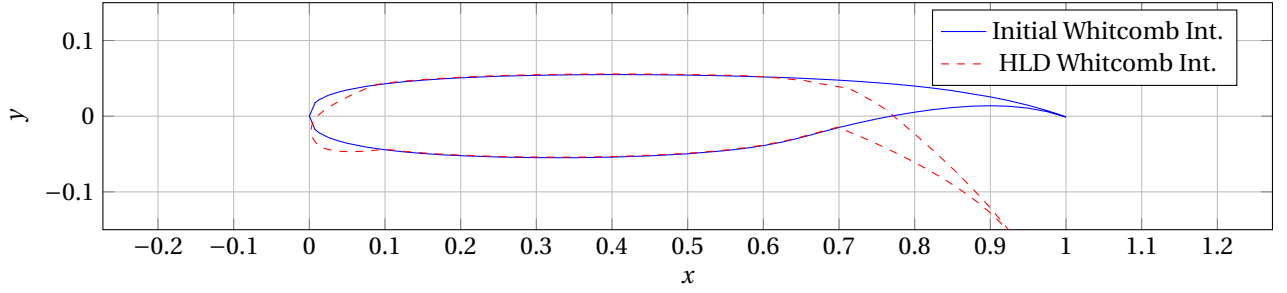
Figure 5.8: Effect of HLDs on the airfoil shape

5.3 Fuselage Aerodynamics

The following section is describing fuselage aerodynamics briefly. Firstly some comments about the wing-fuselage integration are presented in Subsection 5.3.1 and then the nose and tail cone sizing is discussed in Subsections 5.3.2 and 5.3.3 respectively.

5.3.1 Fuselage-Wing Integration

During the previous design phase the decision was made to blend the wing into the fuselage. However, after reconsidering all other design decisions, this does not seem to be a feasible option any more. The previous section shows that a relatively small trapezoidal wing can already generate enough lift. Increasing the wing just for the sake of blending is not a valid option. However, the wing-fuselage integration still needs to be investigated as the aerodynamic effects occurring in this region are of complex nature. Without detailed computational fluid dynamic (CFD) analyses or windtunnel test these effect can not be modelled accurately. Therefore blending the wing remains a recommendation, see also Section 5.6.

5.3.2 Nose Cone

This subsection describes the nose cone design. Generally different nose cone options are feasible. In literature it is stated that an elliptical nose cone is the most efficient for subsonic speeds and a LD-Haack nosecone is the most efficient for transonic speeds [23]. Since our cruise speed equals Mach 0.75, which is the lower bound for transsonic flows, both shapes are considered. Ideally one should determine the drag coefficient of both shapes at various flight conditions and perform a trade-off afterwards. Determining an accurate drag coefficient is unfortunately considered too complex for this design phase (a coarse CFD mesh does not generate meaningful results). As an approximation the wetted area of the two shapes is considered since it generally scales with drag [23]. Table 5.5 shows that the elliptical nose cone has the lowest wetted area. Hence an elliptical nose cone is chosen for the RELOAD aircraft. The wetted area is calculated based on the fuselage size and the previously determined nosecone length [2]. These equations are shown in 5.5 [23] and 5.6 [24]. The nose cone shape is only sensitive to the cross-section of the fuselage and the length of the nose cone. The elliptical shape is constant and adapted to this dimensions. So if one of the first two parameters changes, the nose cone shape changes significantly. An illustration is shown in Figure 10.2.

$$\epsilon = \sqrt{l_{nosecone}^2 - (\frac{w_f + h_f}{2})^2} / l_{nosecone} \tag{5.4}$$

$$A_{wet_{Elliptical}} = \pi l_{nosecone}^2 + 0.5 \frac{\pi (\frac{w_f + h_f}{4})^2}{\epsilon} ln \frac{1 + \epsilon}{1 - \epsilon} \tag{5.5}$$

$$A_{wet_{LD-Haack}} = 0.715 \pi l_{nosecone} \frac{w_f + h_f}{2} \tag{5.6}$$

Table 5.5: Wetted area for different nose cone shapes

Type	A_{wet} [m^2]
Elliptical	57.4 [23]
LD-Haack	76.9 [24]

5.3.3 Tail Cone

The tail cone sizing is not specifically constraint by aerodynamics but rather by ground clearance requirements during the take-off rotation and by the size of the auxiliary power unit (APU). However, for consistency, the tail cone design is also treated in this chapter. Figure 5.9 shows the final tail cone design. The angle θ is determined for both the ground clearance and the APU exhaust requirement. First θ is determined using the ground clearance requirement and the tip-back angle, compare with Chapter 9. Second θ is determined by the APU exhaust requirement. The APU exhaust is assumed to have a diameter of 1.0 [m]. It turns out that θ is maximum for the APU exhaust requirement. Therefore the tail cone is scaled for this θ of 31 [°] in order to minimize weight.

The tail cone shape is sensitive to the tipback angle, APU size, length of the tail cone and the fuselage shapes. When the tipback angle and the APU size changes the tail changes a lot. The other parameters affect the tail cone in the same way as for the nose cone, discussed in 5.3.2.
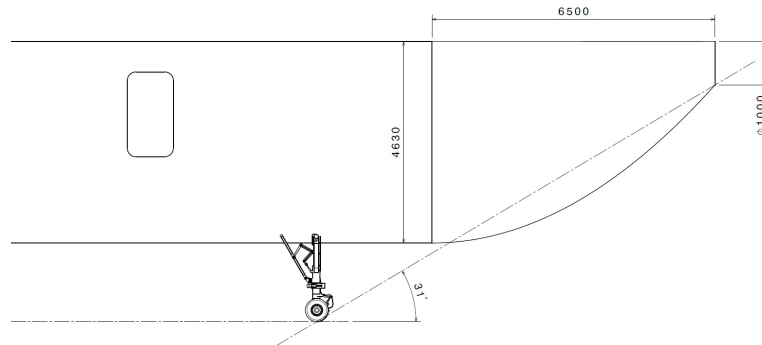
Figure 5.9: Tail cone sketch

5.4 Drag Estimation

This section is devoted to the estimation of the total aircraft drag during different flight phases. The total drag is a direct indicator of the aircraft performance and is eminently important for the engine sizing, as described in Chapter 7. On the other hand the engine shape influences the drag calculations. Due to various interaction effects several iterations are necessary in order to determine sound estimation results.

Nowadays no method for simultaneously estimating the total aircraft drag exists [25]. During the RELOAD aircraft preliminary design phase an advanced component build-up estimation method from literature is used [22]. This methods combines several techniques, e.g. from Hoak [26] and Torenbeek [14]. The considered drag components are depicted in Figure 5.10.
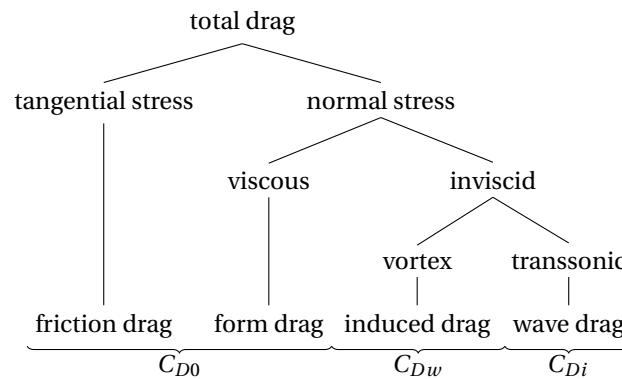
Figure 5.10: Drag components adapted from [22]

The component build-up methods used is based on a set of analytical equations from [22]. Firstly, the zero lift drag coefficient C_{D0} is determined. The C_{D0} build-up is shown in Table 5.6. Except for the contribution of the flaps and the landing gear the $C_{D0_{component}}$ is calculated by Equation 5.7. Extensive formulae for the form factor K and the skin friction coefficient C_F for each component as well as the flaps and landing gear contribution can be found in [22]. Afterwards the wave drag coefficient C_{Dw} and the induced drag coefficient C_{Di} are calculated with Equations 5.8 and 5.9.

$$C_{D0_{component}} = C_F K \frac{S_{wet}}{S} \tag{5.7}$$

$$C_{Dw} = 20(M - M_{cr})^4 \qquad (\forall M \geq M_{cr}) \tag{5.8}$$

$$C_{Di} = \frac{C_L^2}{\pi A e} = \frac{C_L^2}{\pi A \frac{1}{1+A \cdot f(1-\Delta\lambda)} e_b e_D e_M} \tag{5.9}$$

Various factors used in the drag calculations, such as the skin friction coefficient C_F, depend on the atmospheric conditions. Other factors, such as the Oswald coefficient e, depend on the Mach number. Therefore the drag coefficient was calculated for the landing, take-off and cruise conditions for different Mach numbers. It should also be noted that the drag (coefficient) values presented below were obtained after all design iterations. The results are presented in Figure 5.12. Furthermore the thrust required was calculated and is shown in Figure 5.11. A sensitivity analysis shows that the total zero lift drag coefficient C_{D0} is largely influenced by lowering the landing gear and extending the flaps. The effect of atmospheric conditions on the zero lift drag coefficient is comparably small, however the effect of these conditions on the actual drag force is compelling.

Table 5.6: Zero-lift drag coefficient C_{D0} build-up calculated based on [22]

	Wing	Flaps	Canard	Vertical tail	Fuselage	Nac. and pylons	Landing gear	Sum of components	Misc. (5 % of sum)	Total
Landing/ Take-off	0.0030	0.0487	0.0008	0.0018	0.0106	0.0005	0.0234	0.0889	0.0044	0.0933
Cruise	0.0027	-	0.0006	0.0016	0.0095	0.0004	-	0.0150	0.0007	0.0157
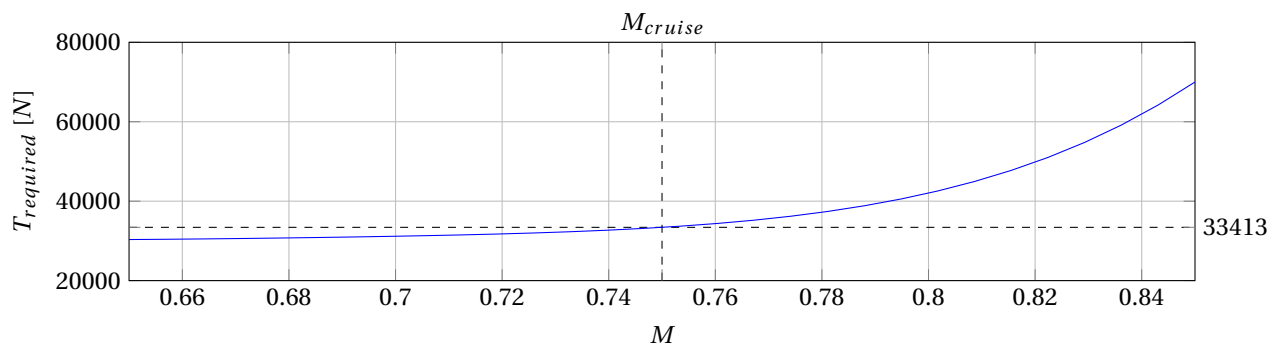
Figure 5.11: Thrust required for cruise configuration at cruise altitude conditions
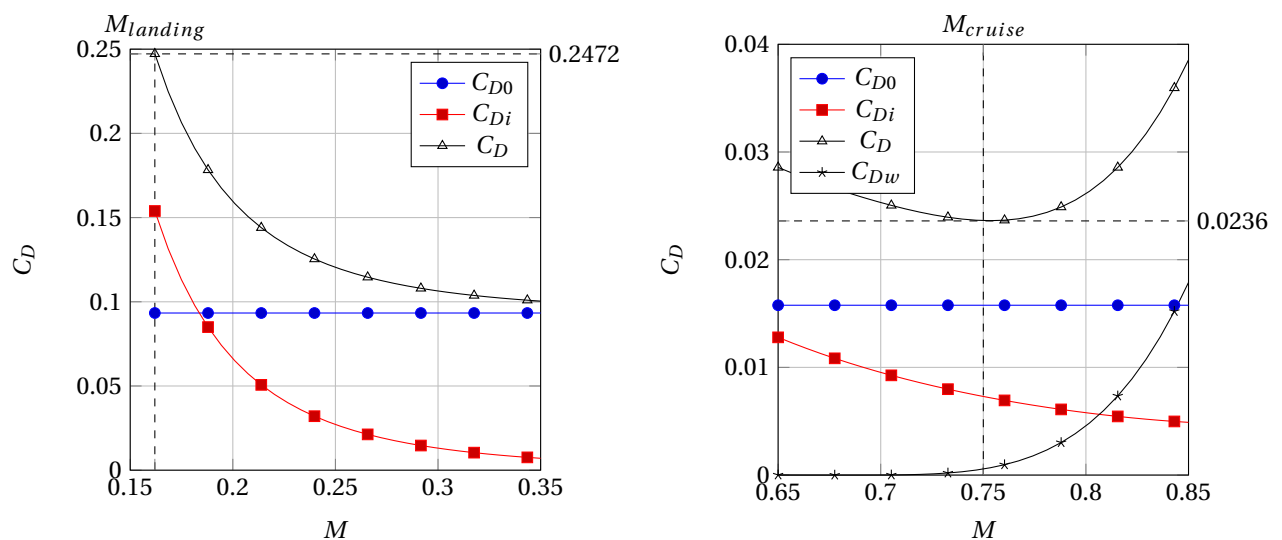
(a) Landing/Take-off configuration at sea level conditions

(b) Cruise configuration at cruise altitude conditions

Figure 5.12: Drag coefficients

5.5 Verification and Validation

The contemporary aerodynamic design is developed using mainly custom code and the scientific tools TSFOIL, XFLR5 and SU2_EDU. Several verification and validation activities are carried out in order to ensure correct and meaningful results. In this section a brief overview of these activities is given.

5.5.1 Verification

The custom code is written in Python. Therefore syntax errors are directly shown to the developer when attempting to execute the code and they are resolved in a straightforward manner. Checking for conceptual errors is more extensive. Wherever possible, different code parts are unit tested against third party codes, i.e. the atmospheric calculations are checked against the Digital Dutch Standard Atmosphere Calculator[12] and wing planform calculations are checked against the Exo Aviation Wing Planform Generator[13]. When no third party code is available the unit tests are conducted by making use of hand-calculations and/or spreadsheets. These spreadsheets are also used to perform quick sensitivity analyses during the design in order to find the most important design parameters.

It is beyond the scope of this project to verify the scientific tools TSFOIL, XFLR5 and SU2_EDU entirely. As these tools are widely used, it is assumed that they are already properly audited. However, the inputs to the tools need to be verified. This is done by implementing a double check performed by two different people. Furthermore singularities are investigated, e.g. the Mach number is increased to 1 and the transsonic drag increase is clearly noticable. When verifying the wing tip analysis the winglet length is set to zero in order to ensure that the tool still generates meaningful outputs (in this case it returns the same performance values as for the wing alone).

5.5.2 Validation

Ideally an aerodynamic design is validated by windtunnel experiments. However this is too extensive for the current development stage and thus it only remains a recommendation, see Section 5.6. Unfortunately no experimental data is found for the selected airfoil sections at the considered Mach and Reynolds numbers. On the other hand the tools used are assumed to be validated and papers analyzing the transsonic performance of the tools using standard airfoils exits. TSFOIL [27] and SU2_EDU [28] show good agreement between tool results and experimental and/or other (full potential) code results). Thus the tools are assumed to be validated.

The results from all aerodynamic subdesign are also validated by comparing values from literature. For example the drag values obtained are similar to the example cases listed in [22]. The shape of the nose and tails cones is validated by comparison to the nose and tail cones of the reference aircraft. Regular sanity checks lead to problems and also changes in the design approach but eventually a solid design methods is generated. Figure 5.12 is a good example of the design quality as the minimum drag coefficient is indeed encountered at the previously specified cruise conditions.

5.6 Recommendations

The last section of this chapter is devoted to recommendations for further design stages. It is of utmost importance that all these recommendations are carefully implemented as small aerodynamic design changes might affect the aircraft performance vigorously.

The airfoil selection presented in Section 5.1 returns the best airfoil from a finite airfoil database. However, there might be better airfoils which are not included in the database. Often the airfoil shape can also be optimized by complicated algorithms which make use of various fluid dynamic codes and this should also be done at an imminent next design stage due to its influence on e.g. the wing box structure.

The wing is designed with a gradual transition between the different airfoils in Section 5.2. Due to the double curvature required, this transition might not be economically manufacturable [29] and thus an alternative solution should be generated as well. Afterwards a trade-off should be performed to determine the best option. A definite decision needs to be made well in advance of the manufacturing stages, hence before 2022 according to the Gantt chart presented in Appendix C.

In Subsection 5.2.5 the wing tip is designed taking into account several assumptions. The effect of splitting the winglet still needs to be investigated. For simplicity the winglet is assumed to feature the same airfoil as the outboard wing section. Optimization with regard both to the winglet airfoil as well as the winglet shape still needs to

---

[12]URL http://www.digitaldutch.com/atmoscalc/ [Cited on 20 June 2016]
[13]URL http://exoaviation.webs.com/airplanewingplanform.html [Cited on 20 June 2016]

be performed. Moreover the winglet performance at cruise conditions also needs to be reconsidered as this is the flight phase with the highest total fuel consumption. As analysis shows that winglets influence the aerodynamic performance significantly this optimization should also be implemented directly during the next design stage.

The flap and slat sizing is performed independently in Subsection 5.2.6. Often the joint use of flaps and slats increases the efficiency and thus the dimensions of these devices can be decreased [22]. This effect should be studied very carefully as the joint use might also have an opposite effect. Also more applied development work is needed regarding morphing HLDs as they are not fully matured yet. Next to that the effect/use of flaps and slats in the airfoil transition region needs to be evaluated in detail. Since HLDs are indispensable for safe take-offs and landings the design should be finalized well in advance of the ground test, thus before 2023.

The effects of blending the body into the fuselage cannot be modelled accurately without using advanced theory. Therefore this should also be a major focal point for the approaching design stages.

The drag estimation also needs to be refined. Although the total aircraft drag cannot be estimated accurately nowadays, see Section 5.4, the wing and fuselage drag estimations can be improved by advanced fluid dynamic calculations. Additional drag smaller sources, e.g. from tubes, sensors and doors, should also be included separately instead of adding a fixed percentage accounting for all miscellaneous items. As an reasonably accurate drag estimation is needed for the engine sizing this also should also be treated immediately after this design stage.

Next to all design features listed in this chapter there are others that have the potential to increase the aerodynamic performance of the aircraft significantly. They are not treated because of time constraints and are thus considered out of the scope of this design phase. Amongst others these are spoilers, coatings and vortex generators. As the engines are not attached to the wing, see Chapter 7, there is plenty of space available for additional design features.

Finally, it is of great importance that the validation procedures are particularized. Especially wind tunnel tests and advanced computational fluid dynamic calculations are needed for proper investigation of interaction effects of different aerodynamic phenomena. This is applicable to all recommendations mentioned above.

6

Structural Design

This chapter aims to first provide all general steps taken in the structural design of the fuselage and wing box in Section 6.1. Section 6.2 discusses the design for fatigue. Then, the actual design of the fuselage and the wing box is considered in Section 6.3 and Section 6.4 respectively. Finally, recommendations for the final design phase are presented in Section 6.5.

6.1 Design Approach

In this section the steps taken in the design of the fuselage and wing are elaborated upon. Firstly, structure specific requirements are presented. Secondly, the constraining load cases are identified. Finally, the assumptions are stated and the methodology is explained.

6.1.1 Requirements

Before starting the design, it is of utmost importance to define and distinguish each function that is required of the fuselage. Partly based on the outcomes, one can determine what design method is suitable, what design cases are considered and how the design space is set up.

The functions of the RELOAD aircraft are described in Chapter 2.3. All of these requirements are also valid for the fuselage. When elaborating on this part specifically however, one can go even more in depth and define the following design constraints with respect to the fuselage design [1]:

REL-STR-FUS-01 The fuselage shall have cutouts for doors and windows according to the configuration described in Chapter 15 and Subsection 6.3.1.

REL-STR-FUS-02 The fuselage shall be integrable with the wing.

REL-STR-FUS-03 The fuselage structure shall withstand 100,000 flight cycles.

REL-STR-FUS-04 The fuselage shall house the cabin layout as described in Figure A.1.

REL-STR-FUS-05 The fuselage shall withstand all aerodynamic loads introduced by the wing and canard.

REL-STR-FUS-06 The fuselage shall withstand the aerodynamic loads according to the gust and manoeuvre diagram of the aircraft, presented in Figure 20.5.

To design the wing box structure, specific requirements apply in a similar manner. These impose constraints and indicate which load cases are of importance. The following requirements are taken into account in the structural design:

REL-STR-WNG-01 The wing box shall structure withstand the aerodynamic loads encountered during all flight phases, taking into account the load factors derived from the gust and manoeuvre diagram presented in Figure 20.5.

REL-STR-WNG-02 The wing box structure shall house the fuel tanks from 30 % to 80 % of the semi-span.

REL-STR-WNG-03 The wing box structure shall fit the local airfoil of the wing.

---

[1]The requirement specific code indicates a structural (STR) fuselage (FUS) or wing (WNG) requirement of the RELOAD (REL) project.

REL-STR-WNG-04 The wing box shall provide access points for refuelling.

REL-STR-WNG-05 The wing box structure shall provide access points for maintenance.

REL-STR-WNG-06 The wing box structure shall provide attachments points for subsystems.

6.1.2   Load Cases:

One of the main inputs for a structural design a set of load cases. One has to answer the question of when the most critical loads occur in an aircraft's flight cycle and define the ultimate loads that it should be able to cope with in extreme conditions. To define just that, a manoeuvre and gust loading diagram is constructed in compliance with the CS-25 regulations [4].

Figure 20.5 in Section 20.2.1 shows the manoeuvre and gust-diagram to find the ultimate loading case for this structural analysis. The manoeuvre diagram considers gravitational load factors of -1g to 2.5g, whilst the gust diagram considers gusts up to the dive velocity at Mach 0.8. Concluding from these diagrams, the constraining load factor is the maximum manoeuvre load of $n_{max} = 2.5$. This factor is then multiplied with the regulatory safety factor of 1.5 to arrive at n_{ult} = -1.5 and 3.75. The figure is displayed in Chapter 20.2 because it is closely related to the topics treated in that chapter.

Fuselage loads: three load cases are considered and evaluated for the fuselage. The first load case considers a regular flight cycle, analyzing load factors from n = -0.5 to n = 2.5. The reason for this range is that a passenger aircraft is highly unlikely to perform a negative g manoeuvre, but can encounter heavy gusts. The second load case is a cruise condition where the aircraft is subjected to the ultimate load factor of 3.75 and -1.5, as follows from the gust and manoeuvre requirements. This situation is one that is not expected to occur, but does constrain the maximum loads that an aircraft has to cope with throughout its life span. A simplified version of this load case on the fuselage is shown in Figure 6.1. The third load case is a $3g$ touchdown where the aircraft touches the ground with all wheels simultaneously, as is observed in Figure 6.2. This load case also features a force, S_y, on the vertical tail in case the pilot has to correct for a crosswind. The actual applied forces and their points of application are summarized in Table 6.1.
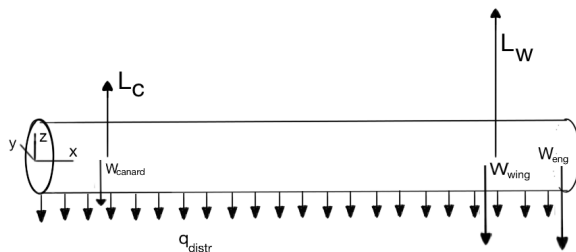
Figure 6.1: Simplified representation of load cases 1 and 2 (flight), including the axis system
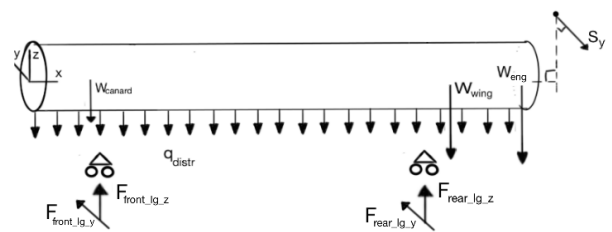
Figure 6.2: Simplified representation of load case 3 (touchdown), including the axis system

Wing box loads: as for the fuselage, the static loads on the wing box are based on the gust and manoeuvring diagram presented in Figure 20.5. Therefore the limit loads occur at 2.5g and -1g. The ultimate loads are thus 3.75g and -1.5g by implementing a safety factor of 1.5 as suggested in CS-25 [4]. A simplified representation of positive loading is shown in Figure 6.3. A representation of a negative loading manoeuvre is resembled in the first load case, but with the weight, lift and reaction forces inverted. For each load case three analyses were performed with 10 %, 50 % and 100 % of the maximum fuel weight to simulate the several flight phases.

During each flight the wing is also subjected to dynamic loading due to turning, climbing, etc. Although a vibrational analysis should be performed later in the detailed design phase, the varying stresses are used for a preliminary fatigue analysis. These load cases, loads and applied number of cycles are presented in Table 6.2. The load cases in this table are constructed in consultation with Dr. C. Kassapoglou[2]. The applied number of cycles spectrum is based on the life expectancy of the aircraft discussed in Section 20.3.

In the structural analysis the fuel weight is varied for both load cases to simulate several phases of a flight. At the end of the flight for example, more fuel will have been consumed, reducing the bending relief in the wing. This significantly increases the stresses in the wing box.

---

[2] Dr. C. Kassapoglou, Aerospace Structures & Computational Mechanics, TU Delft, 15 June 2016, Personal interview.

Table 6.1: Input loads of the fuselage module from the class II design

Aircraft Component	Mass [kg]	Direction	Point of Application in x-direction [m]
Fuselage	8380	-z	0 - 32.78
Furnishing	626	-z	6.51 - 26.28
Chairs	2640	-z	6.51 - 26.28
Passengers + luggage	16500	-z	6.51 - 26.28
Wing	3670	-z	23.10
Main landing gear	1750	-z	22.65
Nose landing gear	365	-z	3.19
Engines & nacelles	5960	-z	27.50
Engine Controls, Hydraulics & Starters	1052	-z	16.38
Fuel system	114	-z	23.11
Anti-icing system	112	-z	21.00
Vertical tail	842	-z	34.38
Canard	929	-z	4.81
Flight controls	465	-z	16.38
Avionics	767	-z	2.29
Auxiliary power unit	169	-z	31.13
Electronics & instruments	481	-z	2.29
Lavatories	368	-z	15.28
Air conditioning	1030	-z	27.86
Cruise reaction forces	Force [kN]		
Wing Lift	473	z	22.32
Canard Lift	73.2	z	3.00
3g Touchdown reaction forces	Force [kN]		
Tail rudder deflection force	17.3	-y	32.72
Nose landing gear (y-direction)	68.9	-y	3.19
Main landing gear (y-direction)	238.9	y	21.77
Nose landing gear (z-direction)	249.3	z	3.19
Main landing gear (right z-direction)	580.8	z	21.77
Main landing gear (left z-direction)	808.9	z	21.77

6.1.3 Assumptions

The basis of any engineering analysis is to know how accurate the method is for a given input. It is therefore of outmost importance to state the assumptions made and their impact on the analysis.

In order to simplify the simulation, assumptions have been made. All these assumptions introduce discrepancies between the results of the simulation and reality. These discrepancies are anticipated and the effects of the assumptions are globally predicted.

AS-STR-01 The aircraft is landing horizontally and on all wheels at the same time.

- The force on the rear wheels is higher in reality than in the simulation, and therefore the force on the front wheel is lower.

AS-STR-02 The landing is treated as a static problem.

- The entire structure is loaded with static forces only in the simulation. Dynamic forces, e.g. vibrations, are not considered, resulting in a less constraining load case on the fuselage.

AS-STR-03 Drag and lift forces during landing are neglected.

- There are no forces considered in x-direction on the fuselage. In reality, the landing gear introduces forces in the x-direction due to braking and rolling drag. The main wings and the canards are also generate forces in the x-direction. This means that the computed stresses are lower in the simulation than in reality.

- The wings are assumed to not generate lift during the landing phase, thus the forces on the landing
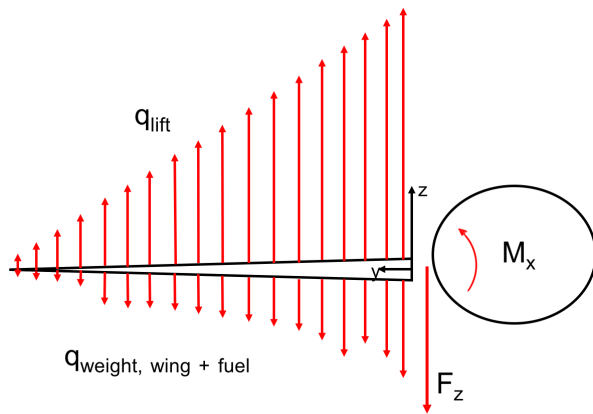
Figure 6.3: Simplified free body diagram of the wing structure (front view), including the axis system
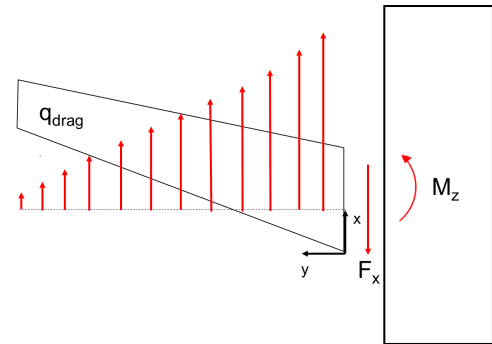
Figure 6.4: Simplified free body diagram of the wing structure (top view), including the axis system

Table 6.2: Load cases taken into account for the preliminary fatigue analysis

Loading case	G load	Applied number of cycles
Take-off	1.3	95850
Landing	1.5 (no lift)	95850
Hard landing	3 (no lift)	135
Limit load manoeuvre	2.5	13692
Ultimate load manoeuvre	3.75	1
Push over with gust	-1.5	9
Small climb	1.25	95850
Small descend	0.75	95850
10° turn	1.015	287550
20° turn	1.064	191700
30° turn	1.547	95850

gear are higher in the simulation as they carry the full aircraft weight and downward deceleration force. Because of this, computed stresses in the fuselage are significantly larger than in reality during landing.

AS-STR-04 The structure of the fuselage is assumed to be uniformly distributed over its length.

- This assumption leads to lower (peak) shear stresses in the yz-plane in the simulation, as loads are less concentrated throughout the fuselage.

- In reality, most of the structural reinforcements are concentrated at the wings and landing gear, thus resulting in a lower peak bending moment in the actual situation as compared to the simulation. This results in higher bending stresses in the simulation.

AS-STR-05 The maximum deceleration during landing equals 3g.

- This value is given in [30] to account for the force of impact during touchdown and is assumed as a reasonable value for a touchdown situation.

AS-STR-06 The reaction forces from the landing gears are introduced into the fuselage as point loads.

- The consequence is that no distributed loads are present in the xy-plane, thus simplifying calculations.

AS-STR-07 The forces at the landing gear are non-zero in x- and y-direction and zero in z-direction.

- There are no moments around the x-axis in the model, which results in lower total stress.

AS-STR-08 The structure is assumed to be thin-walled.

- This assumption is applicable since the skin thicknesses are in general a lot smaller than the overall geometry of the cross-section. However, it affects the maximum stress locations.

AS-STR-09 The structural combination of skin and stringers is idealised using the boom method [31].

- This positively affects the simplicity of the analysis but reduces the accuracy of the model, as described in Chapter 20 of [31]. This accuracy penalty can be mitigated by choosing a higher number of booms.

AS-STR-10 The floor panel area is accounted for in the booms which are closest to its connection point to the fuselage.

- This assumption introduces the risk that the critical stress in the fuselage occurs in the floor. This implies that failure might arise first in the floor. However, this risk is mitigated as the floor is analyzed in detail separately including the transferred loads from the fuselage.

AS-STR-11 The wing structure is modelled as a single cell box, thus the skin of the leading and trailing edge are not taken into account.

- This is conservative and a necessary approach because the trailing edge features morphing high lift devices, demanding a sophisticated mechanism and a careful material selection.

AS-STR-12 The wing box is modeled as a straight structure with a length equal to the calculated wing span divided by the cosine of the sweep angle.

- The longer structure increases bending stress compared to a non-swept wing. However, the stresses at the root are underestimated due to the kink in the structure between the actual wing structure and the continuation of the wing box in the fuselage.

AS-STR-13 The lift and drag forces are modeled as linear force distributions by taking the gradually decreasing chord into account. A simplified representation is displayed in Figure 6.3 and Figure 6.4.

- The wing planform is designed in such a way that it produces an ellipse shaped lift distribution, resulting in a higher lift force near the tip and a lower lift force at the root (compared to the linear distribution). Hence, the stresses on the outboard sections are slightly underestimated.

- By applying this assumption, the differences between the chosen airfoils in terms of aerodynamic performance are not taken into account.

AS-STR-14 The weight distribution of the wing is approximated by a parabolic distribution, taking into account the spanwise decreasing cross-sectional area. Also the weight of the fuel stored in the wing box is modeled in this manner, starting the fuel tank at 30 % of the span and and ending the tank at 80 %. In Figure 6.3 this is shown by the local discrepancies in the parabolic weight distribution under the wing.

- This assumption does not cause a significant decrease in accuracy, as the cross sectional area accurately represents the material and thus weight in each section of the wing.

- Also the parabolic representation of the fuel weight is not expected to have large impact. This because the locally stored fuel depends on the local cross-sectional area, just as the structural weight.

AS-STR-15 The fuselage validation is done using empirical means to estimate the fuselage weight as a function of the operating empty weight.

- The consequence of performing a validation without comparing actual stresses is that the design is over or under designed, thus introducing the risk of an invalid design as a whole. This risk is partially mitigated by comparing the structural weight of the fuselage to reference aircraft, thus performing a partial validation. Furthermore, a recommendation is made to properly validate the model with real-world test data, further mitigating the risk of a faulty final design.

6.1.4 Methodology

The purpose of the structural design approach of the fuselage is to arrive at an accurate model of a fuselage structure that enables the user to design a structure compliant with the requirements. The inputs for this process are all loads acting on this structure with their respective points of application, as well as the layout of the structure, to be tested. The output is a complete breakdown of stresses over the entire structure, thus giving the user an insight in predicted maximum loads and stress amplitudes. The following paragraphs consider the main methods used to arrive at these outputs from the given inputs. Straightforward processes such as the calculation of moments of inertia are not described. An overview of the process is presented in Figure 6.5.

Data input: it is important to ensure that the software tool functions smoothly with a varying set of input parameters, as is the case when performing iterations. The input data is therefore connected directly to the central database of the aircraft for all parameters that are computed by other modules. The inputs include fuselage and floor dimensions, weights and forces, simulation settings and material properties.
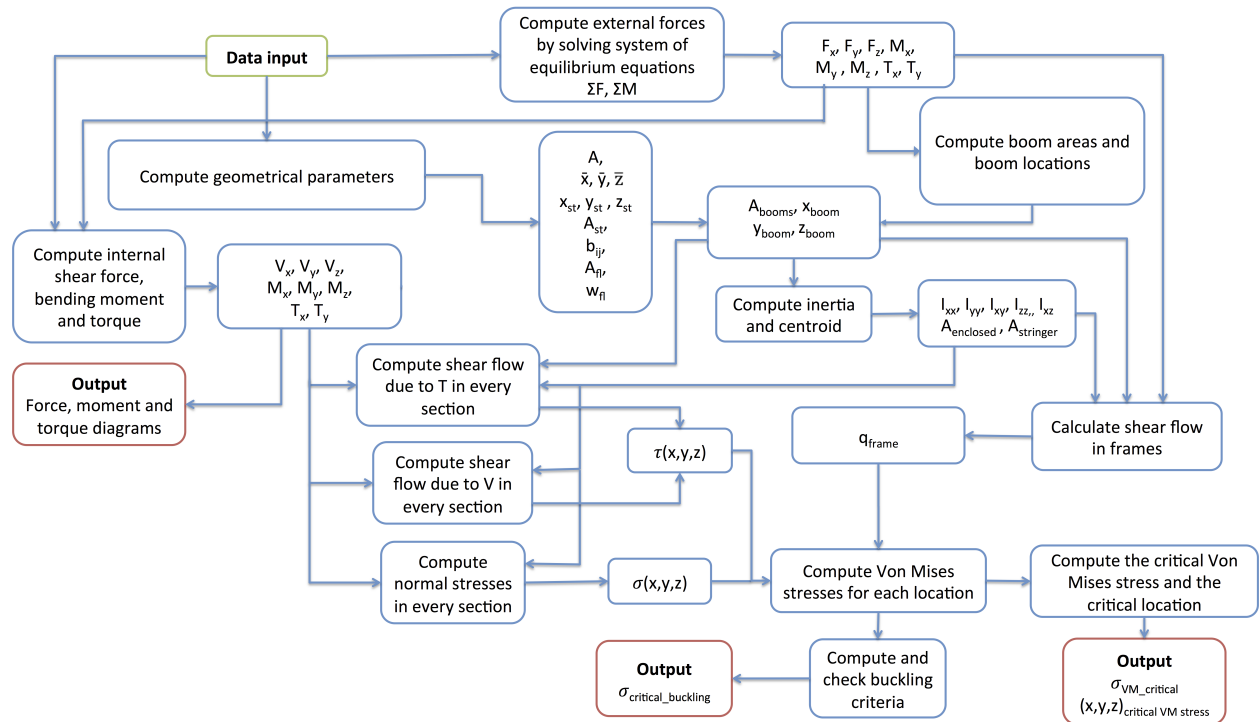
Figure 6.5: Flow chart of the fuselage structural design module

The input parameters for the fuselage design are:

- Fuselage dimensions: l_f, $l_{nose\ lg}$, $l_{main\ lg}$, w_f, h_f, t_{skin}, l_{t_z}, l_{t_x}

- Stringer geometry

- Floor dimensions: core thickness, face thickness

- Loading: component weights, component's centre of gravities, tail force

- Simulation settings: number of stringers, fuselage positions to analyse, rivet spacing, frame spacing

- Material properties: ρ_m, E, ν_m, σ_{yield}, σ_{ult}, G, τ_{max}

- Miscellaneous: h

To construct the wing box structure, the following input parameters were taken into account:

- Wing dimensions: A, S, Λ, c_{root}, λ, t_{skin}, spar locations, spar geometry, stringer geometry, rib locations, rib geometry, rivet spacing, fuel tank geometry, airfoil geometry

- Loading: C_L, C_D, $W_{components}$

- Simulation settings: wing positions to analyse, stringer locations

- Material properties: ρ_m, E, ν_m, σ_{yield}, σ_{ult}, G, τ_{max}

- Miscellaneous: buckling constants C_{rivet}, K_c, K_s

Compute geometrical parameters: the geometrical parameters are only determined by the input data, and are needed to calculate the internal stresses in a structure. The geometrical parameters computed for both the fuselage and wing box are:

- Cross-sectional area

- Centroid of the fuselage

- Stiffener locations

- Cross-sectional area of the stringers

- Distance between the stiffeners

- Area of the floor
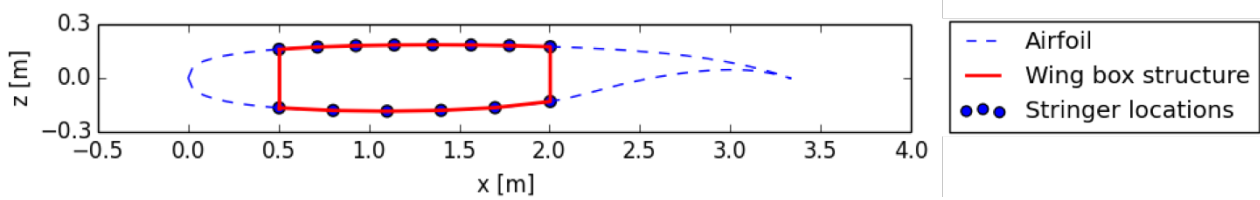
Figure 6.6: Cross-section of the wing at 14.28 [m] from the root

- Width of the floor

For the fuselage also the area and the width of the floor are determined.

The structure of the wing box is set up differently in the tool because the shape of the wing varies along the span, while the cross-section of the fuselage remains constant. Therefore each wing is divided in 100 sections, each with a different geometry. This makes it possible to vary the number and type of stringers on the upper and lower skin. The contour of the wing box is determined by the airfoil coordinates and the local chord length which are taken directly from the aerodynamic design. An example of this cross-sectional geometry setup is displayed in Figure 6.6. The tool also allows to vary the type of airfoil along the span of the wing.

External forces: the external forces block takes a list of aircraft component weights with their respective locations from the class II and III weight estimations. A force and moment equilibrium is set up in the y- and z-direction, taking into account point loads and distributed forces of, for example, the fuselage and payload weight. The reaction force magnitudes and locations are different for each load case. In case 1, only the canard and wing lift are computed to satisfy static equilibrium of forces and moments in the z-direction. In case 2, the reaction forces on the landing gear in y- and z-direction are determined as well as the torque on the fuselage.

For the wing box a linear lift distribution and parabolic weight distribution are assumed as stated earlier and shown in Figure 6.3. Similarly, the drag on the wing is estimated by a linear distribution by dividing the sectional lift force by the three dimensional aerodynamic efficiency. The reaction forces and moments at the root of the wing are calculated by implying a force and moment equilibrium in x- and z-direction. The direction of the reaction forces and moments vary with the several fuel states, and with the positive and negative load factor.

Internal forces: following from the external forces, the fuselage is now divided into 200 sections for which the internal forces are computed. This is done according to the method described in Hibbeler [32], where the equilibrium of a beam is analyzed. From this process one obtains $V_y(x)$, $V_z(x)$, $M_y(x)$, $M_z(x)$ and $T_x(x)$, which are plotted over the fuselage length. Using the same method from Hibbeler and by dividing each wing in 100 sections, the internal forces are calculated in the wing box. The output of this step is $V_x(y)$, $V_z(y)$, $M_x(y)$, $M_z(y)$ and $T_y(y)$.

Boom areas and locations: in order to simplify the structural analysis of the fuselage and the wing box, the boom method is used [31]. Moments about the axes are decoupled, so that one obtains two sets of boom areas and locations. The booms are created at each stringer location and include the stringer area and a part of the adjacent skin area. For the fuselage, the floor area is included in the booms reinforcing the floor.

Shear flow: the shear flow due to shear forces V_y and V_z between all booms in each fuselage section is computed according to Equations 6.3, which are described in Megson [31]. Here, the shear flow q_s is defined as $q_b + q_{s,0}$. Furthermore, the shear flow due to torque is computed by solving the system of equations described in Equation 6.4 [31]. Here, one solves for the shear flows q_{t1} and q_{t2} around the cells above and below the floor respectively. Similarly, A_s refers to the enclosed area of either cell 1 or two and $\sum_{n_{booms}}$ refers to the summation over the booms around these cells.

It is assumed that the wing box is a single cell structure, resulting in a simpler analysis. The shear flow induced by the shear forces V_x and V_z, and the torque $T_y(y)$ are added, taking into account the varying enclosed are of the wing box.

Pressure stresses: the pressure stresses are more complicated for the elliptic cross-section than for a cylindrical fuselage. Due to the elliptic shape, an additional bending stress is introduced in the skin. This bending stress is caused by the tendency of an ellipse to become circular under an internal pressure load. To estimate this effect, a model [33] for elliptical tubes is implemented in the fuselage design tool. In this model the hoop stress equals the sum of the induced bending stress and the membrane stress. These stresses are calculated by Equations 6.1a and (6.1b) respectively. Parameters X, D and θ are used to define the shape of the ellipse, E is the Young's modulus, ν

is the Poisson ratio, Δp is the pressure difference and t is the fuselage thickness. A visualisation of these stresses is found in Figure 6.7. The internal cabin pressure altitude is assumed to be 3000 [m].

$$\sigma_{bend} = \frac{3X\Delta pD}{t^2} \cdot \left(\frac{1}{1 + \frac{p(1-v^2)}{E} \cdot \left(\frac{D}{t}\right)^3} \right) \cdot \cos(2\theta) \quad (6.1a) \qquad\qquad \sigma_{membrane} = \frac{\Delta pR}{t} \qquad\qquad (6.1b)$$

Von Mises stress: the bending stress is determined in each boom and fuselage section and is computed according to the straightforward method described in chapter 20 of Megson [31]. Then, when combining this with the shear stresses computed from the shear flows and pressure stresses , one can easily compute the Von Mises stresses at each location in the fuselage following the method in chapter 9 of [31].

Frame stresses: frames are essential to ensure that external forces are transferred smoothly to the internal structure. Furthermore, they provide resistance to column buckling for the stringers [31]. The frame spacing and size is determined by computing the column buckling requirements and the dimensions are found by finding the required shear flow transmission due to external forces according to the method described in chapter 24 of [31].

Buckling criteria: the considered buckling modes are column buckling determined by Equation 6.2a. L in this formula is determined by the frame spacing in the fuselage and the rib spacing in the wing. Skin buckling is determined by Equation 6.2b where K_c is based on the ratio of stringer spacing and rib or frame spacing and b is the stringer spacing. Inter-rivet buckling is determined by Equation 6.2c, where c varies roughly between 0.1 and 3 and is based on the type of rivet used [34].

$$\sigma_{col} = \frac{I\pi^2 E}{L^2} \qquad (6.2a) \qquad\qquad \sigma_{skin} = K_c E \left(\frac{t}{b}\right)^2 \qquad (6.2b) \qquad\qquad \sigma_{ir} = 0.9cE \left(\frac{t}{L_{rivet}}\right)^2 \qquad (6.2c)$$

Floor stress: the floor is designed as a sandwich panel. To analyse such a panel, a core thickness and a face thickness are provided as an input together with the floor height and material properties of the core and faces. The design approach follows the method described in HexWeb's article on the subject [35], which facilitates the computation of maximum deflections, face stress and core stress. The floor loading following from the class II design is taken as an input here, which is assumed to be uniformly distributed [1]. Additionally, the loads following from the fuselage shear flow and bending moments are computed. These loads are then combined at each location along the fuselage to find the critical stresses and stress amplitudes.

$$q_b = -\frac{V_y}{I_{zz}} \sum B_r y_r - \frac{V_z}{I_{yy}} \sum B_r x_r \qquad (6.3a) \qquad\qquad q_{s,0} = -\sum \frac{q_b b_{ij} \sqrt{y_r^2 + x_r^2}}{2A_s} \qquad (6.3b)$$

$$T_x = 2A_{s1} q_{t1} + 2A_{s2} q_{t2} \qquad (6.4a)$$

$$\frac{b_{ij}}{2A_{s1} t_{skin}} \sum_{n_{booms_1}} + \frac{w_{floor}}{2A_{s1} t_{floor}} (q_{t1} - q_{t2}) q_{t1} = \frac{b_{ij}}{2A_{s2} t_{skin}} \sum_{n_{booms_2}} q_{t2} + \frac{w_{floor}}{2A_{s2} t_{floor}} (q_{t2} - q_{t1}) \qquad (6.4b)$$

6.1.5 Material Selection

When selecting an appropriate material all aspects of the material have to be taken into consideration. These include, among others, the mechanical properties, machinability, material cost, electroconductivity and interaction with the environment. For Aerospace applications, the specific strength of the material performs an important role to construct a light weight structure. Therefore, the most common materials used in modern aircraft are aluminium and composites, such as Carbon Fibre Reinforced Plastics (CFRP).

The newest aircraft, such as the Boeing 787 [3] and the Airbus A350 [4] consist of approximately 50 % composite material. Composites can be considered superior to metal alternatives since they prove to reduce weight and require less fatigue related inspections, hence reducing maintenance costs [5]. However, some considerations regarding composites have to be taken into account. Firstly, the structural analysis of composites is more complicated than the analysis of metals. The second consideration is their interaction with the environment, since they show to be more sensitive to moisture and temperature differences. Thirdly, the limited impact resistance is a well-known issue. A final consideration is the end of life disposal of composites, since the recycling process is complicated and expensive [36]. It is

---

[3]URL http://www.boeing.com/commercial/aeromagazine/articles/qtr_4_06/article_04_2.html [Cited on 19 June 2016]

[4]URL http://www.airbus.com/aircraftfamilies/passengeraircraft/a350xwbfamily/technology-and-innovation/ [Cited on 19 June 2016]

[5]URL http://www.airbus.com/innovation/proven-concepts/in-design/innovative-materials/ [Cited on 19 June 2016]

therefore decided not to threat the analysis of composites in this design phase and to leave it as a recommendation for the next phase.

Therefore, several aluminium alloys are studied. The alloys that are examined and their mechanical properties are summarized in Table 6.3. The mechanical properties are taken from ASM Aerospace Specification Metals, Inc[6]. Although all alloys are commonly used in several industries, it is chosen to take Al 2024-T3 and Al 7075-T6 further into consideration. Al 2024-T3 is characterized by a high E-modulus, which is important for the buckling criteria. However, Al 7075-T6 has the highest specific strength.

Table 6.3: Aluminium alloy overview

Alloy	ρ [kg/m^3]	E [GPa]	σ_{ult} [MPa]	σ_{yield} [MPa]	σ_{ult}/ρ	σ_{yeld}/ρ
Al 2024-T3	2780	73.1	483	345	0.174	0.124
Al 5052 H38	2680	70.3	290	255	0.108	0.095
Al 6061-T6	2700	68.9	310	276	0.115	0.102
Al 6063-T6	2700	68.9	241	214	0.089	0.079
Al 7050-T74	2830	71.7	524	469	0.185	0.166
Al 7075-T6	2810	71.7	572	503	0.204	0.179

It is decided to use Al 7075-T6 for both the fuselage and the wing box since analysis showed it results in the lowest structural weight for both the fuselage and wing box.

6.2 Fatigue

To determine the exact required maximum stresses during a flight cycle in a structure, one should have a thorough understanding of underlying fatigue mechanisms [31]. While a certain material is to bear a certain stress without failure at the beginning of its life, it might not do so after being subjected to a given number of so called load cycles with a given amplitude and mean stress. This subsection shortly introduces the approach and properties regarding fatigue of aluminium and elaborate on how it was specifically applied to the design of this aircraft.

The aircraft is subjected to several load cases during each flight. From take-off until landing several components of the fuselage may experience both tension and compression, which causes metal fatigue at the rivet holes. To investigate this effect on the load carrying structure, Miner's rule is used [37]. Although this method does not consider the damage done by load cycles under the fatigue limit, it proves to be valid to study the fatigue life in a preliminary manner[7].
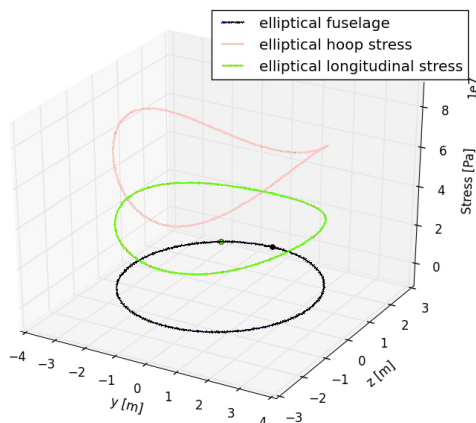
Figure 6.7: Hoop stress and longitudinal stress in [Pa] for the elliptical RELOAD fuselage at 11 [km]
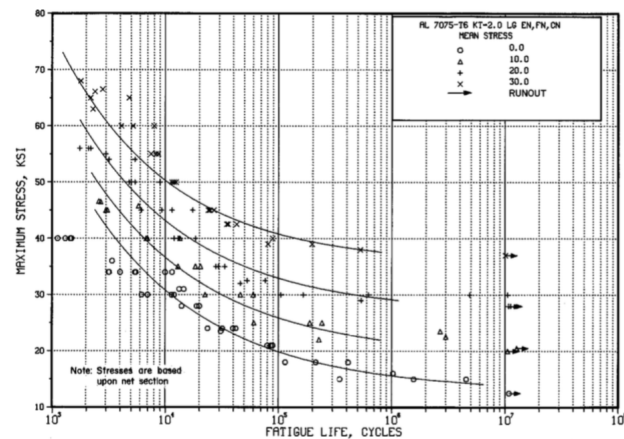
Figure 6.8: SN-curve for notched, K_t=2.0, Al 7075 [38]

Wing box: taking the presented method as a basis for the fatigue analysis, one can analyse the preliminary fatigue behaviour of the wing box. For each load case defined in Table 6.2 the maximum tensile stress in the structure is determined. For this analysis, the maximum payload weight is assumed. A surface roughness correction factor of 0.8 and a reliability correction factor of 0.897 are applied as was done in comparable fatigue studies [39]. The maximum

---

[6]URL http://www.aerospacemetals.com [Cited on 19 June 2016]

[7]Dr. C. Kassapoglou, Aerospace Structures & Computational Mechanics, TU Delft, 15 June 2016, Personal interview

tensile stress at the 1g load condition is taken as the mean stress, and proves to be approximately 168 [MPa]. Using the S-N curve for Al 7075-T6 provided in Figure 6.8, the maximum number of cycles is found for all stresses and cycles. As a final note; a stress factor K_t of 2.0 is used to account for the rivets [34].

The final step of the analysis is to compare the applied cycles to the maximum cycles. This is done by dividing the applied cycles by the maximum cycles for each load case. According to Miner's rule, the total damage in the structure which can be measured by the summation of these ratios, should be lower than one. Since especially the lower skin experiences fatigue, this part is enforced by adding stringers and increasing the sheet thickness. This ensures that Miner's fatigue requirement is met. The final design is found in Table 6.7

Fuselage: for the fuselage, the approach described above is followed with some exceptions. Fatigue failure results from repeated plastic deformation of a material. It is therefore intuitive that the number of load cycles until failure are related to the yield criteria of ductile materials under combined loading, as stated by [40]. Following this method, an equivalent stress amplitude is constructed which is equal to the stress in the fuselage as defined in Equation 6.5. It is found in [40] that Von Mises provides the best fit for fatigue of combined stresses when comparing between Tresca, Von Mises and Rankine principal stresses.

$$\sigma_{eq} = \sqrt{\frac{1}{2} \left[(\sigma_{axial} + \sigma_{p,long} - \sigma_{p,hoop})^2 + (\sigma_{axial} + \sigma_{p,long})^2 + \sigma_{p,hoop}^2 6\tau_s^2 \right]} \qquad (6.5)$$
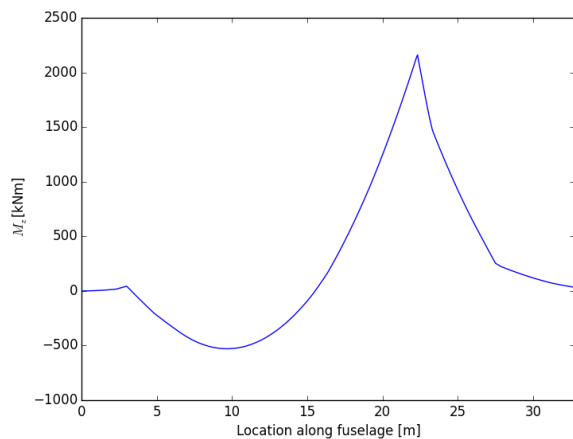
Figure 6.9: Bending moment in the fuselage in cruise, $n = 2.5$
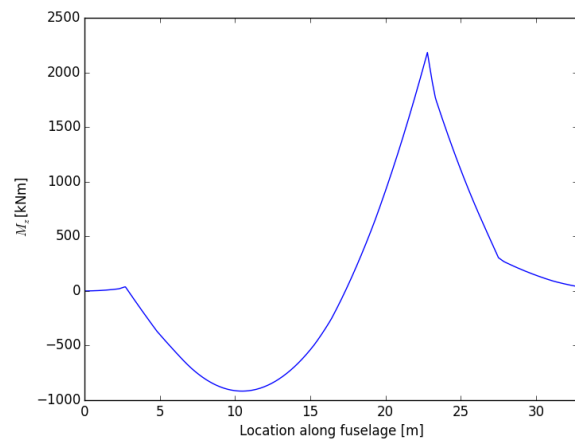
Figure 6.10: Bending moment in the fuselage upon touchdown, $n = 3$

Using Von Mises stresses to motivate an aircraft structural design for fatigue is not a commonly used approach. Therefore it is essential to motivate why this is done in this case. The basis is shown in Section 6.1.2, where the load cases are elaborated on. For a conventional aircraft with a horizontal tail on the aft fuselage, this tail produces a negative lift during cruise flight while the main wing produces positive lift. Together with the distributed weights acting on the fuselage, one is able to derive that the bending moment distribution along the body is highly negative (bottom fuselage in compression) over the main part of the body during cruise. However, the bending moment distribution during landing is largely opposite due to the location of the landing gear and the reaction forces on them. Between the landing gear, the bending moment is expected to be positive while being negative behind the main landing gear.

This is different for the RELOAD aircraft, which is characterised by a very forward placed canard and a relatively aft placed main wing at 10 % and 66 % of the fuselage length, respectively. Furthermore, both the canard and main wing produce positive lift which altogether results in a landing load case and cruise load case that are roughly the same in sign. Figures 6.9 and 6.10 show a 2.5g manoeuvre in flight and landing load case respectively for the bending moments, from which the similarity can be observed. Again taking into account the load cases and cycles described in Table 6.2, the $G_0 = 30$ [μm] S-N curves in Figure 6.11 can be used to derive dedicated fatigue properties of Al 7075-T6 for equivalent stress loadings.

6.3 Fuselage Design

In the coming section, the structural design of the RELOAD fuselage itself is described. Subsequently, the findings are verified and validated to arrive at a final fuselage design.
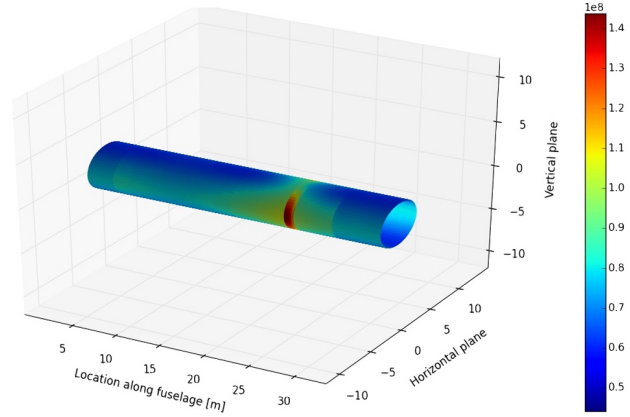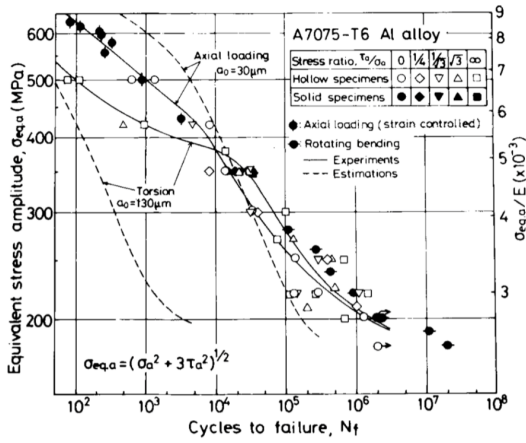
Figure 6.11: Equivalent allowed stress amplitude versus cycles to failure for aluminium 7075-T6 [40]

Figure 6.12: Von Mises stress in $[Pa]$ throughout the fuselage for $n = 3.75$

6.3.1   Structural Design

This subsection elaborates on the final outcomes of the structural design of the fuselage based on the approach described in this chapter. As motivated in Subsection 6.1.5, the chosen material for the fuselage is the aluminium alloy 7075-T6. From Subsection 6.2 it follows that the structure should comply with a list of load cases and cycles according to Table 6.2. Furthermore, it is essential that skin and inter-rivet buckling do not occur under any circumstance below a load factor of $n = 2.5$ and 3g landings. Finally, column buckling is not allowed to occur up till $n_{ult} = 3.75$.

Geometry: the given requirements result in a fuselage design with a number of stringers, a set of stringer dimensions and a skin thickness. The stringer dimensions are mainly influencing the stringer area and inertia, which consecutively dominate the ability of the fuselage to mainly bear bending stresses and resist column buckling. One type of stringers is chosen over the fuselage, which has a so called I-shape. The stringers have a thickness of 2.0 $[mm]$, a width of 10 $[mm]$ and a height of 16 $[mm]$. The amount of stringers necessary to comply with the set requirements is 83, which are evenly spaced over the oval fuselage skin. This number is the minimum required in view of panel buckling of the fuselage skin, which is subjected to combined loadings in multiple directions during flight. Furthermore, the skin thickness t_{skin} is determined to be 1.6 $[mm]$.

The fuselage floor is designed as a honeycomb sandwich panel, for which the chosen materials are aluminium 2024-T3 and aluminium 3003 for the faces and core respectively. The honeycomb faces are both 1.0 $[mm]$ thick and the total floor thickness including the core is 100 $[mm]$. The core has a cell size of 6 $[mm]$ and a density of 54 $[kg/m^3]$ [35].

Forces, moments, torques and stresses: the magnitudes and locations of the extremes are determined for each load case and the results for the landing and ultimate loads are summarized in Table 6.4. Apart from this, the absolute maximum stresses due to the pressure differential when flying at 11 $[km]$ are computed as $\sigma_{longitudinal} = 43.7$ $[MPa]$ and $\sigma_{hoop} = 91.9$ $[MPa]$. The floor is analyzed and designed separately and it is found that at a nominal loading condition at 1g, the maximum deformation in the middle of the floor is 20.5 $[mm]$, while at 3.75g this is 77 $[mm]$. With a fully loaded aircraft, this component experiences a maximum Von Mises load equal to 56 $[MPa]$ in nominal 1g cruise conditions. To display an overview of the global Von Mises stress distribution encountered by the aircraft in the 3.75g load case, a visualisation is presented in Figure 6.12.

Buckling: the structure does not experience plate buckling, column buckling or inter-rivet buckling while subjected to a load factor between $n = -1$ and $n = 2.5$. Above this range, the structure experiences skin buckling between 21 and 23 $[m]$ from the nose. The floor contributes to the stiffness of the fuselage skin as well and is designed to resist intracellular buckling, skin wrinkling and shear crimping up to a load factor of 3.75.

Weight: the weight of the fuselage structure itself is computed from the total materials usage in the fuselage skin, floor, stringers and frames. In order to determine the weight added due to cutouts, the statistical relationship described in Equation 6.6 is used [41]. This equation estimates the mass in $[kg]$ for a cutout in a fuselage as a function of the number of cutouts $n_{cutouts}$, area S_{cutout} in $[m^2]$ and pressure difference Δp in $[bar]$.

$$M_{cutout} = 4.641 \cdot n_{cutouts} \cdot S_{cutout}^{0.976} \cdot (1 + \Delta p)^{4.945} \tag{6.6}$$

Table 6.4: Summary of maximum forces, moments, torques and stresses found in the fuselage

3g Landing	Magnitude	Unit	x [m]	y [m]	z [m]
F_z	882	[kN]	22.79	-	-
F_y	170	[kN]	22.79 - 30.92	-	-
M_y	2.17	[MNm]	22.76	-	-
M_z	1.38	[MNm]	22.76	-	-
T_x	-629	[kNm]	22.79 - 30.92	-	-
$\sigma_{bending}$	66.7	[MPa]	22.78	1.46	2.01
τ_s	73.0	[MPa]	22.78	2.87	-0.54
$\sigma_{VonMises}$	129	[MPa]	22.78	2.94	-0.15
$\sigma_{VonMises,floor}$	168	[MPa]	15.71	-	-
Flight, n=3.75					
F_z	1120	[kN]	22.34	-	-
M_y	3.24	[MNm]	22.32	-	-
$\sigma_{bending}$	87.1	[MPa]	22.78	0.10	2.31
τ_s	91.6	[MPa]	22.78	2.94	-0.15
$\sigma_{VonMises}$	177	[MPa]	22.78	2.94	-0.15
$\sigma_{VonMises,floor}$	209	[MPa]	30.89	-	-

Computing the weights of the individual components results in 2996 [kg] for the fuselage and stringers, a floor weight of 1020 [kg], total frame weight of 986 [kg] and a weight increase due to windows and doors of 437 [kg]. The total weight of the fuselage is then computed as 5439 [kg].

6.3.2 Verification

Verification consists of two main parts. First of all a code verification is performed. Although the program for the fuselage stress analysis has been written carefully and a suitable algorithm was chosen, it is still possible that programming bugs or code inconsistencies are present. These syntax or programming errors are indicated by the program itself and are checked during code verification. When those errors have been solved, the program is 'runnable' and thus able to produce outputs. After that, a solution verification was executed to check whether the numerical model itself does not contain errors.

Singularities: when using the boom method, it is possible that the used algorithm computes either a zero boom area or an infinite boom area due to the automatic boom placement. It is checked if the program correctly deals with these areas by setting them to a finite, but extremely small number so that it does not influence the rest of the program. Furthermore, the code is able to execute computations with the floor at any input height within the fuselage cross-section. Before verification, the area and inertia of the floor explosively rose when placing the fuselage higher than nominal. The equations used here were revised and fixed and with these modifications the verification phase proceeds to the actual comparison of outputs.

Analytical verification: to ensure that the program performs the calculations correctly, beam theory is used to perform a check through analytical calculations [32]. To realise this process in a transparent and effective manner, the fuselage is simplified in the numerical and analytical approach as a circular tube with radius 2.5 [m], a skin thickness of 2.0 [mm] and a floor height of 2.5 [m]. Furthermore, only one distributed weight over the fuselage of 70 tonnes is considered. The results of this verification are presented in Table 6.5. An offset is observed in the moment of inertia about the z-axis, which is an offset that propagates to the shear stress due to the vertical shear force. The discrepancies in the moments of inertia are a consequence of using the boom method, as these are computed based on the boom areas and distances and thus are only an idealised representation of the cross-section [31]. Furthermore, it should be noted that the 24 % offset in vertical shear force at 9.55 [m] is only a result of comparing the relative offset instead of the absolute offset, rendering the small discrepancy as a highly amplified percentage. Based on these outcomes, it is concluded that the fuselage tool is sufficiently accurately performing the desired computations and thus the verification is considered successful.

6.3.3 Validation

Validation is the final step in designing a model that represents a real world accurate fuselage design and can only be performed after verification has been done. When validation is done correctly, one ensures that the model accurately

Table 6.5: Verification results of the fuselage (all forces are in $[kN]$, moments in $[kNm]$ and stresses in $[MPa]$)

	$V_{z,9.55}$	$V_{z,22}$	$M_{y,9.55}$	$M_{y,22}$	$\sigma_{bending,9.55}$	$\sigma_{bending,22}$	$\tau_{s,9.55}$	$\tau_{s,22}$
Numerical	0.041	-229	353	1256	8.99	32.1	0.01	7.29
Analytical	0.054	-229	353	1259	9.01	32.1	0.01	8.10
Discrepancy [%]	24	0.0	0.0	0.2	0.22	0.0	0.0	10.0

	$\sigma_{VonMises,9.55}$	$\sigma_{VonMises,22}$	I_{yy}	I_{zz}
Numerical	9.01	32.1	0.0980	0.104
Analytical	8.99	34.5	0.0982	0.109
Discrepancy [%]	0.24	0.0	0.2	4.6

predicts the stresses in the fuselage and the final layout and properties of the design. Assumption AS-STR-15 is unavoidable for the purpose of this report as proper references on structural test data of fuselages are not available.

For the weight ratio between the fuselage and the OEW, the reference aircraft described in Roskam [42] are used to construct a trendline. Then, this trendline is used to establish estimated fuselage weights for the Airbus A320 and A320neo, as well as the Boeing 737 and 737MAX aircraft.

As presented in Figure 6.13, the RELOAD aircraft, before validation, is not in line with the expected trend. Based on these findings, the requirement on fatigue is reconsidered and adjusted. An ultimate load due to fatigue of 145 $[MPa]$ was previously considered, but deemed too conservative. The current requirement described in Section 6.2 is based on a more in depth fatigue analysis and results in the dimensions and weight as described in Subsection 6.3.1.

6.3.4   Sensitivity Analysis

To visualise the sensitivity of the structural design module to critical input parameters, it is decided that the influence of the fuselage length, fuselage width, center of gravity location and wing position is to be varied with 10 %. These parameters are considered to be most influential and to show their precise influence, the repercussion is tracked through the maximum bending, shear, Von Mises and hoop stresses. The results are presented in Table 6.6, from which is derived that especially the fuselage width and wing position have a large impact on the stresses in the fuselage. Additionally, a statement is made about a potential aircraft family as stated in the system level recommendations in Section 21.2. The structural requirement of having an additional family member is mainly a longer fuselage and more aft wing position. It results from this sensitivity analysis that such measures contribute to an increase and a decrease in stresses for these measures respectively. In total, the fuselage is expected to have roughly the same weight per unit length. This is concluded from a stress analysis where both the wing position and fuselage length are increased and only small differences in maximum stresses are found.

Table 6.6: Results of the sensitivity analysis performed for the RELOAD fuselage

parameter			$\sigma_{bending}$ [MPa]	σ_s [MPa]	$\sigma_{VonMises}$ [MPa]	$\sigma_{p,hoop}$ [MPa]
	Base values		23.21	24.42	90.17	91.92
		%	%	%	%	%
Fuselage length [m]	32.78	+10	8.92	1.68	0.39	0.00
Fuselage length [m]	32.78	-10	-7.24	-2.01	-0.42	0.00
Fuselage width [m]	5.9	+10	-6.89	-0.78	8.55	11.01
Fuselage width [m]	5.9	-10	7.93	0.90	-8.57	-11.42
Center of Gravity [m]	20.3	+10	7.15	0.00	0.01	0.00
Center of Gravity [m]	20.3	-10	-7.11	0.00	0.01	0.00
Wing Position [m]	22.32	+10	-12.88	-9.17	-1.93	0.00
Wing Position [m]	22.32	-10	20.03	9.13	2.10	0.00
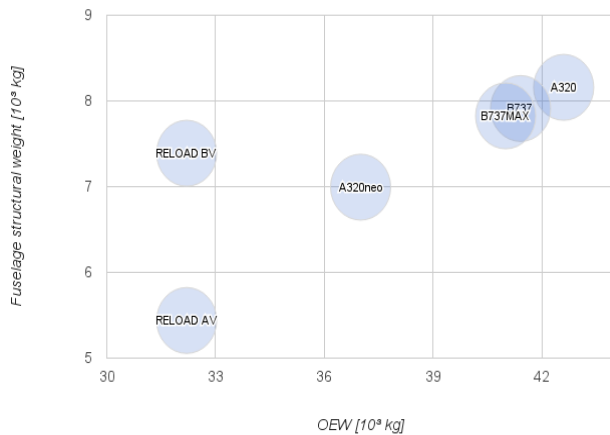
Figure 6.13: Validation weights of the fuselage of RELOAD before (BV) and after (AV) validation, together with reference aircraft
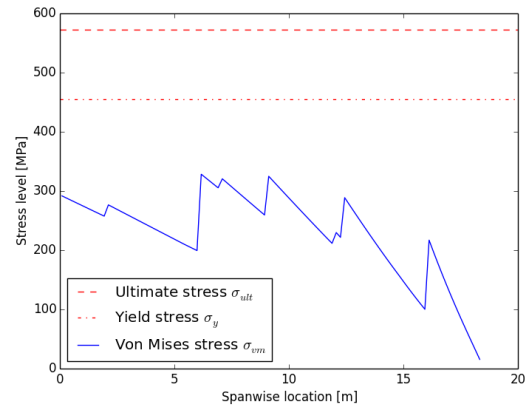
Figure 6.14: Maximum Von Mises stress per element along the span of the wing at 2.5g

6.4 Wing Box Design

In the following subsections, the design of the wing box structure is treated. First the impact of fatigue on the structure is investigated. Then the actual structural design is presented. Finally the outcomes and verification and validation are elaborated on.

6.4.1 Structural Design

In this section the actual structural design of the wing box is presented. The design process includes several iterations and a basic optimisation is done for two types of aluminium, Al 2024-T3 and Al 7075-T6. Finally, it is decided to use the Al 7075-T6 alloy, since it results in a lighter, yet more flexible structure. During the stress analysis only one wing is considered, which is divided in 100 elements.

Geometry: as wing box structure, a "classic" single cell torque box design is selected. This includes two spars at 15 % and 65 % of the chord respectively, a top and bottom skin connecting the two spars, while following the airfoil shape, and stringers to stiffen the structure and avoid buckling. Also ribs are implemented to transfer the aerodynamic loads to the box structure and to provide clamping locations for the skin and stringers.

Due to the variable geometry of the airfoil along the wingspan, the wing box also has to adapt its geometry in span-wise direction. The location of the spars and the length of the skins are automatically updated by the tool using the wing planform geometry set by the aerodynamics group. However, the wing box shape changes abruptly between the two airfoils, not taking into account a gradual change in airfoil as suggested by aerodynamics. A more complex model is required to build and analyse the gradual change. Such an accurate model is therefore recommended for the next design phase.

The thickness and stringer distribution is altered five times, resulting in six different distributions along the span. This is done to render the structure more efficient by removing unnecessary structural elements towards the tip. At every intersection a rib is placed to clamp the skin and the stringers. The average rib spacing is 0.9 [m] to avoid column buckling in the stringers, resulting in a total of 18 ribs in one wing. Each rib has a thickness of 2 mm, based on similar aircraft structures displayed in the Aeroplane Hall of the Faculty of Aerospace Engineering. An overview of the final geometry per section is presented in Table 6.7. After consultation of V. Brugemann [8], it is assumed that the thickness of the spars is varied by riveting additional thin plates together to construct one spar.

Four different types of stringers are used: two I-shaped and two L-shaped types. The I-shaped stringers are placed on the top skin, since they have a higher moment of inertia to resist column buckling due to the compressive loads in the top skin. The width and thickness of all stringers is the same, being equal to 30 [mm] and 1 [mm] respectively. The height of the stringers towards the root is increased due to the higher internal loads.

Forces, moments, torques and stresses: due to the linear lift distribution the internal forces and moments are higher at the root than at the tip. However, this is not true for the Von Mises stress throughout the wing box due to its varying structural geometry. If the Von Mises stress would decrease towards the tip, it would indicate that the structure is overdesigned, resulting in a heavy structure. This indicates the importance of the varying thickness and stringer distribution.

---

[8] V. Brugemann, Structural Integrity and Composites, TU Delft, 10 June 2016, Personal interview

Table 6.7: Thickness and stringer distribution along the span of the wing

Design variable	0 - 2.0	2.0 - 7.0	7.0 - 9.0	9.0 - 12.4	12.4 - 16.1	16.1 - 18.5
Front spar thickness [mm]	20	20	8	7	7	5
Aft spar thickness [mm]	8	8	7	6	6	3
Top skin thickness [mm]	23	21	14	12	9	5
Lower skin thickness [mm]	10	9	9	7	5	2
Number of stringers on top skin	23	23	13	11	6	4
Number of stringers on lower skin	13	13	13	11	4	4
Stringer height [mm]	70	70	50	50	50	50

Figure 6.14 shows the maximum Von Mises stresses for each element of the wing at 2.5g. At this point, the wing box experiences its limit load. The different distributions are recognized by the suddenly increasing stresses. From the graph it is concluded as well that yielding is not limiting the design. However, the analysis showed that for almost all load cases the buckling criteria were constraining.

Buckling: buckling is an important, if not the most constraining failure mode in the wing structure. In total four buckling modes are considered in the analysis: column buckling of the stringers, skin buckling of the top and bottom skin, inter rivet buckling and web shear buckling in the spars. From the analysis it is concluded that skin buckling occurs most often and is mainly avoided by increasing the top skin thickness. The first signs of skin buckling appear at 2.8g near the root of the wing and at 7 [m] from the root at -1.6g.

Weight: the weight of the entire wing box structure (two wings) is determined using the geometry presented above and the density of Al 7075-T6 which is 2810 [kg/m^3] [9]. The total weight is 7135 [kg], of which the combined weight of skin and spar is 6834 [kg]. It is estimated that the fatigue requirement, demanding a reinforced bottom skin at the root and at 7 [m], added approximately 250 [kg] to the design. By assuming a conservative value of 2000 [kg] for secondary wing systems, the total wing weight is estimated to be 9135 [kg].

Although this is rather heavy, the implementation of lightening holes was only considered in the ribs where the weight of each rib was multiplied by a factor 0.7. This factor is based on a visual inspection of wing box structures in the Aeroplane Hall of the Faculty of Aerospace Engineering at Delft University of Technology. Hence, it is expected that the pure structural weight decreases further by a more detailed analysis and by optimising the geometry. A recommendation regarding lightening holes is included in Section 6.5

Deflection and twist: for the wing box structure, also the deflection and the the twist angle are estimated. The deflection is obtained by dividing the internal shear force by the bending stiffness EI, and by numerically integrating it twice with respect to spanwise elements. The twist angle is based on the the torsional stiffness of the closed box structure.

These methods are valid as long as no buckling occurs in the structure. The deformation in that case should also be determined by the post buckling analysis, for which a recommendation is included in Section 6.5. Table 6.8 shows the tip deflection and twist angles for several load cases. The values presented are conservative since they are determined for maximum payload weight.

Table 6.8: Tip deflections and tip angles of twist for several load cases

Load case	Deflection [m]	Twist angle [deg]
-1g	-0.72	0.67
-0.5g	-0.36	0.34
1g	0.72	0.67
2g	1.44	1.34
2.5g	1.80	1.68

6.4.2 Verification

The verification of the wing box structure consists, just as for the fuselage, of two parts: verification of the code and a comparison with an analytical model. Especially the first type proves to be very important for wing box analysis tool.

---

[9]URL http://asm.matweb.com/search/SpecificMaterial.asp?bassnum=MA7075T6 [Cited 20 June 2016]

Code verification: the most complex feature of the wing box program is to set up the geometry correctly. The stress analysis is rather similar to fuselage, if not simpler since it is chosen to use a single cell model for the wing box. The correct geometry and intermediate results are frequently checked by including printing and plotting statements in the code. This highlights a bug which caused the bending stiffness to decrease while increasing the number of stringers.

It is concluded that the tool contains several issues. Firstly, a problem is encountered in how the moment of inertia is calculated using the boom areas. This function requires a different geometry as is outputted by the boom area. Secondly, an inconsistency is found between the function which produces the internal moments and the function which uses these as an input. The first problem is solved by ensuring all functions take the same geometry setup as input, and delivered the results in the same format. The second issue is rectified by implementing more clear names for force and moment variables, referencing to the axis system.

Comparison with an analytical model: to simplify the comparison, the wing box is modeled as a straight box structure with a rectangular, symmetrical and constant cross-section with a length of 20 [m]. The top and bottom skin both have 4 I-shaped stringers, and the thickness of the spars and skin is set to 3 [mm]. The lift and weight are assumed to be constant load distributions, with a small total lift of 50000 [N] and a wing weight of 10000 [N]. Also the number of elements along the span is reduced to ten. In Table 6.9 some parameters are shown to compare the two models. Please note that the values obtained here are only valid for the simplified verification model, and that they are not the results of the actual wing box analysis. From the first three parameters, the conclusion is drawn that the geometry is set up accurately, with all discrepancies below 10 %. The bending stresses along the span are also computed accurately within this margin. Although the difference in shear stress is higher than 10 %, it is assumed that the simplified analytical calculation does not model the situation properly in this case. This assumption is made after careful inspection of intermediate numerical results.

Table 6.9: Comparison of the numerical and analytical model

	I_{xx} [m^4]	I_{zz} [m^4]	Boom area due to M_x [m^2]	$\sigma_{bending,1,top}$ [MPa]	$\tau_s, 1, top$ [MPa]
Numerical	0.00349	0.0103	0.00131	-837	50.6
Analytical	0.0038	0.0105	0.00131	-807.5	44.6
Discrepancy [%]	-8.2	-1.9	0	3.65	13.6

6.4.3   Validation

During validation it is determined whether the tool produces realistic results. Two methods are applied in this section. Firstly, the wing box geometry is compared to similar structures in the Aeroplane Hall. It is concluded that the overall geometry of the final design resembles the similar structures in the Aeroplane Hall. Especially the stringer and rib configuration of the final design seem to be realistic.

Secondly, the weight is compared to the structural wing weight of other aircraft. The wing box of the RELOAD aircraft is heavier than the wing box of the Airbus A320, which is estimated to be 6167 [kg] [43]. The difference is approximately 968 [kg]. This indicates the wing box design is not in line with expectation. However, some considerations have to be taken into account. First of all, the structure is not fully optimised by an algorithm. Next, the initial wing weight estimation to determine the bending relief is 3671 [kg], which is rather low. Also, this number is not updated during the iteration. One can thus expect that the tool set up overestimates the weight. It is also foreseen that more iterations using the current tool, while updating the initial wing weight, already make the weight estimation more realistic.

6.4.4   Sensitivity analysis

It is expected that especially the wing planform parameters such as the aspect ratio, wing surface, sweep angle and taper are influential. These parameters are therefore adapted in the analysis, and their effect is tracked through the compressive stress on the stop skin at the root, on the tip deflection and on the twist angle at the tip. The results are presented in Table 6.10. Analysis shows that varying the wing surface angle has approximately the same impact as varying the aspect ratio.

From the table is derived that especially the aspect ratio has a large impact. This is expected since it determines the wing span. Making the span larger increases the internal bending moment and causes the wing to deflect more. The taper has no effect on the compressive stress. This is because this ratio does not have a big influence on the moment of inertia about the x-axis (I_{xx}), and hence does not affect the stresses produced by the internal moment. Increasing

Table 6.10: Sensitivity analysis of the wing box design

Parameter	Base values		σ_{comp} [MPa] 77.51	Tip deflection [m] 0.94	Twist angle [deg] 0.87
		%	%	%	%
Aspect ratio [-]	7	+10	4.9	27.7	13.8
Aspect ratio [-]	7	-10	-5.2	-26.6	-12.6
Sweep angle [deg]	25.2	+10	2.2	11.7	6.9
Sweep angle [deg]	25.2	-10	-1.9	-10.6	-4.6
Taper [-]	0.3	+10	0	-10.6	-3.4
Taper [-]	0.3	-10	0	12.8	4.6

the sweep angle increases the actual length of the wing box, and has therefore the same effect as increasing the aspect ratio.

6.5 Recommendations

The conceptual design of the fuselage and wing box, as described in this chapter, is carefully performed, verified and validated. Still, the carried out analyses provide no more than a rough sketch of what the final design will be. This section provides a set of recommendations that are considered crucial in service of a successful final design phase.

Specific structural design: the most general, but not least important recommendation is to perform a more in-depth design of the complete aircraft. Up to this point, only an idealised fuselage and wing box are designed. The exact stresses at each point, component placement and dedicated structures such as the tail cone and nose cone are to be investigated for this recommendation. Furthermore, a thorough aeroelastic analysis should be included to ensure structural integrity of the fuselage and wing box under vibrational loads. The more in depth development is scheduled as described in Section 21.1, from which it can be seen that this recommendation is carried out starting in September 2016.

Wing fuselage integration: the integration of the two main structural components of an aircraft is a demanding engineering work package. Not only shall the fuselage allow a cutout the size of a wing box, it is to facilitate landing gear storage as well. The wing fuselage integration is therefore a crucial part of the aircraft, its main objective being to be able to transfer all loads experienced by the wing and fuselage while fulfilling several geometrical constraints. It is therefore recommended to use dedicated computer aided analysis methods to ensure a capable wing fuselage integrating structure, starting in the preliminary design phase (September 2016).

Ribs and frames: one of the components in an aircraft that provide resistance to buckling are ribs and frames. However, these components fulfill multiple other crucial tasks, such as serving as an attachment point for panels and subsystems. Up to this design stage, the ribs and frames are sized conservatively based on reference aircraft and only basic stress calculations are performed. Furthermore their spacing is chosen to fulfill buckling requirements according to the approach formulated in Megson [31]. The recommendation concerning these components is to perform a detailed analysis of what loads each rib and frame should carry and the ideal locations to place them.

Wing tips: wing tips are devices placed at the outer ends of the RELOAD wings which serve multiple purposes, as described in Chapter 5. The current wing box design is based on lift, drag, fuel and component weight forces without taking into account these winglets, as their design is still unfinished. In doing so, the wing box design is ultimately conservative concerning this aspect of the design approach. The reason for this being that winglets can not only cause a vertical bending relief, but a torque relief and horizontal bending relief as well [17]. To potentially reduce the wing box weight, the influence of winglets is to be taken into account by the aerodynamics and structures departments in the preliminary design phase starting in September 2016.

Structural cutouts: when observing the structural designs of frames, ribs, webs and other reinforcing structures throughout existing aircraft, it is noteworthy that most of these components are designed with holes in them. Such a design feature is mainly used to reduce the component's weight while maintaining most of its inertia and to provide means of accessibility inside the structure.[44] For the purpose of this project phase, a detailed structural design is not performed and with that the design of such cutouts is not considered. However, it is expected that these features can offer major weight reductions in both the fuselage and wing box structure. This recommendation is to be carried out by the structural design group in the detailed design phase starting in September 2021.

Composite material usage: for the ambition of the RELOAD conceptual structural design, the boom method approach described by Megson [31] is employed. Although composites were considered and investigated, the choice was made to design a full metal fuselage in line with the expertise of the available structural engineers. However, composites offer clear advantages in the areas of fatigue and weight reduction by optimising the composite build up for a given set of load cases. It is therefore still recommended to investigate composites in future phases of the project, when the degree of expertise and availability of computational tools has surpassed the current state. This recommendation is to be investigated and carried out by a dedicated team of composites experts within the structures department starting in September 2016.

Post buckling analysis: the design choice was made to let the aircraft structure buckle beyond limit load as is done in similar aircraft designs to save weight. However, this implies that the structure weakens beyond limit load as buckling greatly reduces the stiffness of the buckling components. To allow this design option to be implemented, a thorough post buckling analysis should be performed in the preliminary design phase starting in September 2016 to ensure a capable structure in all loading conditions.

<div style="text-align: right; font-size: 4em;">7</div>

Propulsion System Design

In this chapter the propulsion system is tackled. First the tool used to optimise the engine is presented and validated in Section 7.1. The optimisation steps and input values used to reach the final engine design is elaborated on. Next the engine performance and layout are presented and described into detail in Section 7.2. Then the integration of the engine onto the fuselage is discussed in Section 7.3. Finally, a sensitivity analysis is performed and recommendations for further design are made in Section 7.5 and Section 7.6 respectively.

7.1 Software Analysis

In this section the software used for the engine model and performance analysis is presented. The tool is then validated using a reference engine.

7.1.1 Description of the Software

For the optimisation of the RELOAD powerplant it is decided to use a simulation program that is able to replicate gas turbines into detail. The software is called GSP 11 and is designed by NLR [45]. The tool uses non-dimensional modelling of the processes in the different gas turbine components with aero-thermodynamic relations in order to establish a design point. Any deviation from the design point is calculated by solving a set of non-linear differential equations [46].

The tool has an interface which allows the user to first build a model of the engine using components such as inlet, fan, compressors, turbines and combustion chamber. After the model is completed the user can pick a design point, for example the cruise phase, and edit it accordingly. Finally, the user can introduce input values for efficiencies or pressure ratios of each component and then run the program in design mode. The program then generates outputs such as temperatures at different stations as well as the thrust the engine is capable of producing and the inlet and exit area.

The next step is to create an off-design case. Again the ambient conditions need to be set. In this case the user can manually edit the fuel flow in order to size the engine for thrust. The other way around is also possible for an off-design scenario, selecting the desired thrust at take-off and then run the tool to optimise for fuel flow.

7.1.2 Software Validation

Before any engine design and optimisation can be started, the tool needs to be validated. This was done by using the General Electric GE-90 turbofan engine, which is currently being deployed on the Boeing 777 aircraft[1]. The engine was first modelled using GSP 11 and then engine data was introduced in the respective components of the model [47]. The engine parameters can be found in Table 7.1. The values represent the inputs for the design point, which was taken at cruise conditions.

The program is run for the design condition and then for the off-design take-off condition. The inputs which are manually changed for the off-design are the cruise altitude and Mach number, which were both set to 0, as well as the mass fuel flow, which was set to 2.968 $[kg/s]$. It is worth mentioning that the rest of the inputs evaluated in Table 7.1 are adapted by the tool and optimised accordingly for the off-design simulation. The results for both of the

---

[1]URL http://www.boeing.com/commercial/777/#/design-highlights/technology/engine/ [Cited on 1 June 2016]

Table 7.1: Engine data for the GE-90 engine at the design point [47]

Parameter	Unit	Value design point (cruise)
Intake efficiency	[−]	0.98
Fan polytropic efficiency	[−]	0.93
Compressors polytropic efficiency	[−]	0.91
Turbines polytropic efficiency	[−]	0.93
Isentropic nozzle efficiency	[−]	0.95
Spool mechanical efficiency	[−]	0.99
Combustion pressure loss	[−]	0.05
Fuel combustion efficiency	[−]	0.99
Altitude	[m]	10668
Mach number	[−]	0.85
Mass air flow	[kg/s]	576
Mass fuel flow	[kg/s]	1.079
Fan pressure ratio	[−]	1.65
LPC pressure ratio	[−]	1.14
HPC pressure ratio	[−]	21.5
Bypass ratio	[−]	8.1

simulations are compared to engine data in order to check if they match or not. The values from both simulations and the data provided by the manufacturer of the engine can be found in Tables 7.2 and 7.3.

Table 7.2: Output values from GSP simulation compared to engine data at design point conditions [47]

Parameter	Unit	Value manufacturer	Value from GSP	Error margin
TIT	[K]	1380.0	1361.85	1.32 %
SFC	[mg/Ns]	15.6	15.2	2.5 %
Thrust	[kN]	69.2	70.85	2.4 %
OPR	[−]	40.44	40.441	0.003 %

Table 7.3: Output values from GSP simulation compared to engine data at off-design conditions [47]

Parameter	Unit	Value manufacturer	Value from GSP	Error margin
TIT	[K]	1592	1537.98	3.4 %
SFC	[mg/Ns]	7.91	7.90	0.12 %
Thrust	[kN]	375.3	375.84	0.14 %
OPR	[−]	39.97	38.06	4.8 %
Fan pressure ratio	[−]	1.58	1.58	0 %
LPC pressure ratio	[−]	1.1	1.12	1.8 %
HPC pressure ratio	[−]	23.0	21.7	5.6 %
Bypass ratio	[−]	8.4	8.12	3.3 %
Mass air flow	[kg/s]	1350.0	1346.12	0.29 %

As can be concluded from Tables 7.2 and 7.3 the error margins are small. Nonetheless discrepancies are present, due to data which is not available for the GE-90 engine. For example the speed of the rotors at design point or the inertial moment of the spools. The missing inputs are approximated using data from sample models provided by the software. The tool is considered valid since the results provided are sufficiently close to the values provided by the manufacturer.

7.2 Engine Design

In this section the engine, designed in GSP 11, is elaborated on. The model is presented and a description is given for each of its different components. Next, the procedure for the optimisation of the engine is stated and the performance is analyzed. Finally the deterioration and emissions of the engine are briefly touched upon.

7.2.1   Engine Layout

The model that is presented in this subsection is based on the high-bypass turbofan from CFM's LEAP-1A engine[2], the BIGFAN sample model provided by the GSP tool [48] and the General Electric GE-90 engine [47]. The fact is noted that the model presented is not a geared turbofan, but a conventional turbofan. This is because the program does not allow for a geared turbofan to be modelled unless the underlying maps of the model, which are used to define the processes that take place in the gas turbine components, are altered. That is beyond the scope of this report. In Figure 7.1 the layout of the engine is presented as it is modelled in GSP 11. As can be seen the air enters the engine through the inlet, after which the flow is split in a core-side flow, which goes through the core of the engine, and a duct-side flow, which passes through the duct, next to the core. The core flow passes through the low pressure compressor (LPC), into the high pressure compressor (HPC) to be combusted in the combustion chamber. Afterwards the combusted mixture of air and fuel goes into the high pressure turbine, which is attached to the same spool as the high pressure turbine (HPT). After the HPT the flow goes through the low pressure turbine (LPT), which is on the same shaft as the fan and the LPC. Finally, the air passes through the duct of the core and flows into the ambient again through the exhaust.

Before reaching this final layout, other configurations were considered. For example, adding a heat exchanger does not bring any improvements in terms of fuel consumption, only minor benefits in terms of emissions. However, as described in Section 7.2.7, the emissions have to be improved more drastically, therefore the heat exchanger is not needed. A three shafts engine, while providing minor contributions in terms of fuel consumption, is discarded due to the complexity and weight of such a powerplant.
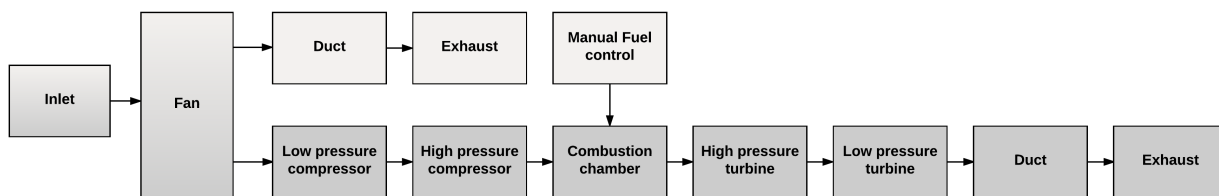
Figure 7.1: GSP 11 turbofan engine model used for RELOAD

7.2.2   Engine Optimisation

The engine design process consisted of several phases. These are described and exemplified below.

- **Referencing:** the first step was to gather reference input data for the model. First the bypass ratio was determined to lie between 10 and 15. The overall pressure ratio of the engine should be 70[3,4] [49–52].

- **Initializing:** the second step consisted of setting the design pressure ratio's and design efficiencies, as well as the inertial spool moments. The initial values used are similar to the GE90's as in Table 7.1. The spool inertial moments were set according to the BIGFAN model.

- **Sizing:** the mass flow at the inlet, the fuel flow and the fuel-to-air ratio are adjusted to reach the required thrust in cruise. The cruise phase is chosen as the design point since this is the most time consuming flight phase of the mission profile.

- **Detailing:** the fourth step is off-design. The atmospheric settings were set to 0 for altitude and Mach. The fuel flow at this stage is adjusted to meet the take-off thrust requirement. The off-design is taken at take-off since this phase requires maximum thrust.

- **Optimising:** the fifth step involved tweaking the values to optimise the engine for the overall pressure ratio which was set in step 1. As a consequence the pressure ratio of the LPT for instance was increased to 1.5 for instance.

- **Iterating:** steps three to five are iterated. After optimisation the thrust is analyzed and the mass air flow and fuel flow are re-evaluated, resulting in a new off-design case which is optimised again. The goal of the iteration was to minimize the fuel flow in cruise and hence lower operating cost and emissions.

- **Exploring:** after the model was optimised other configurations were explored. These other configurations include an engine which is comprised of three shafts or an engine with an added heat exchanger.

---

[2]URL http://www.cfmaeroengines.com/files/brochures/LEAP-Brochure-2013.pdf [Cited on 2 June 2016]
[3]URL http://aviationweek.com/technology/rolls-freezes-design-first-ultrafan-test-gear [Cited on 1 June 2016]
[4]URL http://www.enoval.eu/ [Cited on 1 June 2016]

- **Verifying:** finally the model was verified by MSc. F. Yin[5]. MSc. F. Yin confirmed that the values used were reasonable and in line with the 2030 expectation.

7.2.3 Engine Performance

In Chapter 5, a drag value in cruise of 33.41 [kN] for the entire aircraft is derived. Using this value the required thrust of a RELOAD engine in cruise is calculated to be 16.71 [kN]. Knowing the thrust the process described in Section 7.2.2 is initiated. The same procedure was then applied for the required take-off thrust per engine, which is calculated to be 71.09 [kN]. This value is reached by multiplying the thrust loading of the aircraft with its weight. An overview on the efficiencies and pressure ratios of each engine component at the design point can be found in Table 7.4.

Table 7.4: Efficiencies and pressure ratios of the RELOAD engine components

Parameter	Unit	Value design point (cruise)
Fan core side polytropic efficiency	[−]	0.93
Fan duct side polytropic efficiency	[−]	0.93
LPC polytropic efficiency	[−]	0.91
HPC polytropic efficiency	[−]	0.90
Low pressure shaft design rotor speed	[rpm]	3390
High pressure shaft design rotor speed	[rpm]	10300
Turbines polytropic efficiency	[−]	0.93
Spool mechanical efficiency	[−]	0.99
Spool inertial moment	[kg/m^2]	0.7578
Combustion pressure loss	[−]	0.04
Duct pressure loss	[−]	0.015
Fuel combustion efficiency	[−]	0.995
Fan core side pressure ratio	[−]	1.65
Fan duct side pressure ratio	[−]	1.70
LPC pressure ratio	[−]	1.5
HPC pressure ratio	[−]	23
Heat flux	[kW]	400
Bypass ratio	[−]	13

Finally Table 7.5 comprises the engine performance parameters at design point and off-design. The engine at off-design was sized to make sure that the required take-off thrust is achievable even when deterioration has affected the engine. More information about this aspect can be found in Section 7.2.6.

Table 7.5: Performance parameters of the RELOAD engine at design point and off-design conditions

Parameter	Unit	Value design point (cruise)	Value off-design (take-off)
Mass air flow	[kg/s]	150	319
Mass fuel flow	[kg/s]	0.233	0.595
Net thrust	[kN]	16.84	71.16
SFC	[mg/Ns]	13.8	8.4
TIT	[K]	1561	1907
OPR	[−]	57	38
Inlet area	[m^2]	1.84	1.84
Inlet radius	[m]	0.76	0.76
Exhaust area	[m^2]	1.65	1.65
Exhaust radius	[m]	0.72	0.72

The fuel flow value during cruise of 0.233 [kg/s] per engine is used for determining the reduction of direct operating costs of the RELOAD aircraft. The fuel flow is converted to total fuel cost per hour of 1237 $ per airborne hour using a fuel price of 0.59 [l/h]. Using the fuel cost and Figure 2.1 it can be seen that RELOAD promises to offer a decrease in fuel cost of 911 [$/h]. This translates to a 42.4 % reduction in fuel cost and a 20.42 % reduction in direct operating costs through the use of an improved and low fuel-consuming engine. All the intermediate values of this calculation taken for both engines can be found Table 7.6 and are compared to the average values of the reference aircraft (Airbus A320, Boeing 737-800 and Boeing 737-900). It is worth mentioning that this reduction is only calculated for cruise, it

---

[5]MSc. F. Yin, Propulsion & Power Department, TU Delft, 31 May 2016, Personal interview

is assumed that the weighted average between the high fuel flow during take-off, the low fuel flow during approach and idle cancel each other and do not influence this value considerably, since the cruise phase is the longest part of the flight.

Table 7.6: Improvements in cost and consumption of the RELOAD engines compared to engines used on reference aircraft

Parameter	Unit	RELOAD	Reference aircraft [2]
Fuel consumption	$[kg/h]$	1678	2912
Fuel consumption	$[l/h]$	2097	3640
Fuel price	$[\$/h]$	1237	2148

7.2.4 Nacelle

The purpose of the nacelle is to provide a cover for the engine, while minimising the drag and reducing noise. The nozzle and exhaust system components of the nacelle on the RELOAD engines is designed from titanium alloys, capable of withstanding high temperatures[6]. Meanwhile, the engine casing itself is made from Kevlar honeycomb structures, in order to reduce weight[7]. The nacelle features chevrons in order to reduce the noise created by the mixture of cold and hot air. More information about what kind of chevrons are designed can be found in Section 12.3.3.

7.2.5 Engine Materials

The RELOAD engine is build using high quality, state of the art materials which are implemented in aviation in the coming years. The fans are made of a titanium plated carbon composite[8]. Furthermore the casing of the fan is made of triaxial braded composites which improve the toughness and impact resistance at a lower weight compared to metal casings[9]. The compressors, turbines[10] [11] and combustor[12] feature ceramic matrix composites to increase temperatures, efficiencies and durability[13] [53]. A further recommendation is done in 7.6 for researching the materials of the engine.

7.2.6 Engine Deterioration

Over its lifetime the engine deteriorates. As the number of years in service increases, different aspects start to influence the engine performance more and more . Aspects such as dirt accumulation, mechanical wear or erosion are important and need to be addressed for the safety of the aircraft and its passengers[14] [54].

Fortunately, the GSP tool is able to simulate a certain level of deterioration and provide an overview of how the engine performance is affected by it. The software's interface allows the user to apply deterioration effects and then re-run the tool in order to observe the results. Reductions on performance parameters such as the corrected flow, efficiency and pressure ratio are applied inside compressors, turbines and fan. For an accurate simulation, a reduction of 5% was chosen for all these parameters. This value is considered to be low enough for the aircraft to still be able to operate, even if less efficiently, but high enough to already warn the operating airline to consider replacing the engine. The respective warnings should be given by the Prognostic Health Monitoring System, which is further elaborated on in Section 14.2. However, the possibility of overhauling the engine several times is more than feasible, as it prolongs the engine life considerably and reduce the costs substantially.

The effects of deterioration on performance parameters such as thrust, SFC and OPR for the RELOAD engine in cruise phase can be found in Table 7.7. Table 7.8 shows the required fuel flow, fuel consumption and cost in order for a fatigued engine to achieve the same performance as a new one.

In conclusion it is seen that a deterioration has a significant effect on the operating costs, as it increases the fuel consumption by up to 14 % when compared to an unused engine.

---

[6] URL http://www.safran-group.com/aviation/aircraft-engines-and-nacelles/nacelles [Cited on 16 June 2016]

[7] URL http://www.dupont.com/products-and-services/fabrics-fibers-nonwovens/fibers/uses-and-applications/aerospace-marine-rail.htm [Cited on 16 June 2016]

[8] URL http://www.rolls-royce.com/media/press-releases/yr-2015/pr-180315-rr-composite-technology-hub-in-bristol.aspx [Cited on 3 June 2016]

[9] URL https://spinoff.nasa.gov/Spinoff2006/T_1.html [Cited on 3 June 2016]

[10] URL http://www.geaviation.com/press/other/other_20090309.html [Cited on 3 June 2016]

[11] URL http://www.compositesworld.com/articles/aeroengine-composites-part-1-the-cmc-invasion [Cited on 3 June 2016]

[12] URL http://www.geaviation.com/press/ge90/ge90_20141120.html [Cited on 3 June 2016]

[13] URL http://aviationweek.com/optimizing-engines-through-lifecycle/ge-unveils-cmc-production-ramp-plan [Cited on 3 June 2016]

[14] URL http://www.icao.int/Meetings/EnvironmentalWorkshops/Documents/ICAO-TransportCanada-2006/Hutter.pdf [Cited on 2 June 2016]

Table 7.7: 5% deterioration of the RELOAD engine during cruise

Parameter	Unit	New engine	Deteriorated engine
Thrust	$[kN]$	16.8	14.3
SFC	$[mg/Ns]$	13.8	16.3
OPR	$[-]$	57	52

Table 7.8: Flow, consumption and cost of fuel in cruise for a deteriorated and new engine

Parameter	Unit	New engine	Deteriorated engine
Fuel flow	$[kg/s]$	0.233	0.266
Fuel consumption	$[l/h]$	1049	1197
Fuel cost	$[\$/h]$	619	706

7.2.7 Emissions

As presented in Table 7.6, the improvement of 42.4 % in fuel consumption during cruise also translates to a decrease in emissions. In order to present quantitative results, it is decided to show the amount of CO_2 emissions in $[kg/chair \cdot km]$. These results can be found in Table 7.9. First it should be mentioned that around 2.528 $[kg]$ of CO_2 are emitted per liter of jet fuel[15]. Using the cruise speed, the fuel consumption shown in Table 7.6 and the maximum number of passengers, the emission of CO_2 can easily be computed.

Unfortunately for the NO_X reductions, the same method cannot be applied. There is no exact number that defines the amount of NO_X emitted per kilogram of fuel consumed. However there is an Emissions Databank[16] that summarizes the amount of NO_X emitted during a Landing Take Off cycle (LTO) and also mentions the amount of fuel used during the testing [55]. Using this data, a statistical graph can be produced (see Figure 7.2) and a trend line can be created. Finally, calculating the amount of fuel used by the RELOAD engine for the exact same operations and using the trend line, one can easily approximate the NO_X emissions and compare it with the reference aircraft. The amount of fuel has been calculated for take-off, climb out, approach and idle in the same way that it was done by the ICAO Emission Databank: using the same power settings, times and taking 0.605 $[kg/s]$ as the fuel flow at 100% power setting. The reference aircraft data is taken as the average between the three reference aircraft (Airbus A320, Boeing 737-800 and Boeing 737-900 [55]).
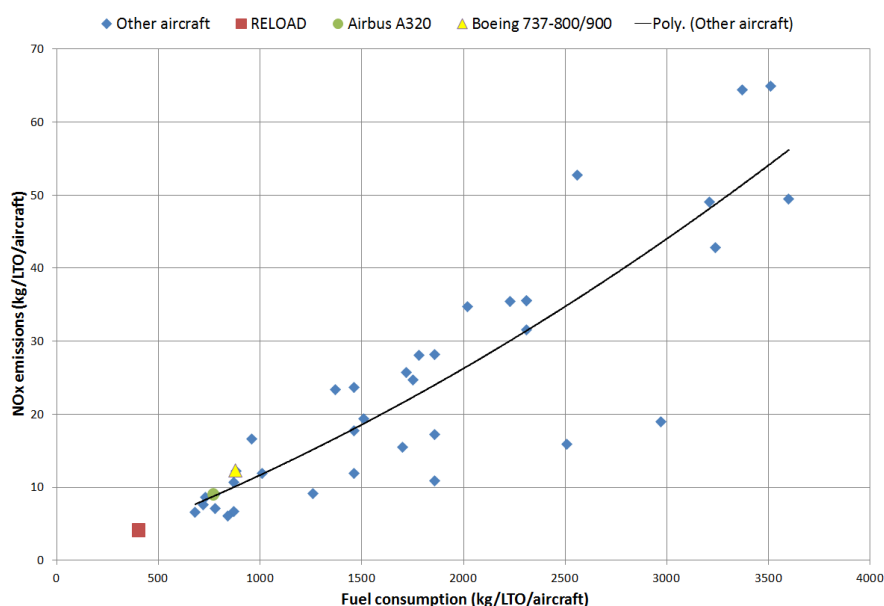
Figure 7.2: NO_X emissions compared to fuel consumption

Lastly the fact is noted that the emission reduction due to bio-fuel are not considered in this analysis, but their potential is further evaluated in Chapter 16.

In conclusion, with a reduction of 39 % in CO_2 emissions and 60.1 % in NO_X emissions, the RELOAD engines do comply with the requirement of 20 % reduction in both emissions.

---

[15]URL https://www.eia.gov/environment/emissions/co2_vol_mass.cfm [Cited on 7 June 2016]

[16]URL https://www.easa.europa.eu/document-library/icao-aircraft-engine-emissions-databank [Cited on 7 June 2016]

[17]URL http://booksite.elsevier.com/9780340741528/appendices/data-a/table-1/table.htm [Cited on 7 June 2016]

[18]URL http://www.airbus.com/aircraftfamilies/passengeraircraft/a320family/a320/ [Cited on 7 June 2016]

Table 7.9: Emission of CO_2 and NO_X of RELOAD and reference aircraft

Parameter	Unit	RELOAD	Ref. AC[2]
Cruise	[km/h]	797.04 [56]	829.69[17]
Fuel use	[l/h]	2097	3640
Fuel use	[l/km]	2.631	4.387
Fuel use	[kg/LTO]	399.2	843.33
Passengers	[$-$]	177	180[18]
CO_2	[kg/km]	6.65	11.09
CO_2	[$kg/chairkm$]	0.0376	0.0616
NO_X	[kg/LTO]	4.47	11.2 [55]

7.3 Engine Integration

This section elaborates on the engine integration of RELOAD. An accurate estimation with respect to its width and length are provided. Several factors were taken into account for the engine positioning, for example safety, noise and structural compliance. The engine placement is evaluated in Sections 12.3.2 and 15.2.

7.3.1 Weight and Dimensions Sizing

In order to size the engine accordingly, an interpolation is done using data from the engines used on reference aircraft, such as the Boeing 737 and A320[19]. A comparison between the diameter of the inlet and the length of the engines is therefore made. For an inlet diameter of 1.52 [m] it resulted that the RELOAD engine will have a length of approximately 2.5 [m]. The nacelle diameter is 10 % larger than the inlet, which measures 1.65 [m][20].

Finally to determine the engine weight, reference engine weight is plotted with respect to the length of reference aircraft engines. As it can be seen in Figure 7.3, the RELOAD engine weights 2350 [kg].

7.3.2 Structural Integration

To check if the engine exhaust heat does not influence the structure of the RELOAD, a comparison is made between the CFM-leap's low pressure turbine inlet temperature. The leap engine is rated at a LPT inlet temperature of 1060 [$degC$] at take-off during certification. In comparison, the RELOAD engine outputs 987.48 [$degC$] at the same stage. This leads to an exhaust temperature at take-off of 517.14 [$degC$]. This is higher than the processing temperatures for aluminium 7075-T6[21], thus a thermodynamic analysis was performed to ensure that the aircraft structure does not suffer from thermostructural effects. To compute the impact of the engine outlet heat on the vertical tail, radiation from the engine exhaust is considered as the supplier of heat. Drainage of this energy from the vertical tail happens both via radiation and convection. To compute these convective effects, a worst case scenario is established with an air temperature of 50 [$degC$] and a conservative convective heat transfer coefficient of air equal to 35 [$-$] [22]. This situation covers full engine thrust at an airspeed equal to taxi velocities. It is found that the maximum temperature occurs at the vertical tail surface, which eventually reaches a maximum equilibrium temperature of 78.15 [$degC$] which is no problem at all for the chosen aluminium alloy. The finding that the engine heat doesn't critically influence the structure is backed up by observing Figure 7.4, from which the heat field of a wing mounted engine can be observed. A similar field can be expected of the RELOAD engine which is of the same engine type.

7.4 Other Subsystems and Components

This section treats the other subsystems and components related to the engine and power generation. The APU is designed here and the fuel type, thrust reverser and bleed air system are described.

7.4.1 Auxiliary Power Unit

In this subsection, the necessity of an APU system is discussed. An APU is a device which acts as a supplement for the main engines during ground operations or engine failure. The APU supplies power for the electrical systems and

---

[19]URL http://www.jet-engine.net/civtfspec.html [Cited on 16 June 2016]
[20]URL http://adg.stanford.edu/aa241/propulsion/nacelledesign.html [Cited on 16 June 2016]
[21]URL http://asm.matweb.com/search/SpecificMaterial.asp?bassnum=MA7075T6 [Cited on 24 June 2016]
[22]URL http://www.engineeringtoolbox.com/convective-heat-transfer-d_430.html [cited on 27-06-2016]
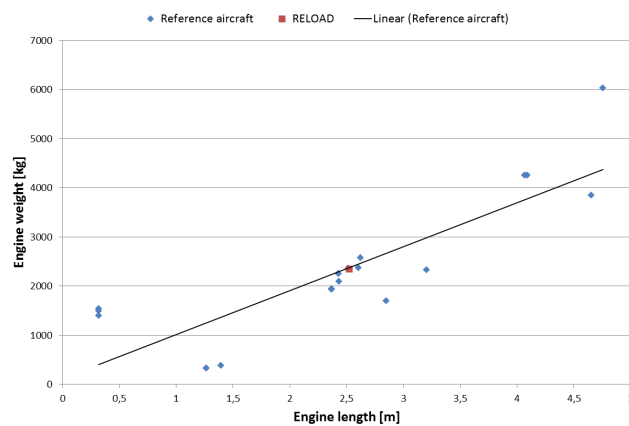
Figure 7.3: Reference aircraft engine lengths plotted against their weights
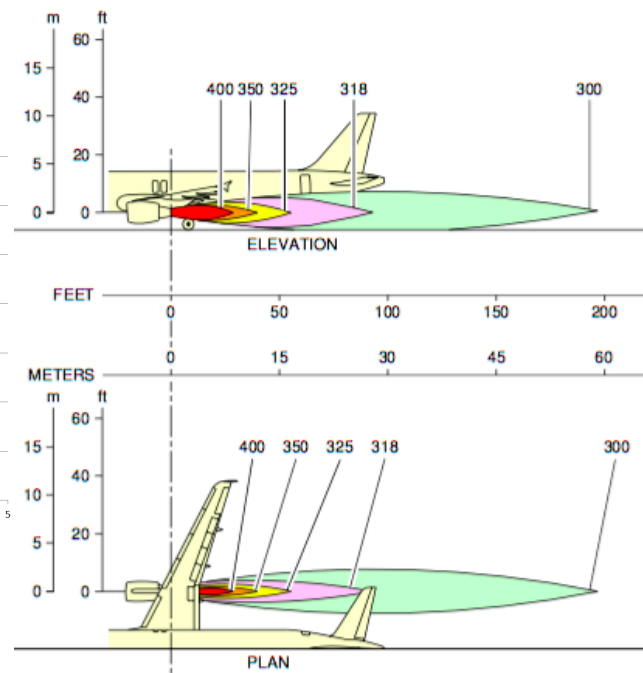
Figure 7.4: Engine heat field of an Airbus A320neo[23]

is used to start the main engines.

For the RELOAD aircraft, an all-electric, variable speed single-shaft APU is used, similar to the APS5000 APU designed by Pratt & Whitney Canada and currently deployed on the Boeing 787 Dreamliner[24]. However, the APS5000 is capable of producing 450 [kVA] at sea level, so the APU placed on RELOAD is sized down to 430 [kVA] according to the power budget requirements which are summarised in Section 11.1. A good visualisation of how the APU is integrated in the electrical system of the RELOAD aircraft is presented in Figure 11.1.

Finally, the APU that is used on RELOAD is expected to have a reduction of at least 50% in noise[25].

7.4.2   Fuel

The fuel used in the GSP 11 model is jet A-1 fuel. The fuel is obtained from fossil resources and has a freezing temperature of -47°. Since these fuels are obtained from crude oil that has been in the ground for millions of years, burning these fuels means putting extra greenhouse gasses into the atmosphere. The RELOAD aircraft is therefore using a mixture of jet A-1 fuel and bio-fuels. The bio-fuels are obtained from renewable resources as plant crops or animal fat [57] and are therefore more CO_2 neutral. The bio-fuels are mixed for 50 % with normal fuel until research allows an even richer mixture of bio-fuel and jet fuel [58].

The main disadvantage of using bio-fuels is the limited supply and a higher price compared to regular bio-fuel. Fortunately the aviation industry is aiming in reducing the carbon based emissions by 50% before 2050, relative to 2005 levels[26]. The most important component in this reduction is undoubtedly going to be the increase in use of bio-fuels. Having said that, it can be safely stated that the demand in bio-fuel is going to increase exponentially, which leads to more efficient and cheaper production techniques and lower the price of bio-fuel to the same level as the Jet A-1 fuel by year 2030 [59].

In conclusion RELOAD uses a fuel mixture of 50 % bio-fuel and 50 % jet A-1 fuel, which reduces the overall fuel life cycle emissions at the same cost.

---

[23]URL: www.airbus.com/fileadmin/media_gallery/files/tech_data/AC/Airbus-AC_A320_01_May_2015.pdf [cited on 27-06-2016]

[24]URL http://www.pwc.ca/en/engines/auxiliary-power-units [Cited on 3 June 2016]

[25]URL http://www.utc.com/News/News-Center/Pages/Hamilton-Sundstrands-Boeing-787-Auxiliary-Power-Unit-undergoes-successful-initia.aspx [Cited on 3 June 2016]

[26]URL http://www.iata.org/policy/environment/pages/climate-change.aspx [Cited on 6 June 2016]

7.4.3 Thrust Reverser

Modern passenger aircraft require high landing speeds and consequently, longer runways in order to have time and space to decelerate. Fortunately, there are other systems besides the wheel brakes that help the aircraft to come to a stop in a relatively short distance. Those system are called thrust reversers and work by diverting the exhaust flow of the engine towards the front of the aircraft.

In high bypass ratio powerplants, such as the RELOAD engine, it is only necessary to divert the flow passing through the duct, also called the cold nozzle, since that flow has a major contribution to the thrust. This makes the system less complex and reduces the cost on materials, since there is no need to obstruct the flow passing through the core of the engine, which is considerably hotter. Nonetheless, the thruster system can represent up to 15% of the engine weight so their mass must not be neglected [14].

In conclusion the RELOAD engine is equipped with a cold stream reverse system. This only comprises cascade vanes which are covered by blocker doors during normal operation. The blocker doors are actuated through the means of an air motor, which opens the blocker doors in order to block the cold nozzle and redirect the output through the cascade vanes[27].

7.4.4 Bleed Air System

In the GSP 11 model of the RELOAD engine the bleed air parameter was not taken into consideration. That is due to the fact that, as further discussed in Section 11.1, RELOAD aims to use a no-bleed architecture in order to improve engine performance, reduce weight and save maintenance costs.

7.5 Sensitivity Analysis

The main parameters defining a turbofan propulsion system are the mass air flow ingested by the inlet and the bypass ratio, because those represent the inputs, while the other parameters are computed by the software. As described in Section7.2.1, for the RELOAD engine, the bypass ratio is chosen to be 13, which is a quite conservative value when compared to the market estimates for 2030, but also slightly higher than the one used by the CFM-LEAP engine[28]. The mass fuel flow is not considered paramount in the design, as it can be varied by the pilot. This parameter remains therefore fixed. In Table 7.10, a sensitivity analysis is performed, where the mass air flow and the bypass ratio are varied and the effect of these variations on thrust, specific fuel consumption and turbine inlet temperature at cruise conditions are shown.

Table 7.10: Sensitivity analysis of the engine at design point

Parameter	Base values	Variation	Thrust [kN] 16.84	SFC [mg/Ns] 13.8	TIT [K] 1561
			%	%	%
Mass air flow [kg/s]	150	+10 %	-0.94	2.9	-0.53
Mass air flow [kg/s]	150	-10 %	4.1	-3.6	4.61
Bypass ratio [$-$]	13	+2	-0.73	0.72	5.9
Bypass ratio [$-$]	13	-2	-0.15	0.72	-5.96

As presented in Table 7.10, a decrease in the mass air flow translates to a decrease in SFC, but also in a consistent increase in the TIT. This is because the fuel to air ratio is higher and the resulting mix has a higher combustion temperature before entering the turbine. Meanwhile, a decrease in bypass ratio would lower the temperature with the cost of also lowering the thrust for the same amount of mass fuel flow. This results in a higher specific fuel consumption.

7.6 Recommendations

This section discusses the recommendations for the further engine design development for the geared turbofan, boundary layer ingestion, fuel cells and materials respectively.

---

[27]URL https://engineering.purdue.edu/ propulsi/propulsion/jets/basics/reverse.html [Cited on 3 June 2016]

[28]URL http://airinsight.com/2011/11/09/comparing-the-new-technology-narrow-body-engines-gtf-vs-leap-maintenance-costs/ [Cited on 24 June 2016]

Geared turbofan   The geared turbofan is a turbofan which makes use of a gearbox in between the fan and the low pressure shaft (LPS). It mimics the use of a third shaft by allowing the fan to rotate at a lower rotation speeds than the LPS. If the fan is coupled directly to the LPS, it has a higher rpm. This may cause the speed at the tips of the fan to be above the speed of sound which distorts the flow into the engine and it increases drag and noise. Therefore by introducing a gearbox, the LPS and the fan can both be ran at optimal speeds[29] [30].

Further analysis of the geared turbofan should involve modelling by a gas turbine simulation programme. Since modelling in GSP 11 would involve changing the maps which are called by the programme and therefore a thorough understanding by the user is needed. Gasturb12 is therefore recommended as this programme is a well known gas turbine simulation programme which features standard maps of geared turbofans. Because it is another programme, a period of a week and a half would be required to get the simulator under control. Another half week to research the influence of the gear ratios, ranging from 1.5 to 5, is needed. Possibly the effect of higher bypass ratio's that can be achieved in the future, ranging from 15 to 20, can be analyzed as well[31].

Boundary Layer Ingestion   Boundary layer ingestion is a method of engine placement where the inlet of the engine is positioned such that it ingests the lower energy flow from the boundary layer. Because of the lower energy flow in the boundary layer, the drag experienced by the engine will be lower. But another consequence is that the pressure recovery by the inlet is lower as well. Although research seems promising, after careful consideration the choice was made to do a recommendation on further research.

At first sight BLI seemed an easy way to improve on fuel consumption. After thorough research though it is concluded that the aerodynamic, mechanical, acoustic and structural effects cannot be assessed in the given time span with the provided tools. Therefore a recommendation is made to assess BLI at a preliminary level in comparison to podded engines. A thorough literature study on the effects of the low-energy flow on the fan should be conducted. Afterwards, a choice for ducted or non-ducted inlet should be made. After the literature study a drag estimation can be made but this should be done on basis of the whole aircraft. It is easy to estimate the division between podded engines and the rest of the aircraft where it is not so straightforward with an engine which is blended into the airframe [60]. Finally, the performance of such a design should be assessed with a CFD tool [61–63]. This should take a month or more, since the knowledge of the researcher with respect to CFD is small.

Fuel Cells   Fuel cells could become a viable replacement for the APU system. Up to 4 % of the fuel that an airline consumes annually is just from taxiing phase[32]. Replacing the APU with fuel cells that would only produce waste such as water, heat and oxygen-depleted air, which would drastically contribute on the reduction of fuel consumption and carbon emissions during the lifetime cycle of an aircraft. This concept has already been tested on a small-scale in 2008, when an Airbus A320 has been fitted with a fuel cell capable of producing 25 $[kW]$ of power[33]. Further, reference based investigations, are expected to take approximately four days.

As the industry is developing and more effort is put on reducing the fuel and emissions, a fuel cell capable of producing at least 100 $[kW]$ of power and entirely replacing an APU become a plausible possibility. However, such an alternative fuel for the aircraft would weigh considerably more, occupy more space and be a potential fire hazard due to its required hydrogen tanks. In the end, the break even point of utilising fuel cells needs to be determined before any such system could be installed on a passenger aircraft [64].

Materials   The materials of the engine are only briefly touched in subsection 7.2.5. For further investigation of the materials of the engine a recommendation is made to investigate all components of the engine and their function thoroughly and do a more elaborate source research new materials and how they are incorporated in the engine. This would take no more than three days.

---

[29] URL http://www.pw.utc.com/PurePowerPW1000G_Engine [Cited on 2 June 2016]

[30] URL https://spinoff.nasa.gov/Spinoff2015/t_1.html [Cited on 2 June 2016]

[31] URL http://www.eurekamagazine.co.uk/design-engineering-features/technology/rolls-commits-to-geared-turbofan/65879 [Cited on 2 June 2016]

[32] URL http://www.ft.com/cms/s/0/dc6235ca-c901-11e5-a8ef-ea66e967dd44.html#axzz4AVTy3zA3 [Cited on 3 June 2016]

[33] URL http://www.airbus.com/innovation/future-by-airbus/future-energy-sources/fuel-cells/ [Cited on 3 June 2016]

<div style="text-align: right; font-size: 3em;">8</div>

Stability and Control Design

During all flight phases and operations the aircraft needs to be stable and controllable. To investigate the aircrafts stability and controllability, this chapter discusses the following subjects. Firstly, the longitudinal and lateral stability and control derivatives are determined. This is shown in Section 8.1. Then, Section 8.2 presents the eigenmode response of the aircraft. The augmented stability and the resulting canard sizing is treated in Section 8.3. The flying characteristics of the aircraft with one engine inoperative are discussed in Section 8.4. Section 8.5 discusses the verification and validation efforts of the software used. Finally, Section 8.6 presents recommendations for the next design phase of the project.

Before emerging in the actual content of this chapter, it is necessary to define the axis system that was used in the computations. Figure 8.1 presents the body axis coordinate system. Please note that all conventions with respect to positive definitions as presented in [65] are followed.
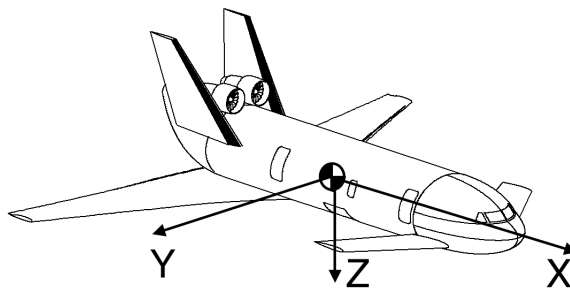
Figure 8.1: The body axis system

8.1 Stability and Control Derivatives

The dynamics of the aircraft are described by a group of parameters, referred to as stability and control derivatives. This section provides the values and formulae used for the longitudinal and lateral derivatives. The definition of each derivative can be found in [65]. The formulae used to obtain the values also originate from [66]. In both references the explanation of each procedure can be found.

To obtain the derivatives, a software tool was created, which allowed the derivatives to be computed using the database previously described [1]. The verification and validation of the tool will be discussed in Section 8.5. The results of the derivative determination are presented in Table 8.1 and 8.2.

For the determination of the control derivatives, it was necessary to size the control surfaces. For the canard, a full moving surface was chosen, such that the elevator surface is equal to that of the canard. The canard will be sized later on in this chapter. The ailerons were chosen to run from 0.7 to 0.95 times the half-span. The rudder runs from 0.1 to 0.9 times the span of the vertical tail-planes. Both the ailerons and rudder start at 0.7 times the chord to the trailing edge. All control surfaces span 30 % of the local chord length.

The linearized equations of motion, as defined in [65], were rewritten in a state-space format and is shown in Equation 8.1 and 8.2 for respectively the longitudinal and lateral motions [65]. The symbols used in the state space system are described in Figure 8.2 and 8.3. In order to excite the state space systems, some parameters still had to be found;

Table 8.1: Longitudinal stability and control derivatives

Deriv.	Sign	Formula	Value
C_{X_0}	-	$-\dfrac{W sin(\gamma_0)}{\frac{1}{2}\rho V^2}$	0
C_{X_u}	<0	$-C_{D_u} + C_{T_{X_u}}$	-0.0286
C_{X_α}	>0	$-C_{D_\alpha} + nC_L$	0.1751
$C_{X_{\dot{\alpha}}}$	-	neglected [65]	0
C_{X_q}	-	neglected [65]	0
$C_{X_{\delta c}}$	-	neglected [65]	0
C_{Z_0}	>0	nC_L	0.4817
C_{Z_u}	<0	$-C_{L_u} - 2nC_L$	-1.3746
C_{Z_α}	<0	$-C_{L_\alpha} - C_{D_1}$	-6.6725
$C_{Z_{\dot{\alpha}}}$	-	neglected [65]	0
C_{Z_q}	>0	$\dfrac{2C_{L_{\alpha_c}}(x_{ac_c}-x_{cg})S_c}{S}$	1.4039
$C_{Z_{\delta c}}$	<0	$-C_{N_{\delta c}}\dfrac{S_c}{S}$	-0.0248
C_{m_u}	<0	$-C_{L_1}\dfrac{\partial x_{ac}}{\partial M}$	-0.0683
C_{m_α}	<0	$C_{N_{w\alpha}}\dfrac{x_{cg}-x_w}{\bar{c}} - C_{N_{c\alpha}}\dfrac{S_c l_c}{S\bar{c}}$	-12.7201
$C_{m_{\dot{\alpha}}}$	-	neglected [65]	0
C_{m_q}	<0	$-1.1C_{Z_q}(x_{ac_c}-x_{cg})$	-0.8439
$C_{m_{\delta c}}$	<0	neglected [65]	0

Table 8.2: Lateral stability and control derivatives

Deriv.	Sign	Formula	Value
C_{Y_β}	<0	$C_{Y_{\beta_w}} + C_{Y_{\beta_f}} + C_{Y_{\beta_v}}$	-1.8243
$C_{Y_{\dot{\beta}}}$	-	neglected [65]	0
C_{Y_p}	<0	neglected [65]	0
C_{Y_r}	>0	$-2C_{Y_{\beta_v}}\dfrac{l_v cos(\alpha)+z_v sin(\alpha)}{b}$	0.9441
$C_{Y_{\delta a}}$	-	neglected [66]	0
$C_{Y_{\delta r}}$	>0	$\dfrac{\partial C_{Lv}}{\partial \delta_r}\left(\dfrac{S_v}{S}\right)\left(\dfrac{V_v}{V}\right)^2$	2.6574
C_{l_β}	<0	$C_{l_{\beta_{wf}}} + C_{l_{\beta_c}} + C_{l_{\beta_v}}$	-0.1908
$C_{l_{\dot{\beta}}}$	-	neglected [65]	0
C_{l_p}	<0	$C_{l_{p_w}} + C_{l_{p_c}} + C_{l_{p_v}}$	-0.6212
C_{l_r}	>0	$C_{l_{r_w}} + C_{l_{r_v}}$	0.3359
$C_{l_{\delta a}}$	<0	$\dfrac{2\frac{\partial C_{Lw}}{\partial \delta_a}\int_{y_{inner}}^{y_{outer}} c(y)dy}{Sb}$	-0.0279
$C_{l_{\delta r}}$	>0	$\dfrac{z_v cos(\alpha)-l_v sin(\alpha)}{b}C_{Y_{\delta r}}$	0.0561
C_{n_β}	>0	$C_{n_{\beta_w}} + C_{n_{\beta_f}} + C_{n_{\beta_v}}$	0.2010
$C_{n_{\dot{\beta}}}$	-	neglected [65]	0
C_{n_p}	<0	$C_{n_{p_w}} + C_{n_{p_v}}$	-0.5326
C_{n_r}	<0	$C_{n_{r_w}} + C_{n_{r_v}}$	-0.3143
$C_{n_{\delta a}}$	>0	$K_a C_{L_w} C_{l_{\delta a}}$	0.0017
$C_{n_{\delta r}}$	<0	$-C_{Y_{\delta r}}\dfrac{l_v cos(\alpha)+z_v sin(\alpha)}{b}$	-0.0893

the dimensionless mass parameters μ_c and μ_b and the mass moment of inertia. The former two could be calculated. The mass moments of inertia, however, were more difficult to ascertain. Initially, the values of the B737 were used. They were extracted from the same source as the validation data used in a later section[1]. The final values of the inertia could be obtained from the CATIA visualization, however, still some uncertainty remains, as the final arrangement of all cabin components (especially the movable ones, such as catering trolleys, and so on) is not fixed.

$$
\begin{bmatrix} \dot{\hat{u}} \\ \dot{\alpha} \\ \dot{\theta} \\ \frac{\dot{q}\bar{c}}{V} \end{bmatrix} = \begin{bmatrix} x_u & x_\alpha & x_\theta & 0 \\ z_u & z_\alpha & z_\theta & z_q \\ 0 & 0 & 0 & \frac{V}{\bar{c}} \\ m_u & m_\alpha & m_\theta & m_q \end{bmatrix} \begin{bmatrix} \hat{u} \\ \alpha \\ \theta \\ \frac{q\bar{c}}{V} \end{bmatrix} + \begin{bmatrix} x_{\delta_e} & x_{\delta_t} \\ z_{\delta_e} & z_{\delta_t} \\ 0 & 0 \\ m_{\delta_e} & m_{\delta_t} \end{bmatrix} \begin{bmatrix} \delta_e \\ \delta_t \end{bmatrix} \tag{8.1}
$$

$$
\begin{bmatrix} \dot{\beta} \\ \dot{\varphi} \\ \frac{\dot{p}b}{2V} \\ \frac{\dot{r}b}{2V} \end{bmatrix} = \begin{bmatrix} y_\beta & y_\varphi & y_p & y_r \\ 0 & 0 & 2\frac{V}{b} & 0 \\ l_\beta & 0 & l_p & l_r \\ n_\beta & 0 & n_p & n_r \end{bmatrix} \begin{bmatrix} \beta \\ \varphi \\ \frac{pb}{2V} \\ \frac{rb}{2V} \end{bmatrix} + \begin{bmatrix} 0 & y_{\delta_r} \\ 0 & 0 \\ l_{\delta_a} & n_{\delta_r} \\ n_{\delta_a} & n_{\delta_r} \end{bmatrix} \begin{bmatrix} \delta_a \\ \delta_r \end{bmatrix} \tag{8.2}
$$

8.2 Eigenmodes

Since all control and stability derivatives are defined and a state space system of RELOAD is formed, it is possible to perform the analysis of the eigenmodes of the aircraft. First of all, the symmetric eigenmotions shall be treated. Secondly, the asymmetric eigenmotions are presented. The dutch roll shall be the main point of focus.

There are four symmetrical eigenvalues associated to the symmetrical system; two pairs of conjugate eigenvalues, as can be seen in Figure 8.4 and 8.5. By applying a step input to the canard, a short period and phugoid response were gained. Figure 8.4 presents the short period response, with the characteristic data for this eigenmotion. Figure 8.5 presents the same for the phugoid, an airspeed versus time plot. As can be seen, both eigenmotions are stable.

For the asymmetrical eigenmotions, again four eigenvalues are found; one conjugate pair and two real eigenvalues, as can be seen in Figure 8.6. They correspond to the dutch roll, Aperiodic Roll and Spiral, respectively. Since the real part of all eigenvalues is negative, all asymmetric eigenmotions are stable. Figure 8.7 presents the results of the dutch roll eigenmotion. The aperiodic roll is stable as well, because its eigenvalue is negative. Finally, the spiral is

---

[1] URL https://github.com/arktools/pydatcom/blob/master/test/data/B-737.out [Cited on 6 June 2016]

	$x_{...}$	$z_{...}$	$m_{...}$
u	$\dfrac{V}{\bar{c}}\dfrac{C_{X_u}}{2\mu_c}$	$\dfrac{V}{\bar{c}}\dfrac{C_{Z_u}}{2\mu_c-C_{Z_{\dot\alpha}}}$	$\dfrac{V}{\bar{c}}\dfrac{C_{m_u}+C_{Z_u}\frac{C_{m_{\dot\alpha}}}{2\mu_c-C_{Z_{\dot\alpha}}}}{2\mu_c K_Y^2}$
α	$\dfrac{V}{\bar{c}}\dfrac{C_{X_\alpha}}{2\mu_c}$	$\dfrac{V}{\bar{c}}\dfrac{C_{Z_\alpha}}{2\mu_c-C_{Z_{\dot\alpha}}}$	$\dfrac{V}{\bar{c}}\dfrac{C_{m_\alpha}+C_{Z_\alpha}\frac{C_{m_{\dot\alpha}}}{2\mu_c-C_{Z_{\dot\alpha}}}}{2\mu_c K_Y^2}$
θ	$\dfrac{V}{\bar{c}}\dfrac{C_{Z_0}}{2\mu_c}$	$-\dfrac{V}{\bar{c}}\dfrac{C_{X_0}}{2\mu_c-C_{Z_{\dot\alpha}}}$	$-\dfrac{V}{\bar{c}}\dfrac{C_{X_0}\frac{C_{m_{\dot\alpha}}}{2\mu_c-C_{Z_{\dot\alpha}}}}{2\mu_c K_Y^2}$
q	$\dfrac{V}{\bar{c}}\dfrac{C_{X_q}}{2\mu_c}$	$\dfrac{V}{\bar{c}}\dfrac{2\mu_c+C_{Z_q}}{2\mu_c-C_{Z_{\dot\alpha}}}$	$\dfrac{V}{\bar{c}}\dfrac{C_{m_q}+C_{m_{\dot\alpha}}\frac{2\mu_c+C_{Z_q}}{2\mu_c-C_{Z_{\dot\alpha}}}}{2\mu_c K_Y^2}$
δ_e	$\dfrac{V}{\bar{c}}\dfrac{C_{X_{\delta_e}}}{2\mu_c}$	$\dfrac{V}{\bar{c}}\dfrac{C_{Z_{\delta_e}}}{2\mu_c-C_{Z_{\dot\alpha}}}$	$\dfrac{V}{\bar{c}}\dfrac{C_{m_{\delta_e}}+C_{Z_{\delta_e}}\frac{C_{m_{\dot\alpha}}}{2\mu_c-C_{Z_{\dot\alpha}}}}{2\mu_c K_Y^2}$
δ_t	$\dfrac{V}{\bar{c}}\dfrac{C_{X_{\delta_t}}}{2\mu_c}$	$\dfrac{V}{\bar{c}}\dfrac{C_{Z_{\delta_t}}}{2\mu_c-C_{Z_{\dot\alpha}}}$	$\dfrac{V}{\bar{c}}\dfrac{C_{m_{\delta_t}}+C_{Z_{\delta_t}}\frac{C_{m_{\dot\alpha}}}{2\mu_c-C_{Z_{\dot\alpha}}}}{2\mu_c K_Y^2}$

Figure 8.2: Symbols appearing in longitudinal state space Equation 8.1 using the stability and control derivatives of Table 8.1

	$y_{...}$	$l_{...}$	$n_{...}$
β	$\dfrac{V}{b}\dfrac{C_{Y_\beta}}{2\mu_b}$	$\dfrac{V}{b}\dfrac{C_{\ell_\beta}K_Z^2+C_{n_\beta}K_{XZ}}{4\mu_b\left(K_X^2 K_Z^2-K_{XZ}^2\right)}$	$\dfrac{V}{b}\dfrac{C_{\ell_\beta}K_{XZ}+C_{n_\beta}K_X^2}{4\mu_b\left(K_X^2 K_Z^2-K_{XZ}^2\right)}$
φ	$\dfrac{V}{b}\dfrac{C_L}{2\mu_b}$	0	0
p	$\dfrac{V}{b}\dfrac{C_{Y_p}}{2\mu_b}$	$\dfrac{V}{b}\dfrac{C_{\ell_p}K_Z^2+C_{n_p}K_{XZ}}{4\mu_b\left(K_X^2 K_Z^2-K_{XZ}^2\right)}$	$\dfrac{V}{b}\dfrac{C_{\ell_p}K_{XZ}+C_{n_p}K_X^2}{4\mu_b\left(K_X^2 K_Z^2-K_{XZ}^2\right)}$
r	$\dfrac{V}{b}\dfrac{C_{Y_r}-4\mu_b}{2\mu_b}$	$\dfrac{V}{b}\dfrac{C_{\ell_r}K_Z^2+C_{n_r}K_{XZ}}{4\mu_b\left(K_X^2 K_Z^2-K_{XZ}^2\right)}$	$\dfrac{V}{b}\dfrac{C_{\ell_r}K_{XZ}+C_{n_r}K_X^2}{4\mu_b\left(K_X^2 K_Z^2-K_{XZ}^2\right)}$
δ_a	$\dfrac{V}{b}\dfrac{C_{Y_{\delta_a}}}{2\mu_b}$	$\dfrac{V}{b}\dfrac{C_{\ell_{\delta_a}}K_Z^2+C_{n_{\delta_a}}K_{XZ}}{4\mu_b\left(K_X^2 K_Z^2-K_{XZ}^2\right)}$	$\dfrac{V}{b}\dfrac{C_{\ell_{\delta_a}}K_{XZ}+C_{n_{\delta_a}}K_X^2}{4\mu_b\left(K_X^2 K_Z^2-K_{XZ}^2\right)}$
δ_r	$\dfrac{V}{b}\dfrac{C_{Y_{\delta_r}}}{2\mu_b}$	$\dfrac{V}{b}\dfrac{C_{\ell_{\delta_r}}K_Z^2+C_{n_{\delta_r}}K_{XZ}}{4\mu_b\left(K_X^2 K_Z^2-K_{XZ}^2\right)}$	$\dfrac{V}{b}\dfrac{C_{\ell_{\delta_r}}K_{XZ}+C_{n_{\delta_r}}K_X^2}{4\mu_b\left(K_X^2 K_Z^2-K_{XZ}^2\right)}$

Figure 8.3: Symbols appearing in lateral state space Equation 8.2 using the stability and control derivatives of Table 8.2

Short period characteristics:
Period P = 1.263 [s]
Damping ratio ζ = 0.065 [-]
$T_{0.5}$ = 2.119 [s]

Eigenvalues:
-0.3269 $\pm$j 4.97322

Figure 8.4: A short period motion, in response to a step elevator input

Phugoid characteristics:
Period P = 65.96 [s]
Damping ratio ζ = 0.015 [-]
$T_{0.5}$ = 477.2 [s]

Eigenvalues:
-0.0014 $\pm$j 0.09525
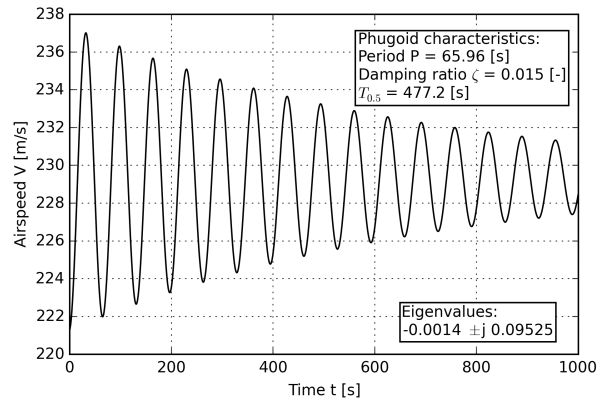
Figure 8.5: A phugoid motion, in response to a step elevator input

just unstable, but the motion is slow (T_2 = 394 [s]). This is therefore an acceptable result. To arrive at this results, some adaptations to the aircraft geometry were executed. Firstly, to enhance the dutch roll stability, a dihedral of $-1°$ was added to the main wing. Furthermore, the vertical tailplane sizing was re-iterated. The results of this iteration are presented in Section 8.3.3.

8.3　Augmented Stability

During the analysis of the stability and controllability of the aircraft it was found that the aircraft had insufficient design space with respect to the allowable center of gravity ranges and canard surface area. This is illustrated in Figure 8.8. To improve the characteristics of the aircraft it is chosen to implement an augmented stability control system with the canard. By itself the canard has a destabilizing effect but by actively controlling the canard during disturbances this destabilizing effect can be converted to a stabilizing effect. Visualizing the augmented stability is done using a gain on the canard contribution. The stability curve of the augmented aircraft is given by Equation 8.3. It should be noted that the canard length (l_c) is negative, since it lies in front of the center of gravity. The down-wash from the canard experienced by the main wing is already incorporated in C_{L_α} and is therefore omitted from the equations. The down-wash is normally not constant due to the augmentation and constant movement of the canard. Assuming a constant down-wash is conservative. If, for example, due to a disturbance the aircraft needs to pitch up, the canard angle of attack will increase which results in a increase in down-wash and therefore a less effective angle of attack of the main wing. The main wing will lose lift which in turn increase the desired pitch up moment further.
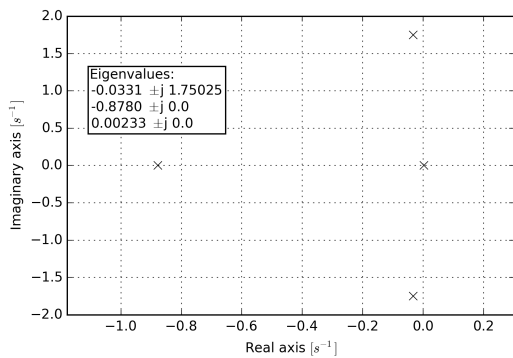
Figure 8.6: The asymmetric eigenvalues plotted
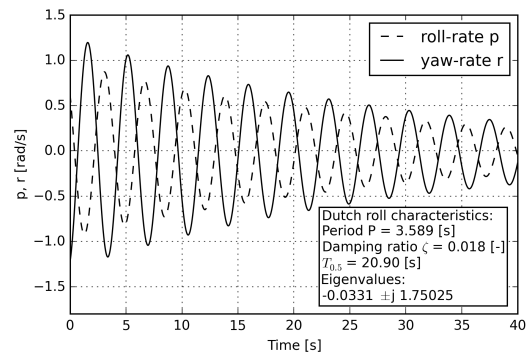
Figure 8.7: A dutch roll motion, in response to an impulse aileron input

$$x^-_{cg} = x^-_{ac} + K_{gain} \cdot \frac{C_{L\alpha_c}}{C_{L_\alpha}} \frac{S_c l_c}{S\bar{c}} \left(\frac{V_c}{V} \right)^2 \qquad (8.3)$$

Equation 8.3 can be rewritten to C_{m_α} and is given in Equation 8.4. C_{m_α} also represents the augmented stability derivative for the RELOAD aircraft used during the eigenmode analysis in Section 8.2.

$$C_{m_\alpha} = C_{L_\alpha} \left(x^-_{cg} - x^-_{ac} \right) - K_{gain} \cdot C_{L\alpha_c} \frac{S_c l_c}{S\bar{c}} \left(\frac{V_c}{V} \right)^2 \qquad (8.4)$$

A gain of one corresponds to an aircraft without augmentation. Lowering the gain decreases the destabilizing effect until a gain of zero. A zero gain effectively is an aircraft without a canard or in RELOAD's case the canard following the undisturbed free stream airflow, resulting in no lift difference due to the disturbance on the canard. A negative gain corresponds to the canard counteracting the disturbance with a negative angle of attack with respect to the effective disturbance angle of attack. Figure 8.8 shows the stability curves for the un-augmented canard as well as the augmented canard. As can be seen, the control curve is not altered.
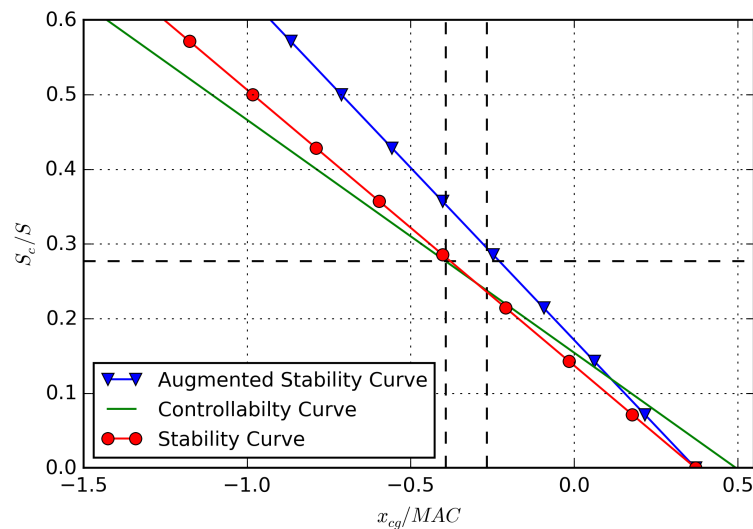
Figure 8.8: Controllability, stability and augmented stability (gain = 0.7) curves for RELOAD

The effect of an augmented stability control system is shown to be effective in Figure 8.8, but to ensure the aircraft is controllable during disturbances limits have to be set to prevent the canard using too large deflections to counter the disturbances. CS-25 regulation stipulate a maximum disturbance of 17.07 $[m/s]$ at sea level [4], which combined with a stall speed of 50.6 $[m/s]$ results in a maximum disturbance angle of attack of 18.8 [deg]. A maximum deflection of 6 [deg] is used for augmenting the stability. resulting in a maximum allowable gain of -0.32. The center of gravity range of RELOAD is shown using the two vertical lines. The horizontal line shows the smallest allowable canard size while complying to stability and controllability. To reduce complexity whilst fulfilling the requirement on the canard actuation system the gain is chosen to just have the center of gravity ranges fit between both curves. This is achieved using a gain of 0.7 which is plotted in Figure 8.8.

To model the augmented stability as described it is needed to have an all-moving canard. A fixed canard with an elevator will stall during large disturbances resulting in a loss of ability to augment the stability. By having an all-moving canard, the whole surface can re-orientate itself to have a desired angle of attack with respect to the free-stream. Thereby retaining the ability to augment the stability. The maximum deflection should at least be equal to the maximum disturbance angle times the needed gain, plus the effective range of angles of attack for the airfoil. For RELOAD it is calculated the canard needs to change its attitude by 23.2 [deg] in either a positive or negative deflection. The aforementioned range of movement is rather conservative, as during a maximum disturbance the canard can stabilize the aircraft and have an additional 10 [deg] range to control and trim the aircraft. Furthermore, the canard can swivel upwards with a 75 [deg] angle, to allow for more effective ground operations. This can be executed by a different actuation system, since it has to be neither fast, nor extremely accurate.

The controllability of the aircraft is limited by the approach phase and the maximum lift coefficient of the airfoil. To enhance the controllability of the RELOAD a morphing trailing edge flap is used on the canard, increasing the curvature of the airfoil during the limiting approach phase and thereby increasing the maximum achievable lift coefficient. The morphing trailing edge does not need the same response rates as the canard control system. A recommendation for the canard design is to further look into curved airfoils combined with morphing HLDs. For now a symmetrical airfoil is assumed for this canard design.

8.3.1 Augmented Control System Design

An overview of the augmented stability control system is given in Figure 8.9. The control system contains a gain, a servo and a feedback loop to stabilize the aircraft. A simple transfer function is used to model the servo using a break frequency of a = 40 [Hz], as suggested by [67]. To measure the error in the feedback loop a direct angle of attack sensor is chosen over a load sensor. An angle of attack sensor can measure the disturbance ahead of the canard reducing the delay between measurement and control of the canard. Several types of angle of attack sensors can be considered. For example a pitot tube with a second pressure port on an angled surface or a small vane which measures the lift force due to the disturbance. Several different sensors are already available and it is believed the sensors will be able to be certified before 2025.
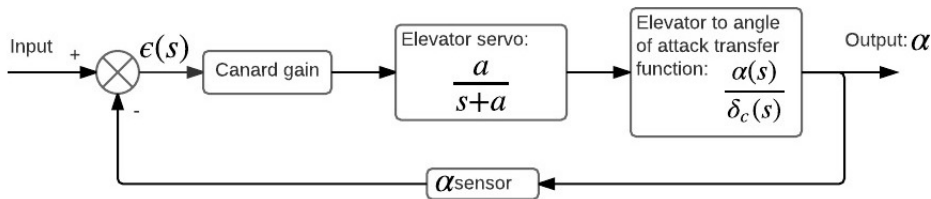
Figure 8.9: The block diagram corresponding to the augmented stability system, inspired by [67]

The elevator deflection angle to angle of attack transfer function was extracted from the symmetric state-space system which was created in the program presented in Section 8.1, 8.2 and 8.5:

$$\frac{\alpha(s)}{\delta_c(s)} = \frac{-0.05744s^3 - 6.674s^2 - 0.02207s - 0.05827}{s^5 + 20.84s^4 + 57.7s^3 + 812.7s^2 + 2.888s + 6.986} \tag{8.5}$$

The F-16 fighter aircraft, which is designed more than 30 years ago, uses an actuation system which is capable of a rate limit of 60 [°/s] for the all moving elevator surface [68]. Fighter aircraft are known for their high performance and therefore need fast and reliable surface actuation systems. The canard size of RELOAD is larger and therefore more heavy than the elevator of a F-16, but does not need the same performance to control and stabilize the aircraft. RELOAD has the added benefit of having more space available to house the control system and actuators than a fighter aircraft. Therefore it is expected to have the technology adapted to the needs of RELOAD before 2030 and is feasible for use in this project. Further recommendations are presented in Section 8.6 for developments needed during the following design phase. These recommendations include further research on the weight of the actuation system, the power needed and the reduction of the actuation range.

8.3.2 Canard Sizing

Using the augmented stability curve from Figure 8.8, the canard surface was found. For the canard a symmetric NACA-0010 airfoil is chosen. A downside of symmetric airfoils is the limited lift coefficient of ∼ 1 at ∼ 10 [deg] angle of attack. For the planform the same equations as in Midterm for the wing planform are used. With the surface area of the canard and a chosen aspect ratio and taper ratio, the span and chords can be calculated. Table 8.3 gives an overview of the resulting sizing of the canard.

Table 8.3: Final results of the canard planform design

Parameter	S [m^2]	A	λ [−]	b [m]	c_r [m]	c_t [m]	MAC [m]	Y [m]	Λ_{canard} [°]
Canard	43.9	5	0.5	14.8	4.0	2.0	3.11	3.29	37.5

8.3.3   Vertical Tail Planform sizing

In the Midterm report the surface area of the vertical tails was sized with an approximating formula from Torenbeek [1, 25]. This surface was updated using the latest values from the Database and iterated to get an optimum design. These design values can be seen in Table 8.4. The vertical tail design was iterated using the results from the stability analysis. It was chosen to use a dual vertical tail. On one hand because the vertical arm between the centre of gravity and the aerodynamic center of the tailplane remains smaller, on the other hand to use the tails to shield the engines and thus reduce noise. The engines are thus placed such that their exhausts are located in between the two vertical fins.

To reach the final surface, a few iteration steps were performed. The initial surface area came from the Class-II design stage and results in an unstable dutch roll mode. By increasing the surface the eigenmotion was rendered stable. The resulting surface is however unfeasibly large. The wing was thus given an anhedral of 1 [deg], such that the surface could be lowered. This poses no problems for the ground clearance and the fuel system requirements. By moving the engines and thus the center of gravity forward, the surface could be lowered while keeping the dutch roll stable. The results of the final design are presented in Table 8.4.

Table 8.4: Final design of the twin vertical tail planform

Parameter	S [m^2]	A	b [m]	λ [−]	C_{root} [m]	Λ_{tail} [°]
Value for each tail fin	29.5	1.3	6.19	0.4	6.0	37.5

8.3.4   Stall Characteristics

It is desired to have the aircraft reduce its angle of attack when the first lifting surface stalls to recover. For RELOAD stall of the main wing would be catastrophic as it increases the angle of attack even further due to the loss of lift behind the center of gravity. Instead it is desired to have stall occur first at the canard as this will reduce the angle of attack and lets the aircraft recover from stall. For conventional canards the planform has to be designed such that it stalls just before the main wing. RELOAD has the benefit of having an active control system to augment the stability of the aircraft and its stall behavior. The sensors used to detect disturbances identify the imminent stall and have the control system act accordingly by deflecting the canard to lower the nose of the aircraft.

8.4   One Engine Inoperative

If the aircraft is to lose one engine, an asymmetrical thrust remains. Therefore a moment is created which needs to be counteracted. The resulting moment is described by the stability derivative of Equation 8.6 [65]. The aircraft will continue to fly with zero sideslip, since this is the most efficient manner to continue. But because of this, there needs to be a roll angle present and the rudder needs a certain deflection. Equation 8.7 [65] gives the equilibrium equations for a one engine inoperative.

$$C_{n_e} = k \frac{\Delta T_p y_e}{\frac{1}{2} V^2 S b} \tag{8.6}$$

$$\begin{bmatrix} C_L & C_{Y_\beta} & 0 & C_{Y_{\delta_r}} \\ 0 & C_{l_\beta} & C_{l_{\delta_a}} & 0 \\ 0 & C_{n_\beta} & 0 & C_{n_{\delta_r}} \end{bmatrix} \begin{bmatrix} \varphi \\ \beta \\ \delta_a \\ \delta_r \end{bmatrix} = \begin{bmatrix} 0 \\ 0 \\ C_{n_e} \end{bmatrix} \tag{8.7}$$

By setting β to zero and adding the moment coefficient to the state-space system for the asymmetric equation of motion, a rudder deflection and rolling angle can be obtained. The results presented here are valid for an approach situation, as low speeds are critical for this flight case [65]. With a thrust difference of 16 kN, and an arm of 2.2 meters, the angles are as follows: rudder deflection angle $\delta_r = 2.27$ deg and roll angle $\phi = −12.52$ deg.

8.5 Verification, Validation and Sensitivity of Tool and Results

The tool used for the canard sizing is already verified and validated in the Baseline Report [2]. The tool which was used in the generation of the control and stability derivatives, the eigenmotions and the subsequent analysis was first verified and then validated. The verification was performed in a rather straightforward manner. After each derivative and analysis, the corresponding sub-block of code was unit tested by following the checklist presented in [1] and checking whether the result was logical. The result was a program which properly produced outputs to the different blocks and performed the analysis correctly. Figure 8.10 presents the structure of the program used, by means of a flow chart. Please note that the sizing of the canard is not included in this figure, as it results from the scissor plot program, presented in [1]. Since the program structure is rather uncluttered, the verification effort proceeded without any mentionable difficulties.
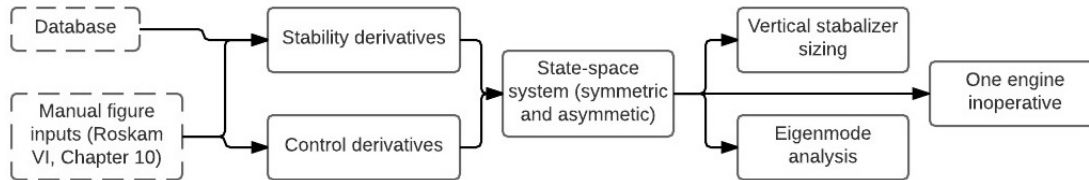
Figure 8.10: Structure of the stability and control program, with the database and manual inputs shown as dashed lines

The validation of the software was executed by comparing the RELOAD derivatives with the ones from a B737[2] and a B747[3]. Since the methods to determine the derivatives are known to produce rather crude results [66], notable differences between the derivatives were present. For instance, the C_{Y_β} of the B737 is -0.95, while RELOAD has one of -1.82. Since the aircraft design features a double vertical tail, this is logical. Another example is the C_{l_β}; for the B737 this is -0.1408. RELOAD has a C_{l_β} of -0.1908. The signs were always congruent as well. Since the aircraft used for validation differ widely in design, the comparison could only be used for high-level comparison purposes. It was found that the program functions correctly in reproducing the stability and control analyses, but a recommendation is made to further validate it by using for instance derivatives found in wind tunnel tests, using an actual model.

The main parameter of influence on stability and control is the location of the center of gravity. A thorough sensitivity analysis is performed to see the effects of small changes of the center of gravity location on the results. For the augmentation and canard sizing the sensitivity is already clearly visualized in Figure 8.8. Moving the vertical lines left corresponds to a more forward c.g. location, increasing the needed surface area of the canard and decreasing the needed augmentation gain. Moving the c.g. more aft will decrease the canard surface area and increase the needed augmentation gain. As can be seen from Table 8.5, moving the c.g. forward, increases the dynamic stability of the aircraft. By moving it aft, the dutch roll eigenmotion is made unstable, which is to be expected. Hence, its half time is negative.

Table 8.5: Sensitivity analysis results

	P_{sp} [s]	$T_{0.5_{sp}}$ [s]	P_{phug} [s]	$T_{0.5_{phug}}$ [s]	P_{dutch} [s]	$T_{0.5_{dutch}}$ [s]	$T_{2_{spiral}}$
c.g. Fwd 5 %	1.18	2.17	67.76	479.50	3.32	7.23	194.48
c.g. ±0 %	1.26	2.17	67.90	489.10	3.59	22.44	304.84
c.g. Aft 5 %	1.36	2.17	68.10	502.20	3.92	-17.3	988.20

Another consideration for the sensitivity analysis is the family concept of aircraft. Two different versions are under consideration, namely an extended range version and a higher capacity version. For the extended range version, the payload has to be reduced or fuel has to be added. Both approaches shift the center of gravity further to the rear of the aircraft. Moving the center of gravity aft improves the longitudinal stability and therefore reduce the canard size, but destabilize the dutch roll and therefore results in a larger vertical stabilizer size. The higher capacity version needs a longer fuselage to house the passengers. Lengthening the fuselage in front of the wing shifts the center of gravity forward. As a result the center of gravity is further from the aerodynamic center. This destabilizes the longitudinal stability, but is countered by the larger distance of the canard with respect to the center of gravity. In addition the dutch roll is stabilized since the vertical tail is further from the center of gravity, which results in a lower surface area of the vertical stabilizer. Lengthening the fuselage behind the wing results in an aft shift of the center of gravity, reducing the size of the canard. The stabilizer size stays roughly constant as the aft shift is countered by the increase in length of the fuselage.

---

[2]URL https://github.com/arktools/pydatcom/blob/master/test/data/B-737.out [Cited on 6 June 2016]
[3]URL http://www.dept.aoe.vt.edu/m̃ason/Mason_f/LDstabdoc.pdf [Cited on 6 June 2016]

8.6 Recommendations

During the preliminary design phase as indicated in Figure C.1 several areas of stability and control are further investigated. The stability and control derivatives have to be refined using CFD analysis and experimental data from windtunnel testing. At this stage the derivatives only give a rough estimate on the control and stability responses of the aircraft. The small contributions of neglected derivatives have to be included to further increase the accuracy of the aircraft model.

Another area of further research is the augmented stability system. The canard is currently only actively stabilizing longitudinal motions. Introducing dihedral or anhedral in the canard planform causes a coupling with lateral motion. The coupling gives the augmented stability system the ability to actively control the yaw of the aircraft using the canard causing the vertical tailplane area to decrease. More research has to be done on the effectiveness of such a system and the needed control system.

Further recommendations for the canard control system are the inclusion of dynamic gains. Dynamic gains can potentially improve the longitudinal response of the aircraft or decrease the needed actuation during different flight phases. Secondly, the requirements of the actuation system have to be set up and worked out, including the allowable response times of the canard control. A potential area of improvement is the canard trim system. Research has to be done on the feasibility of actuating both the canard and simultaneously increasing the curvature of the airfoil using the morphing leading edge. The power required and weight of the system have to be investigated, to give quantitative numbers on the proposed system. Finally the effects of reducing the actuation range have to be researched, since disturbances are short and only cause significant changes in angle of attack during landing and take-off.

Finally, more research in the actuation of the control surfaces is needed. Electric actuators [69] seem promising in replacing hydraulic actuation, which is currently widely used. The required forces and response rates of the actuators need to be determined and compared to the capabilities of both systems and a trade off has to be made. This will have to be decided upon in the preliminary design phase, thus before 2021. This is indicated in Figure C.1

9

Landing Gear Design

This chapter discusses the method used to design the landing gear and the results that followed from that. Section 9.1 explains the method and assumptions made for the design, after which Section 9.2 shows the results. The verification and validation of the landing gear design tool is explained in Section 9.3. Section 9.4 and Section 9.5 closes the chapter with a sensitivity analysis and further recommendations.

9.1 Approach of Detailed Landing Gear Design

Section 4.1.4 elaborated on the decision for a tricycle landing gear. Both the nose and main gear have a dual wheel configuration and the main gear consists of two struts. This section discusses the preliminary design approach of the landing gear, which in the first place is based on the class II estimations from both Roskam [70] and Raymer [5]. Firstly, the landing gear position is determined. Next the loads that follow from this are used in the wheel and shock absorption sizing. Finally, the ground turns and retraction of the landing gear are analyzed.

9.1.1 Positioning

The position of the landing gear is determined first. The track and wheelbase determine whether the landing gear is going to be fuselage or wing podded and is thus important for the further analysis of the landing gear sizing.

The track (see Figure 9.1), which is the distance between the main gears and the longitudinal position of the landing gear, with respect to the most aft center of gravity, is determined first in the design process. To calculate this the required clearances, as defined in Roskam [70], are used. The first angle, angle A as indicated in Figure 9.2, should always be bigger than 15 [°]. The tip-over angle B should be smaller than A to prevent tip-over during landing and take-off.
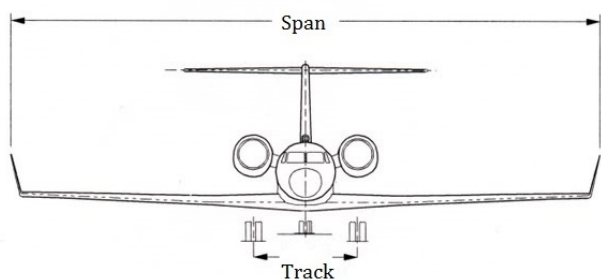
Figure 9.1: Track definition[1]
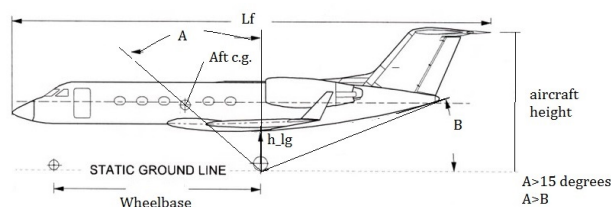
Figure 9.2: Longitudinal tip-over criterion[1]

By looking at the geometry in Figure 9.2, choosing an initial value for A of 32 [°] and selecting a first estimate of the landing gear height of 1.8 [m], the longitudinal position of the main landing gear is calculated. For the wheelbase, the position of the nose landing gear still needs to be known. The fraction of the load that the nose and main landing gear carry is determined by static equilibrium around the center of gravity, see Equation 9.1 and 9.2. Next to the tip-over criteria, these parameters determine the longitudinal position of the landing gear. It is therefore iterated to get a better landing gear position. For the moment equilibrium at the nose, also forward breaking moments have

---

[1]Figure adapted from URL http://s296.photobucket.com/user/JBM4_2008/media/Gulfstream_IV_3_D_Views.jpg.html [Cited on 20 June 2016]

been considered. This forward force is estimated as the total weight multiplied by a factor of 0.45 accounting for deceleration [14].

$$F_{main} = \frac{l_n}{l_m + l_n} \qquad (9.1) \qquad F_{nose} = \frac{l_m + x_{cg_{aft}} - x_{cg_{fwd}} + 0.45 \cdot z_{cg_{lnd}}}{l_m + l_n} \qquad (9.2)$$

Now both the longitudinal positions are known, the lateral positions of the main gear can be calculated. With the wheelbase and a lateral tip-over angle ψ of 55 [°] [70], the track is determined. The inputs are summarized in Table 9.1.

Table 9.1: Inputs for the lateral and longitudinal landing gear position

Parameter	$x_{cg_{aft}}$	Angle A	ψ	Gear height
Value	20.8	32	55	1.8

9.1.2   Wheel Sizing and Configuration

As highlighted in the beginning of this chapter, the main gear consists of two struts with two wheels. The nose gear carries two smaller nose wheels. The sizing of these wheels and their suspension is discussed in this section. This procedure and the equations are obtained from Torenbeek [14].

All calculations in this section relate to the static loads on each strut as discussed in Section 9.1.1. The dynamic loads are accounted for in the design of the shock absorption, which is discussed in Section 9.1.3. The static loads per strut are inserted into statistical relations for the wheel diameter, wheel width, distance between two wheels and the equivalent single wheel load (ESWL). The tyre selection results in a type VII wheel choice. This is the conventional "off the shelf" landing gear tyre for an aircraft of this size since it can withstand high pressures. The internal tyre pressure is approximated from reference aircraft and the tyre diameter[2]. The RELOAD aircraft does not need measures to prevent runway water from spraying into the engines, since they are already protected by the fuselage. The tyre pressure is taken from reference aircraft, but checked for the results for the ESWL. The used equations are applicable for flexible runway pavements. This pavement type is commonly applied at commercial airports, hence it is assumed to be the only runway type at which the RELOAD aircraft operates. Furthermore, a required pavement thickness of 15 inch is assumed from the reference aircraft from the previous design stage [2]. Big commercial airports have thicker layer of asphalt [14], but this value is chosen to design for the critical case. Table 9.2 shows the input values used for the calculations. Section 9.2 shows the design parameters that can be varied and are concluded from the landing gear analysis. Other parameters that are required for these calculations are obtained from and written to the database, as shown in Appendix B.

Table 9.2: Input values for landing gear sizing

Parameter	$\delta[m]$	$P_{internal}[kg/m^2]$
Value main gear	0.38	14.98
Value nose gear	0.38	13.01

Table 9.3: Input values for landing gear shock absorption [14]

Parameter	$\frac{r_{loaded}}{r}$	η_s	η_t	V_t	N_g
Value	0.41	0.8	0.47	3.05	3.0

9.1.3   Shock Absorption

After the static load, position analysis and design of the landing gear, shock absorption must be taken into account. The design is equipped with oleo-pneumatic shock dampers, as these have the highest efficiency. These are "off the shelf" available and are already widely applied to commercial aviation. The wheels take up a part of the dynamics loads, for which the tyre damping is found by the tyre radius minus the loaded radius [5]. To obtain the loaded radius, reference landing gear tyres where used to set up a linear approximation. The fraction loaded radius over tyre radius is shown in Table 9.3. Also the efficiencies η, vertical touchdown rate V_t and the landing load factor N_g can be observed.

From these inputs, the shock strut length and diameter can be obtained. The length of the shock strut is assumed to be 2.5 times the required displacement of the shock absorber [5]. The equations that have been used for this displacement and the diameter of the strut are obtained from [14].

---

[2]URL http://www.boeing.com/assets/pdf/commercial/airports/acaps/737MAXbrochure.pdf [Cited on 3 June 2016]

9.1.4   Ground Turns

One of the medium level requirements is the ability of the aircraft to use current airport infrastructures. Therefore the turn radius of the aircraft is investigated. The smaller the turn radius is, the more types of airports it can land on. But also the risk of damaging the aircraft during taxiing and other ground operations are reduced.

First, the turn around radius is required. This determines the width of the pavement and thus the airports that it can operate at. This can be calculated as shown in Figure 9.3. By determining the intersection of the line connecting the main gears and the nose gear and β, the radius of the ground turn is determined. A value of 60 [°] is chosen for the steering angle β as this is a general value as indicated by [71]. The higher this angle, the easier it can turn on the taxiway and follow the centerline. If the centerline is overshoot by the pilot it must still be able to return to the centerline without driving off the pavement. If the centerline is overshoot the castor angle should remain below the steering angle. The former is calculated using Figure 9.4 and the equations from [71] for a Class III aircraft design group.
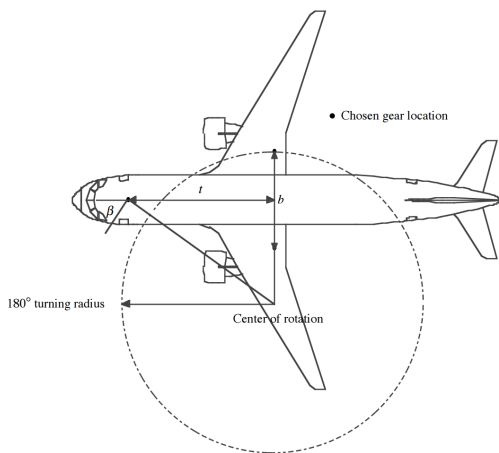
Figure 9.3: 180 [°] ground turn radius [71]
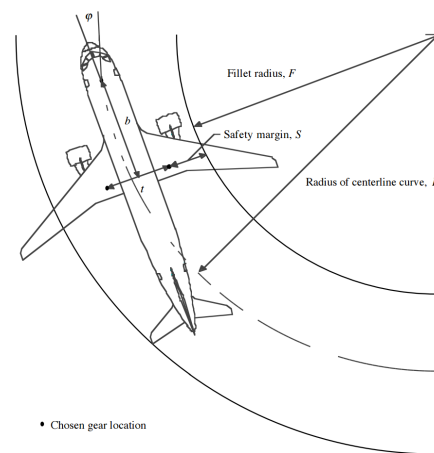
Figure 9.4: Fillet radius design [71]

9.1.5   Retraction

With the preliminary sizing of the landing gear, the retraction must be discussed. Retracting the gear requires both a complicated and heavy hydraulic system together with space inside the fuselage or the wing. Although the location for the landing gear is already set in Section 9.1.1, integration of the gear in the wing and fuselage must be feasible. For this, the design of the fuselage, wing structure, and also aerodynamics are considered.

Due to the determined position of the landing gear with respect to the aft center of gravity which is determined from Figure 8.8, two options are considered for the retraction of the main gear. The landing gear can be either retracted in longitudinal direction or sideways into the fuselage. In the latter case, a slightly larger cut-out would be needed to place the wheels inside the fuselage. The longitudinal retraction is possible, as the aircraft has a lot of space at the root of the wing. This is not needed as extra fuel storage, thus this room could be used for the landing gear. The advantage is that the fuselage fairing can be small and thus no extra drag will be created. However, retracting the landing gear forward would mean that the wing box would be interrupted. Since this would weaken the structure, this option is not chosen. Retracing it backwards is also an option, but the main gear is slightly larger than the room available, which will increase the drag. It is therefore decided that the landing gear will be retracted towards the fuselage. The final landing gear is visualised in Figure 20.1.

9.2   Detailed Landing Gear Design

This section shows all the final results of the landing gear design. They are summarized in Table 9.4. The type of landing gear is a typical tricycle landing gear. After positioning, the distances with respect to the aft center of gravity are known. Now this should be incorporated in fuselage and wings. As said in the previous section, the main gear is placed in the wing. This and the placement of the landing gear can be seen in Figure 20.1.

Table 9.4: Results for landing gear sizing

Parameter	Unit	Value main gear	Value nose gear
D_{strut}	[m]	0.26	0.11
D_{wheel}	[m]	1.03	0.96
h_{lg}	[m]	1.8	1.8
l_{strut}	[m]	0.50	0.54
N_{wheels}	[-]	4	2
N_{struts}	[-]	2	1
$P_{internal}$	[kg/m^2]	14.98	13.01
W_{wheel}	[m]	0.28	0.17
Tyre type	[-]	VII	VII
S_{wheels}	[m]	0.64	0.49
$x_{cg_{gear}}$	[m]	22.8	2.7
Track	[m]	8.44	-

Parameter	Unit	Value
Tip-over angle B	[°]	28.5
$r_{180_{turn}}$	[m]	12.88
φ	[°]	35.8

9.3 Verification and Validation of the Landing Gear Tool

The tool for the sizing of the landing gear is verified and validated such that bugs and wrong assumptions are removed. First, for all inputs the value is checked to make sure that the right units and values are used. Secondly, unit tests on each block of code are performed. The ground turns for example are compared to the Boeing 787-8[3] and the airbus A320[4]. The calculated turning radius of 12.88 [m] is reasonable compared to the turning radius of 13.4 and 15.2 [m] of the A320 and Boeing 787-8. The RELOAD aircraft has a slightly smaller radius due to the smaller track width (8.44 [m] compared to 8.95[m] and 9.8 [m] from Airbus and Boeing). The shock absorption, tire sizes, position and tip-over angle are checked in the same manner, although the latter is much larger compared to the reference aircraft. This is expected though, because of the aft wing position with respect to the fuselage. The program is validated afterwards. All blocks of code are put together and the effects of changing certain parameters on the whole design are checked. An example of this is the change in position and size of the tires by changing the loads on the gears. This shows no unexpected changes, it is found that the program functions correctly.

9.4 Sensitivity Analysis of the Landing Gear

Just as on other technical design, a sensitivity analysis must be performed on the landing gear. The landing gear positioning, shock absorber and tire design is investigated on a 5 % change in main design parameters. The results can be found in Table 9.5, except for the shock absorbers. Their sizing is based on statistics and is therefore not directly related to these input values. The most obvious conclusion that can be drawn is that the landing gear position of the nose gear is very sensitive to the center of gravity location. To account for this in the design, the nose gear is placed as far forward as possible. This will not add extra weight, as the load introduction can then be done at the canard box structure, which is favourable.

Table 9.5: Sensitivity analysis of main and nose landing gear design

Parameter		$x_{cg_{main}}$	$x_{cg_{nose}}$	$D_{wheel,main}$	$D_{wheel,nose}$	$W_{wheel,main}$	$W_{wheel,nose}$
	Base values	22.8 [m]	2.71 [m]	1.04 [m]	0.74 [m]	0.28 [m]	0.17 [m]
	%	%	%	%	%		
Aft. x_{cg} [m]	+5	+0.042	-37	0	0	0	0
Aft. x_{cg} [m]	-5	-0.047	+73	0	0	0	0
P_{strut} [N]	+5	0	0	+1.9	+1.4	+0.4	+2.3
P_{strut} [N]	-5	0	0	-1.0	-1.4	-0.4	-5.9

---

[3] URL http://www.boeing.com/assets/pdf/commercial/airports/acaps/787.pdf [Cited on 14 June 2016]
[4] URL http://www.airbus.com/fileadmin/media_gallery/files/tech_data/AC/Airbus_AC_A320_Jun16.pdf [Cited on 14 June 2016]

9.5 Recommendations

This section treats the design steps that should be included in the next design phase. Still a lot has to be sized into detail.

Specific landing gear design   The design should be further worked out into more detail. First of all, the tires should be sized more specifically. This can be done by contacting tire manufacturers and compare the design specifications as stated in Section 9.2 with existing landing gear tires. Using existing "off the shelf" tires reduces development costs, which is favourable for the BWB design. The same goes for the design of the shock dampers. If feasible, these will be designed as for convenient aircraft, but should be slightly reduced in size to make sure over-designing will not occur. Furthermore, the retraction system including hydraulics should be researched further. A detailed program should be written to ensure integration between the designs of the parts. This should be finished before 2024 as indicated in Figure C.1.

Landing gear weight   To prevent overdesigning, the landing gear weight should be calculated in more detail concluding from the detailed tire, shock absorber and retraction hydraulics design. This can be done once all the dimensions and materials are known from the total landing gear sizing. If this shows out to be different than the estimated weight from the Class II estimation, the gear should be resized due to the "snowball effect". Since this has a lot of influence on the other departments, it should be finished in the preliminary design phase which ends in September 2021.

Dynamic loads   Furthermore, the dynamic loads on each landing gear should be investigated further. Especially braking and landing load factors on each leg can be analyzed in more detail, as they for now have been assumed based on statistical values. This could also mean over- or underdesigning. This investigation can be done simultaneously with the detailed design of the landing gear and should therefore be finished before 2021.

10

Flight Deck Design

The pilots and other aircraft crew are the source of the second major group of direct operating cost [2]. With the purpose of reducing the cost related to this group, it was investigated whether the aircraft control system could be equipped in a manner which would allow for single pilot operations (SPO). In the current standard two pilots operate an aircraft on a flight; the first one performs the "pilot flying" (PF) role and the second is the "pilot monitoring" (PM). These roles are interchangeable between the pilots during a flight. The main reason for this set-up is the presence of a controlling and a monitoring function, such that errors are discovered early on, in a stage where correction is simple [72].

In the current model for direct operating cost, crew cost amounts to 835 $ per hour, as can be seen in Figure 2.1. The largest part of this group of costs is formed by the pilots and co-pilots fees, coming in at 551 $ per hour [2]. By switching to a single pilot configuration, this can thus be halved. By also subtracting one sixth[1] from the other cost sources in this group, the total direct operating cost due to crew can be reduced to 513 $ per hour. This number exceeds the target value of 551 $ per hour proposed in Figure 2.1 and corresponds to a direct operating cost reduction of 7.2 %.

From an economical point of view, designing for a single pilot cockpit is thus an interesting option. To illustrate this, the European low-cost airline Ryanair has already publicly showed interest in truncating one pilot from the flight deck[2]. Furthermore, aircraft manufacturer Embraer aims at having SPO technology available in 2020 to 2025[3]. However, many problems and challenges are associated with it, ranging from a technical basis to public opinion and certification.

For instance, in case of SPO, an incapacitated pilot could lead to a disaster, since the aircraft is left unmanned. This might be solved by implementing a fully automated flight control system, or a ground-based terminal where a monitoring controller is capable to take over control. Both solutions lead to their own problems; a need for an adapted crew resource management (ground-to-air) and a digital connection (with its associated security problems) being just a few of them. Another issue which arises, is the need for a training platform to be present, where new pilots can learn and get used to the work flow and operations of the airline. This could be solved by having a second seat present, where an instructor might take place. Furthermore, the situation where a pilot resides alone in a cockpit for multiple hours, in a highly automated environment, might lead to a lower level of attention being directed to the job at hand. NASA therefore proposes a more involved pilot environment, such that loss of awareness due to a too low work load is avoided [73].

Because of these problems (and more), an airline may choose to continue regular two pilot operations. And although SPO will not impact flight safety, there are other motivations for postponing it. Furthermore, the transition to SPO is not meant to be an abrupt one; perhaps airlines prefer to initiate it in a more gradual time-frame. Therefore, the flight deck of the aircraft shall be designed in a manner which allows for two pilots to operate the aircraft in a conventional way. In addition, a system shall be present which allows for single pilot operations. In this vein, not only is an airline able to choose whether to operate the aircraft on a single or dual pilot basis, but it can also still serve as a training platform when needed. The trade-off between direct operating cost and having two pilots in the cockpit is thus partially placed at the airline. The aircraft is designed such that the cost reduction can be attained. It is up to the airline to decide if they want to meet it fully.

---

[1]The original number is constructed for a crew of six (two pilots and four cabin crew members). It is assumed that pilots and cabin crew members have an equal share in the other cost groups.

[2]URL http://www.theguardian.com/money/2010/sep/08/ryanair-axe-unnecessary-co-pilots [Cited on 3 June 2016]

[3]URL https://www.flightglobal.com/news/articles/embraer-reveals-vision-for-single-pilot-airliners-343348/ [Cited on 3 June 2016]

To cover both aspects of the cockpit and single pilot system design, the remainder of this chapter is split up into two sections. Firstly, Section 10.1 presents the design of the flight deck itself and secondly, Section 10.2 provides a discussion about the SPO system. Since such a system is elaborate and requires research to great extent, it is not be designed in detail. Rather, its needed capabilities and its global architecture are be shown, with recommendations for the final design being present.

10.1 Flight Deck Layout

The flight deck of the aircraft will feature two pilot seats and a jump seat for an instructor or observer. The length of the compartment will be 2.5 [m] [14]. Figure 10.1 shows the layout of the nose cone section, with the cockpit included.
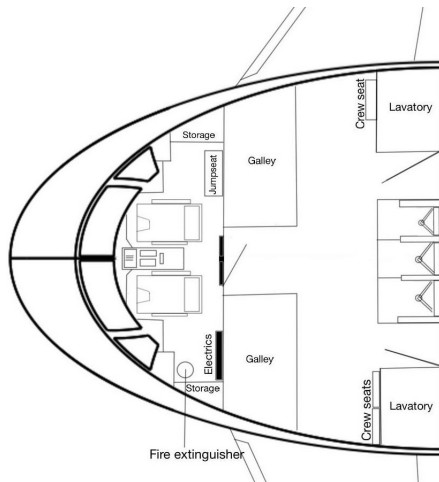
Figure 10.1: The layout of the cockpit and nose cone section
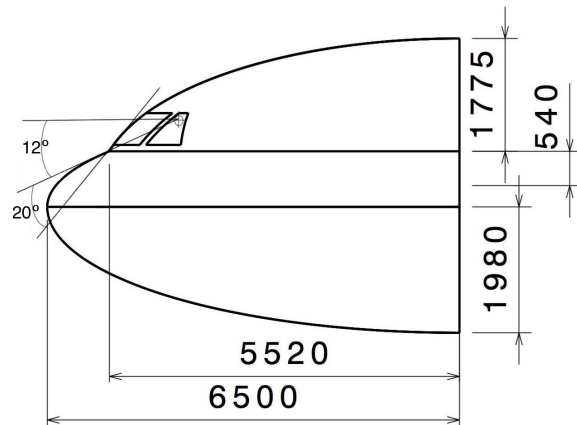
Figure 10.2: The dimensions of the nose cone in [mm] and the pilot visibility angles taken from the eye reference point

The cockpit will feature several innovative instruments, such as Heads Up Displays (HUD) on both pilot positions. The presence of the HUDs allows the pilots to retain situational awareness, while getting instrument data at the same time. HUDs are becoming ever more popular on new aircraft. The Chinese civil aviation authority has even made HUDs compulsary on all aircraft, starting from 2025[4],[5]. The nose cone design allows the cockpit to fulfill all necessary visibility requirements. The over nose angle is equal to 12 degrees and was determined from [74]. The grazing angle is equal to 20 degrees. Figure 10.2 summarizes the design of the nosecone. In the final design stage, it is recommended to investigate the detailed layout of all instruments. Furthermore, since the cockpit windows are made from glass and have a double curved feature, the manufacturing must be investigated. Currently, the techniques exist already[6], but careful attention must be paid to all visibility requirements, such that for instance no distortion of the view occurs.

10.2 Single Pilot Operations

The single pilot operations system consists of two branches; an on-board and a ground-based component. The on-board component aids the pilot in all nominal operations circumstances. It fulfills all tasks that are normally executed by the second pilot in the cockpit. The ground-based component becomes active in all off-nominal circumstances. A ground based terminal in the airline control center serves as a live connection to the aircraft. A so-called "ground operator" assumes the position of aiding the airborne pilot in this live environment to have the aircraft make a safe landing. In this section, firstly the on-board component is described. Secondly, the ground segment is presented, together with its data-link.

10.2.1 Onboard Component

The on-board SPO system component will take over all roles normally fulfilled by the Pilot Monitoring (PM). In order for such a system to be successful, it must at least exhibit the following functionalities and capabilities, as suggested

---

[4]URL http://www.ainonline.com/aviation-news/ain-news-live/airshow-china/2012-11-14/chinese-authorities-commit-aircraft-head-display-mandate [Cited on 7 June 2016]

[5]URL http://www.aviationtoday.com/categories/commercial/China-Prepares-for-Future-Aviation-Growth-With-Avionics-Infrastructure-Investments_83498.html [Cited on 7 June 2016]

[6]URL http://www.pprune.org/archive/index.php/t-523666.html [Cited on 9 June 2016]

by [72]:

- The ability to process language close to human capability, such that the remaining pilot can interact with the system by speech.

- The ability to sense when a pilot makes a mistake and to override its commands in such a situation, even in critical flight phases, such as landing.

- The ability to monitor the aircraft systems on an independent level.

- The ability to inform the captain of external threats.

- The ability to inform the captain what the system "is thinking" and which actions are pending.

A single pilot in a highly automated working environment might succumb to distraction and boredom. The aircraft must be able to detect such an event and alert the pilot or take necessary actions. An analogy is often made with a horse-rider; even when the horse rider is focusing on another task, such as reading a map, the horse makes sure it does not run into an obstacle. The rider is continuously updated by the feeling it gets through his legs and therefore remains in the loop. Therefore, NASA suggest a system which includes a continuous haptic feedback to the pilot, such that he can communicate with the system on another level than visual relationships [73]. The SPO design in this aircraft features a combination of aural and visual links to the pilot to replace this haptic feedback.

Taking into account the high-level requirements of such a system as stated above, an initial architecture is proposed. Figure 10.3 shows this system architecture. The pilot can send inputs to the system via speech or manual (such as via switches). The system settings also allow the pilot to personalize his "virtual first officer", such that operations are adjusted to each individual captain. The system also gathers data of the aircraft and external threats (via a database of objects, Traffic Collision And Avoidance (TCAS), and a visual sensor, for instance). Furthermore, the pilot is closely monitored by the system (for instance his vital functions, such that the system can detect the level of stress in the pilot or his situational awareness). In this vein, the system can adapt to retain the optimal pilot workload (such that it remains at acceptable levels, without over-stressing the pilot). All inputs are sent to a central computing unit, which determines whether to take action and inform the pilot if necessary. The swiftness of this response must be adapted according to the criticality of the situation, which must be assessed at every moment in flight. The outputs are visual and aural. Since this system will take a crucial role in aircraft operations, it has to be designed with sufficient redundancy.
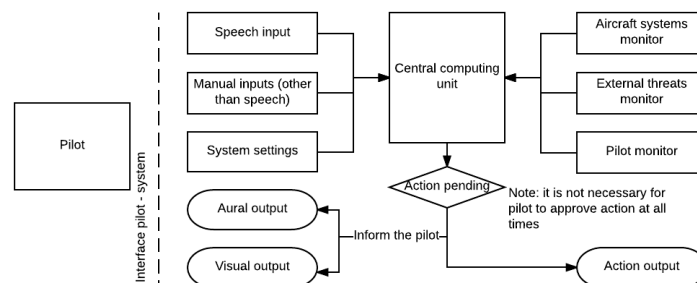
Figure 10.3: The architecture of the on-board single pilot operations system

For this system to be ready by the introduction of the aircraft onto the market in 2030 (and 2025 for certification), the following recommendations are made. These recommendations are set up in a manner that justifies the SMART criteria. There are certain risks associated to each recommendation in the development of such a system, which will be presented in Figure 10.4 and 10.5, pre- and post-mitigation, respectively. The risks associated to this system are presented separately from the technical risks in Chapter 21.3, as this system represents a major part of the cost reduction and is therefore crucial in meeting the requirements. As seen in previous reports ([2] [1]), the "proven flight design" to "feasible in theory" scale is used. Red colors in the upper right corner denote high risks and green risks in the lower left corner are acceptable. These recommendations are to be performed or ready by 2022, such that sufficient time remains to implement and certify the system.

1. **Speech capabilities:** the capabilities of a computer system to comprehend correctly a human voice command (even in a high-stress environment) is a major point to investigate. It forms a critical component in the on-board system. Its development is currently at a level not yet implemented in flight-design, but the area shows promising results nevertheless[7].

2. **Pilot monitoring:** the system needs to determine with great accuracy when the pilot has made a mistake. The monitoring of his or her state is of major importance in this capability. Currently, car technology is already

---

[7]URL http://aviationweek.com/blog/voice-flight-deck-version [Cited on 6 June 2016]

able to assess the drivers state of awareness. The step to aircraft cockpits must be investigated further though. When the system is capable to accurately determine the pilot state, it is considered ready.

3. **Pilot mistake sensing:** the first step in correcting a mistake is to recognize it. By using nominal missions and flight envelopes, the correct pilot inputs can be separated from errors. This capability is paramount and needs more attention in the final design stage. It is considered ready when the system can sufficiently spot potentially dangerous situations.

4. **Visual sensor:** in order to inform the pilot of external threats (such as a high object in the flight path), a visual system is to be added. This will be camera-based. There are already applications of such camera's on micro aerial vehicles[8], but more research is necessary for the step to airliners. Once external threats can be seen and reported through, the capability is attained.

5. **Artificial intelligence to override pilot:** the system must be able to aid the pilot, even in high-workload situations. When a mistake is made, it must be corrected and this sometimes requires action. The system must thus posses the capability to assess on itself (and quickly) whether to take action. This is crucial and currently significantly more research is needed in this area, in order to design the SPO system.

To reduce the risks associated with the development, risk mitigation methods are applied. Please note that for all recommendations and the associated risks, it is possible to fall back on regular two-pilot operations. In addition to that, the following is proposed:

1. **Speech capabilities:** in the development of this function, progress is still to be made. But it is assessed that the risk of uncompleted technology is marginal, since the pace of development is high and systems like these already exist, though less accurate. In the event that this capability is not completed in time, the system can function with manual inputs in a degraded manner.

2. **Pilot monitoring:** since progress is quite far at this point in time, the likelihood of it being not ready is assessed at marginal. Consumer electronics, for example, can already assess the users vital information and level of alertness. If the monitoring function is not available, standard intervals can be used, in combination with statistical data, to assess the pilots awareness.

3. **Pilot mistake sensing:** together with risk number 5, this one features a component of artificial intelligence. Progress is being made, but the risk remains higher than the other recommendations (critical, since its development is crucial). If this capability can not be developed in the desired time-frame, the switch back to two-pilot configuration can be made and more resources can be allocated to stimulate the development.

4. **Visual sensor:** the technology needed here is present, it only needs to be transferred to the aircraft industry. Hence, the risk associated is marginal. The external threats are also stored in a database (and come from TCAS), so the system can operate in a degraded manner without the visual aid.

5. **Artificial intelligence to override pilot:** artificial intelligence is being developed in high pace. Extrapolating the evolution over the past few years, allows to mitigate the risk contained in this recommendation out of the red area. In the case that this capability is not present in time, the SPO system can operate through a different philosophy. Namely, reducing the pilot workload, such that the probability of pilot errors is lower. In this case, the aircraft will not override pilot errors; the pilot has to correct them himself.
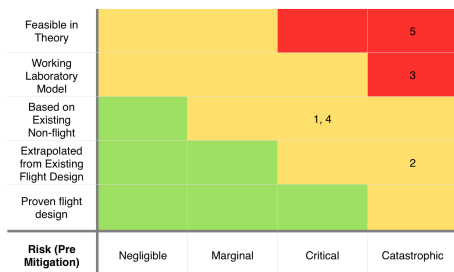
Figure 10.4: Development risk of on-board SPO system component pre-mitigation
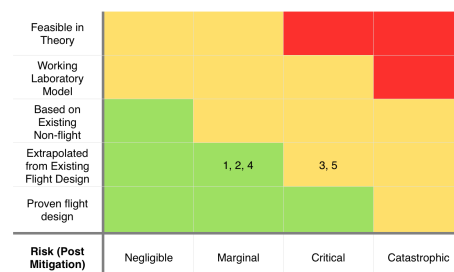
Figure 10.5: Development risk of on-board SPO system component post-mitigation

A final problem that should be noted, results from the situation where the pilot needs to leave the flight deck (in a nominal way), for instance for a bathroom visit. The SPO system is switched to a "guard mode" and a flight attendant could be asked to step in. Some extra training might be required, even if the aircraft enters the "horse-mode" where it functions on its own.

---

[8]URL http://mavlab.tudelft.nl/new-theory-allows-drones-to-see-distances-with-one-eye/ [Cited on 6 June 2016]

10.2.2 Ground-Based Component

In addition to the system proposed above, a ground-based controller position is created, which becomes active when called upon by the captain of the aircraft (or as decided by the ground controller itself, if the captain is incapacitated). This ground controller can perform a standard function in the airline control center in nominal operations, such as flight planner, but remains stand-by to assist the pilot in case of off-nominal flight conditions occurring. In this event, he switches to a terminal allowing to perform all regular copilot functions. One flight controller can oversee multiple aircraft, since he only activates his function in off-nominal conditions. Table 10.1 presents a taxonomy for the levels in which this system might become active, with the colors showing the level of urgency of the situation. As presented in [75], in level 1, the pilot is fully functional and the aircraft is fulfilling its mission in a nominal manner. In this case there will not be a need for help from the ground. Level 2 represents a situation where the pilot asks assistance of the ground controller. In level 3 the ground controller assumes the role of the pilot and lands the aircraft from the remote location. For this to happen, it must become evident to the airline control center that the pilot is incapacitated. Finally, level 4 requires the ground controller to aviate in an off-nominal condition, which is likely to result in the requirement of assistance from another ground controller.

Table 10.1: A taxonomy of the different operating conditions for single pilot operations, assisted by a ground controller [75]

		Flight condition	
		Nominal	Off-nominal
Pilot condition	Normal	1	2
	Incapacitated	3	4

Level	Ground assistance
1	No
2	Yes
3	Yes
4	Yes, multiple

Having an off-site back-up system present, automatically means relying on a data-link, with an up-link and a down-link. In general, the most important capabilities for this data-link are as follows: [76]:

- **Available worldwide:** since a change from nominal to off-nominal flight condition can occur at any location, the data-link must be available at any place on earth. Figure 10.6 presents three alternative networks for the communication. In principle satellite communication can be used, but if this is not available for any reason VHF data shall be used (and HF over oceanic regions, since its waves reflect on the atmosphere [77]) [78].

- **High availability and reliability:** the data-link must be very reliable (and have an availability which is sufficiently close to 100 %). Again, Figure 10.6 suggest an architecture of the underlying networks that could be utilized for the data-link. As can be seen, some alternatives are provided in case one might not be available. There might be some limitations present when using these alternatives.

- **Low probability of intercept:** the following two items are focused on the data security domain. The data-link must withstand actions of malicious intent. The cornerstone of this capability lies in having a low probability of intercept. The information is used to control an aircraft. Making this hard to find is paramount.

- **Security:** if the data-link is intercepted, the information must be unintelligible, due to encoding. Encoding the data makes sure that a third party can not obtain information on the aircraft control, but more importantly, can not inject data into the up-link altering.
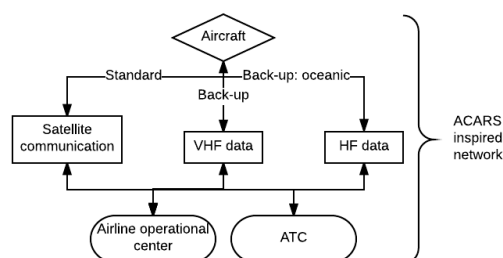
Figure 10.6: The proposed architecture of the network providing support to the pilot from a ground-based terminal in the airline operations center [78]

The data-link must posses the above mentioned capabilities. A general architecture of the network providing the pilot with ground assistance is shown in Figure 10.6. The network is based on the current technology of the ACARS (Aircraft Communications Addressing and Reporting System) network, which is already in use. Some major differences between the ACARS network and the one proposed for SPO are the need for encoding (security) and the higher bandwidth needed for the data-link. [76] suggests a bandwidth of 300 kHz to 10 MHz to send and receive all

aircraft parameters and control information. This might also include a video and audio feed from the cockpit for crew resource management purposes. To control and command an unmanned aircraft, a data rate of 50 to 200 kbps is needed [79]. Since RELOAD carries 177 passengers, the upper data rate of this bound will be assumed. This is still easily supportable by satcom and the back-up line-of-sight VHF communications[79]. Also the oceanic back-up HF band can support such a data rate[80]. With the latter communication band, however, lag might be present due to the fact that the signal bounces of the atmosphere in its path (which allows it to even be used over oceanic areas). This lag disables the possibility for a live control feed. But, by implementing degraded ground based capabilities, the back-up remains. The ground controller could send a simplified command and receive the result with some delay. This requires the on-board system to use its automated capabilities.

In order to develop this component of the SPO system further, the following recommendations are made for the final design. As presented in the previous section, these all have risks associated to them, which are presented in risk maps, Figure 10.7 and 10.8. The recommendations are to be completed by 2022, such that they can be implemented and certified.

1. **World wide availability:** there are already world-wide networks in place to allow communications between aircraft and there home bases. These networks need to be expanded to cover the higher data-rates necessary and the high availability requirement. Failure to do so would be catastrophic.

2. **Security of data-link:** to protect against malicious intent, the data-link needs high security. Both sides of this battle are ever developing. Failure to find a proper solution would be catastrophic. Therefore more research in this area is needed.

3. **Airline operations adaptation:** the airline needs to implement a new ground operations work-flow, such that the ground controller can monitor multiple aircraft at once, while only having a stand-by function in nominal operations. This adaptation requires effort. However, it is inherently one of the lower risk recommendations.

4. **Complete SPO system integration:** this final risk entails the SPO system as a whole (both airborne and ground components). The interface and cooperation of both components and the development of the system is critical and currently based only on laboratory models.

To lower the risks associated with the design of this system in the final design phase, some risk mitigation measures are applied once again:

1. **World wide availability:** since the basis of this network is already present and only its capability needs improvement, the risk of it not being finished on time is marginal. If it were to happen, the SPO could be limited to certain areas where the data-link can be established.

2. **Security of data-link:** the risk associated to this recommendation is critical. Current UAV systems show high security levels already, so therefore the risk of it not being completed can be mitigated. If the capability is not guaranteed completed in time, two pilot operations can be fulfilled until no longer necessary.

3. **Airline operations adaptation:** the cost saving by switching to SPO outweighs the required investment from airlines to ready the infrastructure for the ground controllers. The technology of remote aircraft controlling is already in existence (in the military). Further research is needed in the crew resource management area, but overall this risk can be mitigated to marginal. Again, if necessary, two pilot operations can be sustained.

4. **Complete SPO system integration:** once all individual components are finished, the complete system has to be integrated. Since the individual challenges are solved at that point, the risk is mitigated to the lowest row. Having the option to revert back to conventional dual pilot operations mitigates the risk as well.
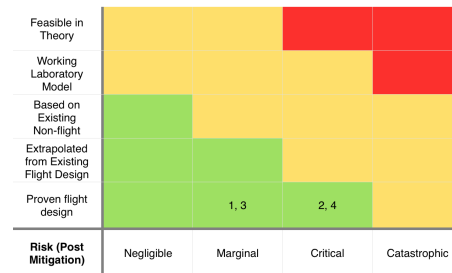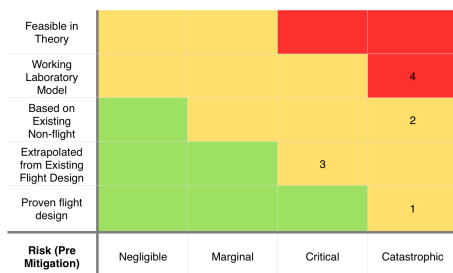
Figure 10.7: Development risk of ground-based SPO system component pre-mitigation

Figure 10.8: Development risk of ground-based SPO system component post-mitigation

<div align="right">

11

</div>

<div align="right">

Aircraft Systems Design

</div>

This chapter covers the design of other important aircraft systems. First of all, the electrical system with its power providers and consumers is discussed in Section 11.1. Section 11.2 elaborates on the command and data handling system and the use of fly-by-wireless. The fuel and hydraulic system are covered in Section 11.3 and Section 11.4 respectively. The pressurization system for the cabin environment is covered in Section 11.5 and Section 11.6 discusses the system for the removal of ice. The last part, Section 11.7 will shortly deal with the passenger service systems.

11.1 Electrical System

The purpose of this section is to provide an overview of the electrical system incorporated in the RELOAD aircraft. First, the generators and other power providers are listed and discussed. Afterwards, the power consumers are presented and the values for the electrical load summary of each component is estimated. Finally, an electrical block diagram is shown in order to provide insight in the inter-connections between the power providers and power consumers.

11.1.1 Power Providers

RELOAD aims to reduce weight and system complexity, while maximizing flexibility. In this regard, the choice was made to make use of the Variable Frequency Starter Generators (VFSG). The main advantage of this type of generator is that it eliminates the need of a constant speed drive, as it is capable of adapting its rotational speed. Also, it can be used as an engine starter, which means that there will be no need for any pneumatic engine starting equipment[1], which will not only lower the weight of the system, but also decrease the amount of maintenance tasks required and therefore reduce the costs in this regard[2].

As discussed in Chapter 7, RELOAD has opted for a no-bleed architecture. That means that the engines do not provide any bleed air for the pressurization system (see Section 11.5), but they provide electric power to air compressors via the VFSG's. An aircraft that is part of the "More Electric Aircraft" (MEA)[3] generation, such as RELOAD requires a real power of 1.6 $[MW]$ for 300 passengers [81]. Sizing this number down to 177 passengers means that RELOAD requires a real power of approximately 0.94 $[MW]$. However, the generators that are used on any aircraft produce alternating current (AC) and their apparent power is measured in $[kVA]$ [82]. Fortunately, there is a simple way to relate the apparent power to real power and that is by using a dimensionless parameter, which is around 95 % for an aircraft [82]. Using this value entails that the generators need to provide an apparent power of approximately 990 $[kVA]$ for the total aircraft.

RELOAD will be equipped with two VFSGs connected to each engine, each one generating 280 $[kVA]$. Two more VFSG's are related to the APU, capable of generating 215 $[kVA]$. In case of a power failure the main battery, APU battery, ram air turbine and permanent magnet generators (PMG) [83] can be used as backup power generators for the critical systems. During flight, in case of an engine generator failure, one APU generator can be started in order to replace the power loss. If an entire engine becomes inoperative, both generators of the APU are sufficient to cover the loss.

---

[1] URL http://utcaerospacesystems.com/cap/products/Pages/variable-frequency-generator.aspx [Cited on 8 June 2016]
[2] URL http://787updates.newairplane.com/787-Electrical-Systems/787-Electrical-System [Cited on 8 June 2016]
[3] URL http://tec.ieee.org/2015/08/28/challenges-in-more-electric-aircraft-mea/ [Cited on 8 June 2016]

11.1.2   Power Consumers

Power consumers carried on board of RELOAD can be split into two categories: critical and non-critical. The critical category includes the hydraulic system, environment control system, avionics system, exterior lighting, flight controls, windshield heating, fuel pumping system and de-icing system. Those systems need to be provided with power at all times and in case a major power failure occurs, the back-up power generators are continuing to supply DC electrical power to keep them functional. As mentioned in [1], the avionics system only includes communication, navigation, collision avoidance and monitoring systems. The flight-control system is taken as an individual power consumer.

On the other side, the non-critical power consumers are: cabin lighting, cargo handling system, the galleys and lavatories, as well as the entertainment and food heating devices. These units and systems are completely dispensable in case a power failure occurs and therefore there is no power redirected to them in case of emergency.

In Figure 11.1, the connections between the power consumers and power suppliers can be observed. It is worth mentioning that the power from the generators first reaches four AC buses, where it is converted to DC if required. This employed architecture means that no ground power is necessary to start the aircraft[4], as the APU battery is used to power the APU generators, which start the APU, that in turn sends power to the engine generators and those are used to start the engines.
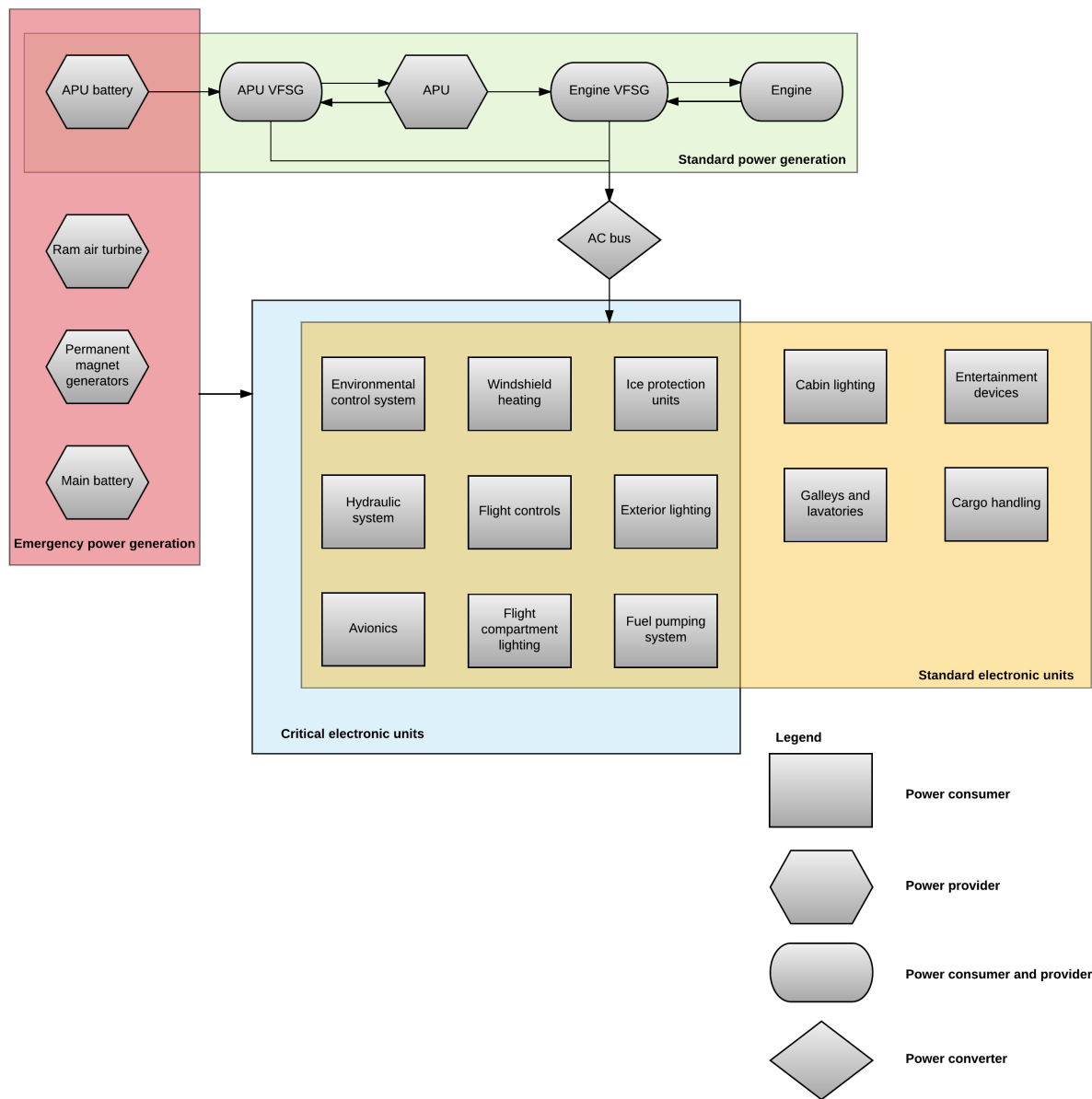
Figure 11.1: Electrical block diagram showing the electrical equipment used by RELOAD and its mutual relations and interactions

---

[4]URL http://787updates.newairplane.com/787-Electrical-Systems/787-Electrical-System [Cited on 8 June 2016]

11.2   Command & Data Handling System

This section will cover the command and data handling (C&DH) system. The C&DH system ensures all data communication throughout the fuselage. There are four main data handling domains. This division is based on aircraft control (avionics), aircraft operations (airline information service domain), cabin operations (passenger information and entertainment services) and in-flight entertainment for each passenger [77][84]. To host all data traffic through the fuselage, a conventional aircraft uses an enormous amount of cables. As discussed in the Design Option Tree in [2], RELOAD considers fly-by-wireless as option for internal communication instead of either fly-by-wire or fly-by-optics. The fly-by-wireless application and technical system data are stated in Subsection 11.2.1. The overall layout of the C&DH system is treated in Subsection 11.2.2.

11.2.1   Fly-by-Wireless

The fly-by-wireless system is a possible replacement for the fly-by-wire or fly-by-optics system, all being the electronic interface of the command & data handling system. The fly-by-wire and fly-by-optics system already achieved a considerable weight saving over the past century by replacing the heavy mechanical controls. Current technologies now allow for even more weight savings by taking out a considerable part of the cabling. As an indication of the savings that are achieved by this: a conventional aircraft carries between 200 and 600 [km] of cables[5].

The advantages for applying fly-by-wire are considerable. Not only the weight is saved, also costs in general are reduced. First of all, the price of copper cables is increasing these years, even four times the price in 2002[6]. Furthermore, development and production of the cabling system is complicated and time consuming, but is going to be more efficient with the new system. For the same reason, maintenance cost will reduce, which is beneficial for the required reduction in direct operating cost. The allocation of system failure is time-consuming if all cables have to be checked individually. This is not required anymore, as the computer can identify error locations. Safety of the complete aircraft can also be increased, as fire hazard is lower without cables [84]. Besides, the flexibility of the interior design is high if cables are not needed and changes can be implemented easier.

On the other hand, some problems with the fly-by-wireless system are encountered. Mostly safety and electromagnetic compatibility is a problem. Safety issues are encountered in privacy, alternation and authentication. Privacy of all aircraft information must be ensured, as "eavesdropping" must be prevented at all times. Also alternation is a source of unreliability and high risks, as this could lead to interception of the signal by malicious people (Man-in-the-Middle). As terrorism attacks are in the spotlights nowadays, a possibility for alternation must be excluded in all ways. This also requires authentication of the signal, which prevents unauthorized access to the network. Another problem encountered for fly-by-wireless is electromagnetic interference (EMI). EMI with e.g. portable electronic devices, satellite communications or radio navigation results in both data rate and quality of service (QoS) degradation or even network collapse (Denial of Service). This must be prevented at all times, as it also leads to high risks [84].

A possible solution for safety and EMI issues is the use of an unconventional type of wireless network and bandwidth. Also a feedback loop can be inserted before original messages are sent to the receiver. Another option that is already widely applied for private WiFi networks is encryption[7]. The sender encrybts the signal, after which the receiver decrybts it again before use. This does not prevent interception, but does ensure privacy and authentication. Interception and EMI of the signal from outside the aircraft can be prevented by making the fuselage a Faraday cage or a principle comparable to this. Radio waves from outside will then be blocked, but can find their way inside this cage. Before applying this technology to the aircraft, a further investigation must be performed on the specific safety and EMI prevention.

To ensure safety further, redundancy is required. Due to the certification problems with the wireless network, a redundant cabling system is considered. This means that if the wireless network fails or is intercepted, the fly-by-wire network is consulted. This fly-by-wireless network is only installed for the critical flight functions, as it is assumed to only be needed in emergency cases. An example of such system is provided by the CANEUS Fly-by-Wireless Workshop[8].

Although several risks are to be overcome, production by 2025 is still assumed feasible as wireless technology is already widely applied these days. Also, a succesfull test flight has already been made by the Gulfstream GV[9]. If this is not the case and safety risks are still rather high, adding cables for the essential functions could be considered.

---

[5]URL http://www.nexans.nl/eservice/Netherlands-en/navigatepub_323737_-33567/Airbus_selects_Nexans_as_main_cable_supplier_for_t.html [Cited on 13 June 2016]

[6]URL http://ntrs.nasa.gov/archive/nasa/casi.ntrs.nasa.gov/20070013704.pdf [Cited on 20 June 2016]

[7]URL http://www.cs.ucsb.edu/ almeroth/classes/tech-soc/2005-Fall/11-01.pdf [Cited on 21 June 2016]

[8]URL https://caneus.org/fbw/downloads/2007/StudorFBWBriefing.pdf [Cited on 21 June 2016]

[9]URL http://www.aviationpros.com/press_release/10403052/gulfstream-demonstrates-fly-by-wireless-aircraft-control-system [Cited on 20 June 2016]

The fly-by-wireless system should, next to the mentioned improvements, fulfill the same requirements as the current fly-by-wire systems. This means it will have a data rate of 100 Mbps, designed for a distance of 6 [m] between each avionics bay and 50-80 end-systems. To achieve this, the ECMA-368 wireless technology will be applied, resulting from a trade-off in [84]. This system has the highest data rate and 14 non-overlap channels. This is beneficial in solving EMI problems.

11.2.2   System Overview

The overall data system is hosted from two avionics bays, both in the nose of the aircraft. These two avionics bays have to interchange a lot of data, which is why they are connected by wires as an exception. This will decrease the risks involved for EMI, improve system scalability and the data transfer time between gateways. From the gateways, the data will be transferred by the ECMA-368 technology at a frequency between 3.1 and 10.6 [GHz] and a bandwidth between 500 [MHz] and 7.5 [GHz] [85]. These properties prevent interference, but consume more power from the generators. This is accounted for and does not require extra adaption to the engines or generators. The system is designed such that multiple sources are able to send to multiple receivers.

In [85], an overview of control systems for comparable aircraft is provided. The C&DH system integrates all these systems, adapted for the RELOAD design, as shown below. For these systems a monitoring and command channel is added, called a COM/MON architecture. The two central computers perform the data handling, data storage and encryption. The overall layout of the Command & Data Handling system is shown in Figure 11.2.
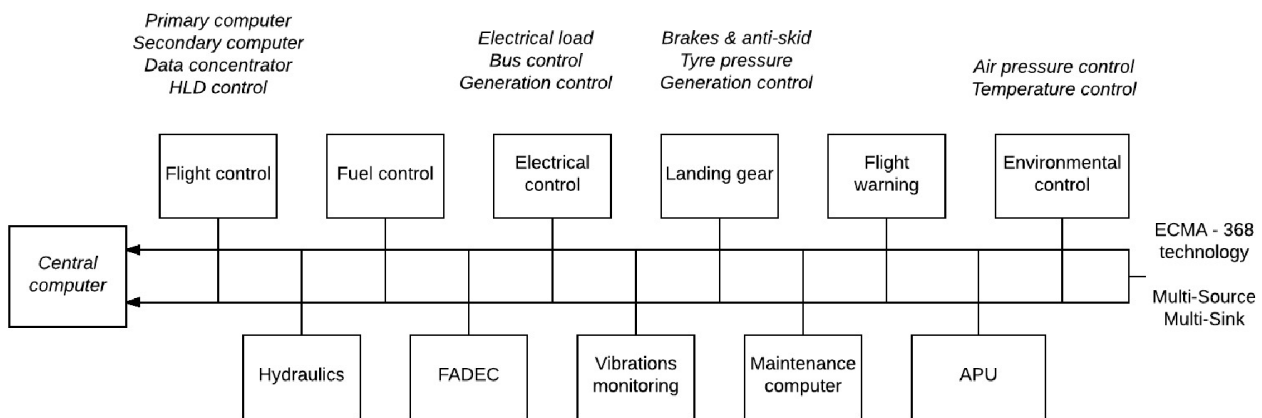
Figure 11.2: Command & Data Handling block diagram[10]

11.3   Fuel System

The fuel system is often not the first system for people to think about when considering an aircraft design. However the fuel system is an integral part of the aircraft and plays a critical role during design, certification and operation of the aircraft. The fuel system should provide the following functions [86]:

- Refuel and defuel the aircraft.

- Engine and APU feed.

- Fuel transfer and jettison.

- Quantity measurement and indication.

- Fuel management and control

11.3.1   Fuel System layout

The fuel system is build up out of a complicated network of pumps, valves, vents, tubes and several safety features. A basic overview of the fuel system is given in Figure 11.3. The two fuel tanks located in both wings run from 30 % till 80 % semi-span between the front and back-spar located at 15 % and 60 % of the local chord length. Both fuel tanks are divided in three sections, connected by baffle check valves which only permit fuel flow from outboard to inboard tank sections. The slight anhedral of 1° of the wings is sufficiently small to still have a natural inboard flow of fuel,

---

[10]FADEC: Full-Authority Digital Engine Control

helped by manoeuvring and disturbances during flight. The lower surface at the tip is still located higher than the lower surface of the inboard part of the wing. This is due to the high thickness of the inboard airfoil combined with the taper and thin airfoil of the outboard airfoil. Two engine feed pumps transport the fuel to the engine. By placing one pump forward and the second pump aft at the root of the fuel tank, a continues fuel flow is ensured during operation and all possible pitch attitudes [86]. A crossfeed is located between both engine fuel lines. The crossfeed ensures access to both feed tanks for each engine, to prevent lateral instability as a result of engine failure. The APU is connected to the crossfeed to ensure access to fuel when needed. The engines and the APU all feature a shut-off valve to cut the flow when required. If an imbalance arises between both tanks the transfer line can be used to pump fuel from tank to tank. Refueling or defueling the aircraft can be done via one or both refuel/defuel adapters located at each wing. To defuel the aircraft, the defuel valves should be opened manually. By using a suction source the fuel can be removed from the tanks. During refueling the aircraft refuel valves will automatically close when sensors detect the tanks are full or detect too high pressures in the tanks.
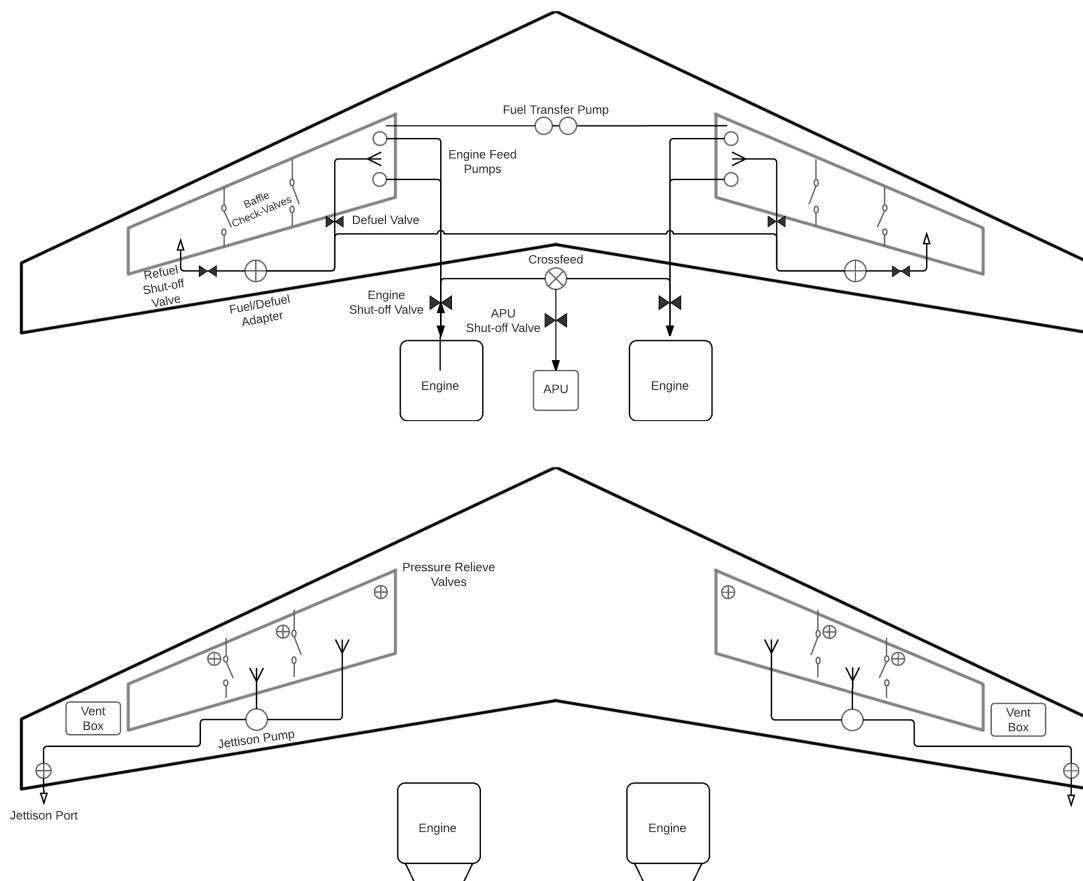
Figure 11.3: Fuel and jettison system layout

The jettison and vent subsystem is shown in Figure 11.3. To prevent the jettison system from interfering with the engine feed, the pumps and fuel lines are separated from the rest of the fuel system. Fuel lines run from the two inboard tanks to the tip of the wing where the fuel is jettisoned. The jettison pump is controlled by the control system to automate the jettison procedure. The inlets of the jettison fuel lines are located such that the inlets will be uncovered when a save amount of fuel remains in the tanks to ensure a failure in the control system cannot fully empty the tanks. The vent system is also shown in Figure 11.3, featuring a vent box and several vent valves. The vent system is needed to prevent pressure build-up in the tanks during flight. The increased pressure difference causes higher stresses for the structural components increasing the needed structural weight. The vent box shown is connected to several venting lines running through the fuel tanks and collects fuel caught in the venting lines, preventing fuel from being vented out. At each tank section a vent valve is present which will open when the pressure rises above design limits. The vent valves serve as a backup in case the vent lines fail or get blocked.

The fuel systems shown in Figure 11.3 fulfill several of the functions needed for the fuel system of RELOAD. The functions which are not treated in the layout are quantity measurement & indication and fuel management & control. These systems have to be researched further and designed in the coming final design phase. For the quantity

measurement & indication, sensors have to be placed within the tanks to measure temperature, pressure and fuel volume to calculate the fuel quantity left in the tanks. The fuel management &control function will interconnect the fuel system with the complete aircraft control system and control all valves, pumps and subsystems. The management and control will automate several processes to lessen the workload of the pilot. For example controlling the jettison process and continues balancing of the fuel tanks.

11.4 Hydraulic System

The hydraulic system is one of the most efficient systems integrated in the aircraft, thanks to the negligible losses due to fluid friction. It it used to move or actuate systems such as flaps, landing gear and thrust reverser. As in any aircraft, the RELOAD hydraulic systems aims to achieve the required redundancy and reliability [87]. This is done in two ways. First one, by having multiple pressure sources, which translates into having multiple pumps available to pressurize the system. Secondly, by having three separate hydraulic systems, which allows for failure of two of these systems without compromising the control of the aircraft[11].

As it can be read in [87], an aircraft usually has a left, right and central hydraulic system. The same architecture will be employed on RELOAD. The only difference is that the central system will be powered by electric-motor-driven hydraulic pumps, as opposed to air-turbine-drive pumps used in the more traditional architectures. This system is similar to the one used on Boeing 787[12] and is in line with the MEA approach followed by RELOAD [81].

11.5 Environmental Control System

In this section the environmental control system is presented, of which mostly the pressurization is covered in this design phase. The pressurization system is not a conventional one in the sense that it does not make use of bleed air of the engines. It rather makes use of air inlets outside the cabin. The air goes through electrically driven compressors and through air conditioning packs as can be seen in Figure 11.4. The free-stream air is captured by the inlets after which the air is compressed by electrical compressors. These compressors ensure the right pressure at all altitudes. Before the air goes into the cabin the quality and temperature is assured in the air conditioning segment. In Figure 11.4 one type of valve can be distinguished: A cross flow shut-off valve, this valve ensures flow to the other side of the system in case of failure[85].

The no-bleed architecture of the aircraft has a few advantages over the industry standard bleed system. Since no bleed flow is extracted from the engines, a relative improvement in efficiency is expected and hence an improvement in fuel burn [88]. The compressor of the pressurization system is adjustable in speed which implies that it can be run at energy efficient, optimal speeds during each stage of the flight. Another consequence of the no-bleed system is the reduction of engine parts, like pre-coolers, valves and ducts. Because ambient air is used the air does not have to be cooled, as is the case with bleeded engines. These improvements are expected to translate in improved maintainability and reliability [81][89].
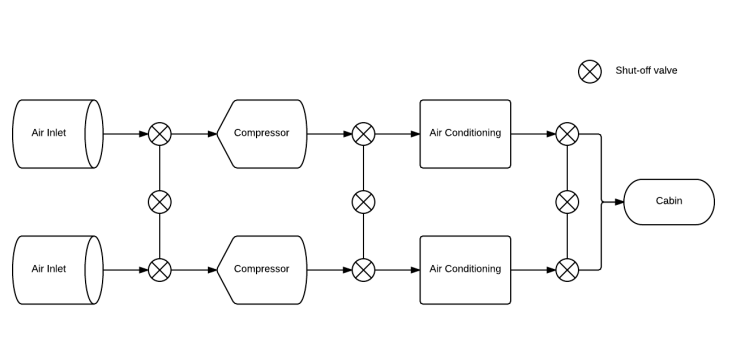
Figure 11.4: Flow diagram of pressurization system

11.6 Ice Removal

The aircraft does not operate in perfect weather conditions at all times. When it is expected to operate in conditions where icing is present, special measures must be present to ensure this does not develop into a problem. In

---

[11]URL =http://www.skybrary.aero/index.php/Hydraulic_Systems#Hydraulic_System_Redundancy [Cited on 9 June 2016]

[12]URL http://www.boeing.com/commercial/aeromagazine/articles/qtr_4_07/article_02_3.html [Cited on 9 June 2016]

this section, the anti-icing system is presented, which ensures that the ice build-up on the aircraft is retained to a minimum.

The anti-icing and de-icing systems normally are separated [70], but in RELOAD they will be formed by one single system. The role of de-icing (to remove an existing ice build-up) and the anti-icing (to prevent ice build-up) will both be tackled by an electric heating system. Due to the aft placement of the engines, it is impractical to have hot air be directed to the wing leading edges. Hence, the choice for an electrically based heating system was made. The anti-icing system is present on the wing leading edges, the canard leading edges and the engine air intakes. Finally, the leading edge of the vertical tail-planes will also be fitted with electric heating.

In the final design stage, it will be investigated how to exactly integrate the electric heating with the aircraft components. A point to pay attention to is the risk of a fire starting, due to the electrics. Furthermore, for now no power budget associated with this system was set up. This is also recommended for the final design stage.

11.7 Passenger Service Systems

The last part of aircraft systems is related to the passenger service systems. The positioning of the passenger seating, lavatories and galleys inside the fuselage has already been discussed in [1] and Figure A.1 in Appendix A. The lavatory system makes use of a blue liquid such as Anotec Blue SFTY-100[13] to disinfect and flush the toilet. Furthermore, passenger service includes the entertainment system. RELOAD will feather wireless personal screens and audio and LED lights for cabin lighting.

---

[13]URL http://toilet-guru.com/aircraft.php [Cited on 8 June 2016]

12

Noise Assessment

The RELOAD aircraft is not designed to be just sustainable, it is designed to be silent as well. In this chapter an analysis of the noise produced by the aircraft is presented and a preliminary approach to noise design is shown based on references. First a brief overview of noise and its sources is given in Section 12.1. Secondly, in Section 12.2 the noise requirements are revisited and investigated. Thirdly, the engines are placed in an optimal position to shield noise in Section 12.3. Finally, other means of noise reduction and the recommendations are discussed in Sections 12.4 and 12.5 respectively.

12.1 Overview on Noise Propagation

The airframe and the engines are the two most important sources of aircraft noise. The main sources that produce noise within the engine are the fan, compressor, combustor, turbine and the exhaust jet, where noise is produced by the mixing of hot exhaust and cool ambient air in a flow-flow interaction. The noise generated by the engine can be split up into different sources of noise [90].

- **Fan:** the noise generated by the fan is mainly due to the rotational speed of the fan tips. If supersonic velocities are reached by the fan tips a significant increase in noise can be observed due to shockwave formation.

- **Jet:** the jet of the engine has a characteristic noise directivity. Large velocity, temperature and density gradients cause strong refraction, which is the bending of waves due to moving into another (state) medium. This is shown in Figure 12.1. Due to the same refraction there is virtually no sound directly behind the exhaust of the engine, which is called the "cone of silence".

- **Combuster, turbine and compressor:** these sources are also experiencing the consequences of refraction and therefore show a maximum emission away from the engine symmetry axis, see Figure 12.1.
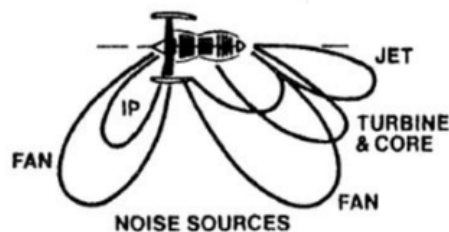
Figure 12.1: Noise emitted by the engine [90]

Not only the engines produce noise, also the airframe has a nonnegligible contribution to the total noise. This noise is generated mostly by turbulent airflows over the outer surface of the aircraft. Different sources of airframe noise are:

- **Landing gear:** the landing gear is responsible for most of the noise created by the airframe, if it is isolated fr0m the rest. This is because the structure of struts, wheels and bits is directly dropped down into the flow. This causes a flow-object interaction which emits noise.

- **Flaps:** flaps create noise due to the flow through the slots of the flaps and the interaction with their own wake. More noise is created by the flaps due to interaction with the landing gear.

- **Interaction of elements:** some aircraft objects that are placed within the free stream create turbulent wakes. These wakes create noise when they interact with other elements further downstream. The interaction noise can have a significant contribution to the total noise of the aircraft.

As can be concluded from the above stated, engine noise is a complex process that is build up by many different, small, building blocks. Not every element that contributes to noise is mentioned but only the ones relevant for this report.

12.2 Re-defining the Requirements

In the Baseline report [2], the requirements are defined without a good understanding of how the fly-over, lateral and approach measurements are performed. As such, the reference values for all three measurements are taken from different aircraft, as there is no aircraft that performs best in all three aspects. After further research it is decided that the most correct way of defining the requirements is in respect with the lowest cumulative noise of either a reference aircraft or the ICAO Annex 16 Volume 1 chapter 4 regulations[1]. That is found to be 266 $[EPNdB]$[2], therefore the new noise requirement values that RELOAD has to comply with is a cumulative noise level of 239 $[EPNdB]$.

In respect to the cabin noise requirements defined in [2], ICAO regulations do not mention anything. Because of that it is decided to not investigate this further, as they cannot be established correctly. However, one can expect that the noise levels inside the cabin and cockpit would be at acceptable levels. This because RELOAD uses turbofans and not propellers which are much louder. Also, the engines will be located at the back of the fuselage as shown in Section 12.3, which will further reduce the noise inside the aircraft [91]. Nonetheless, this aspect will be analyzed more in-depth at a later stage of the project.

The engines used by RELOAD are based on the CFM-LEAP engine, which already complies with the Chapter 14 noise regulation that will come into effect starting with 2017[3]. Therefore, the assumption that the RELOAD engine also complies to the Chapter 14 noise requirements is made. In Figure 12.2 the cumulative noise requirements for the RELOAD aircraft, which has a MTOW of 55744.2 $[kg]$, can be observed.
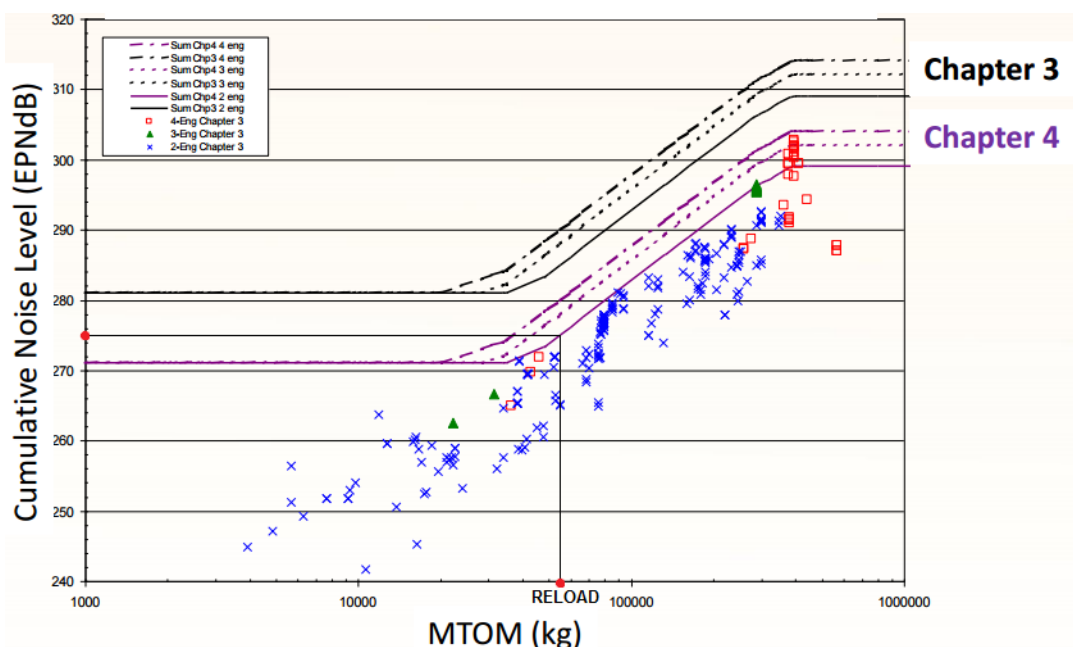
Figure 12.2: Noise requirements for the RELOAD aircraft based on Chapter 4 regulations [1]

This means that if RELOAD has to comply with Chapter 4 rules, it needs to have a cumulative noise of under 275 $[EPNdB]$. However, Chapter 14 aims at reducing the cumulative noise regulations with 7 $[EPNdB]$ compared to Chapter 4 [4]. Since the CFM-LEAP engine already complies to these future regulations, it means that an aircraft

[1]URL http://www.icao.int/Meetings/Green/Documents/day%201pdf/session%202/2-Dickson.pdf [Cited on 10 June 2016]
[2]URL https://www.easa.europa.eu/document-library/noise-type-certificates-approved-noise-levels [Cited on 10 June 2016]
[3]URL https://www.cfmaeroengines.com/files/brochures/LEAP-Brochure-2013.pdf [Cited on 10 June 2016]
[4]URL http://www.icao.int/SAM/Documents/2014-ENV/3.2.Noise%20TechnologyV3_notes.pdf [Cited on 10 June 2016]

the same size as RELOAD but with a more conventional look would have a cumulative noise level of at most 268 $[EPNdB]$.

In conclusion, RELOAD needs to decrease the cumulative noise from 268 $[EPNdB]$ to 239 $[EPNdB]$, which translates into a reduction of 29 $[EPNdB]$.

12.3 Noise Reduction Methods

In this subsection the engines are placed making use of reference data considering engine noise shielding. Although most of the references are not directly applicable to our aircraft, they provide the means to give a preliminary estimate of the engine noise. In this section only the shielding capabilities of the structures are assessed and the reflection of sound is not taken into account.

12.3.1 Engine Shielding

One of the most important aspects in noise reductions is the placement of the engines, as the shielding provided by the fuselage or by the wing is not negligible at all. One way of analyzing this reduction is by comparing different aircraft configurations in order to assess the best location of the engines.

These type of analysis is performed for different aircraft sizes and configurations. In [92], a comparison is performed between different engine placement configurations: tube-and-wing (TW), with engines mounted underneath the wing, over-wing-nacelle (OWN), with engines placed on top of the wing, mid-fuselage-nacelle (MFN), with engines also placed on top of the wing but just behind the trailing edge, and finally the hybrid-wing-body (HWB) configuration, which has the engines placed on top of the fuselage of a hybrid wing body aircraft. In Figure 12.3 the noise reduction results from these configurations are summarized [92]. It should be mentioned that the number in the name of the configuration represents the passenger capacity of the aircraft while "GTF" stands for Geared Turbo Fan Engine and "DD" stands for ultra high bypass ratio Direct Drive engine.
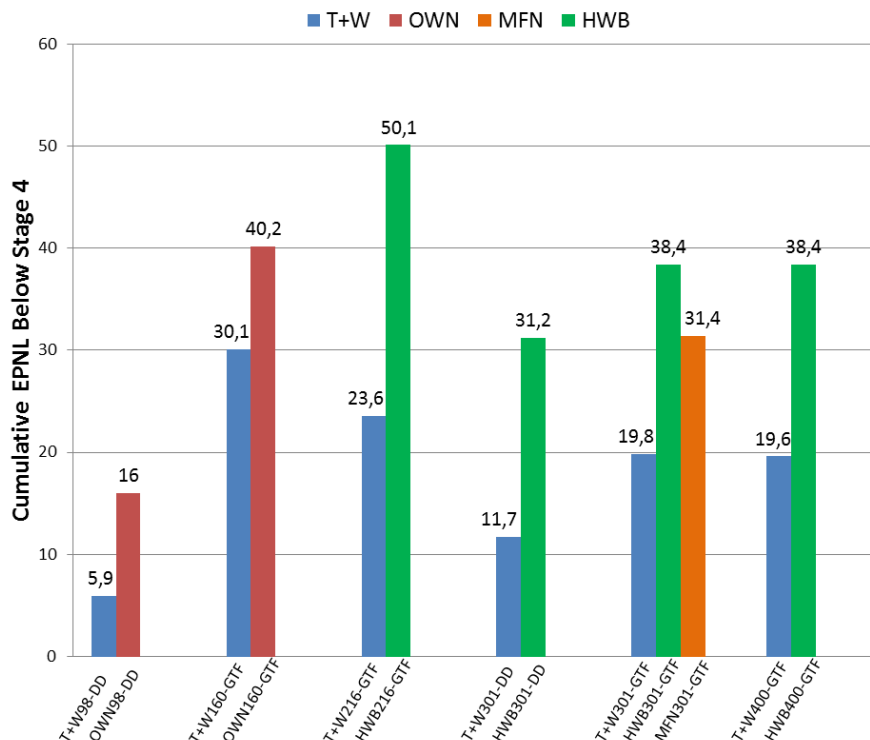
Figure 12.3: Noise reduction based on engine positioning

As can be noticed, for the same capacity and the same engine the most beneficial configuration is the HWB configuration. This one has, on average, a reduction of 20.85 $[EPNdB]$ when compared to the conventional configuration with engines mounted underneath.

In conclusion, in order to obtain a considerable noise reduction RELOAD will place its engines on top of the fuselage and they will be located between the vertical stabilizers. A factor of 0.9 is applied as the configuration of the HWB modeled in [92] and the configuration of RELOAD, although similar, are not entirely identical and also because the

models used for measurements are scaled down. This means that only by placing the engines on top of the fuselage with the core nozzle exit plane one fan nozzle diameter (FND) upstream of the tail [92], a noise reduction of approximately 18.7 [$EPNdB$] is achieved when compared to the same engine being placed under the wing.

12.3.2 Engine Placement

However, it is decided to place the engines at 2 inlet diameters in front of the trailing edge of the fuselage. As presented in Chapter 7, the inlet diameter of the RELOAD engine is 1.5 [m]. This results that the plane of the engine exhaust is located at approximately 3 [m] in front of the trailing edge of the fuselage along the centerline of the engine. This configuration and position provides a reduction of approximately 31.6 [$EPNdB$] below Chapter 4 standards [93]. This means that the reduction with respect to Chapter 14 is 24.6 [$EPNdB$], which results in a further reduction of 5.9 [$EPNdB$] just by moving the engine one more fan diameter to the front of the aircraft. A visualization of the RELOAD engine placement can be found in Figure 12.4.

12.3.3 Chevrons

Chevrons can be found at the exhaust of the engine. Basically they are a geometrical sawtooth pattern at the end of the cylindrical exhaust that makes the mixing of fan, core and ambient streams more efficient than a normal exhaust[94][95]. The chevrons create vortices which reduce the velocity and therefore the noise. Chevrons focus mainly on reducing the low frequencies while trying to minimally affect the higher frequencies. The latter can even increase[95]. Chevrons may affect the performance of the aircraft by decreasing the thrust and thus requiring more fuel to be burned in order to compensate for it. However, for the type of chevrons used by RELOAD engines and shown in Figure 12.5, the effect on fuel burn is considered to be minimal and in the order of 0.05 % [96].
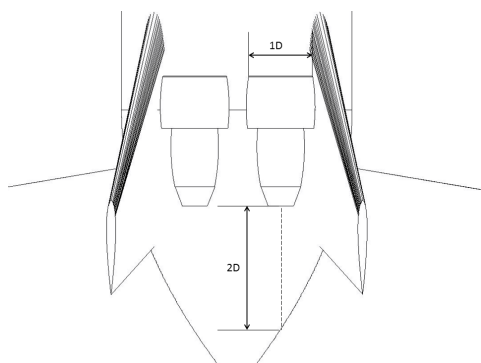
Figure 12.4: Engine placement in respect to the trailing edge of the fuselage
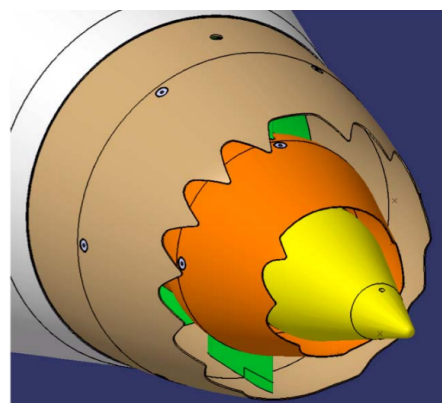
Figure 12.5: F8 type outer chevron and C2 core chevron [96]

In [96] an experiment is conducted with different type of chevrons configurations on an engine with a bypass ratio of 10. According to the research, the greatest reduction in noise is achieved by the nozzle equipped with the F8 chevron, as shown in Figure12.5. From [96] a reduction of 2[$EPNdB$] can be obtained at 2 times FND, with the F8 nozzle in clean configuration from an angle which corresponds mostly with the sideline. However, this engine is not identical to the RELOAD engine and this value is only approximated, therefore a recommendation is made in 12.5 for further analysis.

12.3.4 Vertical Stabilizer Placement

Adding a vertical stabilizer provides extra shielding, especially for the sideline reference measurements . Again, from [93], adding vertical stabilizers and chevrons lowers the noise by 3.5 [$EPNdB$]. However, as stated in Section 12.3.3, the chevrons are expected to reduce the noise by 2 [$EPNdB$]. This means that the vertical stabilizers only contribute with approximately 1.5 [$EPNdB$] reduction. Furthermore it is calculated that with a rudder deflection of 15 °, the shortest distance between the rudder and the engine center line is roughly one meter, it is recommended to investigate this further. Finally it is assumed that an unpeturbed flow enters the engine. A recommendation is made to further investigate the affect of the vertical stabilizers on the flow that enters the engine in 12.5

12.3.5 Landing Gear

As mentioned in section 12.1, the landing gear is one of the most important sources of airframe noise. As studied in [97], [94] and [98] a reduction of roughly 1.5 [$EPNdB$] can be established by adding fairings on the brakes and

a bogie beam undertray, wheelcaps and leg-door fillers[99]. Further investigation is needed to see where and how these parts should fit on the RELOAD landing gear.

12.4 Conclusion

In conclusion a cumulative noise reduction of approximately 29.6 [$EPNdB$] is achieved by using engines based on the CFM-LEAP, by placing the engines on top of the fuselage, adding chevrons and refining the landing gear ensemble. This indicates that RELOAD complies with the requirements re-defined in Section 12.2. Figure 12.6 provides an overview of the design choices and shows where RELOAD is situated in comparison to the Chapter 4 and Chapter 14 regulations. It is also compared to other reference aircraft with noise reductions, which is the Boeing 737-800[2].
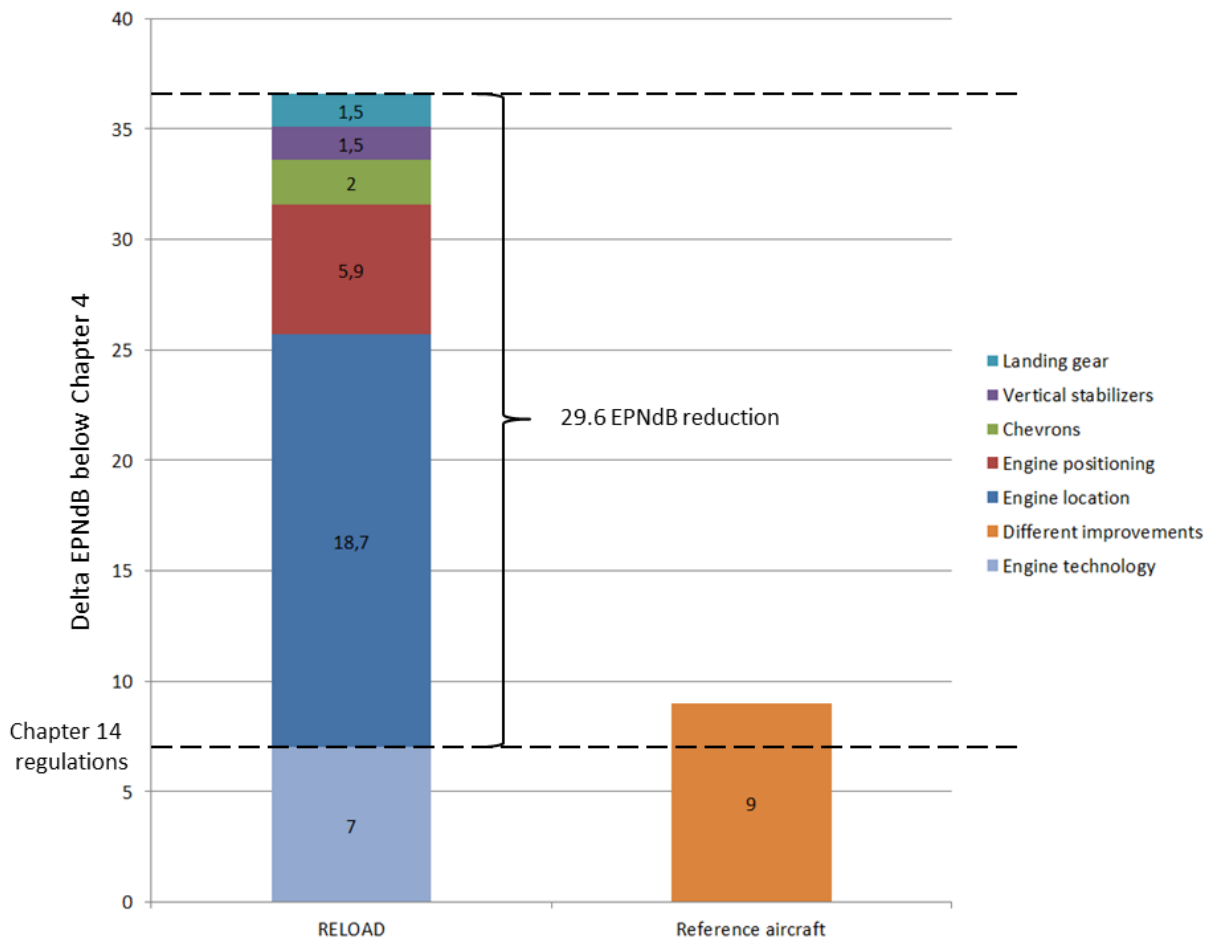
Figure 12.6: RELOAD noise reductions from different improvements

12.5 Recommendations

As experienced during the noise research, nothing certain can be said about the noise produced by the aircraft. Therefore the recommendation is made to build a model and test it in an aeroacoustic facility. Every aspect mentioned in chapter 12 should be tested first separately and afterwards together on the aircraft to fully grasp the impact on the total noise produced by the aircraft. Detailed information about how such an experiment is set up and conducted is described in [100]. At least six months are estimated to be needed in order to provide sufficiently reliable results.

A recommendation for assessing cabin noise by references is made as well. Due to the lack of time a cabin noise assessment could not be executed for this report. In three days it should be possible to asses the cabin noise through references and express this in [dB].

Due to the limited amount of space between the vertical stabilizers and the engines, a more in-depth analysis of the flow interaction between the two engines, as well as the flow interaction between the engine inlet and the stabilizers

should be performed. This should be performed through references, and start with investigating flow peturbations and the boundary layer. A week is estimated as sufficient time to finalize this research.

The effects of the hot exhaust jet on the rudder when its at maximum deflection should be investigated. The maximum deflection angle at which the rudder is deflected should be determined. It is possible to restrict the inward deflection of the rudder towards the engine. Decreasing the inward deflection engine should relieve the (if present) thermal stresses on the rudder. It is recommended to first analyse these effects at zero velocity. If the results are alarming, the cooling effect of the flowing air should be considered as well. A duration of one week is expected to conduct a preliminary analysis.

Finally, influence on the exhaust flow of the engines on the fuselage should be investigated. The temperature of the material underneath the exhaust flow should be measured. If the results are above the processing temperatures, either the pylon length should be increased or a more heat resistant material should be selected for the top of the tailcone. A reference study could be conducted in approximately three days.

III

Design Objectives

Optimising just one component of an aircraft is already quite a complex and arduous task. However, designing an entire flying vehicle while making sure that its components interact in an optimal way is even more difficult. Regardless, this has been tackled in the detailed design, while keeping in mind at all times that the integration of these components must accommodate all the design objectives.

In this regard, each department defined in Part II was aware from the beginning of all design objectives that needed to be fulfilled. For example, the propulsion department took into account the sustainability of the aircraft when sizing the engines, such that they would produce a reasonable low amount of emissions. At the same time, the aircraft systems were designed for safety by introducing redundancy. All the effort placed in the design objectives resulted in an aircraft that is, among others, safe and easily maintainable, while minimising the technical risks of such a project.

This Part is divided as following: the operations and turnaround time of the aircraft are explained in Chapter 13, while the maintenance of its systems is taken care of in Chapter 14. The aircraft is proven to be safe and sustainable in Chapters 15 and 16, respectively. A cost analysis including the return of investment is performed in Chapter 17. Manufacturing is also an important point and is analyzed in Chapter 18, while the reliability as well as availability of the aircraft are elaborated on in Chapter 19 Finally, Chapter 20.6 makes a recapitulation of the requirements and briefly shows how the final design complies with them.

13

Design for Operations

This chapter will discuss the ground operations of the RELOAD aircraft design. Section 13.1 will discuss the services and operations at the terminal, resulting from which the turnaround time is elaborated on in Section 13.2. Section 13.3 explains the design of the landing gear from an operations perspective.

13.1 Terminal Operations

The RELOAD aircraft will be designed for an optimal flight performance, but must also be efficient during ground operations. From the moment that the aircraft touches down until the moment it takes off, operations on the ground are in full progress. Figure 13.1 shows the Work Flow Diagram for all tasks performed simultaneously.

Figure 13.1: Work flow diagram for ground operations [101]

This section discusses the design and access points for service systems. In general, money is lost every minute that the aircraft is inoperative. An efficient terminal operations scheme thus saves operating cost or at least ensures that it remains the same as compared to reference aircraft. The canard up front of the aircraft and the blended wing give rise to problems concerning accessibility, which are to be solved. The overall layout of these points with service

vehicles can be observed in Figure 13.2. The rest of this section will discuss the placement of each service system and what they are used for, based on Airbus A320 and Boeing 737 operations. [102, 103]
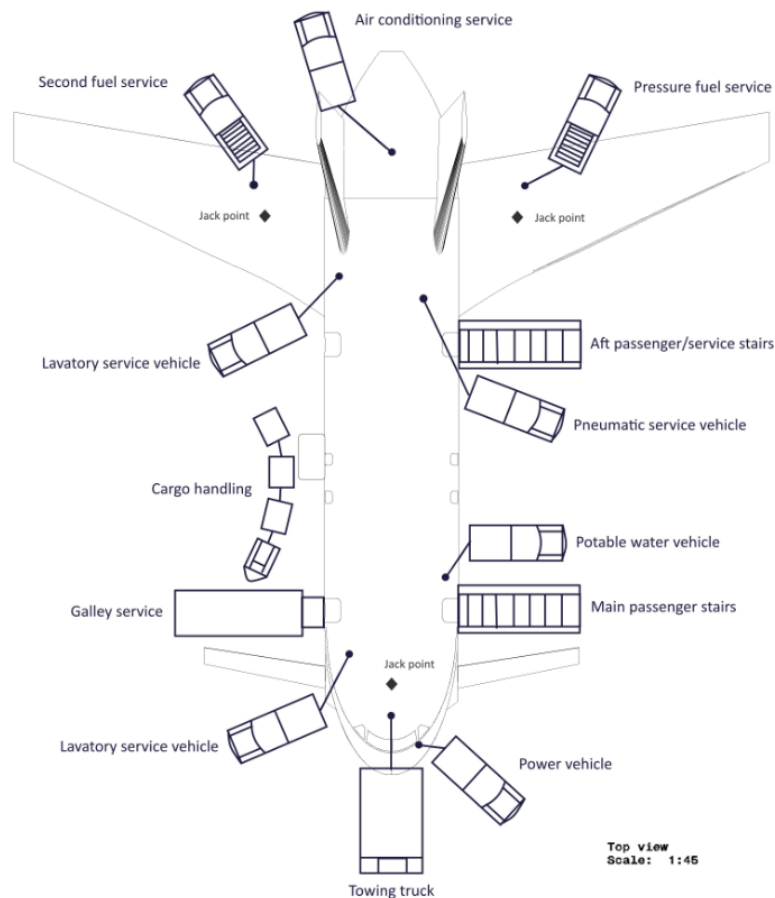
Figure 13.2: Airport terminal operations turnaround

To board and deboard the passengers, two staircases can be used. The main stairs up front of the aircraft can only be placed after the canard is tilted at least 75° upwards. This is possible as the canard is designed as a full-movable surface. Using stairs instead of a conventional jetway is less expensive and faster as well. A second staircase could be added in the back to ensure even faster deboarding and boarding of the aircraft or to allow the cleaning service crew to enter the aircraft directly. Furthermore, the double aisle interior design supports the pace of this process.

The portable water system requires a filling and draining point beside each other, such that one cart can handle both simultaneously. As most water is required at the galleys and lavatories and the center of gravity of the aircraft are already rather aft, the water tanks are placed towards the nose of the aircraft. Due to the elliptical fuselage shape, there is storage room next to the cargo compartment which will be used for two slender water tanks.

As mentioned in Section 11.7, the lavatory system uses Anotec fluids to flush the toilets. During lavatory service, both the Anotec tank is refilled and the waste tank is emptied. Two lavatory access points and two tanks of both fluids are installed in the aircraft. Two sets are positioned in the front and back of the aircraft respectively, as lavatories are placed here.

Cargo handling ensures the unloading and loading of the passenger cargo. For efficient storage of cargo Unit Loading Devices, ULD3-45 are used as elaborated on in [1] in service of a high-pace storage process. As can be observed in Figure A.2 in Appendix A, the cargo compartment offers room for eight ULD3-45 units, which is more than the initially stated and required seven. As just eight units need to be unloaded and loaded, one cargo door is installed. This reduces structural weight with respect to installing a second as on conventional aircraft. In addition, installing a second door is inconvenient combined with the large wing root which covers a large portion of the fuselage. The size of the cargo door is designed the size of an ULD3 unit with inaccuracy margins to ensure smooth cargo handling[1].

The pneumatic service vehicle ensures the pneumatic systems are all ready for flight. That means that they check tire pressure and hydraulic pressure, but are not used to start up the engine. This is covered by the VFSG and as

---

[1]URL http://www.premiumjetcargo.com/about-us/aircraft-types/a320-pax.php [Cited on 8 June 2016]

explained in Section 11.1, together with the air conditioning. As this system uses inlet air and APU power to refresh the cabin air, the air conditioning packs and system are located in the tail cone. Therefore the connection for the service cart is placed here as well, next to the pneumatic inlet. The fresh cabin air is pumped from the back of the aircraft towards the front over the ceiling and "old" air is abducted towards the passenger floor. From here, used air is blown out of the aircraft through the front valve. As the engine are positioned on top of the body, this used air will not enter the engine inlet and thus the cabin anymore.

Another key service cart required during ground operations is the refueling cart. Most conventional airports have a fuel system or storage in the pavement for each gate, such that the refueling cart just needs the hoses to fuel the aircraft. One conventional pressure fueling inlet is placed on the bottom side of the left wing to quickly refuel at high pressure. Another inlet is added to fuel with two carts at the same time, to reduce turnaround time, but using this inlet is optional. Two fuel vents are added on the underside of each wing to relieve air during fueling. Please refer to Section 11.3 for a detailed description of this system.

The ground power supply is connected to the nose of the aircraft below the cockpit. This system will ensure power for the cockpit, cabin entertainment, catering and cleaning during ground time as engines are turned off.

The cleaning and galley service team enters the cabin when all passengers are deboarded via the main stairs. The cleaning team then cleans the aircraft from the inside and performs tasks that the flight attendants can not do. The galley service switches the empty trolleys and garbage for full trolleys with foods and drinks. additionally, duty free items and entertainment systems are provided by the galley service. For this purpose the exit next to the galley is occupied by the catering truck. Both the cleaning and galley service mostly take place at the home airport of the airliner.

The jack points are used to jack the aircraft in case of aircraft landing gear maintenance or other moments that the landing gear does not provide enough clearance. The main jack points in the wing are located at the wing spar close to the landing gear. The nose jack point is positioned below the canard wing box. This is favourable for the structural integrity.

13.2 Turnaround Time

The turnaround time of the aircraft must be reduced as much as possible to keep operating cost low. To find the turnaround time of the RELOAD aircraft, the reference aircraft and differences with these have been analyzed [104] [102]. This system considers the positioning and removal of stairs, carts, cables and hoses, the rotation of the canard and the opening and closing of doors. In 1 minute it is found that 20 passengers can deboard the aircraft and 12 passengers can later board the aircraft in the same time slot for reference aircraft. The RELOAD design is assumed to handle 25 and 14 passengers per minute respectively due to the double aisle. Unloading and loading one ULD-3 cargo unit takes approximately 1,5 minute and all units will be loaded through the same door. Concluding, a turnaround time of maximum 40 minutes is required to completely prepare the aircraft for the next flight. The results of this analysis are visualised in Figure 13.3.
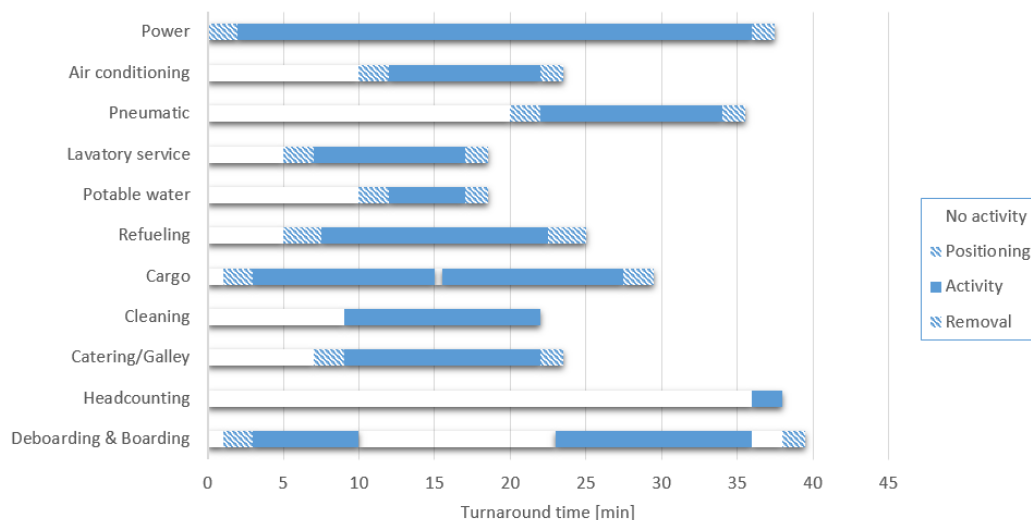
Figure 13.3: Airport terminal operations turnaround time

A note must be made on Figure 13.3 and its outcome, as this turnaround time is based on the home base of the airliner. Only at this place, catering and extensive cleaning are required. If the aircraft performs short flights, these tasks are only needed at the end of the day thus shortening the overall turnaround time by twenty minutes as deboarding now directly happens after boarding. The cargo unloading and loading is now constraining due to the single cargo door, resulting in a minimum turnaround time of 28 minutes. The power, air conditioning and pneumatic service can be shifted forward for this if needed. The layout of the RELOAD therefore allows for a fast continuation of operations.

13.3 Landing Gear

Now looking into operations for the landing gear design, it is considered beneficial that the conventional tricycle gear is applied. This ensures that accessibility to the front section of the aircraft at the gate is very comparable to most other aircraft. Additionally, it retains stability during loading and unloading. Furthermore, the aircraft is levelled on the ground, which is useful for loading and unloading of passengers, luggage and catering. With a landing gear height of 1.8 [m], also ground operations underneath the aircraft are still possible. Furthermore, the aircraft has been designed for a turn radius that is required on conventional airports as explained in Section 9.1.4.

Design for Maintenance

Aircraft maintenance is the third highest source of direct operating cost, as can be seen in Figure 2.1. In the current market, this amounts to 770 $/h. Therefore, it is crucial to investigate the aircraft design for ease of maintenance, or rather, adapt the design for it. Requirement SAFE-3, as defined in [105], states that the aircraft design shall be compliant with industry practice and regulations as defined in the MSG-3 logic. Section 14.1 describes maintenance logic. Furthermore, Section 14.2 presents a Prognostic Health Monitoring system, which is capable of aiding in determining tailored maintenance intervals. The landing gear is one of the only components of the aircraft that is designed according to the safe life principle, instead of fail safe. Section 14.3 therefore discusses it separately. Finally, Section 14.4 proposes some recommendation for the final design with respect to designing for maintenance.

By implementing the PHM system, maintenance intervals will be determined on a basis of necessity. Especially for engine maintenance this is expected to result in a cost reduction, since the technology is already operational[106, 107] and will thus be perfected more during the final design phase. At this moment PHM systems can already save 10 % on maintenance cost[108]. By careful design of the maintenance program and implementation of the Fly-By-Wireless (see Section 11.2.1) and the PHM system, maintenance cost can be reduced by 15 %, from 761 $/h to the targeted value of 647$/h, by the year 2025. This corresponds to a direct operating cost reduction of 2.6 %. Project risk is included inherently in this assumption. This risk will be treated and mitigated in Section 21.3.

14.1   Maintenance Program

The MSG-3 logic is a program envisioned by the aviation industry for the creation of aircraft maintenance programs. Since the creation of such a program takes roughly an equal amount of time as the aircraft design itself [109], only the higher level structure of the program shall be presented here. First of all, the MSG-3 procedure shall be initiated by the setting of the different components of the logic [109]; the Industry Steering Committee, which comprises of representatives of the authorities, the operators and the manufacturer will direct the work. Furthermore, the Maintenance Working Group, with representatives of the manufacturers and the operators, develops the requirements. Finally, the Maintenance Review Board approves the work. The entire MSG-3 logic is summarized by Figure 14.1. Once the committees are defined, the MWG's will start with the analysis of the requirements. The following MWG's are proposed:

- MWG 1: Hydraulics & Flight Controls
- MWG 2: Environmental systems
- MWG 3: Powerplants & APU
- MWG 4: Avionics
- MWG 5: Structures

- MWG 6: Zonal
- MWG 7: Fuel systems
- MWG 8: Landing gears
- MWG 9: Interior
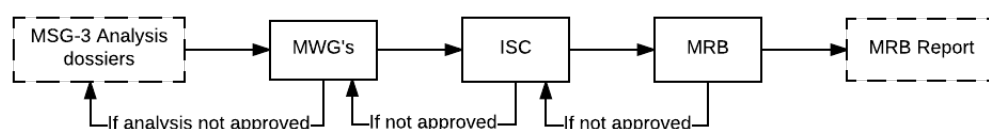
Figure 14.1: Maintenance Steering Group 3 logic summarized, based on [109]

The result of the MSG-3 program is a MRB report. It will act as a basis for each individual operator to develop its own maintenance program subject to approval of his regulatory authority. The report features the maintenance tasks, their interval and description of how to perform it.

The maintenance program shall be set up in a manner which allows for the task intervals to be determined on a basis of necessity, instead of flight cycles, hours or fixed times, as is now often the case. To determine when maintenance must be performed on a certain part, a prognostic health monitoring system shall be implemented in the aircraft. The following section describes this system.

14.2 Prognostic Health Monitoring

To optimize the interval at which maintenance of specific parts is to be executed, a prognostic health monitoring system will be included in the aircraft design. By optimizing the maintenance intervals, the cost related to maintenance can be lowered. Tasks shall only be performed when necessary, instead of on a fixed basis. Also, by using the prognostics capabilities, maintenance can be planned in advance. In this manner, less problems will arise by because of planning issues.

The PHM system will be based upon an in-flight health monitoring segment and a ground based segment. Firstly, the in-flight segment will be discussed. The in-flight system will have the main task of monitoring the aircraft health. All main components will have sensors continuously collecting data on their performance. In the engine, for instance, pressure and temperature sensors monitor the combustion process. Vibration sensors are used to assess whether all rotating parts still operate nominally. All these sensors feed their information to the health monitoring computer, which uses diagnostic observation algorithms and a diagnostic model to determine the aircraft health. These algorithms are still to be developed, which will be further elaborated on in Section 14.4. A reasoning engine uses the diagnostic model to output the health of certain parts. It is however still up to a human to execute the actual maintenance action. This is where the ground segment comes in. The ground based system will aid the maintenance crew to assess the need for tasks, but the action itself still needs to be performed by qualified crews. The in-flight segment outputs the health monitoring results. This data is available to the maintenance crew via a download or via a mobile platform (represented by a tablet interface in Figure 14.2). The mobile application allows the maintenance crew to go to the aircraft and assess its health in site. The data is then distributed on to various operator departments. The engineering department may analyse it for trends. The flight operations department could use it for optimizing operations to lower maintenance cost. And the platform manager such that aircraft can be scheduled. Current aircraft, such as the B787, produce as much as 500GB data per flight[1,2]. The PHM system must be configured such that this number will not increase majorly. It is expected to remain in the same order of magnitude. The central computed will have the capability to store all this data. Using the diagnostic model, the component reliability and feedback from encountered failure, the failure of a component can be predicted in the range of weeks ahead[110]. The entire PHM system is visualised schematically in Figure 14.2.
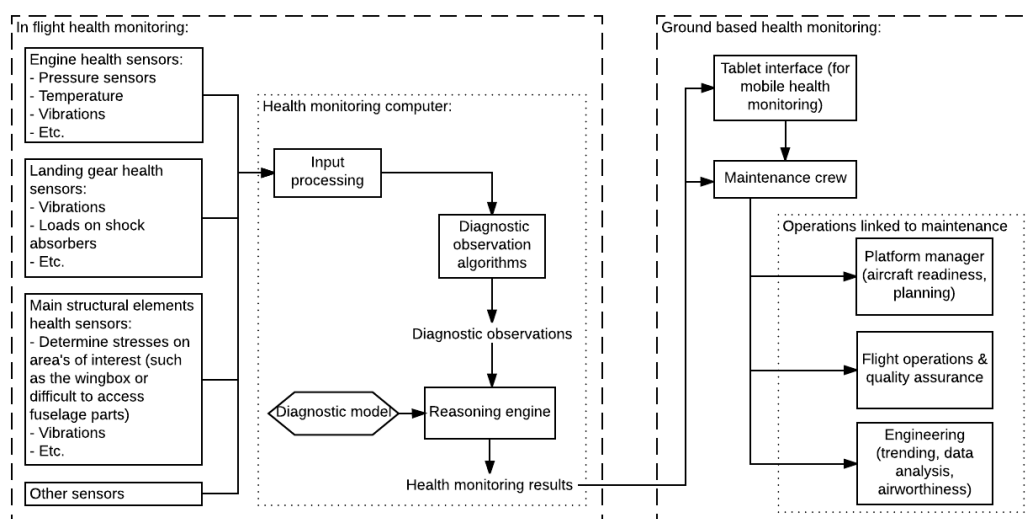
Figure 14.2: Architecture of the prognostic health monitoring system, based on [111, 112]

---

[1]URL http://www.geek.com/news/the-boeing-787-produces-over-500gb-of-data-during-every-flight-1542105/ [Cited on 24 June 2016]

[2]URL http://www.computerworlduk.com/news/data/boeing-787s-create-half-terabyte-of-data-per-flight-says-virgin-atlantic-3433595/ [Cited on 24 June 2016]

14.3   Landing Gear and Engine Maintenance

The landing gear is one of the moving parts. Furthermore, it is a safe life part, rather than a fail safe one. Due to the high landing loads and friction on the gear, maintenance is done regularly and is thus an expensive endeavour. To reduce the direct operating cost, design for maintenance is thus paramount. A conventional landing gear is chosen in the RELOAD design, making maintenance on the gear itself rather straight forward.

One thing that is often applied to retain safe operations, is a complete landing gear overhaul[3]. Roughly once every 10 years, the landing gear is replaced[1]. This means that each leg should be easily detachable and completely replaceable quickly to lower the costs associated with this task. In this way it does not require large downtime for the aircraft. To make sure this is possible, jacking point are located in the fuselage as can be observed in Figure 13.2. The forward jacking point is located aft of the nose landing gear to prevent tip forward and high nose loads. The aft jacking points are located in the wing for stability.

Apart from the entire gear replacement, several routine tasks and inspections need to be performed on the landing gear regularly. These tasks are always required, and always will be. A large cost reduction can thus be only attained by severely lowering the time and effort associated to them or by lowering the frequency at which they need to be performed. By implementing a the PHM system, the latter can be done. However, lowering the time associated to these tasks without impacting safety, requires intricate knowledge of the maintenance program and all systems. It shall therefore be recommended for the final design stage.

Looking at the engines, it is concluded they from the largest cost group inside maintenance. The cost related to engine maintenance are reduced by the implementation of two measures: first of all, the PHM system allows for a cost reduction, because it allows for more accurate necessity driven maintenance planning. Second of all, the engines are sized such that they can produce take-off thrust in a derated manner. This implies that at the beginning of life, the thrust needed for take-off is 86 % of the total engine thrust. By using the engines in this derated manner, the components last longer and the maintenance cost decreases.

14.4   Recommendations

To lower the direct operating cost resulting from maintaining the aircraft, more research and design effort has to be produced. This section presents some recommendations for the final design. Firstly, some recommendations towards the general design of RELOAD shall be stated. Then, the PHM system will be elaborated on more.

The first recommendation pertains to the development of the maintenance program of the aircraft. Because the MSG-3 logic is vast and requires complex analyses, only the general outline was presented above. It is recommended to start the development of the maintenance review report soon in the final design stage. The development of a proper maintenance program is paramount for efficient operations of the aircraft. The global planning of the MSG-3 maintenance program can be found in Figure C.1. The second recommendation is made towards the domain of aircraft structures and the engines. Because the engines are on top of the fuselage, their accessibility is low. In case the engine needs to be replaced (or if less invasive maintenance needs to be performed), its accessibility is an important issue. To accommodate daily line maintenance tasks, it is recommended to install a system which allows for crew to easily mount the aircraft and access the engines. Such a system might take the form of fuselage integrated steps up to the engines. Furthermore, that part of the fuselage must be designed to carry maintenance crew. For more invasive tasks, such as replacing the engine, it is recommended to investigate the design of specialized jigs, to mount and dismount the engines from in between the tail planes. The creation of these jigs can take place concurrent with the maintenance program, explained above. The third and final recommendation pertains to the PHM system. It is recommended to investigate the health monitoring sensors further and to determine what placement and type of sensors lead to the optimal health monitoring capabilities. Furthermore, the diagnostic model needs to be defined, verified and validated until it is certain it will function as desired. The reasoning engine will feature some artificial intelligence capabilities, which must be developed as well. It is recommended to finish this development before 2024, such that there remains enough time to certify and test the system.

---

[3]URL http://www.boeing.com/resources/boeingdotcom/commercial/services/assets/brochure/landgearoverhaulexchpgm.pdf [Cited on 15 June 2016]

<p style="text-align: right;"># 15</p>

Design for Safety and Risk

In this section, all the major safety measures taken by RELOAD in order to provide its passengers a safe and pleasant flight are discussed. Some aspects that contribute to safety, such as data analysis or sensors that analyse the material integrity are discussed in Chapter 14, while others, such as the possibility of remote controlling the aircraft or video cameras that aid the pilot are further elaborated upon in Chapter 10. It should also be noted that other safety systems that are currently used by any aircraft, such as seat belts, life vests, emergency lights and navigation lights, although taken into consideration, are not specifically described. This chapter starts off with Section 15.1 in which two safety systems are analyzed. Section 15.2 and Section 15.3 discuss the engine and landing gear safety safety respectively. Afterwards, Section 15.4, Section 15.5 and Section 15.6 contain the external, passenger and avionics safety issues. Each section contains a numbered set of potentially risk-sensitive components. These numbers refer to the technical risk maps, which are presented in Section 15.7 with a corresponding fault tree analysis in Section 15.8.

15.1 Safety Systems

This short section discusses two safety systems implemented in the RELOAD aircraft. These systems are vital to ensure safe flight by avoiding collisions.

A Traffic Collision Avoidance System (TCAS) is installed on RELOAD. This has the potential to assess any other aircraft located in proximity and warn the pilot if it seems that their paths interact. This system also advices the pilot to take on the necessary avoidance measures, such as climbing or descending at a specific rate.

RELOAD also benefits from the use of the Enhanced Ground Proximity Warning System (EGPWS). This system is designed to warn the pilot in case the aircraft is in danger of flying into the ground or other obstacle. Although classic systems only use a downward looking radio altimeter, RELOAD also has the Forward Looking Terrain Avoidance (FLTA) function, which is able to scan the vertical and lateral paths of the aircraft and advise the pilot accordingly[1].

15.2 Engine Safety

This section summarizes the risks and safety measures taken in order to prevent any threats the engine may pose to the structural integrity of the aircraft and the safety of its passengers and crew.

1.1 Fatigue crack failure: A failure due to fatigue can have a catastrophic impact and a probable likelihood of occurrence if not managed properly. To mitigate this risk, the Prognostic Health Monitor System (PHM) described in 14.2 shall be capable of detecting any fatigue cracks or defects that may result in an engine failure. This way no blade or materials can endanger any aircraft component. However, if the PHM fails to give any warning about a potential engine failure then the second safety measure should prove its usefulness. That is the engine containment capability. Engines used by RELOAD are designed such that they pass any airworthiness standards of aircraft engines, such as blade failures. More specifically, the RELOAD engines are capable to prevent or at least minimise the damage from a blade rotor failure through the compressor and turbine rotor cases [113]. The two engines are placed approximately 0.8 $[m]$ apart, which should be enough to avoid any flow interaction, as it has been proven before on the Lockheed JetStar aircraft [2]. Also, the damage containment system is sufficient to protect the other engine in case one has problems. After these means of risk mitigation, the probability of such an event is reduced to improbable and the impact

---

[1]URL http://www.skybrary.aero/index.php/Terrain_Avoidance_and_Warning_System_%28TAWS%29 [Cited on 16 June 2016]
[2]URL http://barrieaircraft.com/lockheed-jetstar.html [Cited on 21 June 2016]

is reduced to critical.

1.2 Pylon tear down: A potential scenario is a pylon tear down, resulting in the engine disconnecting from the fuselage. The consequence is that the engine becomes an uncontrolled projectile, which is completely unacceptable in any situation. It is recognized by the RELOAD engineers that the placement of the engines has a negative influence on the probability of an impact with the fuselage in the case of a pylon tear down. Therefore, the likelihood of occurrence is defined as remote and the impact is deemed catastrophic and measures are necessary to mitigate this risk. As with any aircraft design, the pylons are designed for extreme load cases and energy levels to minimise the likelihood of occurrence of such an event. The described PHM is able to monitor the structural status of the pylons as well, thus the main risk lies in the event of a crash or crash landing. To further mitigate this risk a recommendation is made to design the tail cone as a crumple zone, which deforms and buckles before the pylons fail. This way the tail cone facilitates a damper effect for the pylons and engines, further lowering the likelihood of occurrence of such an event to negligible.

1.3 Engine fire: Aircraft engines accommodate high performance combustion tanks, thus it is not unthinkable that a contained or uncontained fire occurs at this component. This is a risk with a remote probability of occurrence and a critical impact, as very little of such events occur but fatalities are not ruled out. These statements are based on the 2014 statistical summary of Boeing[3] and are a valid basis for the RELOAD aircraft as it refers to jet engine aircraft. The aircraft can in most cases deal with such an event by using on-board systems such as fire extinguishers. Furthermore, the fuel flowing towards that engine is cut-off automatically in order to minimise the damage. By these measures, the impact of such an event is reduced to marginal[3].

1.4 Engine cooling failure: If an engine has either a fan failure or no cooled air is provided from the compressor, the engine can easily become overheated. Should one of these events occur, then a fire is most likely the result and the same measures are taken as for an engine fire (Risk 1.3). Such events happen only by remote likelihood and have a marginal impact as seen from the list of accidents between 2006 and 2016 [4].

1.5 Ignition system failure: The risk of the ignition system failing is insignificant when on the ground. It can however pose a threat if one or two engines disengage while flying, for example due to a dust cloud. The likelihood of such an event is considered remote and the impact negligible, as each engine has an ignition system and the aircraft is designed to fully function with one engine inoperative.

15.3   Landing Gear Safety

This section discusses the safety considerations for the landing gear design.

2.1 Landing gear actuation: A failure in such a system has a critical impact on the aircraft, as a belly landing is risky. From the statistics of Boeing[3] it is seen that the likelihood of occurrence is relatively small and therefore set to remote. The retraction of the landing gear is a crucial system. According to the Federal Aviation Administration (FAA) [114] next to the standard retraction hydraulics, an emergency system must always be present. This regulations state that the landing gear should be able to extract even in case of main system failure. Examples for this are backup hydraulic systems, stored nitrogen gas bottles that can be directed into actuating cylinders, mechanical systems that can be operated manually, or free-fall gravity systems. The latter is most lightweight, as it just uses gravity and no extra system. This is why this option is applied. The convenient option is to install three bars in the cockpit floor that can be pulled in case of emergency. This releases the uplocks of the retraction system, such that the gear free falls into its position. For the RELOAD design, this system is applied to reduce the impact of a retraction mechanism failure to negligible.

2.2 Landing gear strut failure: Weather conditions could cause the aircraft to touchdown on just one leg in stead of the complete main gear or to land under a side slip angle. An insufficiently capable landing gear design can then fail under the high loads, which would have a critical impact on the aircraft. As the problem happens on the ground this event is not considered catastrophic, since such a failure doesn't necessarily result in fatalities. Harsh weather such as high energy cross winds are a common phenomenon, so the likelihood of occurrence is probable. To prevent failure in this situation, the main gear track has been designed for a lateral tip over of 55 degrees in case of a banked landing. Furthermore, the main gear legs are sized to carry a landing load factor of 3g which is be sufficient to touchdown and roll straight in crosswinds. The same landing load factor is applied to the nose gear for rough landings. Lastly, the tires have been sizes to carry more than just the load on the leg divided by two, for the same crosswind problems and for tire failure. After mitigation, the likelihood is reduced to remote.

2.3 Tire failure: A flat tire on an aircraft is a significant risk, as it means that large amounts of heat through friction can set the tires on fire. In a large aircraft, it is not obvious that such an event is immediately noticed by the pilots,

---

[3]URL http://www.boeing.com/resources/boeingdotcom/company/about_bca/pdf/statsum.pdf [Cited on 17 June 2016]
[4]URL http://www.skybrary.aero/index.php/Bleed_Air_Systems_Accident_2̇6_Incidents [cited on 17 June 2016]

as aircraft often have multiple wheels per landing gear which can bear the loads. There are multiple possibilities in how a tire is damaged. Gusts can cause an aircraft to perform a so called "hard landing" which compresses the tires possibly beyond their limit load. Additionally, debris on runways and taxiways can have the same effect. As risk mitigation, aircraft taxi- and runways are checked multiple times per day for debris and modern aircraft tires are equipped with pressure sensors to detect flat tires on time. Through these means, the probability of this event is reduced from probable to occasional with a marginal impact.

15.4   External Influences

The environment also performs a major role in an aircraft's life cycle. How RELOAD is able to cope interact with the environment threats is discussed in this section.

3.1 Bird impact: The likelihood of a bird strike event is probable and the impact is catastrophic, as such an event can cause system level failures and fatalities as seen from statistics (EASA[5]). Bird strikes can present a safety hazard, especially in case it damages an engine or the wing. Fortunately, due to the placement of RELOAD engines, they are protected against bird strikes by the fuselage, especially during climbing. For the fuselage, wing and canard the nosecone and leading edges respectively are reinforced in order to make sure that they could sustain bird strikes without affecting the aircraft's performance. Fibre Metal Laminates with layers of aluminium alloy and high strength glass fibre composite is proven to be capable to withstand very high impacts [115] and is therefore a suitable material for the reinforcing of leading edges and nosecone. The impact is thereby reduced to marginal and the likelihood to occasional.

3.2 Lightning: Lightning strikes are not uncommon, but nowadays very few aircraft experience serious accidents due to this phenomenon as seen from statistics on Aviation Herald[6]. Therefore, lightning strikes are considered occasional and of marginal impact. RELOAD is able to cope with lightning strikes, in order to prevent damage due to power spikes for example. The fuel tanks have been designed to not allow any sparks or current inside them even if the lightning connects at their proximity. This protection system can be viewed in Section 11.3.1. Any access doors, fuel filler caps or vents are designed to seal properly in order to keep the current generated by the lightning on the exterior of the fuselage[7]. Surge protection devices and wire shielding are installed on RELOAD in order to avoid any damage done to the electrical system[8]. Finally, RELOAD is covered with a fine layer of conductive meshes that minimise the damage of the skin at the point where the lightning hits[8]. With the taken measures, the impact of a lightning strike is reduced to negligible.

15.5   Passenger Safety

Designing for a safe flight is one of the major task of an aerospace engineer. Several aspects need to be considered to comply with CS25 regulations [4]. This section discusses the design of the safety exits as well as the equipment located on board and deployed in case of emergency situations.

4.1 Emergency evacuation: Should the aircraft be forced to make an emergency landing, it is well imaginable that all passengers have to be evacuated as quick as possible. Such a situation is extremely dangerous if the right safety measures are not taken and can easily result in fatalities. As aircraft are subjected to strict safety regulations, the likelihood of an unsuccessful evacuation is estimated as remote, but has a catastrophic impact. CS-25 regulations [4] state that an aircraft with 177 passengers should have at least two Type I and two Type III doors on each side of the fuselage. However, since the design allows it and the aft 8 rows have no exit behind them, it is chosen to scale up to two Type A doors and two Type III doors on either fuselage side. Furthermore, the doors were sized larger than the minimum requirements and the aircraft features two aisles which double the capacity. The required door sizes together with the applied design dimensions for these door types are stated in Table 15.1. A seat map configuration including the placement of exits, lavatory and galleys can be found in Figure A.1 in Appendix A. To disembark the passengers in a quick manner (under 90 seconds) in case of an emergency, slides are present at each door which can serve as life rafts in case of a water landing. Figure 15.1 shows the configuration of the emergency slides. Furthermore, it can be seen that the cockpit features an emergency exit for the pilots on the top side through which they can reach the ground via an escape rope. By means of the described methods, the impact of an emergency situation in general is reduced to marginal.

---

[5]URL http://essi.easa.europa.eu/documents/EASAReportBirdpopulationandimpact.pdf [Cited on 17 June 2016]
[6]URL http://avherald.com/ [Cited on 17 June 2016]
[7]URL http://www.scientificamerican.com/article/what-happens-when-lightni/ [Cited on 14 June 2016]
[8]URL http://www.airspacemag.com/flight-today/how-things-work-lightning-protection-161993347/?no-ist [Cited on 14 June 2016]
[9]URL https://www.behance.net/gallery/2609097/Chemical-Aviation-Oxygen-Box [Cited on 10 June 2016]

Table 15.1: Emergency exit dimensions

Door type	Required		Design	
	Width [m]	Height [m]	Width [m]	Height [m]
Type A	1.06	1.83	1.06	1.95
Type III	0.51	0.914	0.6	1.00
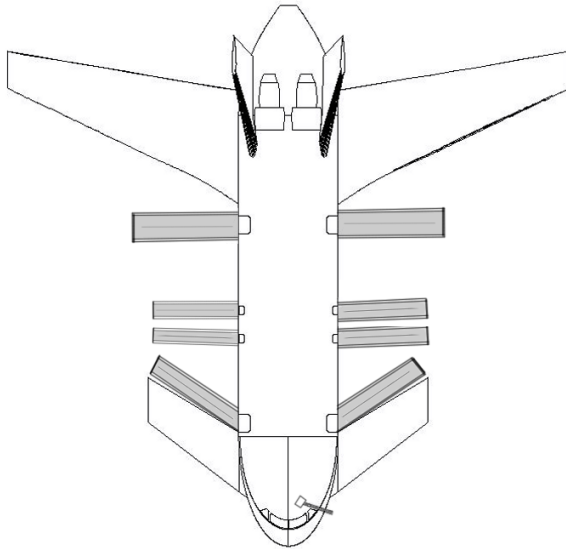
Figure 15.1: Top view of the aircraft with all the emergency slides deployed
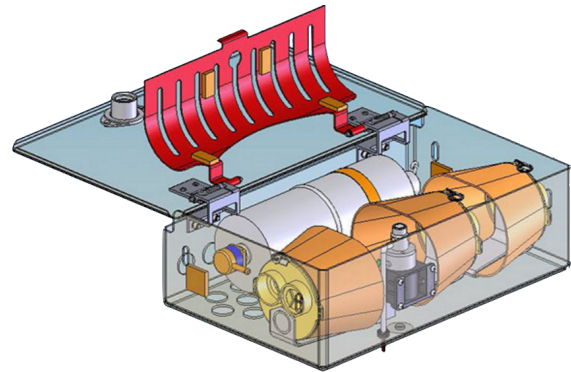
Figure 15.2: Oxygen mask storage system[9]

4.2 Cabin depressurisation: In the situation of a pressure loss in the cabin at 11 [km] altitude, passengers can get seriously injured. Even fatalities are not ruled out, depending on the magnitude of the pressure differential. Therefore this risk is estimated to have a critical impact with a remote possibility of occurrence. Cabin pressure can be lost due to a fault in the pressurization system or a structural failure of the fuselage. Furthermore a problem with the air conditioning system, air inlet or a compressor failure can also cause a drop in cabin pressure. Just as in regular commercial aircraft, oxygen masks and a pressure vessel with liquid oxygen are stored in the ceiling above each passenger row in RELOAD to mitigate the associated risks. An impression of such a system can be found in Figure 15.2[10]. This needs only to be replaced after usage, which is rare. It does need inspections and tests regularly to ensure proper functionality. Furthermore, the aircraft is able to rapidly descent to below 3 [km] should depressurisation occur. Altogether, the impact of cabin pressure loss is reduced to marginal with the stated measures.

15.6 Avionics Safety

5.1 Control surface actuation: The control surfaces are imperative in ensuring stability and controllability. These features are achieved more specifically through a full movable canard surface and ailerons that can be trimmed over a wide range of angles, as described in Chapter 8. The angular setting is attained through the usage of servo actuators, which are electrically driven. There is, of course, always a possibility that such an actuator fails. Following such a failure, the control surface is either fixed in one position or rotating without constraint which can easily result in an extremely dangerous unstable and uncontrollable situation. The impact associated with an actuation system failure is therefore deemed catastrophic with a probable likelihood of occurrence. To diminish the impact of one free rotating surface to negligible, a dual redundant servo-actuation system is applied to each of the control surfaces. A means of disconnecting each servo is to be implemented simultaneously, such that the impact of one canard jamming can be reduced to negligible as well. However, even though the defect actuator needs to be replaced immediately once the aircraft lands, the risk of a dual failure during flight still remains. Therefore the impact of a complete canard actuation system failing is still catastrophic, but the likelihood after risk mitigation is reduced to improbable.

5.2 Fly-by-wireless system: The chosen command and data handling system in the RELOAD poses some serious challenges, as described in Section 11.2. Its main functions are to ensure a high rate and quality data stream, which

---

[10]URL https://www.behance.net/gallery/2609097/Chemical-Aviation-Oxygen-Box [Cited on 8 June 2016]

is not always ensured. The risks concerning various forms of command and data handling failure has already been elaborated on in the cited section and can be discretized as having a catastrophic impact with a probable likelihood of occurrence. The efforts of risk mitigation include insertion of feedback loops to ensure data quality and so, for example, reduce the probability of a system hijack. Furthermore, multiple transponders are used, each utilizing multiple non-overlapping frequency ranges to provide redundancy. For a single failure, these measures reduce the likelihood of occurrence to remote and the impact to negligible. When considering the failure of multiple (redundant) components, the impact is still catastrophic but with an improbable likelihood.

15.7 Technical Risk Overview

Risks evolve and disappear over time. They should therefore be tracked over time, to ensure that they do not suddenly fire. This section treats the technical risks related to the development of the product. As a basis, the per component preliminary analyses in Part 4.2.2 are considered. These are, where possible, grouped and summarised in Sections 15.2 to 15.6.

All risks are plotted in a risk map, which visualises the likelihood of occurrence against the consequence for each considered event. Five categories are considered for the likelihood of occurrence of an event; Improbable, Remote, Occasional, Probable and Very probable. Four categories are defined for the impact axis; Negligible, Marginal, Critical and Catastrophic. Since the risks is seen as the multiplication of the two, the risks in the upper right corner are critical and must be mitigated to ensure the very continuity of the project.

Figure 15.3: Technical risk map before risk mitigation

Figure 15.4: Technical risk map after risk mitigation

15.8 Fault Tree Analysis

With the information found above a complete fault tree analysis is performed. This analysis can be found in Figure 15.5.
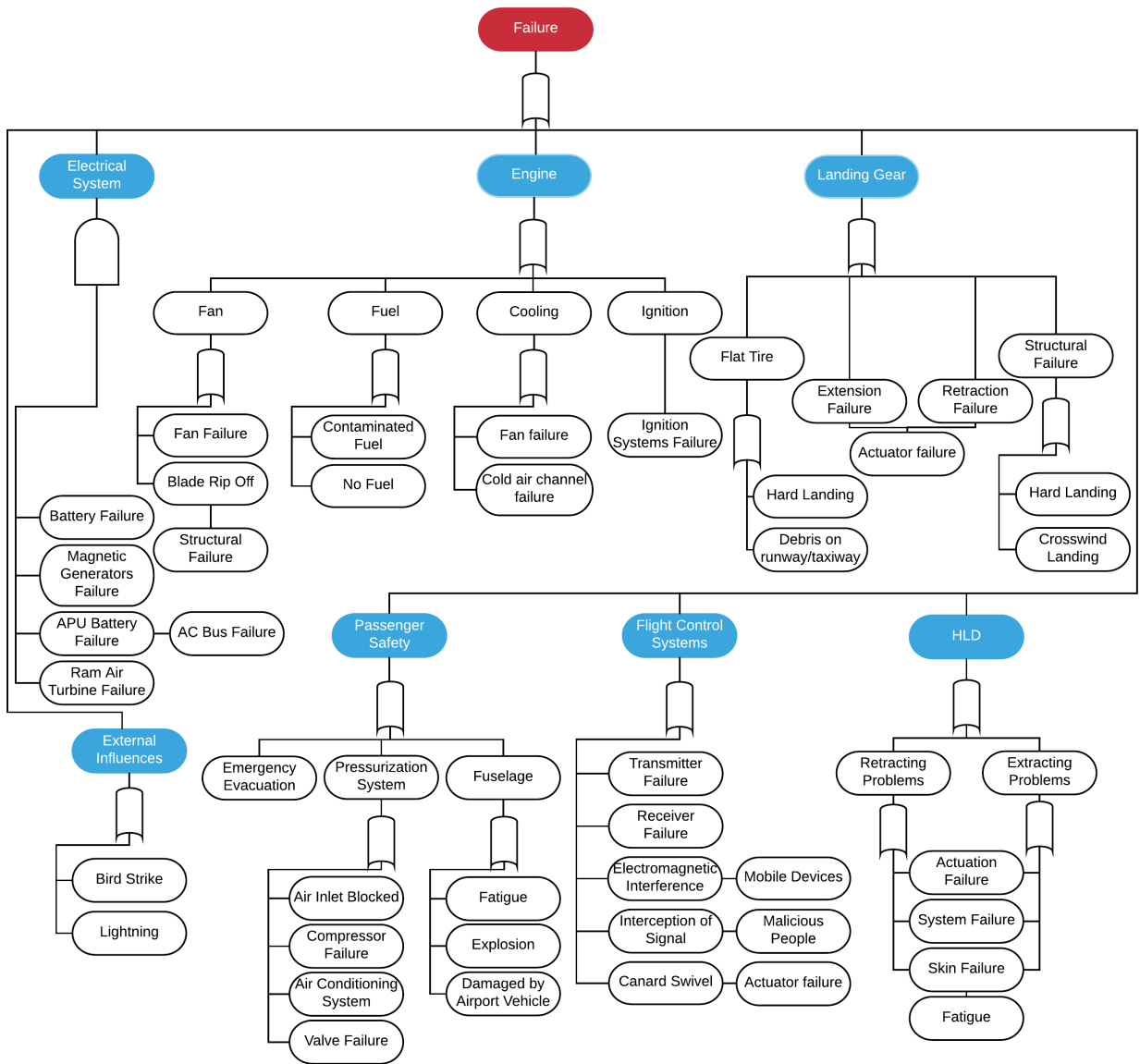
Figure 15.5: Fault Tree Analysis

16

Design for Sustainability

Although the performance of RELOAD is important, also its impact on the environment should be considered. This chapter elaborates on the method used to analyse the environmental impact in Section 16.1. Then this method is applied to the RELOAD project to study and mitigate the impact in Section 16.2.

16.1 Method

The methods used in this chapter on sustainable development are roughly the same as in Mid Term Report [1]. Most notably the Red Flag, treated in Chapter 13 of the Mid Term Report, is used again. The life cycle assessment is updated to current standards and a visualisation of the product's life is displayed in Figure 16.1 . Furthermore the flag method is expanded with the Green Flag method: the Green Flag method highlights the design choices that are made keeping sustainability in mind. As can be seen in Table 16.2, most improvements are made in the operational phase, which is the most important phase. However, in every phase of the life cycle analysis improvements are accomplished.
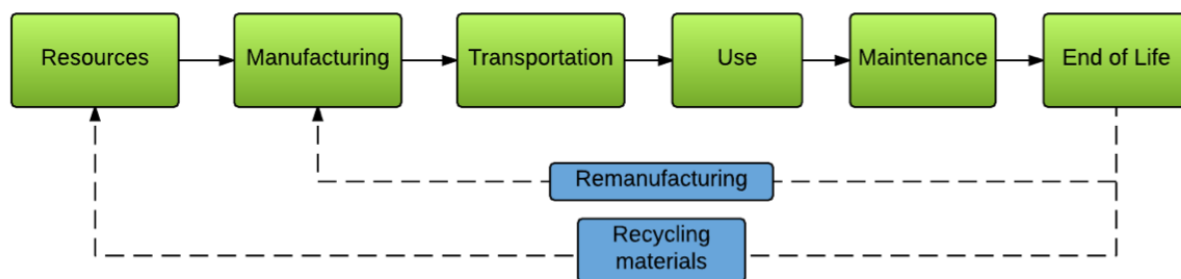
Figure 16.1: Visualization of the life cycle of RELOAD

16.2 Sustainable Development Analysis

Each part of RELOAD's life cycle raises different sustainability concerns. In this section each part is treated and investigated using the Red and Green Flag method, after which the risks are mitigated.

16.2.1 Resources

During the preliminary design several material choices are made. The materials selected during this stage of the design are discussed. The main material groups are:

1.1R **Aluminium:** In the midterm report [1], a brief overview of the environmental impact of aluminium is already given. At this point the preliminary structural weights of the wingbox and fuselage are known and therefore the impact of using new produced aluminium can be assessed, compared to recycled aluminium. The results are presented in Table 16.1. As can be seen, more than 124000 [$kgCO_2$] can be spared per aircraft by using recycled aluminium only on the wingbox and fuselage. The aim of RELOAD is therefore to use as much recycled aluminium as possible. It has to be noted that pure aluminium is assumed for these calculations and not the alloy.

Table 16.1: CO_2 reduction by recycling aluminium [116]

Parameter	Mass[kg]	Aluminium [$kgCO_2/kg$]	Recycled aluminium [$kgCO_2/kg$]	Reduction [$kgCO_2$]
Reference	1	11.6	1.68	9.92
Fuselage	5439	63092.4	9137.52	53954.88
Wingbox	7135	82766	11986.8	70779.2
Total	12574	145858.4	21124.32	124734.08

1.2R Titanium: New production methods for titanium are on the rise. As demand is growing, the search for faster processes which consume less energy is urgent. For now though, the energy consumption and costs remain high [117].

1.3R Steel: As mentioned in [118], a 10 to 15 % reduction in CO_2 can be achieved in the steel industry by logistics. RELOAD aims not to only minimise the usage of steel, but also to optimise the transport of (un)treated steel.

1.4R Rubber: This resource is already assessed in the midterm report [1].

1.5G Biofuel: Biofuels are, when compared to normal jet-A fuel, more CO_2 neutral. This means that the production and use of biofuels produces less CO_2 emissions than jet-A fuel. In [119], a reduction of 75 % in greenhouse gasses is presented on the life cycle of camelina based biofuels compared to normal jet fuels.

16.2.2   Manufacturing

2.1R Vertical stabilizer: RELOAD features two vertical stabilizers of 29.5 [m^2] each. The size is, compared to comparable aircraft, significantly larger and thus demands more material to manufacture the sub-assembly. Aluminium is red flagged as a resource in Subsection 16.2.1, due to its environmental impact.

To mitigate the negative influence of the amount of resources used to manufacture the vertical stabilizers, it is opted to reduce the needed size of the stabilizers. One of the recommendations during the vertical stabilizer sizing is to utilize the canard for augmented yaw stability by introducing dihedral or anhedral. Using the canard to stabilize the yaw motions of the aircraft it is expected to reduce the needed vertical stabilizer surface by 7 to 10 % and thereby the amount of needed resources. Mitigation approaches specific to the used resource is already treated in Subsection 16.2.1.

2.2R Wing: RELOAD has a different design point with respect to current competitors, most notably the wing loading is lower. RELOAD has a wing loading of 4000 [N/m^2] compared to a wing loading of 5950 [N/m^2] of a Boeing 737 [1]. As a result the wing surface area is larger, requiring more resources to manufacture the wing.

The increased footprint caused by manufacturing the larger wing surface is mitigated by the low drag of the wing design during use. The use phase of the aircraft can be 45 years, making the use life cycle phase have a larger impact compared to the slight increase in footprint during the manufacturing phase.

2.3G More Electric Aircraft: RELOAD is a More Electric Aircraft. A MEA is less dependant on hydraulics and pneumatics power. Pneumatic power is commonly provided by the bleed air of the engines, resulting in lower efficiency of the engines. Hydraulics are heavy, prone to leakage, need maintenance and the installation is tricky [69]. RELOAD utilises electric power over pneumatic and hydraulic power to increase efficiency, lower weight and reduce maintenance needed. All of which contribute positively to the overall sustainability of RELOAD.

2.4G Fly-by-wireless: One of the advantages of RELOAD is the use of fly-by-wireless eliminating the need of a large amount of cabling. Fly-by-wireless is treated in full in Subsection 11.2.1. Sustainability wise it is beneficial since it reduces the amount of resources needed to manufacture the cabling harness of the RELOAD aircraft.

2.5G Lean manufacturing: Using Lean manufacturing approaches, RELOAD is minimizing waste while creating value. The method is described in further detail in Section 18.1. By minimizing waste RELOAD contributes to a lower footprint made by manufacturing of the aircraft. At the same time value is created for the RELOAD project because it wants to brand itself as a sustainable aircraft designer.

16.2.3   Transportation

3.1G Factory location: Special attention has gone in selecting manufacturing locations for sub-assemblies of RELOAD.

---

[1]URL http://www.b737.org.uk/techspecsdetailed.htm [Cited on 15 June 2016]

In Section 18.3 a more in depth explanation is given on the choice of location. The locations are purposely chosen to be in close proximity to minimize transportation distance and therefore environmental impact.

3.2R **Type of transport:** Transport by train results in the least amount of carbon-dioxide, only 0.03 - 0.1 $\left[\frac{g_{CO_2}}{kg \cdot km}\right]$ [2]. A promising concept for transportation are airships like the Varialift[3] and Aeroscraft[4], which only have a footprint of 0.055 $\left[\frac{g_{CO_2}}{kg \cdot km}\right]$ [2]. The majority of parts have to be shipped by plane, namely the nose cone, tail cone, fuselage, wings, canard and vertical stabilizers. These sub-assemblies are too large to be transported by train. Transport by boat is not possible, since the factories are located inland. The engines are 1.5 [m] in diameter and 2.5 [m] long, and are thus suitable to be transported by train. The landing gear is 1.8 [m] long and the wheels have a diameters of up to 1.03 [m]. The landing gear sizes also permit these sub-assemblies to be transported by train.

To mitigate the impact of transportation, the sub-assembly factories are chosen to be relatively close to minimize the amount of transportation distance. The two factories which are furthest from the final assembly line supply the engines and landing gear. These parts can be transported by train, which has a lower footprint than transport by plane. A more in detail explanation on the factory locations is given in Section 18.3.

16.2.4 Use

4.1G **Fuel consumption:** The total fuel consumption of the RELOAD aircraft is lowered by 37.7 % with respect to reference aircraft, as treated in Subsection 7.2.7. This is mainly due to the engine design and the low drag of the aircraft, on which is elaborated on in the next two points.

4.2G **Low drag:** The overall aerodynamic design results in a drag of 33.4 [kN] during cruise. The drag is covered in more detail in Section 5.4. Due to the drag value, RELOAD is able to significantly reduce the fuel use and therefore emissions.

4.3G **Engine:** The engine is specifically designed for this aircraft and therefore optimised for the low drag. The engine is designed with sustainability on the forefront, reducing the fuel consumption as much as possible.

4.4G **Biofuels:** The use of biofuels does not influence the amount of CO_2 emitted into the air by the aircraft but it does influence the source of the fuel as can be found in 7.4.2. The CO_2 emissions caused by biofuels are part of a closed emission circle and do therefore not affect the environment during this life cycle phase [119].

4.5G **Noise:** As can be read in Chapter 12 noise is a key design point. With the appropriate measures, RELOAD is able to lower the cumulative noise of the aircraft by 29.6 [$EPNdB$] with respect to reference aircraft 12.4.

4.6G **Cabin waste:** By implementing two aisles in the fuselage, as can be seen in A.1, RELOAD offers the possibility to recycle on-board. Garbage can be retrieved faster and therefore the cabin crew can make different rounds to retrieve different kinds of garbage[5].

4.7R **Emissions per kg fuel:** This is still red flagged because of the fact that, although the total emissions are lowered, the emissions of CO_2 per kilogramme of fuel burned are not lowered, even when using biofuels. This is mainly because of the molecular structure of the fuels. Although this can not be altered, the overall emissions are more CO_2 neutral with biofuels [120].

16.2.5 Maintenance

5.1G **Prognostic health management:** In 14.2 the Prognostic Health Management system is described, which provides not only a decrease in maintenance cost, but also affects the location and frequency of the maintenance.

5.2G **Location:** By implementing the PHM system, optimisation calculations can be easily implemented with respect to location. A database of maintenance facilities and parts in stock could be uploaded to the aircraft after which the most optimum planning can be be made with respect to flights, maintenance and destinations.

5.3G **Frequency:** The frequency of maintenance is improved as well since precise action can be taken according to the health monitoring system. This prevents the aircraft from unnecessary down time.

---

[2]URL http://timeforchange.org/co2-emissions-shipping-goods [Cited on 16 June 2016]

[3]URL http://www.varialift.com/ [Cited on 15 June 2016]

[4]URL http://aeroscraft.com/aeroscraft/4575666071 [Cited on 15 June 2016]

[5]URL http://www.sustainableaviation.co.uk/wp-content/uploads/2015/09/Aircraft-Cabin-Waste-Recycling-Guide1.pdf [Cited on 15 June 2016]

16.2.6   End of Life

6.1R **Remanufacturing:** Airliners actively maintain their aircraft to maximize the lifetime. As a result most structures and components are at their end of life and therefore are not remanufacturable. Having unlimited lifetime is not wanted either, since new technologies emerge and result in old technology to become outdated.

Most ideally every component of RELOAD reaches end of life at the same instance in time. This is complicated by the end of life being dependant on vastly different factors, like time, cycles or even uncertainties. To minimize waste RELOAD aims to optimise each component for the expected lifetime depending on the limiting factor. RELOAD intents to design all components to be recyclable after this end of life stage is reached, so the resources can be reused.

6.2G **Metals:** The metals used to manufacture RELOAD are recyclable. The energy required to recycle Aluminium, Steel and Titanium is lower than the energy needed to produce new resources [116], making the recycling process more favorable. RELOAD is most likely not remanufacturable, so effort is put into designing RELOAD such that the parts can be recycled. Steel and Aluminium are easy to recycle, with a reduction of respectively 84.4 % and 85.5 % in the amount of carbon-dioxide emitted [116]. For Titanium it is more complicated to recycle since Titanium is highly reactive at high temperatures. Nevertheless recycling still is more favorable and results in a reduction of 84 % in carbon-dioxide emissions [121].

6.3R **Rubber:** Recycling rubber is a hazardous process, which is treated in Chapter 13 of the Midterm Report [1]. To recycle rubber it has to be devulcanized, shredded and vulcanized. Waste processing is hazardous due to the release of toxic elements during combustion of rubber[6].

6.4R **Composites:** These types of materials are hard to recycle due the bonding between fibers and resin. The industry has not yet developed a reliable and economic method to separate the components used in composite materials. To prevent landfill, the industry is researching methods to separate the components and recycle composites [36].

6.5G **Ease of disassembly:** A general design strategy should be that the structure allows for easy disassembling. This makes the maintenance and the end of life phase easier. Simple strategies are presented in Table 15.4 in reference [122]. Main design rules are to minimise the number of fasteners where possible, minimize the number of interconnecting wires and cables, fasteners should be easily removable and easily reachable.

---

[6]URL http://www.conserve-energy-future.com/RecyclingRubber.php [Cited on 16 June 2016]

Table 16.2: Life Cycle Assessment of the aircraft

1. Resources	2. Manufacturing [123]	3. Transportation
Materials:	Lean manufacturing (2.5G)	Factory location (3.1G)
-Aluminium (1.1R)	Subsystems:	Type of transport (3.2R)
-Steel (1.2R)	-Nose	
-Titanium (1.3R)	-Fuselage	
-Carbon epoxy	-Tailcone	
-Rubber (1.4)	-Engines	
-Polymers	-Vertical stabilizer (2.1R)	
-Ceramic matrix composite	-Landing gear	
-Jet-A fuel	-Canard	
-Biofuels (1.5G)	-Wings (2.2R)	
	-HLD	
	-More Electric Aircraft (2.3G)	
	-Wing tips	
	-Fly-by-wireless (2.4G)	
	-Fuel system	
	-Hydraulic system	

4. Use	5. Maintenance	6. End of life
Fuel consumption (4.1G)	PHM (5.1G)	Remanufacturing (6.1R)
-Low drag (4.2G)	-Location (5.2G)	Material recycling:
-Engine (4.3G)	-Frequency (5.3G)	- Metals (6.2G)
-Biofuels (4.4G)		- Composites (6.4R)
Noise (4.5G)		- Rubber(6.3R)
Reachability		- Polymers
Safety		Ease of disassembly (6.5G)
Cabin waste (4.6G)		Disposal
Personnel		
Emissions per kg fuel (4.7R)		

<div align="right">

17

</div>

<div align="right">

Cost Analysis

</div>

Since three important requirements are related to cost, it is of utmost importance to consider this during the design. This chapter investigates the life cycle cost (LCC) of the aircraft in Section 17.1. Afterwards the expected return on investment is discussed in Section 17.2.

17.1 Life Cycle Costs

During a life cycle, more costs than just the development are included. In general the total life cycle costs are split up according to 4 life phases; development cost, manufacturing cost, operational cost and disposal cost. To estimate the performance of the aircraft and its compliance with the requirements it is important to determine its performance in terms of cost. This section estimates the cost of the entire life cycle.

17.1.1 Development and Manufacturing Cost

For the cost estimations of development and manufacturing, Roskam part VII [124] is used. The first cost that is estimated is Research, Development, Test and Evaluation (RDTE) cost that takes into account seven different estimations such as RDTE profit, test and simulation cost and development support. Since not all parameters are known yet at this stage, several estimations and judgement factors are chosen to account for this. The estimated parameters are shown in Table 17.1. The second cost is the manufacturing and acquisition cost which takes into account the manufacturing costs and profit made by the manufacturer. Again, the assumptions used for the calculations are summarized in Table 17.1[1][2][3][4]. The final results are calculated for a range for produced aircraft, as is explained in Section 17.2. For both costs, the avionics and engine costs have to be estimated. The engine costs are estimated from the CFM LEAP engine, which costs approximately 13 million [\$] per engine [5]. According to Roskam [124], the avionic equipment costs can be estimated to be in between 5-15 % of the total aircraft price. However, since rather new trailing edges technologies are used, a slightly higher percentage is taken, thus 20%. For the same reason an additional safety factor of 1.05 is included to account for the extra implementation costs of the Prognostic Health Management and the top mounted engines.

Both calculations are verified using the example application in Roskam at the end of each chapter to see whether the same inputs would generate the correct output. Validation is performed with values of the Airbus A320 and Boeing 737. The price of the RELOAD aircraft proves to lie in between the price of the two competitors.

17.1.2 Operating Costs

One of the most constraining requirements in the RELOAD project is to reduce the Direct Operating Cost (DOC) by 30 %. The DOC considers expenses that are directly related to the amount of flying hours an aircraft makes, as stated in Section 2.1. The following operating costs are considered in the design:

---

[1] URL http://aviationweek.com/paris-air-show-2015/production-rates-are-airbus-and-boeing-aiming-too-high [Cited on 17 June 2016]

[2] URL http://www.payscale.com/research/US/Job=Aeronautical_Engineer/Salary [Cited on 17 June 2016]

[3] URL https://www.measuringworth.com/uscompare/ [Cited on 17 June 2016]

[4] URL http://www.keith.seas.harvard.edu/Misc/AuroraGeoReport.pdf [Cited on 16 June 2016]

[5] URL http://www.cfmaeroengines.com/press/ryanair-to-purchase-200-cfm-leap-1b-engines-at-a-value-of-more-than-1-3b/776 [Cited on 17 June 2016]

Table 17.1: Estimated parameters for the life cycle cost calculation

	RDTE parameters			Acquisition cost parameters	
Symbol	Description	Value	Symbol	Description	Value
W_{AMPR}	AMPR weight from eq (3.5) in [124]	39148 [lbs]	F_{pro_m}	Manufacturing profit percentage	0.05
N_{RDTE}	Number of test airplanes built	5	R_{e_m}	Engineering manhour rate program	133 [\$/h] [4]
F_{diff}	Factor for difficulty of the program	1.5	F_{int}	Interior cost factor	2000
F_{CAD}	Factor for computer aided design	1.2	R_{m_m}	Manufacturing labour rate of the program	81 [\$/h]
R_{e_r}	Engineering manhour rate	133 [\$/h][1]	R_{t_m}	Manufacturing tooling labour rate	81 [\$/h]
CEF	Cost escalation factor [3]	6.1	N_{r_m}	Airplane manufacturing rate	3[2]
N_{st}	Number of static airplanes	2	t_{pft}	Number of flight test hours [124]	10
R_{m_r}	Manufacturing labour rate	81 [\$/h]	F_{ftoh}	Overhead factor [124]	4
F_{mat}	Factor for type of materials [124]	1	F_{fin_m}	Factor for manufacturing interest rate	0.1
N_{r_r}	RDTE production rate [124]	0.33			
R_{t_r}	Tooling labour rate	58 [\$/h]			
F_{obs}	Factor of observable importance	1			
F_{stf}	Cost adjustment factor	0.2			
F_{pro}	RDTE profit percentage	0.05			
F_{fin}	Factor for interest rate	0.1			
C_{RDTE}	**Total RDTE cost**	**3.07 B\$**			

- Fuel & Oil is the most significant part of the DOC, such that the biggest saving can be obtained here. By designing a new turbofan engine, a considerable reduction is achieved. This is explained in Section 7.2.3.

- Maintenance cost decreases by the application of a Prognostic Health Management system. This is elaborated on more in Section 14.2.

- Crew cost decreases significantly by the implementation of the single pilot system. This is elaborated upon in Chapter 10.

- Depreciation depends on the price that is paid for the aircraft, its residual value and its lifetime. A lifetime of 45 years is assumed, see Section 6.1. Using the aircraft price as determined in Section 17.2 and the residual value as 5 % of the price[6], a calculation of the depreciation cost per year can be made. This is normalized per flight hour by assuming six 3-hour flights per day with ten inoperative days for big maintenance every year.

- Rentals include the rent of aircraft, terminals, gates, airport equipment, etc. These costs reduce with efficient operations, as the aircraft stays shorter at the terminal and gate and lends the airport equipment shorter. On the other hand, a new operational system may be required to serve this innovative design. A concrete estimation can not be made on this number as no direct relation to operations could be found. This is why this cost reduction is set to zero percent in the most conservative case.

- Insurance costs are related to the aircraft price, which is therefore assumed non-changing with respect to conventional aircraft. Also, reliability and safety is ensured in the RELOAD project, so insurance costs are not expected to increase due to the innovation.

- Other costs are considered to remain the same, as no conclusion can be drawn on what this part includes precisely.

The indirect operating cost is also estimated using Roskam [124]. This gives a relation for the block distance as a function of the IOC/DOC fraction. From the Baseline report [2], the block distance is calculated to be 7356 [km] which results in a fraction of 0.5. With this fraction, the IOC would be 1553.5 [\$].

---

[6]URL https://www.kpmg.com/Global/en/IssuesAndInsights/ArticlesPublications/Documents/components-of-aircraft-acquisition.pdf [Cited on 17 June 2016]

Table 17.2: Direct operating cost in [$/$hr$] of reference aircraft and RELOAD

Aircraft type	Fuel & Oil	Maintenance	Crew	Depreciation	Rentals	Insurance	Other	Total
Boeing 737-800	2011	816	948	305	509	7	4	4600
Boeing 737-900	2217	674	543	438	79	2	5	3958
Airbus A320	2252	748	858	249	441	9	10	4567
Weighted average	2148	761	834	308	400	7	7	4464
RELOAD	1237	647	513	297	400	7	7	3108
Saving [%]	42	15	38	3.6	0	0	0	30.4

17.1.3   Disposal cost

For the disposal cost no estimation method is available, nor reference data. However,it can be reasoned that the disposal cost of the RELOAD aircraft is likely to remain the same. The RELOAD aircraft has a conventional aluminium wing and fuselage, which reduces the disposal costs compared to composites. Furthermore, it uses off-the-shelf parts for example the morphing high lift devices and engines, such that not much difference will occur in the costs.

17.2   Return on Investment

Airbus and Boeing are currently the clear winners when looking into production rates and market share. They both approach a 50 % market share these days and produce approximately 50 narrow-body aircraft (A320 or Boeing 737) every month[7]. Now RELOAD is coming into place with a completely new innovative design to take further steps in reducing noise, emissions and especially operating costs. As production rates and sales of the Boeing and Airbus are not achievable in the upcoming years, a production and sales of three aircraft per month is assumed. The aircraft price is then based on this number and a return on investment of 5 % over the upcoming five years as stated in the requirements. This means that the total refunds must be 105 % of the investment in development and manufacturing. Figure 17.2 shows that for an aircraft price of 90M $ (2016) a ROI of 5 % is achieved in 2035, indicated by the upper horizontal dashed line. The break even point, indicated by the lower horizontal and vertical dashed lines in Figure 17.2, is achieved in 2034.

Section 20.5 elaborates further on the market share that is required for this return on investment.
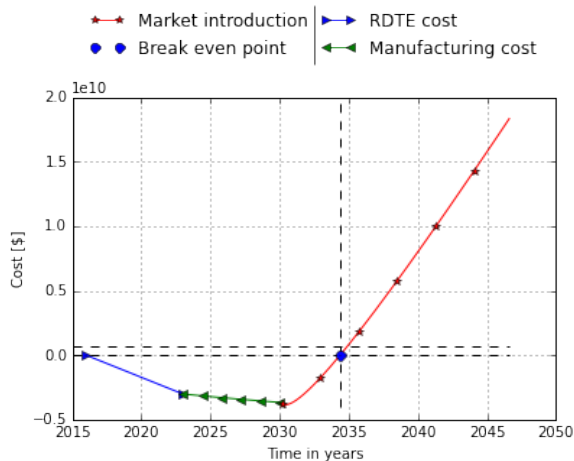
Figure 17.1: Life Cycle Cost for the RELOAD aircraft
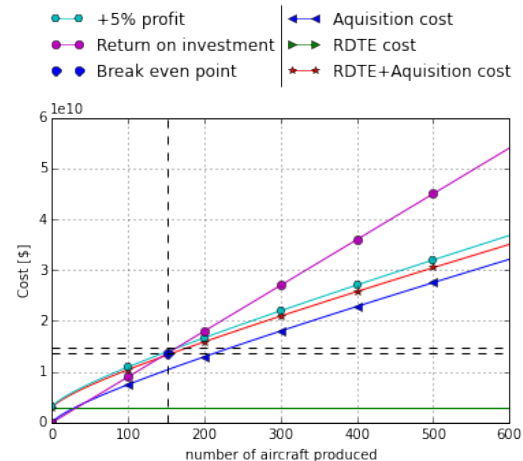
Figure 17.2: Return on investment from start of the RELOAD project

---

[7]URL https://leehamnews.com/2015/02/03/airbusboeing-production-rates-forecast-through-2020/ [Cited on 17 June 2016]

18

Manufacturing Analysis

In this chapter the manufacturing process is described. The manufacturing philosophy is stated in Section 18.1. The assembly order of the different subsystems is elaborated on in Section 18.2 and Section 18.3 presents the locations of the factories. Finally a note is made on production scaling in Section 18.4.

18.1 Manufacturing Philosophy

The manufacturing process is an important one for the RELOAD project since a lot of waist can be spared, and thus cost can be reduced. To incorporate this in our design the lean manufacturing philosophy is adopted, which is defined as: "Lean thinking is the dynamic, knowledge driven, and customer-focused process, through which all people in a defined enterprise continuously eliminate waste with the goal of creating value" [125]. The definition is elaborated on in the enumeration.

- **Knowledge driven:** a full understanding of the system is required so all types of waist can be identified. This means that all the knowledge of the different employees involved in the manufacturing process is focused on eliminating waste.

- **Customer-focused:** respond to customer demands and therefore reduce lead times.

- **Eliminating waste:** the main focus of lean manufacturing is to reduce waste. Waste is defined as "everything that uses resources but does not add value to the final product" [126].

- **Creating value:** as there are many different stakeholders involved, many different types of value need to be defined. But in the end they all come down to generating economic profit.

- **Dynamic and continuous:** lean manufacturing is an ongoing process that changes continuously: adapting the manufacturing process to eliminate waste and create more value.

A direct implementation of this philosophy in the RELOAD project can be found in Section 16.The information in this section is obtained from [126].

18.2 Parts for Assembly

In the aerospace industry a common practice is the use of an assembly line. An assembly line uses different workstations to efficiently manufacture parts. The parts move up in the assembly line where they are combined into a sub-assembly. Each workstation produces the same part using the same crew. The advantages of an assembly line are [127]:

- Minimal transport

- Simple planning

- Good indication of delay

- Maximal equal shaped products

- Routine forming per crew

RELOAD is divided in several sub-assemblies to be assembled at a central location. To assemble the whole aircraft at one location would be impractical due to the needed size of the facility and the differences in required expertise for the sub-assemblies. Section 18.3 elaborates further on manufacturing locations. The sub-assemblies of RELOAD, as seen in Figure 18.1, are divided in the nose cone, tail cone, fuselage, landing gear, engines, wings, winglets, canard and vertical stabilizers.
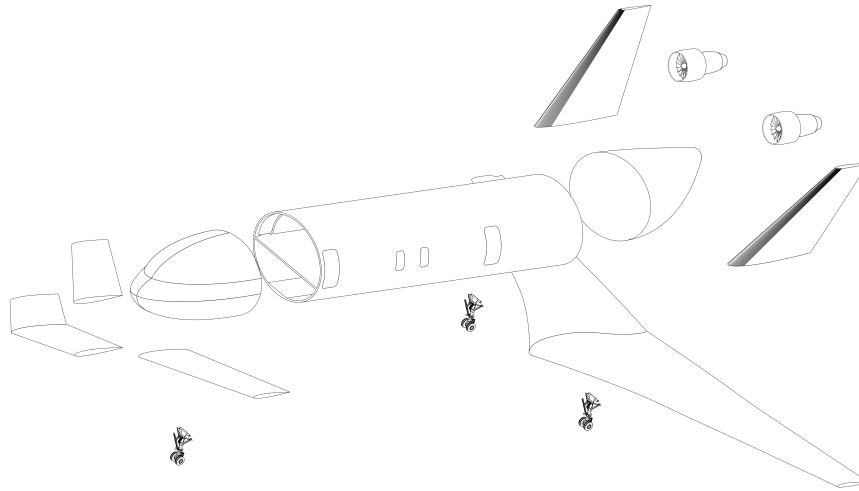
Figure 18.1: Exploded view showing the different sub-assemblies of the aircraft

The different sub-assemblies have a strict assembly order, ensuring a quick assembly while still providing enough workspace for the different crews. Firstly, the tailcone, nosecone and fuselage section are put together to form the whole fuselage. Next, the wings and the engines are installed. The vertical stabilizers are installed after the engines enabling easy placement of the engines. The engines are protected with airbags to ensure they are not damaged during the installation of the vertical stabilizers. After the wings are placed, the landing gear can be installed, simultaneously with the canard, vertical stabilizer and winglets.

18.3   Manufacturing Locations

To determine the manufacturing locations of the in Section 18.2 mentioned subsystems, a close eye is kept on the manufacturing location of one of our competitors in Europe. Here the assumption is made that in these regions, the expertise, space and infrastructure is already available for the subsystem manufacturing. Europe is chosen because distances are relatively small, therefore minimising travel time and emissions between different subsystems.

The main assembly line will be located around Madrid. Together with the factories where the vertical stabilizers, canard and main wing are produced. The region around Madrid is chosen because it is a large industrial region which could easily facilitate the employees of RELOAD. In Getafe, a city in the same region, they are already familiar with the assembly of horizontal planes for the A380[1]. By housing the factories of the canard, main wing and the vertical stabilizers near the main assembly line a decrease in shipping time, cost and emissions is expected. Furthermore because the manufacturing techniques used are roughly the same, expertise between the different facilities can be easily exchanged. The fuselage, nosecone and tailcone will be manufactured in Nantes, where large-sized, light alloy structures can be produced[2]. The engines will be manufactured in Dahlewitz, Germany where the Rolls-Royce engine factory is as well[3]. Finally the landing gear will be manufacturing in the United Kingdom, Filton[4].

The fuselage is flown over to Madrid using an Airbus Beluga[5], the engines could be transported by train or even by a normal lorry from Germany and the same goes for the landing gear from the UK.

18.4   Production Scaling

A combined effort of marketing, certification and performance of the prototype determine the actual interest of airliners in RELOAD. Clear arrangements are made with the sub-assembly manufacturers to scale up production if

---

[1]URL http://www.airbus.com/company/worldwide-presence/airbus-in-spain/ [Cited on 14 June 2016]
[2]URL http://www.airbus.com/company/worldwide-presence/airbus-in-france/ [Cited on 14 June 2016]
[3]URL http://www.rolls-royce.com/worldwide-presence.aspx[Cited on 14 June 2016]
[4]URL http://www.airbus.com/company/worldwide-presence/airbus-in-uk/[Cited on 14 June 2016]
[5]URL http://www.aerospace-technology.com/projects/stbeluga/ [Cited on 14 June 2016]
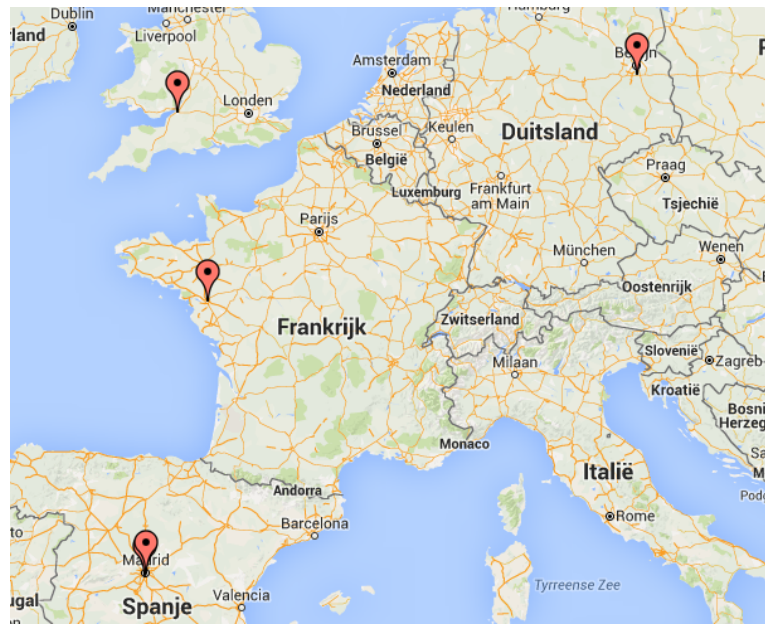
Figure 18.2: Manufacturing locations of sub-assemblies and main assembly

the demand exceeds the manufacturing rate based on the amount of orders. The initial production rate will be based on the needed rate to meet the return of investment requirement treated in Section 17.2. Orders will be taken from 2022 onward, to have an early overview of the actual demand of RELOAD in advance of the market introduction and to update the initial production rates. The manufacturers are of course limited in the amount of sub-assemblies which can be produced. If the backlog increases faster than the production rate can increase, additional facilities are build or contracted. The decision point to contract/build additional facilities will be in 2029, when mass production of RELOAD start. A more detailed description of the planning is given in Section 21.1.

<div align="right">

19

</div>

Dispatch Reliability and Availability Analysis

Requirement SAFE-1, as defined in [105], states that the dispatch reliability should be 99.7 % or higher. This chapter presents a method to compute the dispatch reliability in Section 19.1. Furthermore, the aircraft availability is discussed in Section 19.2.

19.1 Dispatch Reliability

To determine the dispatch reliability, a method proposed by [128] and [129] is used. This method determines the delay rate (DR) for numerous aircraft components, combines them and relates it to the dispatch reliability via Dispatch Reliability = 100 - DR. The individual DRs are found as presented in Table 19.1 and are summed to obtain the total DR. The different components are extracted from the Air Transport Association 100 document[109]. The most important ones are represented in the table below. The inputs for these equations are presented in table 19.2. The formulae and inputs in the tables are attained by investigating reference aircraft and finding trend lines. This explains the presence of the negative results for some individual system DRs. It is thus concluded that the single components are not representative, but the total is. Please note that this method is verified and validated as described in [128] and [129]. For multiple aircraft, including the B737NG, this method produces reasonable results. Using all these DRs, a final dispatch reliability of 99.0 % is found.

Table 19.1: Delay rate formulae [129]

Component	Formula	Result
Air conditioning	$ln(DR) = 0.5479 ln(NP/FL) - 5.3721$	0.0479
Auto pilot	$DR = -0.0063(FL) + 0.0318$	0.0161
Communications	$DR = 0.0002(NP) - 0.0449$	-0.0095
Electric power	$DR = -0.0003(NP/FL) + 0.0668$	0.0456
Equipment	$DR = 0.0186(FL) + 0.008$	0.0545
Fire protection	$DR = -0.0001(Thr) + 0.0559$	0.0413
Flight control	$DR = -0.0008(NP/FL) + 0.1937$	0.1371
Fuel	$ln(DR) = -0.0161(NP/FL) - 2.1535$	0.0371
Hydraulic	$ln(DR) = 0.2265 ln(FL) - 2.5852$	0.0928
Ice protection	$DR = -10^{-6}(MTW/FL) + 0.0892$	0.0668
Instruments	$DR = -3 \cdot 10^{-7}(MTW) + 0.054$	0.0372
Landing gear	$DR = 0.0012(NP) - 0.3128$	-0.1004
Lights	$DR = 0.0001(NP) + 0.0003$	0.0180
Navigation	$DR = -0.0005(NP) + 0.1548$	0.0663
Oxygen	$DR = -6 \cdot 10^{-7}(MTW/FL) + 0.0303$	0.0169
Pneumatics	$DR = 0.0013(CS) - 0.531$	0.4440
Water waste	$DR = 3 \cdot 10^{-7}(MTW) - 0.0067$	0.0101
APU	$DR = -0.0002(NP) + 0.0702$	0.0348
Structures	$DR = 0.0002(Thr) - 0.0725$	-0.0433
Doors	$DR = 0.0006(NP) - 0.1351$	-0.0475
Engine	LEAP brochure[130]	0.0200

Table 19.2: Inputs for delay rate functions [128]

Input	Symbol	Value
Maximum take-off weight	$MTW\ [kg]$	56000
Number of passengers	$NP\ [-]$	177
Flight length	$FL\ [h]$	2.5
Max aircraft thrust	$Thr\ [kN]$	146
Cruise speed	$CS\ [kts]$	430

Although the requirement is thus not met, the reliability is still comparable to reference aircraft. Boeing 737NG comes in at 97.1 % [128]. The A320 has a reliability of 99.3 %[1]. The reliability of RELOAD thus overpasses the Boeing 737NG. The Airbus A320 has a marginally higher reliability. It can be concluded that RELOAD meets the standards set by the current competitors. The requirement of 99.7 % would drive the design to such an unacceptable extent, that it is decided to challenge this requirement and to adapt it.

19.2 Availability

The aircraft availability A can be determined with Equation 19.1 [109]. A duty day has a length of 10 hours and it is assumed the aircraft will be out of service due to maintenance or other occurances for 25 days every year[2].

$$A = 100 \cdot \left(1 - \frac{\text{duty hours out of service}}{\text{total duty day hours}} \right) = 93.2\% \tag{19.1}$$

With the current assumption that the aircraft will be serviceable 340 days per year, the availability will thus be 93.2 %. Figure 19.1 shows all reasons why the aircraft might be taken out of service.
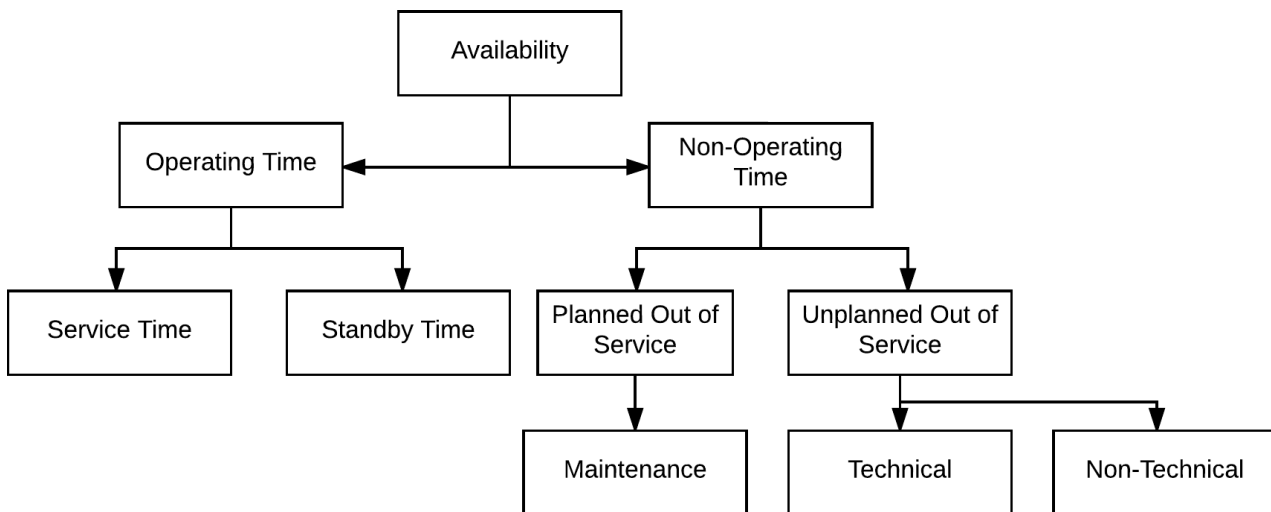
Figure 19.1: Aircraft availability breakdown

---

[1] URL http://www.boeingblogs.com/randy/archives/2012/04/the_space_between.html [Cited on 17 June 2016]
[2] URL https://www.conklindd.com/t-higherutilization=lowercosts.aspx [Cited on 17 June 2016]

IV

Design Overview

Part I, II and III together have formed the Detail Design of the RELOAD aircraft by considering all pieces of engineering. Combining the baseline preparation with the conceptual design and concept selection, the detail engineering phase has been started. In this, the engineering subjects as aerodynamics, structural analysis and propulsion have been covered. But also the influence of other requirements and post-development phases of the product life cycle were discussed. This included the design for manufacturing and maintenance, such that clearance and a low cost design are guaranteed. Furthermore, the cost analysis is performed to find a selling price, the Direct Operating Cost and return-on-investment. At last the safety, risk and reliability of the aircraft were discussed, such that a costumer will not only buy the aircraft for its performance, but also knows it is safe to fly.

This part will wrap up the design as discussed in the report. An overview of all design features and the verification of the requirements is performed in Chapter 20. Afterwards, a planning and recommendations for further development is provided in Chapter 21. Finally, a conclusion on the Final Review is drawn in Chapter 22.

<div align="right">

20

</div>

<div align="right">

Final Design

</div>

The purpose of this chapter is to provide a final design overview, by summarizing the most important aspects of the RELOAD aircraft, as well as how it evolved through the design process, in Section 20.1. The flight performance factors are also evaluated in Section 20.2 and Section 20.4.1 discusses the final aircraft weight. The lifetime of the RELOAD aircraft is elaborated on in Section 20.3. All these results are used in Section 20.5 to analyse the market gap that the aircraft is going to fill. Finally, the design will be validated in Section 20.6.

20.1 Design Overview

The design process started by creating a very extensive design option tree, with all the feasible and non-feasible solutions for each component. The solutions that would immediately seem either non-feasible or too futuristic were crossed out straight away and then the rest were extensively evaluated in order to see if they are possible. In the end, only a few were left, which created the basis for the four design concepts [2].

A software tool was written which proved its usefulness when iterating during the conceptual design phase. The tool also helped in creating the trade-off tables which decided the final design choice. This choice was further analyzed in the detailed design phase. The results of this analysis will be presented in this section.

The final RELOAD concept is a canard aircraft with a tapered and backward swept wing placed towards the aft of the elliptical fuselage. It uses two ultra high bypass turbofans for propulsion, which are podded on top of the fuselage and in-between two vertical stabilizers. The wings includes morphing flaps, its contour is based on transonic airfoils and it ends up with two blended split winglets. The commands from the cockpit to the flight controls are sent using fly-by-wireless technology, while the actuation is performed electrically and hydraulically only. Augmented stability has been implemented in order to have an all-moving canard and the latest state-of-the-art systems, such as TCAS, EGPWS and PHM are implemented in order to ensure the safety and ease the maintenance of the aircraft. A more extensive overview of the aircraft's qualities and capabilities can be found in Figure 20.1.

Once the final design is concluded, the function flow diagram (FFD) and function breakdown diagram (FBD) can be reviewed. In respect to the diagrams presented in Baseline report [2] which were already quite-extensively defined, the post-flight functions are the only ones that have further been detailed. The detailed diagrams can be found in Figure 20.2 and Figure 20.4, respectively.

Finally, the design option tree can be found in Figure 20.14 and is also used to provide a better overview of the design selection of each component and sub-component. This has been created based on the results provided in the Chapters 5 to 10.
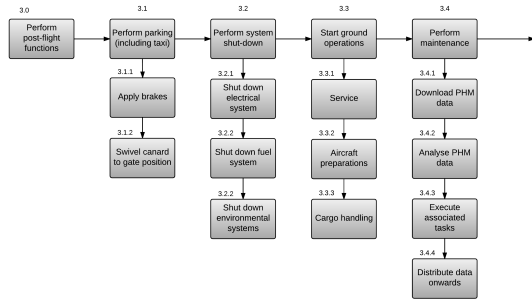
Figure 20.2: Update on the functional flow diagram of the final design
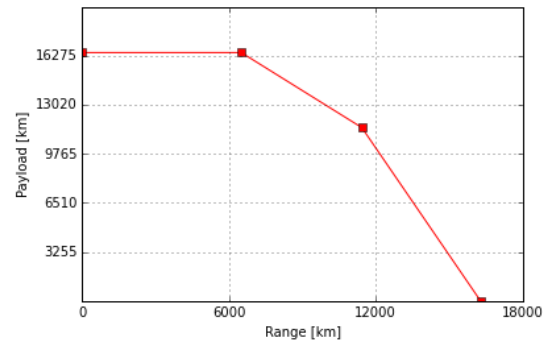
Figure 20.3: Payload range diagram
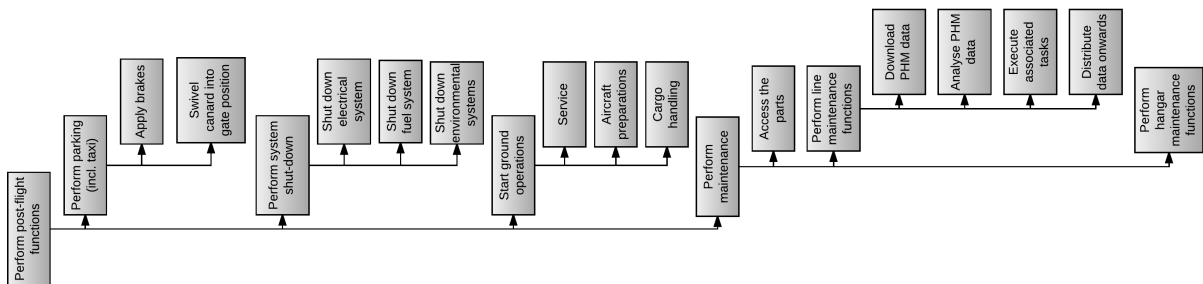
Figure 20.4: Update on the functional breakdown diagram of the final design

20.2 Flight Performance

This section discusses the flight performance of the RELOAD aircraft design. Section 20.2.1 shows the manoeuvre and gust loading diagram, after which the flight envelope is shown in Section 20.2.2. The take-off, landing and climb performance are discussed in Section 20.2.3 and Section 20.2.4. These performances are calculated for the selected mission as discussed in Chapter 2.

20.2.1 Manoeuvre and Gust Loading Diagram

One of the main inputs for a structural design are the load cases. One has to answer the question of when the most critical loads occur in an aircraft's flight cycle and define the ultimate loads that it should be able to cope with in extreme occasions. To define just that, a manoeuvre and gust loading diagram can be constructed according to the CS-25 regulations [4]. Concerning the manoeuvre diagram, one can observe that any aircraft falling under CS-25 regulations with a MTOW above 22.7 tonnes should be able to perform manoeuvres between -1g and 2.5g, thus ranging the load factors from n = -1 to 2.5. Furthermore, the gust loading diagrams are constructed similarly according to the CS-25 procedure [4], evaluating the load factors at mach numbers of M_B = 0.619, M_C = 0.75, M_D = M_C + 0.05 = 0.8. Here, M_B is constrained by the intersection of the manoeuvre incremental load factor curve and the maximum lift curve. Furthermore, the height considered is the cruise altitude of 11 km as specified in the requirements in Chapter 2.3. The resulting loading diagram can be observed in Figure 20.5.
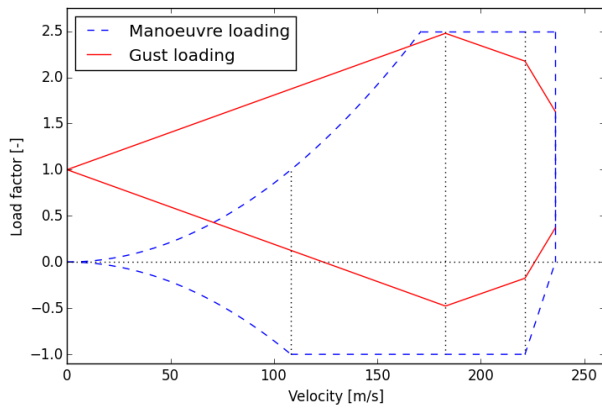
Figure 20.5: Manoeuvre and gust loading at cruise altitude in accordance with CS-25 regulations
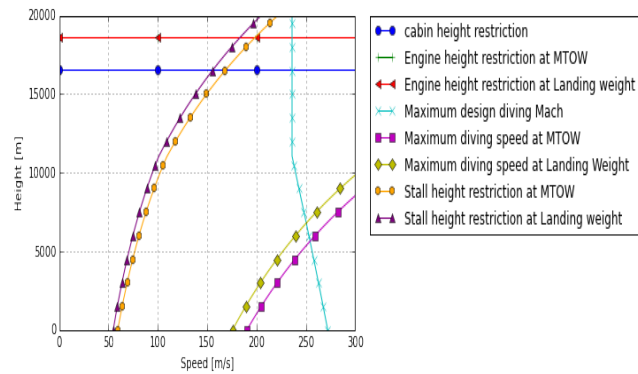
Figure 20.6: Flight envelope in accordance with CS-25

20.2.2 Flight Envelope

For operations, it is important to know the speed and height ranges that can be reached by the aircraft. These parameters are highly depended of each other and are therefore visualised by means of a flight envelope as depicted in Figure 20.6. The left speed ranges are restricted by the stall speeds of the aircraft, which is $\sqrt{h}$ depended on the height due to the air density. The height that can be reached is restricted because of the maximum pressure difference that is allowed by the structure. This was calculated using [25]. The maximum speed that can be reached is restricted by the loads that the aircraft can withstand. As explained in Section 20.2.1, the RELOAD aircraft is designed to withstand a limit load factor of 2.5 (and an ultimate load factor of 3.75) and a diving speed mach number of 0.8. This figure thus shows the outer restrictions that can be reached in the whole flight regime.

All equations if the flight envelope are verified by hand calculations and the total flight envelope diagram is compared to the diagram from [25]. Since the result after debugging was reasonable, the program was found to work correct.

20.2.3 Landing and Take-off Performance

Even though there is designed for a Take-off field length of 2000 m and a landing field length of 1500 m, it is still needed to check whether these requirements are met. To calculate these distances, the equations in [131] and [132] are used. These equations however, are only valid for constant weight. Furthermore, it assumes that there is no wind and that the thrust is parallel to the velocity vector. The calculation can be done for small slope angles, however the results shown in Table 9.4 is only for a horizontal runway.

For the equations, the values from the database are used. Next to that, some values for speeds and constants are assumed [131]. These are summarized in Table 20.1. Most assumption originate again from [131, 132], except for the effective friction coefficients μ. These are taken from [70]. Lastly, the climb angle γ is taken from reference aircraft[1] and checked whether it still remained below the maximum climb angle as determined in the Mid term Report [1]. It was found that aircraft complies with the landing and take-off requirement as expected. For the take-off distance and the landing distance safety factors of 1.15 and 10/6, respectively, are included. Furthermore, no thrust reversers were considered for this calculation. Since these will be implemented in the aircraft as described in section 7.4.3, an extra safety margin is present during landing. The final values are shown in Table 20.1.

Furthermore, if an engine fails during the take-off run, the aircraft should either take-off with one engine inoperative, or decide to abort the flight. However, the aircraft should reach the situation that it can no longer stop in time and overshoots the end of the runway in case the flight is aborted. Thus a decision speed V_1 is defined. If the aircraft reaches a speed higher than this, it is no longer allowed to abort, as this field length would be longer than the remaining runway. This speed is calculated using [131, 132]. By setting the ground phase distance for accelerating plus the ground phase for decelerating to 1900 [m], the decision speed is calculated. A slightly lower value than the maximum take-off field length is used as a safety margin. The decision speed can also be seen in Table 20.1.

The program was checked with hand calculations and validated by using the inputs from several take-off and landing distance examples calculation from [131, 132]. Since the same answers were found, the program was concluded to work correctly.

---

[1]URL http://www.bangaloreaviation.com/2009/05/typical-takeoff-and-climb-angles-of-all.html [Cited on 2 June 2016]

Table 20.1: Inputs to calculate the landing and take-off requirements

Take-off inputs			Landing inputs		
Parameter	Unit	Value	Parameter	Unit	Value
V_2	[m/s]	$1.2V_{min}$	$V_{approach}$	[m/s]	$1.3\ V_{min}$
$V_{screen_{height}}$	[m/s]	$V_2 + 5.14$	$V_{touchdown}$	[m/s]	$1.2V_{min}$
$h_{screen_{height}}$	[m]	15.2	$h_{screen_{height}}$	[m]	15.2
μ_{TO}		0.02	$\mu_{L_{fullbrakes}}$		0.4
γ_{climb}	°	9	$\gamma_{descent}$	°	3
$S_{Take-off}$	[m]	1809	$S_{Landing}$	[m]	1456
V_1	[m/s]	37			

20.2.4   Climb and Payload Range Performance

As can be seen in Figure 20.7 and 20.3, the climb and payload-range performance is investigated using the latest design parameters from the database[1]. The steady climb performance remained the same, as no large increases in weight and thrust were made. However, the code was adapted to incorporate the change in climb rate with an unsteady climb using [133]. The solid lines shows that the maximum rate of climb decreased from 29.8 [m/s] to 26.0 [m/s]. The payload-range diagram however, changed considerably compared to the conceptual design. This resulted from resizing the fuel tanks. In the Midterm report, it was assumed that all the space in between the wing spars, except for the tips because of safety, could be occupied with fuel. However, more space was needed at the wing root for the design of the landing gear and high lift devices. To reach a range of 6500 [km] a fuel volume of 12 [m^3] is needed. With the resizing of the fuel tanks, a maximum fuel volume of 18 [m^3] is still possible. This means that 1.5 times the needed fuel can be loaded and a range of 11300 [km] can be reached without trading the range for payload. If this is still needed, a maximum range of 16085 [km] can be reached as indicated in Figure 20.3.
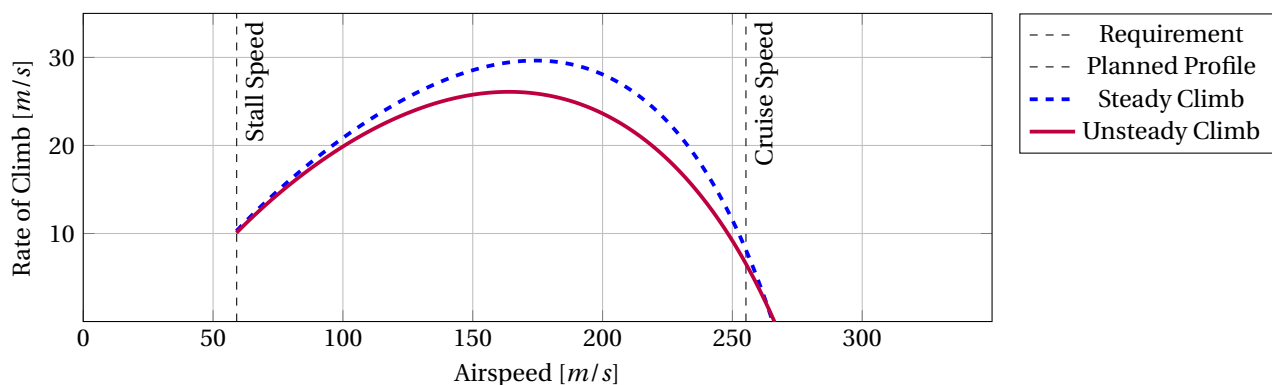
Figure 20.7: Unsteady rate of climb at sea level

20.3   Lifetime of RELOAD

RELOAD is designed to last for 45 years of service. The lifetime is assuming an average of 6 flights per day, or 100 000 flight cycles. Current aircraft are retired on average after 25 years, but some are kept in service for up to 45 years[2]. By designing for a lifetime of 45 years RELOAD enables airliners to prolong the use of their aircraft fleet and have airliners decide when they want to retire their aircraft.

20.4   Technical Performance Management

In this section, an overview on the direct operating costs reduction as well as the aircraft weight evolution is being provided. In respect to the sizing of the wing, canard or vertical tails, too little iterations are performed in order to be worth showing them.

---

[2]URL http://avolon.aero/airfinance-annual-2012-industry-review-and-outlook/ [Cited on 20-06-2016]

20.4.1   Aircraft Weight

The predicted MTOW of the aircraft evolved over the course of the project to a value of $58\,687$ $[kg]$ and is visualized in the Technical Performance Management (TPM) chart of Figure 20.8. The OEW of the aircraft is predicted to be $32\,237$ $[kg]$ at this stage of the project. The mass is below the planned profile, so no action is taken at this point in time. Figure 20.9 shows the contribution of the major mass groups for RELOAD. The masses follows from the Class 2 weight estimation described by Raymer [5] and are updated to include more precise structural weights of the wing and fuselage.
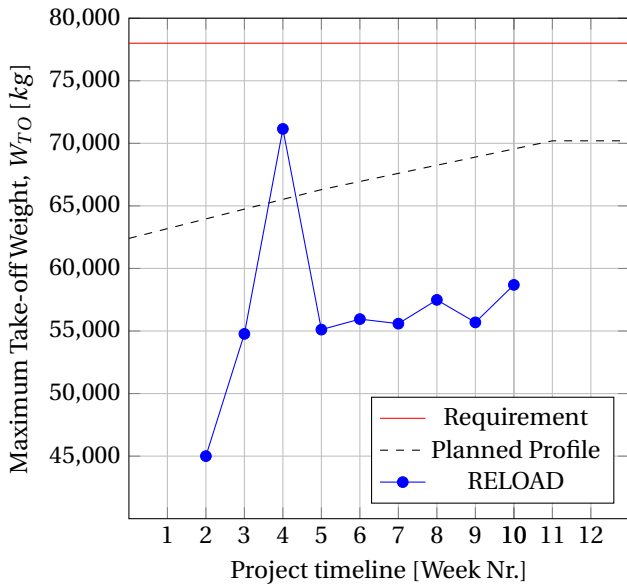
Figure 20.8: Technical Performance Management diagram
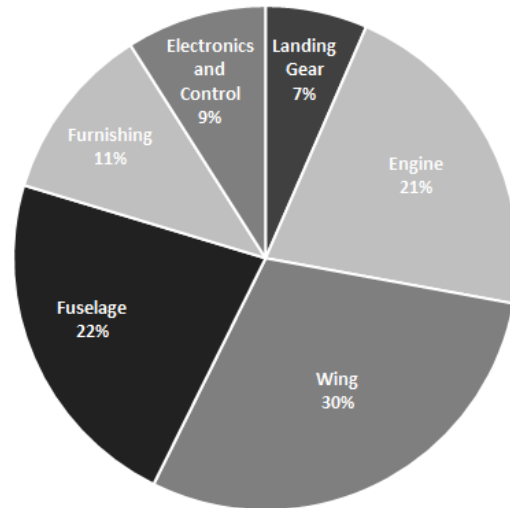
Figure 20.9: Mass overview for RELOAD

20.4.2   Cost reduction

The evolution of the direct operating costs reduction is also interesting to visualize. As it can be seen in Figure 20.10, the engine model is initially built with a higher bypass ratio and higher efficiencies of components. The drag at that point is assumed to be the same with the competitors which results in a very efficient engine that can on its own save approximately 28.6 % of the total direct operating costs. However, as the efficiencies, pressure ratios and bypass ratio are changed to more conservative values, the cost reduction also decreases to roughly 20.8 %. Unfortunately, at this point, the cost of fuel in $ per liter was found to be approximately 50 % more that assumed. This resulted in a revised cost reduction of only 7.7 %. At this phase, the aerodynamics department began producing estimations for the drag of the aircraft and as those estimations became were refined, the cost reduction due to fuel consumption ended up being 20.4 %. Combined with the reduction due to crew, maintenance and depreciation, the final cost reduction result becomes 30.4 %.

Direct operating costs reduction
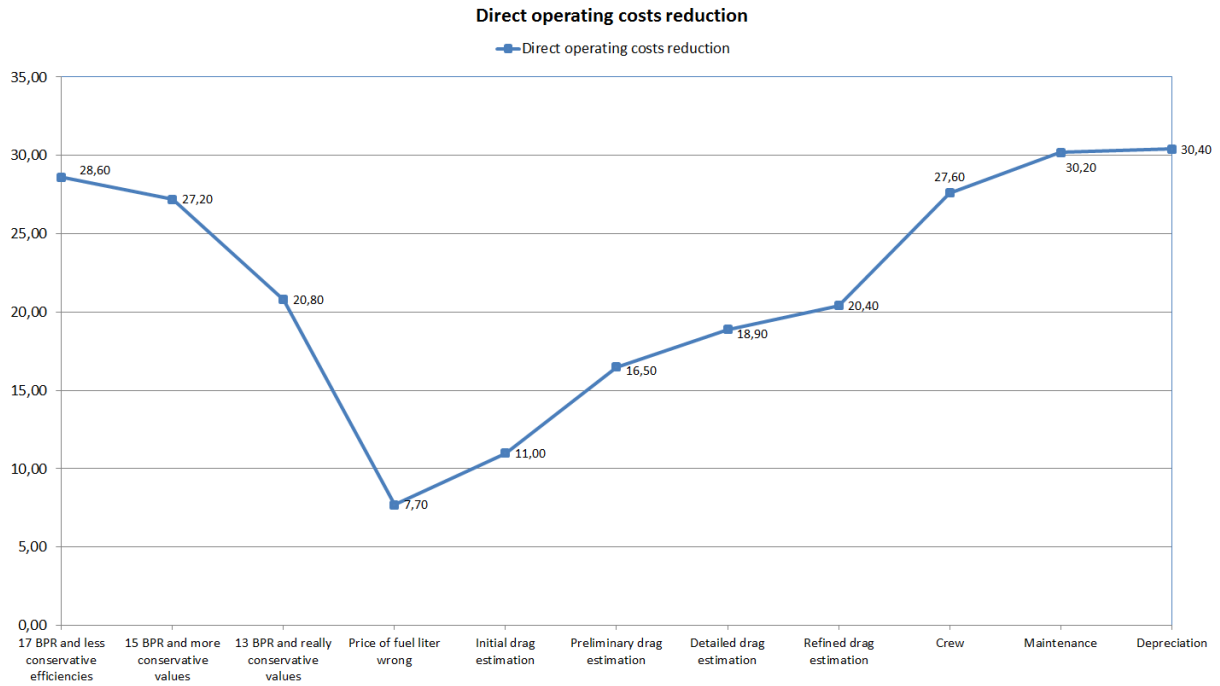
Figure 20.10: Technical Performance Diagram showing the cost reduction of RELOAD

20.5 Market Position

This section elaborates on the foreseen market position of RELOAD. First, a comparison is made of our current competitors and our position with respect to them, in Section 20.5.1. Based on our position and on the return of investment needed an expected market share is forecast, in Section 20.5.2

20.5.1 RELOAD & Competitors

For airliners to consider buying RELOAD, the aircraft needs to differentiate itself from competitors. Figure 20.11 and 20.12 show the position of RELOAD with respect to current and future competitors. The range of RELOAD is only rivalled by the future Boeing 737MAX series and the current A319. The A319 has a slightly longer range at the cost of less capacity. Looking into the cost per air hour RELOAD shows a significant cost reduction with respect to current and future competitors.
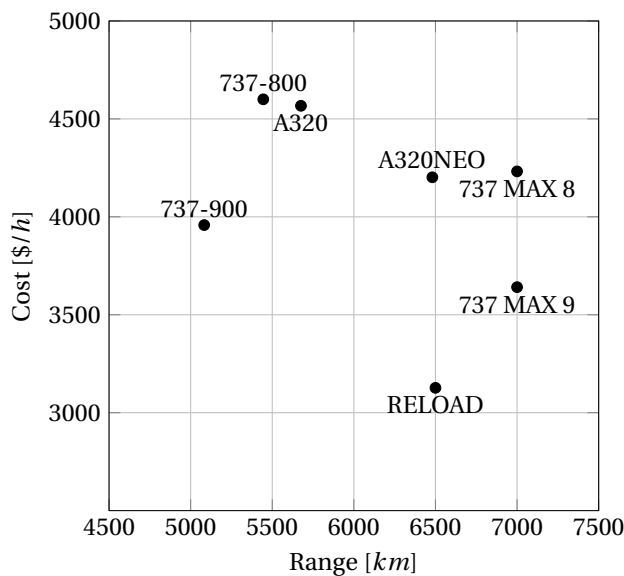
Figure 20.11: Direct operating cost per air hour for RELOAD and direct competitors [2]
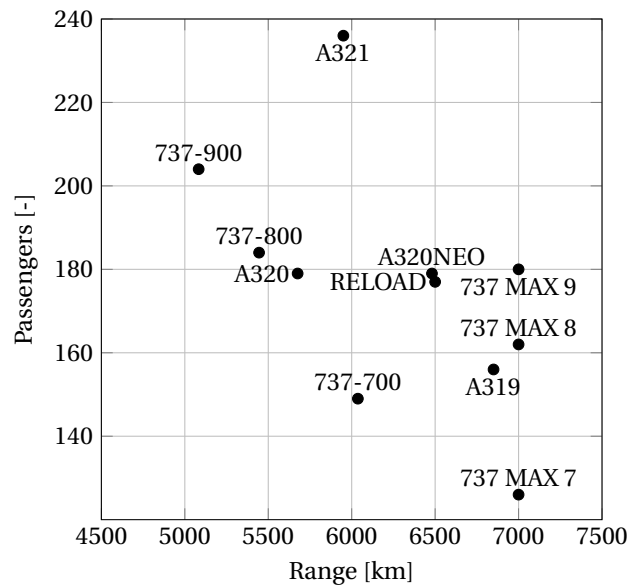
Figure 20.12: Number of passengers and range for current and future aircraft [2]

RELOAD has a promising position on the overall narrow-body market, differentiating itself from other aircraft mainly on the low direct operating cost. The current range of 6500 [km] is currently the only limiting factor compared to competitors. One of the recommendation for the continuation of the RELOAD project is the addition of several versions of the RELOAD aircraft, this recommendation is treated in Section 21.2. A long range RELOAD version will fit the gap between RELOAD and longer range options like the 737 MAX series aircraft.

20.5.2   Market Share

RELOAD is designed to be delivered on the market in 2030. During the Baseline Report [2] an extensive market forecast was done to verify the need of RELOAD in the near future. An overview of the market deliveries up until 2034 is shown in Figure 20.13. Asia, North-America and Europe are the three most promising markets up until 2034 and will be the main focus for the RELOAD aircraft.

From Chapter 17 it is found that 172 RELOAD aircraft need to be sold in less than five years to meet the return of investment requirement (COST-1, as defined in [105]). The forecast amount of sold aircraft is 5346 units for the period of 2030 to 2034 [134]. If all 172 RELOAD aircraft have to be sold before 2035, a market share of 2.57 % in sales is required. RELOAD will have a significant lower direct operating cost than competitors. In a market driven by profit airliners will be very interested in RELOAD in the state it is described in this Design Overview. A market share of 5 % with the current position of RELOAD is conservative, but will result in a needed 268 RELOAD aircraft to be manufactured in a period of four years.
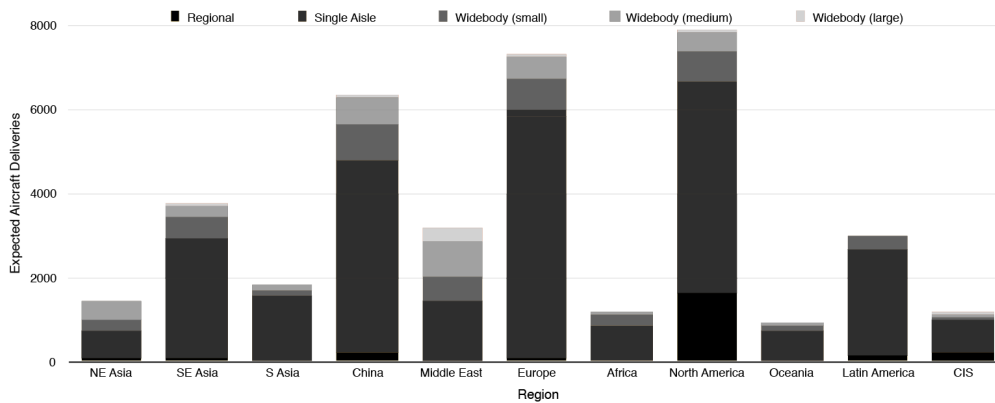
Figure 20.13:   Expected market deliveries during 2014-2034 [2]

20.6   Requirements Verification

Changing a requirement is not always possible or wanted by the customer and should therefore always be done under consultation. Strict management is therefore needed such that the same design constraints are used during all design phases. Now that the detailed engineering has come to a closing, it should be checked whether all the requirements are met, or could be met. If not, this should either be consulted with the client or re-design is needed.

For this, a compliance matrix is made of the requirements considered in Figure 2.3. This shows the requirements in a table with an indication of the status of the requirement. In this case, three indications are used:

- A check mark (✓) is used to show when a requirement has been met.

- A tilde (~) is used to indicate that a requirement is likely to be met, but that no certain numbers are yet available at this stage.

- A ✗ mark has been used to indicate whether a requirement has not been met.

The complete matrix is shown in Table D.1. There are still 3 requirement of which no exact values known and are thus checked with a ~. Also, one requirement could not be met.

The first two requirements with no exact value are the entering to the production line at 2025 and introduction to the market at 2030. Although every design and selected technology was selected with these requirements in mind, a lot more still has to be investigated for a complete aircraft design. Already the planning to meet the requirements, such as the production plan discussed in chapter 18, has been made and it is therefore considered very unlikely that

his requirement will not be met. However, certain values are never possible for this kind of requirements as schedule slip always happens unintentionally and rather unexpectedly.

The last requirement which is no exact value, is the requirement TLR-NES-6, which states that the cabin noise should remain below 80 dB. This requirement was not deeper investigated due to time constraints and resource constrictions.

The requirement that could not be met is the dispatch reliability requirement. The dispatch reliability was calculated to be 99.0 % as explained in Section 19.1. This does not meet the target value of 99.7 %, however it is comparable to the reference aircraft. Boeing 737NG has an dispatch reliability of 97.1 %[128] and the Airbus A320 is 99.3 %[3]. New technologies implemented in the design decrease the dispatch reliability. However, this will improve by 2025, but it is difficult to obtain exact numbers at this project stage. Improvements can also be made if the reliability per system is investigated deeper, as this might be higher than estimated from the reliability relations. Adapting the design to meet this requirement is also possible, but that would mean to redesign the whole aircraft, with no guarantee that it can be met. Compared to competitors, this requirement is too strict and would drive the design to an unacceptable extent. It is therefore decided to waive the requirement and accept the dispatch reliability of 99.0 % as being sufficient.

---

[3]URL http://www.boeingblogs.com/randy/archives/2012/04/the_space_between.html [Cited on 17 June 2016]
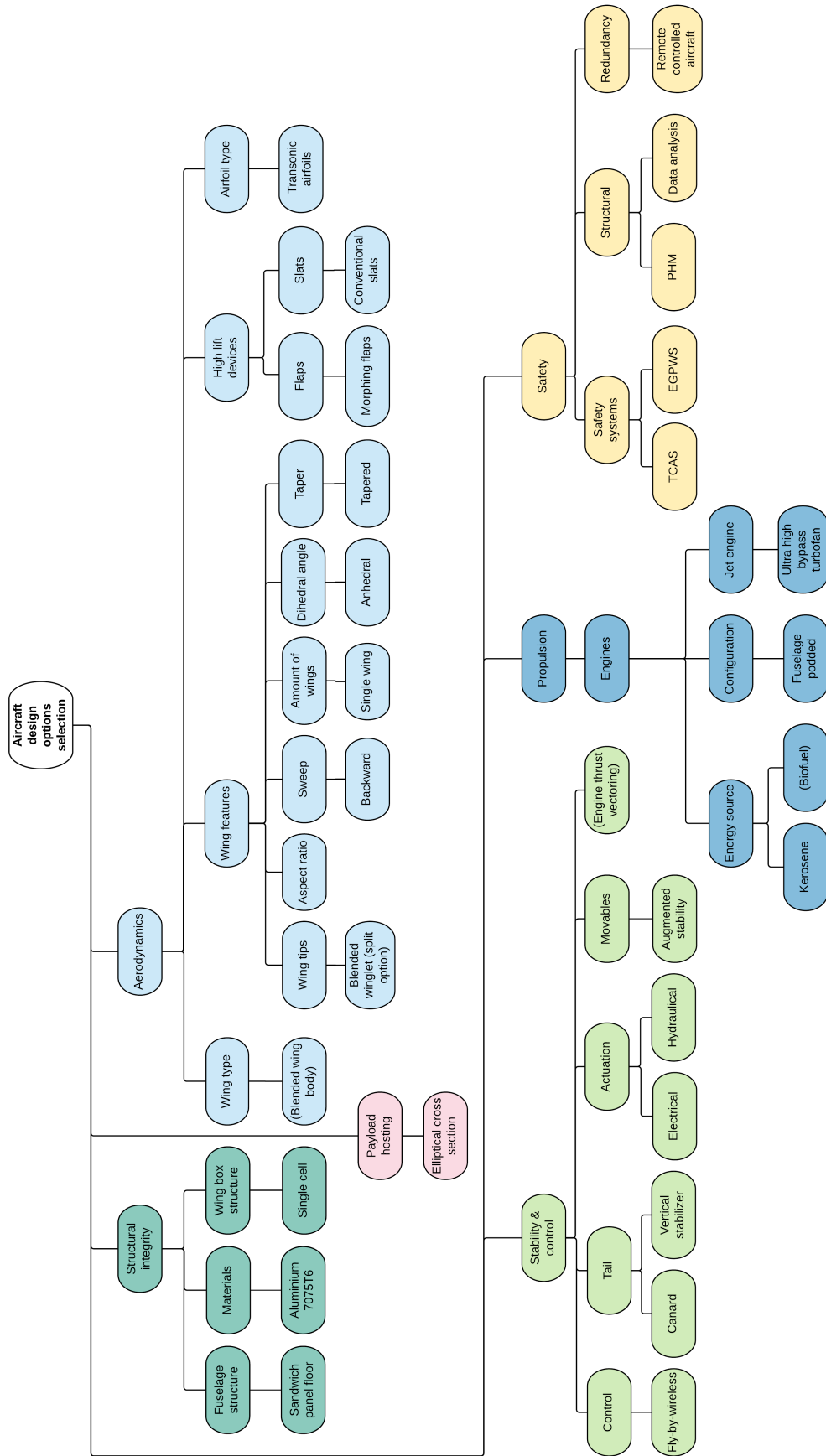
Figure 20.14: Design option tree of the final design

1 Single Pilot Operations cockpit
2 Fully-movable canard
3 Conventional sealed slats
4 Morphing trailing edge flaps
5 Main fuel tanks and jettison system
6 Forward retracting, fully steerable nose landing gear –
two wheels
7 Landing gear fairing used for noise reduction
8 Augmented stability system
9 Vertical stabilizer
10 All-electric, variable speed single-shaft APU
11 Four-wheel main landing gear – side retracting
12 Transonic airfoil

13 Ultra High Bypass turbofan
14 'Cold stream' thrust reverser
15 Control system commands using fly-by-wireless
16 Elliptical fuselage – twin-aisle –177 passengers
17 F8 type chevrons used for noise reduction
18 One low pressure and one high pressure spools
19 No bleed air system – 'more electrical aircraft'
technology
20 Cargo unit load devices – ULD 3
21 Engine containment system
22 Two Variable Frequency Starter Generators per engine
23 High lift devices on the canard
24 Split winglets

Figure 20.1: Schematic of the RELOAD aircraft including its functional capabilities

<div align="right">

21

</div>

<div align="right">

Continuing the Development

</div>

The RELOAD project phases, as defined in Figure 1.1, are completed at this stage. However, the design of the RELOAD aircraft is not. There are more phases to come to fully designing the aircraft. This chapter presents the future planning of the project. Section 21.1 shows the coming stages and a Gantt chart. Furthermore, some system-level recommendation, which need to be investigate in these coming design stages, are made in Section 21.2. The risk of the project itself is discussed in Section 21.3.

21.1 Future Project Planning

After the completion of this 11 week project, the following project phases are grouped together under the name "final design". The final design consists of the phases preliminary design, the detail design, manufacturing, and testing and certification. The two foremost of this list share their name with the two final phases of this project. Nonetheless, they are very different since they go more into detail and develop the design further [135]. Figure 1.1 summarizes this naming convention. Each of the phases in the final design is now described.

The first phase in the final design is the preliminary design phase. The 11 weeks of RELOAD project delivered a "baseline configuration". This configuration provides the needed confidence that the design can fulfill all the requirements. The goal of the first final design phase is to further develop the RELOAD design until sufficient understanding of the design is achieved, such that the design can be frozen and the detail design phase can start [135]. This phase must provide confidence in that the aircraft can be manufactured and certified in the right time frame and with the appropriate budget. Again the division is made into larger engineering groups. Some of the tasks that need to be executed include:

- **Structural design** Structural designers and FEM specialists will optimize all structural parts of the aircraft.
- **Aerodynamic design** The aerodynamicists will optimize the design using CFD and windtunnel tests.
- **Control design** Control specialists will design and optimize the aircraft control system and all control surfaces.
- **Propulsion design** The engines will be elaborated.
- **Landing gear** Since the landing gear constitutes to a large part of the aircraft mass special attention is paid in its design.
- **Other:** The aircraft power, command and data handling systems etc. also have to be designed in detail.

Some of the typical concerns in this design phase are fatigue, aeroelasticity and vibrations [135]. The interactions between the different components are researched and results are validated by windtunnel tests.

The second phase in the final design is called the detail design. In this phase the configuration has been frozen. The aircraft will be designed and analyzed up until the very last rivet hole. Furthermore, the tools and fixtures needed in the creation of the aircraft will be designed and manufactured. There will be tests on full-scale aircraft and all systems will be tested on an iron bird. The planning of this phase is based on the different aircraft components again as each component requires high detail.

The third final design phase, manufacturing, starts not long after the second phase; they run simultaneous for most of the time. In this phase the aircraft prototypes are build, including the aircraft that will be used in the ultimate load test. The second and third phase are concluded at the same time with the roll-out of the first prototype which will be used for testing and certification. This final phase focuses on validating the entire design and certifying it. This phase can take multiple years and therefore has to be planned out in detail.

Together with the start of the detail design, the creation of the maintenance program starts. The process takes as much time as the detail design and the manufacturing phase and it is crucial for the operational life of the aircraft. The planning of this phase follows the MSG-3 logic and is based on [136].

All the tasks outlined above need to be planned and defined, such that the remainder of the aircraft development will be executed in a smooth manner. Figure C.1 presents a Gantt chart for the top-level activities, goes a bit more into detail and attributes time slots to them.

21.2 System Level Recommendations

In the further development of RELOAD, the following system level recommendations should be taken into account.

The first recommendation pertains to the size of the vertical tail surfaces. In the current design, their communal size is 59 [m^2]. This number is this high since the center of gravity is rather aft and thus the tail arm is small. The tail volume coefficient V_v of RELOAD is equal to 0.12. For jet transport aircraft, this value is typically 0.09 [6]. Hence it is recommended to investigate lowering the tail surface. A measure that might be taken is placing the canard under a dihedral angle such that it also features a vertical projected surface. Furthermore, by implementing a differential thrust system, the lateral stability can be augmented. The biggest reduction in tail size might result from installing a yaw damping system, which would increase dutch roll stability significantly. Two reference aircraft, the Beechjet 400A and the Tupolev TU-334, differ highly in configuration but also have their cg at an aft location. This is illustrated by their vertical tail volume coefficients, which are $V_v = 0.123$ and $V_v = 0.103$ respectively [6]. Using their vertical tail plane surface to wing surface ratio $\frac{S_v}{S}$ (0.26 and 0.28 respectively [6], with RELOAD's 0.37), it is determined that the vertical tail plane surface can be reduced by 7 to 10 % by implementing these measures.

The second recommendation pertains to the long operational life RELOAD is designed for (10^5 cycles). In the conceptual design stage that the first 11 weeks of the project took place, it was decided to research composite materials for the fuselage. Specifically filament winding the fuselage was an interesting option. But due to the high level of computational power needed and the relatively low amount of quantitative results that could be produced at this stage it was decided to move back to aluminum. However, since RELOAD is meant to have a long operational life, with multiple flights per day, the aircraft will experience many pressurization cycles. Composite materials show less fatigue than metals[1] and thus can the aircraft sustain this longer operational life. It is therefore recommended to broaden this research and focus on where to apply this kind of material and how to manufacture it.

The third recommendation regards the measure of blending the wing into the fuselage. From an aerodynamic and efficiency perspective, it is interesting to blend the wing into the aircraft [1]. However, due to constraints with the operations it was decided for now to revert back to a low wing configuration. Furthermore, the amount of processing power needed to accurately compute the aerodynamic advantages was simply too high at this project stage. It is therefore recommended to continue this research and assess the manner in which the wing will be blended in the fuselage.

Another recommendation pertains to the maintenance of the aircraft. Firstly, it is recommended to investigate the usage of smart materials; materials which actively combat and restore degradation and damages. Secondly, the maintenance program of the aircraft must be defined in such a manner, that minimal cost will be spent, while still retaining high levels of safety. Both will help in reducing the maintenance related direct operating cost.

The fifth recommendation pertains to the improvement of the engine. At this stage a conventional turbofan engine was used. The engine can be made more efficient by implementing the geared system, which was not done now since the assumptions needed in the design would invalidate the results. It is recommended to continue the research on this area and implement a geared turbofan in the final result. Finally, a recommendation is made to at every stage in the project redefine and deepen the tasks as shown in Figure C.1.

After developing the RELOAD aircraft, it is worth wile looking into different version from a market position. There might be a need to develop a long range version of the aircraft which, as a compromise, carries less passengers on a longer range. Furthermore, a cargo version could be investigated such that the shift to this market can be made.

21.3 Project Risk

New risks also develop as long as the project continues. These new risks are tracked and listed below. They are applicable to the new technologies that are recommended to be implemented in the RELOAD aircraft, namely carbon materials, PHM system, SPO, blending the wings into the fuselage, BLI engines, geared turbofans, split winglets, morphing HLD, augmented stability and smart materials.

---

[1]URL http://www.astm.org/DIGITAL_LIBRARY/STP/PAGES/STP27745S.htm [Cited on 17 June 2016]

1. **Non-feasible before 2025** To meet the strict reduction in cost a lot of new technologies were investigated and implemented. The most import ones are the SPO, morphing HLD etc. If research to these devices is halted or when certification becomes a problem it might be possible that these techniques are not ready in time for the production of the aircraft. The same holds for the PHM system, for which still some algorithms need to be developed. The consequence is therefore critical, as a large adaption of the design would be needed.
2. **Overestimated results** The new technologies that might be implemented on the are now being researched on individual scale. The effect on the efficiency of implementing this on the aircraft might be lower than expected. This holds specifically for BLI, geared turbofans and blending the wing. To a lesser extend because some test flights have already been done also for morphing HLD and split winglets. The consequence is considered marginal as a very conservative design approach is taken.
3. **Schedule slip** Several technologies still have to be investigated and this increases the risks for schedule slip. Still, the new aircraft is expected by 2030 and many technologies are to be investigated, thus delay is probable to happen in this time. However, at the moment the design is in a very early stage thus the consequences are still negligible.

A risk can be managed in four ways; it can be terminated, mitigated, transferred or if the consequences are low enough, it can be taken. Transferring and terminating risks is at this stage of the development phase hardly possible, so only the other options will be considered. Per risk mentioned above the actions taken to decrease the risk is shortly summarized below:

1. **Non-feasible before 2025** Since the technologies depend on other research, it is hard to decrease the likelihood of occurrence. The risk of not meeting the requirements can therefore be mitigated by considering a conservative design that allows to implement the new technologies when possible. This was done for the HLD and engine design and the consequence is therefore considered negligible. For the morphing HLD, this risk was terminated for the leading edge device, as too many certification and safety issues remained uncertain. For the trailing edge it is still considered as this technology is more matured. However, switching to Fowler flaps is still a possibility. The PHM system has already some features that are used, thus it is likely to be available by 2025. However, if this is not the case this risk can be mitigated by applying a conventional maintenance scheme until the complete PHM system is available.
2. **Overestimated results** To mitigate this risks, two persons have checked the assumptions made, and whether they where not to optimistic. For the wing, wingtips and wingbox, these were investigated using CFD tools and boom equations. These results need to be refined to see whether the inputs were correct using wind tunnels and FEM calculations. This should be done as soon as possible to reduce the change of extensive resizing. The same holds for the wing-fuselage integration, especially when a more blended integration is considered. This reduces the consequence to marginal.
3. **Schedule slip** As explained, with the amount of research still to be done it is likely that delay will happen somewhere in the future. To mitigate this, planning is executed carefully, with plenty of slack time, such that the chances are lower that this will occur.

Figure 21.1: Final design stage project risk pre mitigation

Figure 21.2: Final design stage project risk post mitigation

22

Conclusion

Airbus and Boeing are implementing small changes to make their aircraft more efficient. However, current designs are reaching their limits in the performance improvement that can be reached. So what if a new aircraft would be developed? This series of reports aims to design a new aircraft with 30 % reduction in cost, while maintaining the other costs at a similar level. Likewise, the emission and noise should be reduced by 20 %. A conceptual design is developed by 10 students of Delft University of Technology in 11 weeks time. This chapter concludes the final design that is developed in this report, which is the last in a series of four reports.

Before the scope of this report, the design of four different concepts was performed and by means of a trade-off, the best concept was selected. This concept, the blended wing body (BWB), consists of a large wing at the end of the fuselage and a canard and twin tail for stability. Furthermore, it was decided to use a conventional tricycle gear, wingtips and morphing high lift devices for optimum performance. The previous report investigated, among others, on high level the landing gear, fuselage layout and wing planform design. This report is a continuation on this design and went more deeply into the aerodynamics, stability, engines and strength of the aircraft. However, over the design phases the BWB is considerably adapted to fit the needs and design choices. For example, the wing is only placed at the end of the fuselage instead of along the whole length. This was done for safety reasons, such that enough emergency exits could be placed. Furthermore, due to time and knowledge constraints the wing fuselage integration could not be accurately determined. Thus, only a large, low wing is investigated at this point. The main conclusions will be shortly summarised below:

- The aerodynamic design looked into the optimum airfoil and planform. By iterating over 1000 airfoils on their performance at cruise conditions a "Whitcomb Integral Supercritical" airfoil is selected for the outboard wing sections until half of the semi-span whereas the "Grumman K-3 Transonic" airfoil is used at the root section. For this airfoil, the sweep and twist were updated to a sweep angle of 30 [°], a inner twist angle of -1.56 [°] and a outer twist angle of -3. [°]. Furthermore, the wingtips and HLD were sized. The HLD run from 0.3 until 0.7 of the span and generate a $\Delta C_{L_{max}}$ of 0.673. For the wingtips blended winglets were considered due to technical constraints and these increased the lift over drag ratio on average by 10.8 %. However, it is recommended to investigate split winglets further, as these can improve the efficiency by another 2%.

- Regarding the structural strength, the fuselage loading and wingbox was designed to withstand 10^5 load cycles. This resulted in the wingbox dimensions and material selections for the fuselage and wing. For both, Al 7075-T6 is chosen due to its specific strength qualities.

- The engine was designed for a top mounted turbofan, giving for example values for a bypass ratio of 13 and specific fuel consumption of 2097 [l/h]. This resulted in a inlet radius of 0.76 [m] and a outlet radius of 0.72 [m]. This engine achieves a 39 % in CO_2 emissions and 60.1 % in NO_X emissions, such that the emission objectives have been met.

- The landing gear position was also calculated, such that the nose gear can be retracted forward and the main gear retracts towards the fuselage. Furthermore, dimension for the strut height and wheel dimensions of the type VII tyres are found, giving a total landing gear height of 1.8 [m].

- The aircraft remains has stable eigenmotions using augmented stability for the canard, which resulted in a canard size of 43.7 [m^2]. In the same way, the vertical twin tails were sized, which have a surface area of 29.5 [m^2].

Next to these topics also the cockpit and aircraft systems have been investigated, such that the aircraft is able to operate using a single pilot. By using prognostic health management systems, the maintenance efficiency can be

further increased. In general, the aircraft is able to reach a turn around time of 40 minutes during operations at the home base and 28 minutes in a degraded fashion at outposts.

This RELOAD aircraft can already reach a 5% Return on Investment after 5 years and selling a 172 aircraft at a price of 90 M$. This would mean that RELOAD should only capture 2.2 % of the expected aircraft to be sold in between 2030 and 2034. However, it is expected that due to the good performance in costs the aircraft is at least able to capture 5 %. RELOAD is able to reduce the direct operating cost by 30.4 % using for example efficient engines (-20.4 %) and single pilot operations (-7.2 %). The remainder is achieved from the prognostic health management program for maintenance and from depreciation. Furthermore, this aircraft will meet the noise reduction requirements of 29 $[EPNdB]$ by using engines based on the CFM-LEAP, placing the engines on top of the fuselage and shielding the noise with the vertical tails, a cumulative noise reduction of approximately 29.6 $[EPNdB]$ is achieved. Lastly, this aircraft has a dispatch reliability of 99.0 %. Although this is just not enough to meet the requirement of 99.7 % , it is still highly competitive with the Airbus A320 and Boeing 737, which have a dispatch reliability of 99.3 % and 97.1 %, respectively.

Bibliography

[1] Gulikers, T. et al., "DSE Mid Term Report (Project 07)," Delft University of Technology, 2016.

[2] Gulikers, T. et al., "DSE Baseline Review (Project 07)," Delft University of Technology, 2016.

[3] United States Bureau of Transportation Statistics, "Transtats Database [online database]," OST-R, 2016.

[4] EASA, *Certification Specification and Acceptable Means of Compliance for Large Aeroplanes CS-25*, 17th ed., European Aviation Safety Agency, Cologne, 2015, chap. 1–2.

[5] Raymer, D., *Aircraft Design: A Conceptual Approach*, 2nd ed., AIAA, Washington, DC, 1989, chap. 11,15,18.

[6] Sadraey, M., *Aircraft Design: A Systems Engineering Approach*, 1st ed., Wiley, New Hampshire, 2012, chap. 6,5.

[7] Steenhuizen, I. D., "Wing Design Part II," *Aerospace Design and Systems Engineering Elements II Wing Design Part II*, Delft University of Technology, Delft, 2013. Lecture slides.

[8] Murman, E. M., Bailey, F. R., and Johnson, M. L., "TSFOIL - A Computer Code for Two-Dimensional Transonic Calculations, Including Wind-Tunnel Wall Effects and Wave Drag Evaluation," NASA SP-347, 1975.

[9] Drela, M., "XFOIL," Software Package, Ver. 6.99, Cambridge, 2013. Software available at: `http://web.mit.edu/drela/Public/web/xfoil/` [Cited on 24 June 2016].

[10] Hepperle, M., "Javafoil," Software Package, Ver. 2.219, Braunschweig, 2014. Software available at: `http://www.mh-aerotools.de/airfoils/javafoil.htm` [Cited on 24 June 2016].

[11] Palacios, F. et al., "SU2 Educational," Software Package, Ver. 1.1.0, Stanford, 2014. Software available at: `https://github.com/su2code/SU2_EDU` [Cited on 16 June 2016].

[12] Roskam, J., *Airplane Design Part III: Layout Design of Cockpit, Fuselage, Wing and Empennage: Cutaways and Inboard Profiles*, 1st ed., DARcorporation, Lawrence, 1986, chap. 6.

[13] Raymer, D., *Aircraft Design: A Conceptual Approach*, 2nd ed., AIAA, Washington, DC, 1989, chap. 4.

[14] Torenbeek, E., *Synthesis of Subsonic Aircraft Design*, 8th ed., Kluwer Academic Publishers, Dordrecht, 1982, chap. 3,6,10,7, pp. 77,210,342–363,258–259.

[15] Roskam, J., *Airplane Design Part II: Preliminary Configuration Design and Integration of the Propulsion System*, 1st ed., DARcorporation, Lawrence, 1985, chap. 9.

[16] Deperrois, A., "XFLR5," Software Package, Ver. 6.14, Paris, 2016. Software available at: `http://www.xflr5.com/xflr5.htm` [Cited on 24 June 2016].

[17] ir. R. Vos, D., "Advanced Aircraft Design I Root and Tip Effects," *AA283 Aircraft and Rocket Propulsion*, TU Delft, Delft, 2016. Lecture slides.

[18] Wakefield, I. and Dubuque, C., "Exceeding Tire Speed Rating During Takeoff," *Aero Quarterly*, Vol. QRT_02.09, No. 34, 2009, pp. 14–19.

[19] Monner, H. and Riemenschneider, J., "Morphing high lift structures: Smart leading edge device and Smart single slotted flap," *Proceedings of the Sixth European Aeronautics Days*, IOS Press, Amsterdam, 2012, pp. 94–102.

[20] Wölcken, P. C. and Papadopoulos, M., "Smart Intelligent Aircraft Structures (SARISTU)," *Proceedings of the Final Project Conference*, Vol. 1, Springer International Publishing, Switzerland, 2016, pp. 1–1021.

[21] Sodja, J., Martinez, M. J., Simpson, J. C., and Breuker, R. D., "Experimental Evaluation of the Morphing Leading Edge Concept," *AIAA Journal*, Vol. 23, No. 2015-0791, 2015, pp. 1–12.

[22] Sforza, P., *Commercial Airplane Design Principles*, 1st ed., Elsevier Science, Oxford, 2014, chap. 5,9.

[23] Sr., G. A. C., "The Descriptive Geometry of Nose Cones," VCP program, 1996.

[24] Filippone, A., *Advanced Aircraft Flight Performance*, 1st ed., Cambridge University Press, The University of Manchester, 2012, chap. 2.

[25] Torenbeek, E., *Advanced Aircraft Design, Conceptual Design Analysis and Optimization of Subsonic Civil Airplanes*, 1st ed., Wiley, Delft, 2013, chap. 5,11,4.

[26] Hoak, D. E. et al., "The USAF Stability and Control DATCOM," TR-83-3048, 1978.

[27] Mason, W., "Transonic Aerodynamics of Airfoils and Wings," *AOE 4124 Configuration Aerodynamics*, Virginia Polytechnic Institute and State University, Blacksburg, 2016. Lecture notes.

[28] Palacios, F. et al., "Stanford University Unstructured (SU2): Open-source Analysis and Design Technology for Turbulent Flows," *AIAA Science and Technology Forum and Exposition*, Vol. 1, AIAA, Maryland, 2014, pp. 1–7.

[29] Sharma, S. C. and Ganessan, B., "Optimisation of Aircraft Structures For Minimizing Costs," *Aerospace Manufacturing Technologies*, Vol. 1, Allied Publishers Limited, New Delhi, 1997, pp. 98–106.

[30] E. Mooij, E. and Papp, Z., "Structures assignment," *AE3212 SVV 2016*, TU Delft, Delft, 2016. Reader.

[31] Megson, T., *Aircraft Structures for Engineering Students*, 8th ed., Elsevier, Kidlington, Oxford, 2013, chap. 1–24.

[32] Hibbeler, R., *Mechanics of Materials*, 5th ed., Prentice Hall, Jurong, 2011, chap. 1-14.

[33] Austin, A. and Swannell, J., "Stresses in a pipe bend of oval cross-section and varying wall thickness loaded by internal pressure," *International Journal of Pressure Vessels and Piping*, Vol. 7, No. 4, 1979, pp. 167–182.

[34] Brügemann, V. et al., "Project Manual Design and Construction," *AE1222 - I*, TU Delft, Delft, 2014. Reader.

[35] HexWeb, "Honeycomb sandwich design technology," `http://www.hexcel.com/resources/technology-manuals`[Cited on 17 June 2016], 2000.

[36] Yang, Y. et al., "Recycling of composite materials," *Chemical Engineering and Processing: Process Intensification*, Vol. 51, No. 12, 2012, pp. 53 – 68.

[37] Schijve, J., "Fatigue of structures and materials in the 20th century and the state of the art," *International Journal of Fatigue*, Vol. 25, No. 8, 2003, pp. 679–702.

[38] Department of Defense, *Military Handbook, Metallic Materials and Elements for Aerospace Vehicle Structures*, 2nd ed., Department of Defense, Washington DC, 1998, chap. 3.

[39] Sarath, S., Issac, J. C., and Girish, K., "Analysis of the Wingbox with Spliced Skin and Estimation of the Fatigue Life for the Wingbox," *International Journal of Mechanical Engineering and Robotics Research*, Vol. 2, No. 2, 2013, pp. 155–163.

[40] Tanaka, K., Matsuoka, S., and Kimura, M., "Fatuque strength of 7075-T6 Aluminium alloy under combined axial loading and torsion," *Fatigue & Fracture of Engineering Materials & Structures*, Vol. 7, No. 3, 1984, pp. 195–211.

[41] Masseanalys, A., *Luftfahrttechnisches Handbuch: Masseanalyse*, 3rd ed., LTH-Koordinierungsstelle, München, 1994, chap. 1,4,7.

[42] Roskam, J., *Airplane Design Part V: Component Weight estimation*, 1st ed., DARcorporation, Lawrence, 1985, chap. 2,3,4.

[43] Ajaj, R. et al., "A conceptual wing-box weight estimation model for transport aircraft," *Aeronautical Journal*, Vol. 177, No. 1191, 2013, pp. 533–551.

[44] Kuhn, P., "The Strength and Stiffness of Shear Webs with and without Lightening Holes," *Wartime Report*, NACA, Washington, 1942. `http://www.dtic.mil/dtic/tr/fulltext/u2/a801095.pdf` [Cited on 23 June 2016].

[45] NLR, "Gas Turbine Simulation Program," Software Package, Ver. 11.4.4.0, Amsterdam, 2014. Software available at: `http://www.gspteam.com/` [Cited on 16 June 2016].

[46] Kogenhop, O. et al., "GSP 11 User Manual," National Aerospace Laboratory NLR, 2016.

[47] Cantwell, B. J., "The GE-90 - An Introduction," *AA283 Aircraft and Rocket Propulsion*, Stanford University, Stanford, 2010. Lecture slides.

[48] Visser, W. and Broomhead, M., "GSP, A generic object-oriented gas turbine simulation environment," NLR, 2000.

[49] Epstein, A., "A 2030 Technical Vision For Sustainable Commercial Air Transport," *Technology & Environment Pratt & Whitney*, Pratt & Whitney, Madrid, 2011. Lecture slides.

[50] Benzakein, M. J., "What does the future bring? A look at technologies for commercial aircraft in the years 2035–2050," *Propulsion and Power Research*, Vol. 3, No. 4, 2014, pp. 165–174.

[51] McKay, B. and Barlow, A., "The UltraFan Engine and Aircraft Based Thrust Reversing," *48th AIAA/ASME/SAE/ASEE Joint Propulsion Conference & Exhibit*, AIAA, Atalanta, 2012, pp. 2–3.

[52] Haselbach, F., Newby, A., and Parker, R., "Concepts & Technologies for the next generation of large civil aircraft engines," *29th Congress of the International Council of the Aeronautical Sciences*, ICAS, St. Petersburg, 2014, p. 4.

[53] Halbig, M. C. et al., "Evaluation of ceramic matrix composite technology for aircraft turbine engine applications," *51st AIAA Aerospace Sciences Meeting including the New Horizons Forum and Aerospace Exposition*, Aerospace Sciences Meetings, Grapevine (Dallas/Ft. Worth Region), Texas, 2013, pp. 07–10.

[54] Roberts, G. D. et al., "Design and testing of braided composite fan case materials and components," *19th ISABE Conference (ISABE 2009)*, NASA, Montreal, 2009, p. 10.

[55] International Civil Aviation Organization, "Airport Air Quality Manual," ICAO, 2011.

[56] Verhagen, W., "Project Guide Design Synthesis Exercise: Low Cost Narrow Body Aircraft," Delft University of Technology, 2016.

[57] Daggett, D. et al., "Alternative fuels and their potential impact on aviation," *National Aeronautics and Space Administration, NASA/TM*, Vol. 25, No. 6, 2006, pp. 2–3.

[58] Rahmes, T. et al., "Sustainable bio-derived synthetic paraffinic kerosene (Bio-SPK) jet fuel flights and engine tests program results," *9th AIAA Aviation Technology, Integration, and Operations Conference (ATIO)*, Vol. 7002, AIAA, Hilton Head, South Carolina, 2009, pp. 1–19.

[59] Eisentraut, A., "Technology Roadmap - Biofuels for Transport," International Energy Agency, 2011.

[60] Kawai, R. T., Friedman, D. M., and Serrano, L., "Blended wing body (BWB) boundary layer ingestion (BLI) inlet configuration and system studies," *NASA CR*, Vol. 214534, No. 20070006754, 2006, pp. 9–10.

[61] Plas, A. et al., "Performance of a boundary layer ingesting (BLI) propulsion system," *45th American Institute of Aeronautics and Astronautics Aerospace Sciences Meeting and Exhibit*, Vol. 2007-450, AIAA, Reno, Nevada, 2007, pp. 8–11.

[62] Daggett, D. L., Kawai, R., and Friedman, D., "Blended wing body systems studies: boundary layer ingestion inlets with active flow control," *NASA CR*, Vol. 212670, No. 2006-214365, 2003, p. 2003.

[63] Plas, A. P. et al., "Performance of a Boundary Layer Ingesting (BLI) Propulsion System," *AIAA Journal*, Vol. 45, No. 2007-450, 2007, pp. 450–471.

[64] Spencer, K. M., "Investigation of Potential Fuel Cell Use in Aircraft," *IDA*, Vol. Institute for Defense Analysis, No. D-5043, 2013, pp. 1–28.

[65] Mulder, J. et al., *Flight Dynamics, Lecture notes AE3202*, 1st ed., TU Delft, Delft, 2013, chap. 2.

[66] Roskam, J., *Airplane Design Part V: Component Weight estimation*, 1st ed., DARcorporation, Lawrence, 1985, chap. 72-73,44-46.

[67] Roskam, J., *Airplane Flight Dynamics and Automated Flight Controls, Part 2*, 2nd ed., DARcorporation, Lawrence, 1998, chap. 1–4.

[68] Gabernet, A. F., "Controllers for Systems with Bounded Actuators: Modeling and control of an F-16 aircraft," Ph.D. Dissertation, University of California, Irvine, 2007.

[69] Goupil, P., "AIRBUS Electrical Flight Control System (EFCS)," *AA283 Aircraft and Rocket Propulsion*, Airbus France S.A.S., Toulouse, 2016. Lecture slides.

[70] Roskam, J., *Airplane Design Part IV: Layout of Landing Gear and Systems*, 1st ed., DARcorporation, Lawrence, 1985, chap. 2.

[71] Chai, S. T. and Mason, W. H., *Landing Gear Integration in Aircraft Conceptual Design*, 2nd ed., NASA Ames Research Center, Virginia Polytechnic Institute and State University, 1996, chap. 3.

[72] Cummings, M. L., Stimpson, A., and Clamann, M., "Functional Requirements for Onboard Intelligent Automation in Single Pilot Operations," *AIAA*, Vol. 1, No. 1, 2016, pp. 1–7.

[73] Flemisch, F. O. et al., "The H-Metaphor as a Guideline for Vehicle Automation and Interaction," *NASA STI*, Vol. 2003-212672, No. 20040031835, 2003, pp. 1–26.

[74] Vos, R., Melkert, J., and Zandbergen, B., "Fuselage design," *AE1222-II Aerospace Design and Systems Engineering Elements I*, Delft University of Technology, Delft, 2013. Lecture slides.

[75] Bilimoria, K. D., Johnson, W. W., and Schutte, P. C., "Conceptual Framework for Single Pilot Operations," *International Conference on Human-Computer Interaction in Aerospace*, NASA, Santa Clara, California, USA, 2014, pp. 1–8.

[76] Fahlstrom, P. G. and Gleason, T. J., *Introduction to UAV Systems*, 4th ed., Wiley, West Sussex, 2012, chap. 12.

[77] Rondeau, J.-L., "Systèmes de Bord: Communication," *Avionics Module*, Ecole Nationale De L'Aviation Civile, Toulouse, 2015. Lecture slides.

[78] Perrin, A., "FANS: Future Air Navigation System," *Avionics Module*, ENAC, Toulouse, 2015. Lecture slides.

[79] Gundlach, J., *Designing Unmanned Aircraft Systems: A Comprehensive Approach*, 2nd ed., American Institute of Aeronautics and Astronautics, Inc., Reston, 2012, chap. 12.7.

[80] Scheible, M. P. et al., "High Data Rate, Reliable Wideband HF Communications Demonstration," *MITRE*, Vol. 1, No. 1, 2014, p. 2.

[81] Rosero, J. et al., "Moving Towards a More Electric Aircraft," IEEE A&E Systems Magazine, 2007.

[82] FAA, "Aircraft Electrical System," Federal Aviation Administration, 1998.

[83] von Meier, A., *Electric Power Systems: A Conceptual Introduction*, 1st ed., Wiley-IEEE Press, Hoboken, New Jersey, 2006, chap. 4.

[84] Dinh-Khanh Dang, T. G., Ahlem Mifdaoui, "Fly-By-Wireless for Next Generation Aircraft: Challenges and Potential solutions," *Wireless Days (WD), 2012 IFIP*, Vol. 93, No. 6559, 2012, pp. 1–8.

[85] Moir, I. and Seabridge, A., *Aircraft systems: mechanical, electrical and avionics subsystems integration*, 3rd ed., John Wiley & Sons, West Sussex, England, 2011, chap. 12.

[86] Langton, R. et al., *Aircraft fuel systems*, 1st ed., Wiley Online Library, Chippenham,Wiltshire,UK, 2009, chap. 2–4,12.

[87] FAA, "Hydraulic and Pneumatic Power Systems," Federal Aviation Administration, 2012.

[88] Gandolfi, R. et al., "Aircraft air management systems trade-off study using exergy analysis as a design comparison tool," *19th International Congress of Mechanical Engineering*, ABCM, Brasilla, DF, 2007, pp. 1–10.

[89] Sinnet, M., "787 No-Bleed Systems:Saving Fuel and Enhancing Operational Efficiencies," *Aero Quarterly*, Vol. QRT_04|07, No. 2, 2007, pp. 1–11.

[90] Bertsch, L., "Advanced Aircraft Noise Modeling and Measurement," *Avionics Module*, ENAC, Delft, 2016. Lecture slides.

[91] G.J.J, R., *Elements of Aviation Acoustics*, 1st ed., Delft University Press, Delft, 1993, chap. 12.

[92] Thomas, R. H., Burley, C. L., and Nickol, C. L., "Assessment of the Noise Reduction Potential of Advanced Subsonic Transport Concepts for the NASA Environmentally Responsible Aviation Project," *AIAA SciTech*, Vol. 54, No. 2016-0863, 2016, pp. 1–25.

[93] Thomas, R. H., Burley, C. L., and Olson, E. D., "Hybrid Wing Body Aircraft System Noise Assessment With Propulsion Airframe Aeroacoustic Experiments," *AIAA*, Vol. 16, No. 2010-3913, 2010, pp. 1–28.

[94] Leylekian, L., Lebrun, M., and Lempereur, P., "An overview of aircraft noise reduction technologies." *Aerospace-Lab*, Vol. 7, No. 1, 2014, p. 1.

[95] Martens, S., "Jet noise reduction technology development at GE aircraft engines," *ICAS Paper*, Vol. 842, No. 2007-214495, 2002, p. 1.

[96] Thomas, R. H., Czech, M. J., and Doty, M. J., "High Bypass Ratio Jet Noise Reduction and Installation Effects Including Shielding Effectiveness," *AIAA Paper*, Vol. 541, No. 51, 2013, pp. 1–21.

[97] Dobrzynski, W. et al., "Research into landing gear airframe noise reduction," *AIAA*, Vol. 8, No. 2002-2409, 2002, p. 2002.

[98] Chow, L., Mau, K., and Remy, H., "Landing gears and high lift devices airframe noise research," *AIAA paper*, Vol. 8, No. 2002-2408, 2002, pp. 1–10.

[99] Khorrami, M. R. et al., "Aeroacoustic Evaluation of Flap and Landing Gear Noise Reduction Concepts," *AIAA Paper*, Vol. 2478, No. 20150000546, 2014, pp. 1–28.

[100] Heath, S. L. et al., "NASA Hybrid Wing Aircraft Aeroacoustic Test Documentation Report," *NASA Technical Report server*, Vol. 16, No. 2016-219185, 2016, pp. 1–85.

[101] Unknown, "Ground handling operations: a technical perspective," *Groundhandling*, MIT, Michigan, 2016. Reader.

[102] Airplanes, B. C., *737 Airplane Characteristics for Airport Planning*, 6th ed., Boeing Commercial Airplanes, Seattle, Washington, U.S.A, 2013, chap. 5.

[103] A321, A. I. A. ., *Ground Operations Manual: Aircraft Data, Limitation and Description*, 15th ed., LTU International Airways, Hamburg, Germany, 2003, chap. 1.1.

[104] Airbus, "Aircraft characteristics airport and maintenance planning," Airbus, 2015.

[105] Gulikers, T. et al., "DSE Project Plan (Project 07)," Delft University of Technology, 2016.

[106] Bense, W., "Prognosis and Health Monitoring Systems for Aircraft Engines," *SAE 2013 AeroTech Congress & Exhibition*, SAE International, Warrendale, 2013, pp. 1–8.

[107] Orsagh, R. F. et al., "Prognostic Health Management for Avionic Systems," *2005 IEEE Aerospace Conference*, IEEE, Rochester, 2005, pp. 1–7.

[108] Scanff, E. et al., "Life Cycle Cost Impact of Using Prognostic Health Management (PHM) for Helicopter Avionics," *Microelectronics Reliability*, Vol. 47, No. 12, 2007, pp. 1–16.

[109] Simonetti, G., "Aircraft Maintenance Management," *Maintenance*, Ecole Nationale de l'Aviation Civile, Toulouse, 2015. Lecture slides.

[110] Saxena, A., "Prognostics: the science of prediction," *Annual Conference of the PHM Society (PHM2010)*, Stinger Ghaffarian Technologies Inc., NASA Ames Research Center, Moffett Field CA 94035, Portland, OR, 2010, pp. 1–70.

[111] UTC Aerospace Systems, "Health and Usage Management Systems (HUMS)," `http://utcaerospacesystems.com/cap/systems/sisdocuments/Health%20and%20Usage%20Management%20Systems%20(HUMS)/Health%20and%20Usage%20Management%20Systems%20(HUMS).pdf` [Cited on 13 June 2016], 2016.

[112] Przytula, K. W. et al, "Health monitoring for commercial aircraft systems," *26th International congress of the aeronautical sciences*, Vol. 6.1.2, ICAS-2008, Anchorage, Alaska, USA, 2008, pp. 1–7.

[113] Yang, B., "Blade containment evaluation of civil aircraft engines," *Chinese Journal of Aeronautics*, Vol. 26, No. 1000-9361, 2013, pp. 9–13.

[114] FAA, "Aircraft Systems and Components," Federal Aviation Administration, 2012.

[115] McCarthy, M. A. et al., "Modelling of Bird Strike on an Aircraft Wing Leading Edge Made from Fibre Metal Laminates – Part 2: Modelling of Impact with SPH Bird Model," *Applied Composite Materials*, Vol. 11, No. 5, 2004, pp. 317–340.

[116] Hammond, G. and Jones, C., *Inventory of carbon & energy: ICE*, 1st ed., Sustainable Energy Research Team, Department of Mechanical Engineering, University of Bath Bath, UK, 2008, chap. 1, pp. 1–64.

[117] Cui, C. et al., "Titanium alloy production technology, market prospects and industry development," *Materials & Design*, Vol. 32, No. 3, 2011, pp. 1684–1691.

[118] Yellishetty, M., Ranjith, P., and Tharumarajah, A., "Iron ore and steel production trends and material flows in the world: Is this really sustainable?" *Resources, conservation and recycling*, Vol. 54, No. 12, 2010, pp. 1084–1094.

[119] Shonnard, D. R., Williams, L., and Kalnes, T. N., "Camelina-derived jet fuel and diesel: Sustainable advanced biofuels," *Environmental Progress & Sustainable Energy*, Vol. 29, No. 3, 2010, pp. 382–392.

[120] Marsh, G., "Biofuels: aviation alternative?" *Renewable Energy Focus*, Vol. 9, No. 4, 2008, pp. 48–51.

[121] Fraser, H. L. et al., "Recycling of Ti-6Al-4V Chips: Influence of the Machining Process on the Chip Quality," *2015 World Conference on Titanium*, John Wiley & Sons, Inc., Hoboken, New Jersey, USA, 2016, p. 293.

[122] Otto, K. and Wood, K., *Product Design: Techniques in Reverse Engineering and New Product Development*, Prentice Hall, Upper Saddle River, New Jersey, 2001, chap. 15, pp. 719–779.

[123] Young, P., Byrne, I. G., and Cotterell, M., "Manufacturing and the environment," *The international journal of advanced manufacturing technology*, Vol. 13, No. 7, 1997, pp. 488–493.

[124] Roskam, J., *Airplane Design Part VIII: Airplane Cost Estimation*, 1st ed., DARcorporation, Lawrence, 1990, chap. 3-5,8,9.

[125] Murman, E. et al., *Lean enterprise value*, 1st ed., Palgrave Macmillan UK, New York, USA, 2002, pp. 177–287.

[126] Sinke, J., "Lean Manufacturing," *AE4ASM004 Manufacturing of Aerospace Structures & Materials Chapter 10*, Delft University of Technology, Delft, 2016. Lecture notes.

[127] Sinke, J., "Lean Manufacturing," *AE3211-II Production of Aerospace Systems Chapter 11*, Delft University of Technology, Delft, 2016. Lecture notes.

[128] Chu, S. et al., "The Study on Dispatch Reliability Prediction Model of Civil Aircraft," *The Open Mechanical Engineering Journal*, Vol. 1, No. 8, 2014, pp. 828–832.

[129] Bineid, M. and Fielding, J., "Development of a civil aircraft dispatch reliability prediction methodology," *Aircraft Engineering and Aerospace Technology*, Vol. 75, No. 6, 2003, pp. 588–594.

[130] Drouin, E. and Hemberger, M., "Leap," CFM International, 2015.

[131] Voskuijl, M., "Take-off performance (Flight Mechanics)," *AE22330-I Flight and Orbital Mechanics*, Delft University of Technology, Delft, 2016. Lecture slides.

[132] Voskuijl, M., "Landing performance (Flight Mechanics)," *AE22330-I Flight and Orbital Mechanics*, Delft University of Technology, Delft, 2016. Lecture slides.

[133] Voskuijl, M., "Unsteady Climb (Flight Mechanics)," *AE22330-I Flight and Orbital Mechanics*, Delft University of Technology, Delft, 2016. Lecture slides.

[134] Airplanes, B. C., *Current market outlook: 2015-2034*, 1st ed., The Boeing Company, Seattle, 2015, chap. 1, pp. 1–58.

[135] Vos, R., Melkert, J., and Zandbergen, B., "Introduction and Organization," *AE1222-II Aerospace Design and Systems Engineering Elements I*, Delft University of Technology, Delft, 2013. Lecture slides.

[136] Echeveste, G., "Development of a Maintenance program, MRB process & MSG-3 Method," *Maintenance*, Airbus, Toulouse, 2015. Lecture slides.

Fuselage Design

This appendix provides an overview of the passenger floor and cargo floor design of the fuselage. Figure A.1 shows the passenger seating and service layout of the upper compartment. This setting is based on the double aisle concept with emergency exits according to CS-25 regulations. Three lavatories are installed and the galley is positioned up front.
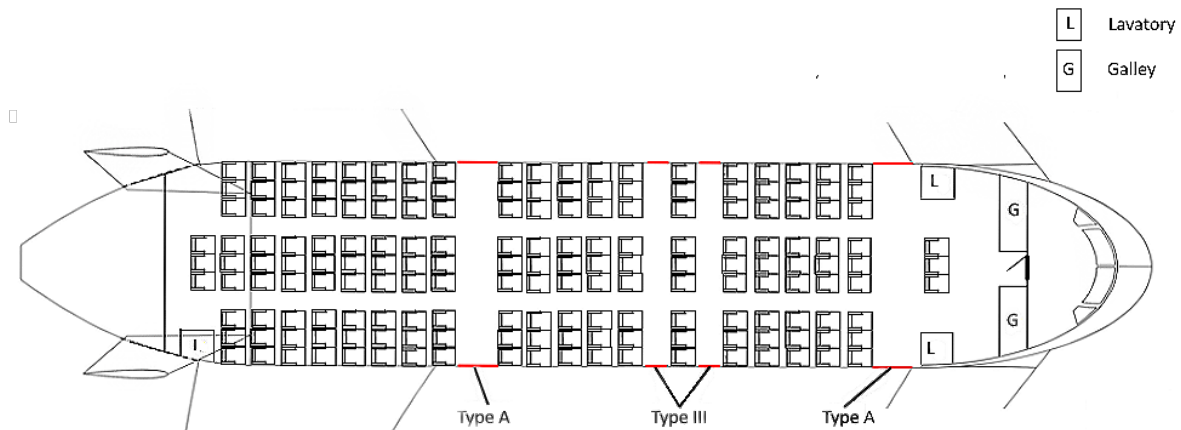
Figure A.1: Seat map configuration of the RELOAD aircraft

Figure A.2 shows the layout of the belly of the fuselage. This layout is based on several design aspects. The air conditioning packs are placed close to the APU and engine such that bleed air can directly be converted to fresh cabin air. The storage of lavatory fluid and deposit is positioned below the lavatories and close to the service inputs. The cargo compartment has room for eight ULD-3 devices, three in front of the cargo door, four behind it. The potable water storage is positioned next to the cargo compartment to move the center of gravity forward and use the remaining space of the fuselage. The air pressure system sucks out air and outlets it into the atmosphere. The data and computer storage of the aircraft and cockpit is positioned below the cockpit.The remaining room of the elliptical fuselage is filled with structures, cables, pipes and hydraulics.
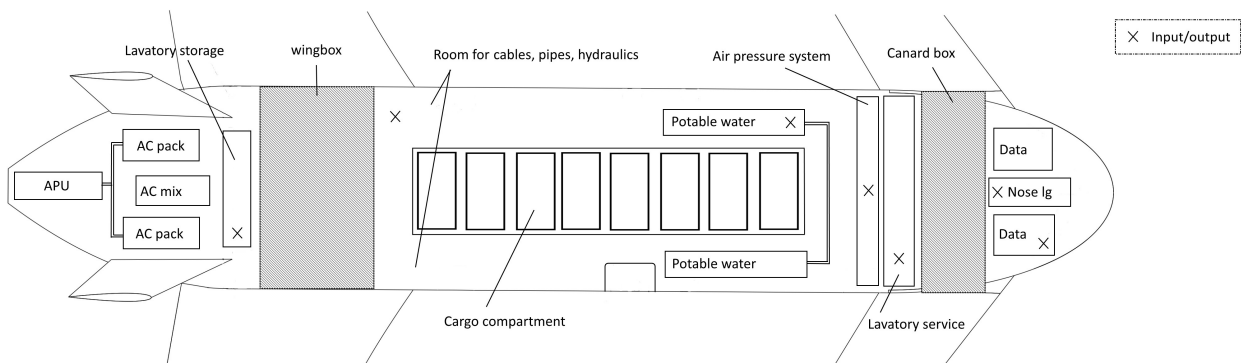
Figure A.2: Layout of fuselage belly of the RELOAD aircraft

Database

This appendix provides an overview of the most recent database in the RELOAD development process, indicating all relevant parameters and its corresponding value.

Table B.1: Updated midterm report database

Parameter	RELOAD	Unit	Parameter	RELOAD	Unit	Parameter	RELOAD	Unit	Parameter	RELOAD	Unit
ind	152	[-]	A	7	[-]	A_c	5	[-]	z_v	4.	[m]
A_v	1.3	[-]	$a_{0,h}$	-0.05	[rad]	α	-0.035	[rad]	α_{stall}	0.331613	[rad]
$Castor_{angle}$	0.656	[rad]	$C_{D_{0,fuselage}}$	0.0916	[-]	$C_{D_{Lfuselage}}$	0.0001927	[-]	$C_{D_{0,w}}$	0.008256	[-]
$C_{D_{Lw}}$	2.88e-05	[-]	$C_{D_{0,v}}$	0.00182	[-]	$C_{D_{Lv}}$	0.00028	[-]	$C_{D_{0,c}}$	0.0024	[-]
$C_{D_{Le}}$	0.00052	[-]	C_{D_0}	0.0125	[-]	C_{L_0}	0.622	[-]	$C_{L_{ac}}$	0.35	[1/rad]
$C_{L_{uv}}$	1.43	[1/rad]	C_{L_a}	4.21	[1/rad]	$C_{L_{uwf}}$	5.364	[1/rad]	C_L	0.4817	[-]
$C_{L_{landing}}$	1.6	[-]	$C_{L_{max}}$	1.6	[-]	$C_{L_{TO}}$	1.6	[-]	C_{L_c}	0.6	[-]
$C_{m_{engines}}$	0.2	[-]	c_{root}	7.329	[m]	c_{root_c}	4.0	[m]	l_c	18	[m]
C_{m_0}	-0.114	[-]	$Control_{effec_{morphing}}$	0.095	[-]	ψ	0.5585	[rad]	c'/c	1.05	[-]
h	1.1e+04	[m]	$\rho_{kerosine}$	800	[kg/m³]	$\rho_{biofuel}$	870	[kg/m³]	$D_{strut_{main}}$	0.26	[m]
$D_{strut_{nose}}$	0.17	[m]	$D_{wheel_{main}}$	1.03	[m]	$D_{wheel_{nose}}$	0.96	[m]	$D_{engines}$	1.72	[m]
Γ	-0.0745	[rad]	e	0.95	[-]	e_c	0.8	[-]	BPR	13	[-]
$V_{biofuel}/V_F$	0	[-]	d_f	0.1524	[m]	$r_{180turn}$	12.88	[m]	H_t/H_v	1	[-]
h_f	4.63	[m]	h_{lg}	1.8	[m]	$h_{nacelle}$	1.38	[m]	I_y	1.91e6	[kg m²]
K_door	1.12	[-]	K_lg	1.12	[-]	K_mp	1	[-]	K_n	-4	[-]
K_ng	1.02	[-]	K_np	1	[-]	K_p	1.4	[-]	K_r	1	[-]
K_tp	1	[-]	K_tr	1.2	[-]	K_uht	1.	[-]	K_uht_c	1.143	[-]
$l_{strut_{main}}$	0.50	[m]	$l_{strut_{nose}}$	0.54	[m]	$l_{landing}$	1500	[m]	$LEMAC$	21	[m]
$l_{fstructure}$	19.76	[m]	l_a	28	[m]	l_{engine}	2.327	[m]	l_u	0	[m]
l_f	32.78	[m]	$l_{MAC_{root}}$	6.84	[m]	$l_{MAC_{root_c}}$	3.	[m]	$l_{nosecone}$	6.5	[m]
l_{vortex}	1.93	[m]	$l_{tailcone}$	6.5	[m]	$P_{maingI_{landing}}$	4.22e+05	[N]	$P_{mainlg_{TO}}$	5.06e+05	[N]
$P_{nosel g_{landing}}$	0.703e+05	[N]	$P_{nosel g_{TO}}$	0.843e+04	[N]	MAC	5.26	[m]	MAC_c	3.11	[m]
MAC_v	4.4	[m]	M_{cruise}	0.75	[-]	$M_{c_{airfoil}}$	0.677	[-]	M_{min}	0.162	[-]
m_{engine}	1540	[kg]	m_F	9542.	[kg]	$m_{landing}$	4.7506e+04	[kg]	m_{OE}	2.97e+04	[kg]
m_{PAX}	79.4	[kg]	$m_{pax_{luggage}}$	13.6	[kg]	m_{UAV}	500	[kg]	mu_1	0.2	[-]
mu_2	0.93	[-]	mu_3	0.05	[-]	n_{aisles}	2	[-]	$n_{c_{functions}}$	7	[-]
n_{crew}	5	[-]	$n_{engines}$	2	[-]	$n_{generators}$	1	[-]	$N_{ult_{landing}}$	3	[-]
$n_{mfunctions}$	2	[-]	n_{mss}	2	[-]	$n_{mwheels}$	4	[-]	$n_{nwheels}$	2	[-]
n_{pax}	177	[-]	$n_{pax/row}$	9	[-]	n_{tanks}	4	[-]	$n_{mstruts}$	2	[-]
$n_{nstruts}$	2	[-]	N_z	3.75	[-]	$P_{internal_{main}}$	14.98	[kg/m²]	$P_{internal_{nose}}$	13.01	[kg/m²]
R_{kva}	50	[kvA]	Re	2.44e+09	[-]	S	158.8	[m²]	S_c	41	[m²]
S_{cs}	6	[m²]	S_{csw}	4	[m²]	S_e	1	[m²]	S_{ec}	1	[m²]
S_f	578.0	[m²]	S_v	65	[m²]	$S_{wheels_{main}}$	0.64	[m]	$S_{wheels_{nose}}$	0.49	[m]
$S_{total_{main}}$	0.5	[m]	$S_{total_{nose}}$	0.538	[m]	$S_{wet_{nacelle}}$	15	[m²]	S_{wf}/S	0.15	[-]
c_j	7.855e-06	[kg/Ns]	Λ	0.445	[rad]	Λ_c	0.65	[rad]	Λ_v	0.6545	[rad]
l_t	11.	[m]	l_{TO}	2000	[m]	λ	0.3	[m]	Λ_c	0.5	[rad]
λ_v	0.3	[rad]	t/c_{root_c}	0.16	[-]	t/c_{root}	0.173	[-]	t/c_{root_v}	0.1	[-]
T/W	0.26	[-]	$Tip-over_{angle}$	0.497	[rad]	$Tyre_{type}$	VII	[-]	l_{track}	8.44	[m]
V_1	37	[m/s]	V_h/V	0.922	[-]	V_{stall}	50.6	[m/s]	V_f	18.07	[m³]
V_p	395.3	[m³]	$w_{fuselage_c}$	5.9	[m]	w_{f_t}	5.9	[m]	w_f	5.9	[m]
$w_{nacelle}$	1.38	[m]	$w_{wheel_{main}}$	0.28	[m]	$w_{wheel_{nose}}$	0.17	[m]	x_{ac}/c	0.269	[-]
x_{ac}/c_{wf}	0.269	[-]	$x_{cg_{aft}}$	19.91	[m]	$x_{cg_{main}}$	22.8	[m]	$x_{cg_{nose}}$	2.7	[m]
$x_{cg_{engine}}$	27.5	[m]	$x_{cg_{fwd}}$	18.33	[-]	$x_{cg_{OEW}}$	20.3	[m]	$y_{cg_{engine}}$	1.82	[m]
Y_lg_nose	0	[-]	z_{gE}	6.89	[m]	$z_{cg_{landing}}$	4.588	[m]	$z_{cg_{TO}}$	4.189	[m]
z_w	1.8	[m]									

Final Phase Planning

This appendix visualises the project planning of the RELOAD aircraft development process starting the 1st of September 2016 until 31st of December 2029.
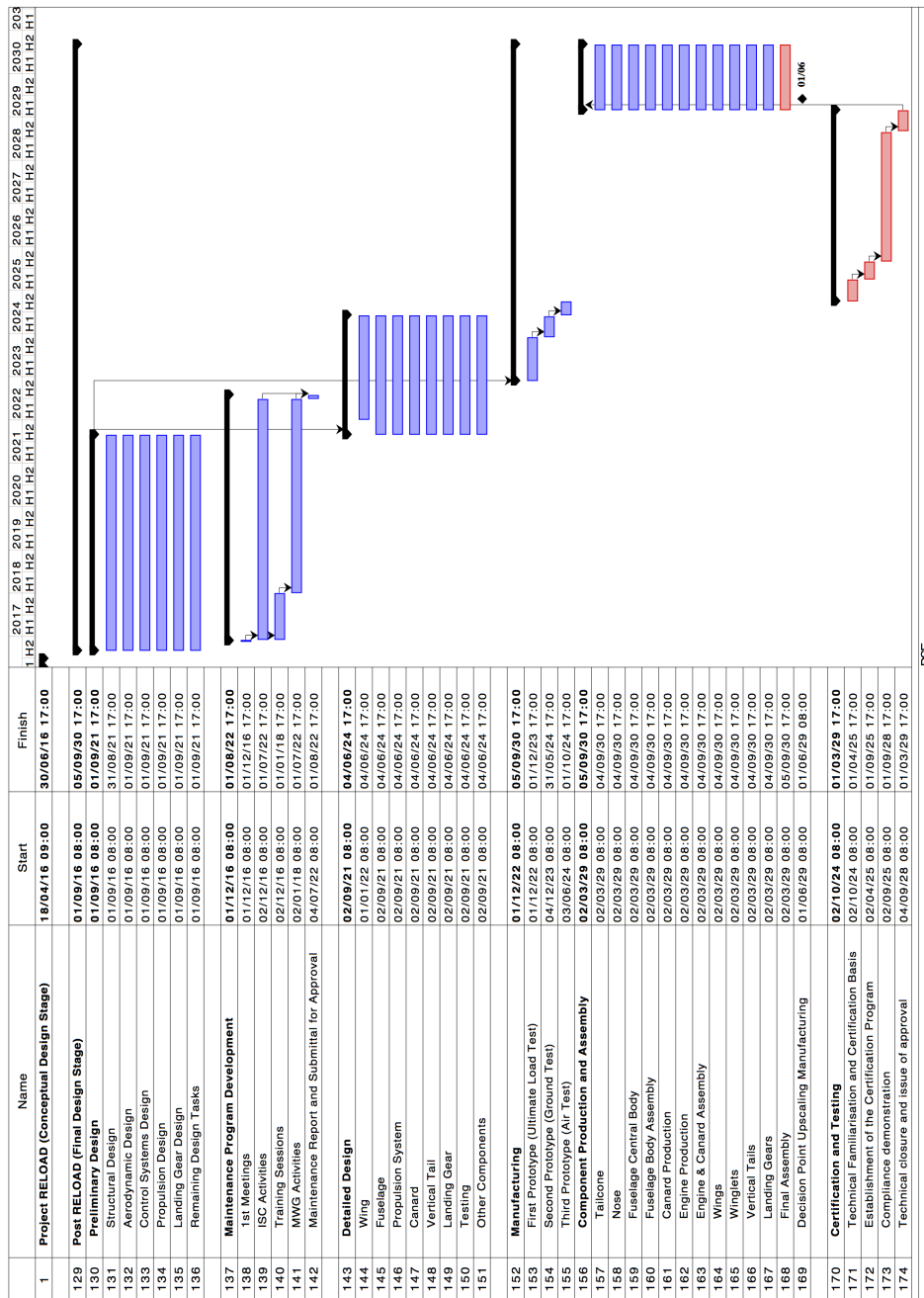
Figure C.1: The Gantt chart associated with the final design phase

D

Requirements Compliance Matrix

Table D.1: Requirements compliance matrix

Requirement identifier	Requirement	Met: yes (✓)/ not yet (~)/ no (✗)
Top Level Requirements - Technical Specifications		
TLR-TS1	The aircraft shall have a seating capacity of 175 in a typical 1-class configuration.	✓
TLR-TS2	The aircraft shall have a range of 6500 km with maximum payload.	✓
TLR-TS3	The aircraft shall have a cruise speed of at least Mach 0.75.	✓
TLR-TS4	The aircraft shall have a cruise altitude of 11 000 m.	✓
TLR-TS5	The aircraft shall have a take-off field length of 2000 m.	✓
TLR-TS6	The aircraft shall have a landing field length of 1500 m.	✓
TLR-TS7	The aircraft shall have a MTOW ≤ 78 000 kg.	✓
Top Level Requirements - Development specifications		
TLR-DS-1	The aircraft shall have a 99.7 % technical dispatch reliability.	✗(99.0 %)
TLR-DS-2	The aircraft shall be introduced to the market by 2030.	~
TLR-DS-2.1	The aircraft shall use proven technology already available by 2024.	✓
TLR-DS-2.2	The aircraft shall enter the production line by 2025.	~
TLR-DS-3	The return on investment shall be 5 % after 5 years.	✓
TLR-DS-4	The direct operating cost shall not exceed $3125 /h.	✓
TLR-DS-5	The aircraft shall be manufacturable.	✓
TLR-DS-5.1	The production shall use available facilities.	✓
TLR-DS-5.2	The aircraft components shall be transportable.	✓
TLR-DS-6	The aircraft shall be maintainable.	✓
Top Level Requirements - Noise and emissions specifications		
TLR-NES-1	The aircraft NOX emission shall be lower than 51.28 g/kN.	✓
TLR-NES-2	The aircraft CO_2 emission shall be lower than 0.05472 kg/chair/km.	✓
TLR-NES-3	The aircraft cumulative noise shall be lower than 239 EPNdB.	✓
TLR-NES-6	The aircraft cabin noise shall be maximum 80 dB.	~
Top Level Requirements - Design regulations		
TLR-DR-1	The aircraft shall comply with the CS25 regulations.	✓
TLR-DR-1.1	The aircraft shall be stable during all stages of flight.	✓
TLR-DR-1.2	The aircraft shall be controllable during all stages of flight.	✓
TLR-DR-1.3	The aircraft shall be manoeuvrable during all stages of flight.	✓
TLR-DR-1.3.1	The nominal climb slope shall be 1.5 degrees.	✓
TLR-DR-1.3.2	The nominal descend glide slope shall be 3 degrees.	✓
TLR-DR-1.4	The aircraft shall be capable of transitioning from one flight condition to any other, without any exceptional skills from the pilot.	✓
TLR-DR-1.5	The landing gear must remain extended throughout the accelerate-stop distance.	✓

TLR-DR-1.6	During the acceleration to speed V_2, the nose gear may be raised off the ground at a speed not less than V_R.	✓
TLR-DR-1.7	Landing gear retraction may not be begun until the aeroplane is airborne.	✓
TLR-DR-1.8	The aircraft shall be able to be evacuated within 90 seconds.	✓
TLR-DR-1.9	The aircraft shall be equipped with two Type I and two Type III emergency exits.	✓
TLR-DR-1.10	The aircraft shall provide a cabin pressure of at most 2438 m at the maximum operating altitude of the airplane under normal operating conditions.	✓
TLR-DR-2	The aircraft shall comply with the MSG-3 process.	✓
Medium Level Requirements -Technical specifications		
MLR-TS-1	The aircraft shall have a seating pitch of 0.8128m in a typical configuration.	✓
MLR-TS-2	The aircraft shall use current airport infrastructure.	✓
MLR-TS-2.1	The aircraft shall be capable of taxiing for at least 9 km.	✓
MLR-TS-2.2	The Take-off climb gradient shall be of at least 3 degrees.	✓
MLR-TS-3	The aircraft flight envelope shall encase the flight envelopes of the A320 and B737.	✓
MLR-TS-3.1	The loiter duration shall be 900 seconds.	✓
MLR-TS-3.2	The loiter height shall be at 2 km altitude.	✓
Medium Level Requirements -Development specifications		
MLR-DS-1	The aircraft shall provide interfaces for adding standard equipment.	✓
MLR-DS-2	The aircraft conceptual development shall be completed within 4000 man hours.	✓
MLR-DS-3	The typical life cycle cost and their distribution, excluding direct operational costs, shall remain at the same level as the A320 and B737NG.	✓
Medium Level Requirements -Other specifications		
MLR-OS-1	The aircraft shall be stable during ground operations.	✓
MLR-OS-2	The aircraft shall be controllable during ground operations.	✓
MLR-OS-3	The aircraft turn around time shall be equal or smaller than the A320 and B737NG turn around time.	✓
MLR-OS-4	The aircraft shall perform communications.	✓
Low Level Requirements -Technical specifications		
LLR-TS-1	The cruise 2 height shall be 3 km.	✓
LLR-TS-2	The cruise 2 duration shall be at least 3600 seconds.	✓
LLR-TS-3	The cruise 2 velocity shall be 246.43 m/s.	✓

E

Technical Drawings

This appendix provides the technical drawings of RELOAD. All the significant dimensions and sizes are shown from a top view, side view and front view of the RELOAD aircraft.
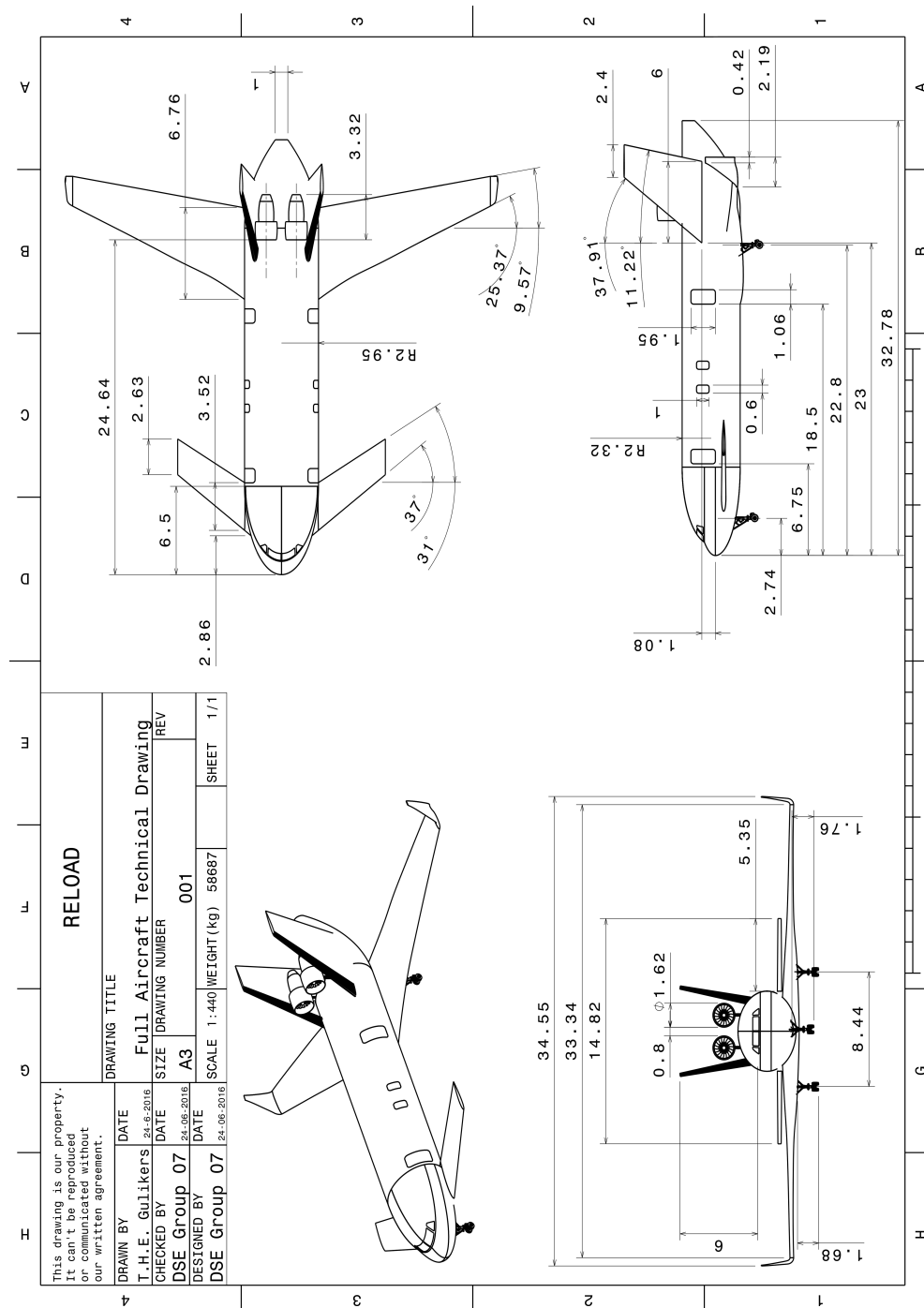
Figure E.1: Technical drawings